## Copyright Statement

# Investigation of primary productivity along the Atlantic Meridional Transect (50°N to 33°S) through fast repetition rate fluorometry

by

**Claudia Yuki Omachi**

A thesis submitted to the University of Plymouth
in partial fulfilment for the degree of

**Doctor of Philosophy**

Faculty of Science
School of Earth, Ocean and Environmental Sciences

In collaboration with
Plymouth Marine Laboratory

November 2003

*Aos meus pais*

*To my parents*

# Investigation of primary productivity along the Atlantic Meridional Transect (50°N to 33°S) through fast repetition rate fluorometry

Claudia Yuki Omachi

## Abstract

Phytoplankton physiology and primary productivity at basin scales were determined using *in situ* data from fast repetition rate (FRR) fluorometry. Samples were collected along the Atlantic Meridional Transect cruise 11 (AMT11, September-October 2000), between 50°N and 33°S in the Atlantic Ocean.

Because of the large-scale nature of the study, consistent knowledge about oceanographic conditions and the phytoplankton community structure of each sampling station were required. The province analysis was carried out by detecting the regional variations of water mass characteristics in the upper 200 m layer. Temperature versus salinity diagrams were plotted at each station and further analyses of nitrate and chlorophyll were carried out for confirmation of the provinces. The structure of phytoplankton community and its distribution were assessed by statistical analyses of the phytoplankton pigments detected by high performance liquid chromatography. The phytoplankton physiology was assessed with FRR fluorometry to retrieve the quantum yield of photochemistry (Fv/Fm), the effective absorption cross-section ($\sigma_{\mathrm{PSII}}$) and the turnover time of photosystem II ($\tau_{\mathrm{QA}}$). Some assumptions and parameterisations allowed the determination of primary productivity fractionated for prochlorophytes and eukaryotes from Fv/Fm and $\sigma_{\mathrm{PSII}}$.

The classification of the regional variation of water masses through temperature and salinity relationships turned out to be a quick and simple analysis for the detection of provinces, defining eight provinces along the transect. Phytoplankton were distributed in three communities which were stratified along the transect. The limits between the communities were at variable depths depending on the province. The shape of the vertical profile of Fv/Fm and its pre-dawn to mid-day variation were also dependent on the province. In the Equatorial upwelling region and at the depth of deep chlorophyll maximum in the oligotrophic gyres, e.g. where nitrate was replete, values of Fv/Fm were relatively low at both pre-dawn and mid-day stations. This persistent low value of Fv/Fm at pre-dawn, e.g. after overnight darkness in nitrate replete conditions, leads to the proposition of iron limitation. In the upper layer of the oligotrophic gyres, nocturnal recovery of Fv/Fm was observed, indicating nitrate limitation rather than iron limitation. In the light limited part of the water column ($P_B$) varied proportionally and consistently to the light intensity. Station analysis of $P_B$ showed photosaturation at low light levels at which the radiocarbon method was insensitive. The FRRF method was more precise, reflecting better the environmental conditions at the time of sampling than the results of radiocarbon P-E experiments. The upper layer of Atlantic Ocean was photosaturated due to the physiological impairment caused by either nitrate or iron limitation yet the zone of photosaturated photosynthesis contributed more to the primary productivity of the water column than the zone of light limited photosynthesis. The primary production fractionated for prochlorophytes and eukaryotes, indicated that the former contributed to more than half of the total production in the gyres.

FRR fluorometry has been demonstrated to be a promising option for primary productivity studies, especially at basin scales, that allows 'continuous' measurement through the water column. Exploiting the capability of this method is valuable for the understanding of photosynthesis in the natural environment and more important than attempting to reconcile it to the traditional method of radiocarbon incorporation.

# Contents

# List of Figures

# List of Tables

# List of Acronyms and Symbols

**ALL** Alloxanthin

**AMT** Atlantic Meridional Transect

**BENEFIT** Benguela Environment Fisheries Interaction and Training Programme

**BUT** 19'-Butanoyloxyfucoxanthin

**C** carbon

**Ca** calcium

**CC** Province influenced by Canary Current

**CHA** (total Chl$a$)/(total pigments)

**Chl**$a$ Chlorophyll $a$

**Chl**$b$ Chlorophyll $b$

**Chl**$c_2 - Eh$ Chlorophyll $c_2$ MGDG (monogalactosyldiacylglyceride ester) *Emiliania huxleyi*

**CHBC** (Chl$b$ + total Chl$c$)/(total pigments)

**Chl**$c_2 - Cp$ Chlorophyll $c_2$ MGDG (monogalactosyldiacylglyceride ester) *Chrysochromulina polylepis*

**Cl** chlorine

**CNPq** Conselho Nacional de Desenvolvimento Científico e Tecnológico (The National Council for Scientific and Technological Development) - Brazil

**Co** cobalt

**Cu** copper

**D1** polypeptide located in the PSII reaction centre and has a role in donor and acceptor side of electron in the photosynthetic electron tranport through PSII, with the binding sites for the phaeophytin and the $Q_B$

**DCM** Deep Chlorophyll $a$ Maximum

**ECMWF** European Centre for Medium-Range Weather Forecasts

**EPTOMS** EARTH PROBE Total Ozone Mapping Spectrometer

**ETRA** Eastern Tropical Atlantic Province

$f$ proportion of functional photosystem II to the total photosystem II

**Fe** iron

**FRR** Fast repetition rate

**FRRF** Fast repetition rate fluorometer

**FUC** Fucoxanthin reaction centre

**Fv/Fm** quantum yield of photochemistry of photosystem II

**Fv/Fm$_{dawn}$** Fv/Fm sampled at pre-dawn, by bench-top mode with dark chamber. Discrete water sampling.

**Fv/Fm$_L$ and Fv/Fm$_D$** Fv/Fm sampled with light and dark chambers, respectively

**Fv/Fm$^\infty$** Fv/Fm measured after dark adaptation (at least 30 min in the dark)

**GREEN pigments** Lutein + prasinoxanthin + violaxanthin + neoxanthin

**HEX** 19-Hexanoyloxyfucoxanthin

**HPLC** High Performance Liquid Chromatography

**ILD** Isothermal Layer Depth

**K** potassium

**Mg** magnesium

**MgDVP** Divinyl protochlorophyllide *a*

**Mn** manganese

**Mo** molybdenum

**N** nitrogen

**n$_{PSII}$** number of photosystem II reaction centres per chlorophyll *a*

**Na** sodium

**NADR** North Atlantic Drift Region

**NASE** North Atlantic Subtropical Gyral Province - East

**NCEP** National Centers for Environmental Prediction

**NECS** Northeast Atlantic Shelves Province

**NPQ** non-photochemical quenching

**P** phosphorus

**P$_B$** Chl*a*-specific primary production

**P$_{col}$** primary production integrated in the water column (from the shallowest FRRF measurement down to 0.1 % PAR)

**PAR** Photosynthetically Available Radiation

**PER** Peridinin

**PML** Plymouth Marine Laboratory

**PPC** (total photoprotectant carotenoids)/(total pigments)

**PQ** photosynthetic quotient

**PSI and PSII** Photosystem I and Photosystem II

**PSC** ratio of total photosynthetic carotenoids to the total pigments

**PSU** Photosynthetic Unit

**$Q_A$** first electron acceptor, a bound form of plastoquinone

**$Q_B$** second electron acceptor, a plastoquinone

**$q_E$** pH controlled non-photochemical quenching

**$q_P$** photochemical quenching

**$q_T$** state transition non-photochemical quenching

**RCBC** Recirculation Cell of Brazilian Current Province

**RCI and RCII** Reaction centre in photosystem I and reaction centre in photosystem II, respectively

**RRS JCR** Royal Research Ship *James Clark Ross*

**RuB** Pribulose bisphosphate, a five-carbon compound, which is the first substrate of Calvin-Benson Cycle

**S** sulfur

**SATL** South Atlantic Gyral Province

**Si** silicon

**WTRA** Western Tropical Atlantic Province

**UoP** University of Plymouth

**ZEA** Zeaxanthin

$\Phi_{RC}$ number of electrons transferred from $P_{680}$ to $Q_A$ per quanta absorbed

$\phi_e$ quantum yield of electron transfer by photosystem II

$\sigma_\theta$ potential density

$\sigma_{PSII}$ effective absorption cross-section of photosystem II

$\tau_{QA}$ turnover rate of $Q_A$ re-oxidation

# Acknowledgments

I would like to thank the many people who gave me assistance and support throughout this work. I've been very lucky to have Jim Aiken supervising me and discussing many aspects of this work. He's been offering me opportunities to always improve and I am very grateful for that. I would like to thank Derek Pilgrim for his supervision and aid during the work. Thanks to the people who I worked with in the PML, who helped me in field works and corrected my English, in special: James Fishwick especially for the sampling in the E1 and many other assistance in the PML, Matt Pinkerton and Gerald Moore.

Thanks go to Malcom Woodward for his excellent leadership in the AMT11 cruise and for providing me with nutrient and CTD data; Emilio Fernández (Vigo, Spain) for $^{14}C$ primary production and HPLC pigments; Ramiro Varela (Vigo, Spain) for coefficient of absorption and P-E experiments data. I am indebted to Dave Suggett and Richard Geider at Univesity of Essex for providing the equation of production from the FRRF, many explanations and discussions about nuances of fluorescence. Dave also aided me to collect FRRF data during the AMT11. I am grateful to Tim Smyth for modelling, many times, the light field required for primary production determination. I also want to thank Ray Barlow (Cape Town, South Africa) for the HPLC pigment data, coefficient of absorption data, many discussions and the opportunity for sampling in the Benguela upwelling. Sam Lavender and Peter Miller helped me to process remote sensing images. I also want to thank Sam Lavender for reading drafts of some chapters. Thank you to Bob Clarke and Chris Ricketts for always finding time to advise me about statistics. Thanks also to Dave Parry and Alex Poulton (SOC) for discussions. Thanks to all my officemates who helped me a lot correcting my English: Nigel, Guy, Josh, Gavin and recently Anne.

I want to thank the crews and people on board RRS James Clark Ross during the AMT11, FRS AFRICANA for BENEFIT-L1 and RV Squilla for E1 sampling.

This work was possible due to the PhD studentship given by the Brazilian government (CNPq).

Coming to a new country and settling in were very smooth with the help of Gilberto & Elisa, who opened their home to receive us. Friends are who make any place a home and we felt at home with Caina & Marquinhos, Coba & Pablo, James Lee, Gilberto & Elisa, Kelmo, Cecília & Ismael, Alex and Gize, Sandrine & Giovanni, Claudinha & Christophe, Linda and little Kevin, Kate & Paulo and lately the mexican community. Muito conveniente, como diria o Marquinhos.

Thank you to my parents, who always supported and gave everything for the best of their sons, and my brother and sisters, who are always my mates. Arigatoo.

All the personal acknowledgments were referred to as *us* instead of *me* because of Êdu, who showed me that life is much better as *we* than *I*.

# Author's Declaration

At no time during the registration for the degree of Doctor of Philosophy has the author been registered for any other University award.

This study was financed with the aid of a studentship from the Brazilian National Council for Scientific and Technological Development (CNPq) and carried out in collaboration with Plymouth Marine Laboratory.

Relevant scientific seminars and conferences were regularly attended at which work was often presented; external institutions were visited for consultation purposes.

**Presentations and Conferences attended**:

Ocean Optics XV, 16-20 October 2000, Musée Océanographique, Monaco.

Phytoplankton Productivity - an appreciation of 50 years of the study of oceans and lakes, 18-22 March 2002, University of Wales, Bangor, UK. Oral presentation: *Basin scale measurements of phytoplankton photosynthetic parameters using FRRF* (CY Omachi, DJ Suggett, G Moore, J Aiken and D Pilgrim).

Challenger Centenary Conference: Marine Science 2002, 9-13 September, University of Plymouth, Plymouth, UK. Poster presentation: *Assessment of phytoplankton physiology and primary productivity through fast repetition rate fluorometry in the Atlantic Ocean* (CY Omachi and J Aiken). Co-author of: *Assessment of photosynthetic capacity using fast repetition rate fluorometry in the Atlantic Ocean, 50°N to 40°S* (DJ Suggett, CY Omachi and J Aiken).

AMT Student Research Forum, 23 January 2003, Plymouth Marine Laboratory, Plymouth, UK. Oral presentation: *Basin Scale Analyses of Phytoplankton Production* (CY Omachi and J Aiken).

Functional Biodiversity Discussion Group, 25 April 2003, Plymouth Marine Laboratory, Plymouth, UK. Oral presentation: *Pigment analysis to assess the phytoplankton community structure* (CY Omachi, R Barlow, J Aiken and D Pilgrim).

HABWATCH-Workshop on real-time coastal observing systems for ecosystem dynamics and harmful algal blooms, 11-21 June 2003, Villefranche-sur-Mer, France. Oral presentation: *Estimating group fractionated primary production for prochlorophytes and eukaryotes using fast repetition rate fluorometry* (CY Omachi and J Aiken).

Sensing and mapping the marine environment from near and far, 16 July 2003, London, UK. Oral presentation: *Phytoplankton community structure and pigment characteristics across the Atlantic Ocean* (CY Omachi, R Barlow, J Aiken and D Pilgrim).

Two oral presentations in the Institute of Marine Studies, University of Plymouth, Research Seminar Series 2000-2003.

**External Contacts**:

Departamento de Ecoloxía e Bioloxía Animal, Universidad de Vigo (Vigo, Spain)

Grupo de Oceanografía Física, Universidad de Vigo (Vigo, Spain).

School of Biological Sciences, University of Essex (Colchester, UK).

Marine and Coastal Management (Cape Town, South Africa).

Signed _____

Date _____

# Chapter 1

# Introduction

Primary production is the amount of organic carbon synthesised by organisms from inorganic carbon. Amongst those organisms are plants and bacteria. They incorporate $CO_2$, converting it into carbohydrate, using sunlight.

Primary production by marine phytoplankton accounts for about 40 % of the global primary production, although their contribution is only 1 % to the global plant biomass (Falkowski 1994). Phytoplankton are important not only to sustain the food web in the oceans but they play an important role in biogeochemical cycles (Falkowski 1994). Oceans can sequestrate greenhouse gases, for example $CO_2$, into the deep ocean by the sinking of fecal pellets, the process known as ocean carbon pump (Holligan 1992). Some oceanic phytoplankton are linked to the emission of volatile sulphur compounds, that can influence the world climate (Jeffrey *et al.* 1997). These microscopic algae also contribute to the alteration of ocean surface temperatures (Sathyendranath *et al.* 1991). The process of absorption of light and its dissipation as heat by phytoplankton, increases the surface temperature of the oceans and this can affect the depth of mixed layer (Holligan 1992).

The term phytoplankton is from the Greek *phyton*, plant, and *planktos*, meaning wander-

ing passively with the water parcel. Surface ocean circulation and regional environmental characteristics can influence primary production, by influencing water mixing and nutrient supply. Oceans have contrasting regions, which are described as provinces and characterised in terms of physics, nutrient conditions and chlorophyll *a* concentration and also due to the seasonal variability in these terms (Longhurst 1998). The division of the ocean into provinces was proposed to estimate the primary production of the ocean from satellite data (Sathyendranath *et al.* 1995). In contrast to terrestrial ecosystems, however, boundaries are not easily identified in the ocean, either because of weaker differences between provinces or because the boundaries are not fixed geographically and may change in location seasonally (Longhurst 1998).

Physical oceanography determine the supply of nutrients and light levels. These factors influence in the composition of phytoplankton community, by affecting differently the physiology of phytoplankton, and determine the primary production of the ocean.

## 1.1 Objectives

The general objective of this thesis is to understand how oceanographic conditions affect the primary production of phytoplankton and to identify the limiting factors of primary production in the Atlantic Ocean. To achieve this goal, four objectives were set as following:

1. Develop a simple tool for an identification of provinces in terms of the physical and nutritional conditions that the phytoplankton are exposed to. The difficulty in identifying the province where the sample has been collected can lead to a misinterpretation of the data. Easily identified characterististics that can support province determination will be sought to allow comparison with previous works carried out in the Atlantic Ocean.

2. Characterise how the phytoplankton are distributed along the provinces meridionally through the Atlantic Ocean. Taxonomic and physiological characteristics of the community structure will be assessed.

3. Identify the possible factors which limit primary production by affecting the phytoplankton physiology. This will be achieved by analysing the physiological parameters derived from fast repetition rate fluorometry (FRRF) measured at mid-day and also after an overnight recovery from light exposure.

4. Determine primary productivity in the natural environment using the physiological data from the fast repetition rate fluorometry. Advantages of the new method (FRRF method) will be exploited to investigate primary production. Limits of the new technique will be highlighted and some comparisons between the results from the FRRF method and from the traditional technique of $^{14}C$ uptake will be presented.

## 1.2 Structure of the thesis

This thesis is presented in eight chapters and an appendix to each chapter is attached as required. Figures and tables indexed by numbers are found in the main Chapters and those indexed by letters are presented in the Appendixes. Chapters 2 and 3 provide the scientific background required to understand the subject covered by this thesis. In Chapter 2, a brief review of phytoplankton, of photosynthesis in the ocean and of some limiting factors is presented. Then, the link between photosynthesis and fluorescence is described to introduce fast repetition rate fluorometry and the estimation of primary productivity using this method. A relevant background of the Atlantic Ocean, e.g. the upper circulation, water masses, provinces and primary production, is presented in the Chapter 3. In this same chapter, there is a description of the programme and the cruise that provided

the data for this thesis. Chapter 4 presents the determination of a method to identify provinces in an objective way and the characterisation of the provinces where sampling took place. The phytoplankton community structure characterisation is presented in the Chapter 5. With the knowledge acquired in previous chapters about environmental conditions and phytoplankton community structure, analysis of the physiological state of phytoplankton community structure is undertaken in Chapter 6. This leads to the identification of possible factors that affect phytoplankton physiology in the Atlantic Ocean. Primary productivity is assessed in Chapter 7, and the environmental factors affecting it are discussed. Fast repetition rate fluorometry is compared to the classical methods of measuring primary productivity, and the advantages and limitation of the novel method are identified. Subjects of each chapter (Chapters 4 to 7) are very different between each other and they analyse different data, so each of these chapters presents methodology for the data analysed and there is not a specific chapter for all the methodology. A list of acronyms and symbols is given in the beginning of the thesis.

# Chapter 2

# Review of phytoplankton photosynthesis and fluorescence

## 2.1 Introduction

Phytoplankton are microscopic plants with sizes ranging from 0.5 $\mu$m to 200 $\mu$m and they can be unicells, endosymbionts, filament or colony formers, found in fresh water or marine environments (Jeffrey *et al.* 1997).

They are phototrophs because they use sunlight as a source of energy, and their ability to fix $CO_2$ for carbon supply makes them autotrophs and important contributors to the biogeochemical cycle. Because of their need for light, they live in the upper layer of the water column known as the '*euphotic zone*', which extends downwards to where the light level at just below the surface is reduced to 1 % (Kirk 1994).

The sunlight is harvested by the means of pigments and the solar radiant energy is used to split water ($H_2O$) molecule to get the electrons necessary, transferring the energy through a chain of electron carriers until that energy is incorporated as chemical bonds, converting $CO_2$ into carbohydrate.

The pigments and electron carriers are contained in a specialised type of membrane called *thylakoid*. Higher plants and eukaryotic algae have the cellular functions compartmented within separate organelles, and the photosynthesis is carried out within organelles known as *chloroplasts* which contain the thylakoid and also the enzymes for $CO_2$ fixation. Phytoplankton with thylakoids lying free in the cytoplasm are named prokaryotes. The knowledge of prokaryotes increased recently when oceanographers started to use the epifluorescence microscopy and flow cytometry more often (Partensky *et al.* 1999). Prokaryotes are the smallest phytoplankton, hence more difficult to be detected and special methods are required for their sampling. Although prokaryotes are abundant in most part of the oceans, their genera are almost exclusively limited to *Trichodesmium*, *Synechococcus* and *Prochlorococcus*. Eukaryotes in the other hand, are bigger cells. The main marine eukaryotic phytoplankton are diatoms (Bacillariophyta[1]), dinoflagellates (Dinophyta), green algae (Chlorophyta), silicoflagellates (Chrysophyceae), golden-brown flagellates (Prymnesiophyceae) and cryptomonads (Cryptophyceae) (Jeffrey *et al.* 1997). Diatoms have big range of size (2 to 200 $\mu$m), and they require high nutrient conditions (Margalef 1978), especially silica for their exoskeleton (frustule). Dinoflagellates are motile due to their paired flagella, and they are capable of locomotion in their search of nutrients or light in conditions of low mixing. Prymnesiophyceae are found in most parts of the ocean, and some release dimethyl sulfide (DMS), the main source of cloud condensation nuclei in the ocean atmosphere, altering the cloud albedo and affecting the global climate (Charlson *et al.* 1987, Bates *et al.* 1987, Legrand *et al.* 1991). Other prymnesiophytes (e.g. coccolithophores) can form blooms, being important in the biogeochemical cycle (Holligan *et al.* 1993). Chlorophytes (green algae) are largely distributed from fresh water to ocean, hence their importance (Jeffrey *et al.* 1997). Cryptomonads are common in marine,

[1]The word ending in *phyta* means Division and the *phyceae* means Class

estuarine and freshwater environments but are very fragile and require non-destructive fixation methods for sampling, making pigment measurements very important (Jeffrey *et al.* 1997)

Phytoplankton have a ubiquitous pigment, chlorophyll *a* (Chl*a*), and normally, although erroneously, the Chl*a* concentration is used as a measure of phytoplankton biomass (Cullen 1982). One advantage is that it can be remotely sensed optically (Clarke *et al.* 1970, Aiken *et al.* 1995, O'Reilly *et al.* 1998), providing global images of phytoplankton distribution and patterns of ocean circulation (Gordon *et al.* 1980).

Because Chl*a* is the main pigment for photosynthesis, global mapping of its distribution can be used for determination of primary production over large spatial scales (Longhurst *et al.* 1995, Antoine *et al.* 1996), providing a important means for understanding the global biogeochemical cycle of $CO_2$.

## 2.2 Photosynthesis

It is important to make a distinction between definitions regarding to primary production studies. The main process of inorganic carbon ($CO_2$) fixation in the oceans is the *photosynthesis* in which solar radiant energy is converted into chemical energy incorporated in the organic compound ($CH_2O$). The product of photosynthesis, e.g. the amount of plant biomass, is defined as *primary production* and the rate of change in that amount is the *primary productivity* (Falkowski and Raven, 1997), hence the importance of understanding photosynthesis in primary production studies.

Extensive reviews of photosynthesis are available in the literature (e.g. Lehninger 1970, Kirk 1994, Jeffrey *et al.* 1997, Falkowski and Raven 1997, Nelson and Cox 2000) and an

overview is presented here based on these.

Photosynthesis can be represented as in the Equation 2.1:

$$\mathrm{nCO_2 + nH_2O \xrightarrow{light} nO_2 + (CH_2O)_n} \tag{2.1}$$

where light is absorbed by Chl*a*. Light absorption is the first step for the photosynthetic process. Plant pigments absorb the light with the release of $O_2$, transferring the electron excited by the photon through a series of electron carriers until that energy is used for $CO_2$ fixation. The first stage of the photosynthesis is when light is absorbed and its energy is stored in other forms (NADPH and ATP) with the split of $H_2O$ and release of $O_2$. These reactions are dependent on the light, so they are commonly known as the *light-dependent reactions*. The subsequent stages (although dependent on the products of light-dependent reactions, NADPH and ATP) assimilate $CO_2$ and produce organic carbon. As they do not need light they are commonly known as dark reactions or *carbon-assimilation reactions*.

In higher plants and eukaryotic phytoplankton, the light-dependent reactions take place in the thylakoid membrane system while the carbon-assimilation reactions occur in the stroma of the chloroplast.

### 2.2.1 Light-dependent reactions

The light energy is absorbed by the antenna and then transferred to reaction centres where the energy is used in electrical charge separation. These processes are fundamentally similar in all photosynthetic organisms. The absorbed energy is used to extract electrons from $H_2O$, and those electrons are transferred to hydrogen carriers, $NADP^+$, reducing it to NADPH, releasing $O_2$, incorporating inorganic phosphorus, $P_i$, into adenosine diphosphate, ADP, and generating the adenosine triphosphate, ATP. The NADPH and ATP

are used for inorganic carbon fixation in the dark reaction. All the light reactions can be summarised as photosynthetic electron transfer (PET) (Equation 2.2):

$$2H_2O + 2NADP + 3ADP + 3P_i \xrightarrow{\text{light}} O_2 + 2NADPH + 2H^+ + 3ATP \qquad (2.2)$$

Figure 2.1 shows a schematic representation of PET. Two photochemical reactions occur in the light phase of photosynthesis: the *light reaction 1*, the functional component of which comprises *Photosystem I* (PSI) and is associated with the reduction of NADP; and the *light reaction 2*, the functional component of which comprises the *Photosystem II* (PSII) and involves the liberation of oxygen. The two photosystems are served by the pigments or antenna for light harvesting process.

Photosynthesis starts (Figure 2.1) when the $P_{680}$, the chlorophyll molecule in the PSII, absorbs light energy and becomes excited ($P^*_{680}$). To transfer this excitation energy, it expels an electron, becoming $P^+_{680}$, which is a strong oxidant. That electron reduces the phaeophytin molecule (Phaeo), and is transferred rapidly to reduce a bound form of plastoquinone ($Q_A$) the electron of which is lost to reduce another specialised plastoquinone ($Q_B$). After receiving two electrons, $Q_B$ binds two protons, dissociates from PSII and diffuses throughout the thylakoid membrane until it reaches the cytochrome b6/f, taking with it the two electrons. These two electrons reduce the cytochrome b6/f molecules oxidised by PSI. Meanwhile, the $P^+_{680}$ oxidises a donor Z (tyrosyl residue), taking an electron from it, reforming itself to $P_{680}$. The oxidised form of Z in association with the Mn-containing water-splitting complex removes electrons from $H_2O$, releasing $O_2$. In the PSI, when light energy excites the $P_{700}$, this chlorophyll molecule acquires energy and loses an electron, becoming the oxidised form, $P^+_{700}$. The electron is passed rapidly through a series of electron carriers $A_0$, a chlorophyll monomer, $A_1$, phylloquinone, $FeS_x$, iron-containing proteins ($FeS_A$ and/or $FeS_B$) and then to ferrodoxin (Fd). Via the flavo-

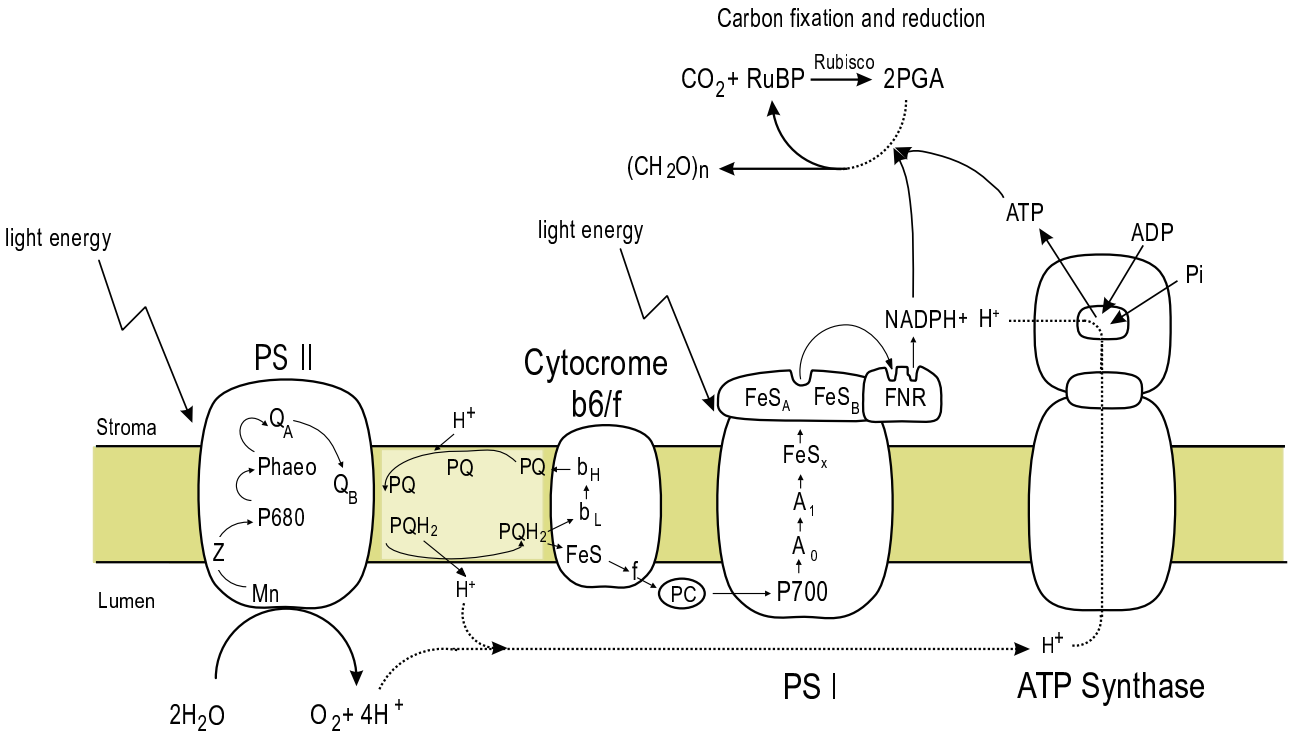


Figure 2.1: The light reactions of photosynthesis. The chlorophyll molecule in the PSII absorbs light energy and becomes excited ($P^*_{680}$). The excited form ($P^*_{680}$) expels an electron, becoming a strong oxidant ($P^+_{680}$). By oxidising the donor Z $P^+_{680}$ reforms itself back to $P_{680}$. The oxidised form of Z in association with the Mn-containing water-splitting complex removes electrons from $H_2O$, releasing $O_2$. The electron expelled by $P^*_{680}$ reduces the Phaeo, and is transferred successively to $Q_A$ and then to $Q_B$. After receiving two electrons, $Q_B$ dissociates from the PSII and diffuses thoroughout the thylakoid membrane to reach cytochrome b6/f. In the PSI, $P_{700}$ absorbs light and loses an electron, becoming oxidised, $P^+_{700}$. The electron is passed through the electron carriers ($A_0$, $A_1$, $FeS_A$, $FeS_B$ and Fd) and then transferred to NADP to form NADPH. The cytochrome b6/f reduces the plastocyanin PC which transfers the electron to restor $P^+_{700}$ into $P_{700}$. Besides PET chain, the thylakoid membranes contain the ATP synthase that draws the $H^+$ released from water split to synthesise ATP (From Falkowski and Raven 1997, Geider *et al.* 2002).

protein ferrodoxin-NADP reductase (FNR), electrons are transferred to NADP to form NADPH. The $P_{700}^{+}$ is restored to its original state by an electron from the plastocyanin (PC), which was reduced by the cytochrome b6/f.

Associated with this hydrogen transport, ATP synthase converts ADP and inorganic phosphate to ATP, and dissipates $H^+$ across the membrane (lumen to stroma), keeping the equilibrium of the ATP (Figure 2.1). When the ATP level is higher than its consuming rate by carbon fixation cycle, ATP synthase operates in reverse pumping $H^+$ back from stroma to lumen.

### 2.2.2 Carbon assimilation reactions

The energy stored in the products from the light-dependent reactions, ATP and NADPH, is used to fix $CO_2$ in the carbon assimilation reactions (Equation 2.3):

$$CO_2 + 2NADPH + 2H^+ + 3ATP \xrightarrow{\text{enzymes}} (CH_2O) + H_2O + 2NADP + 3ADP + P_i \quad (2.3)$$

This process is commonly known as Calvin-Benson Cycle. The energy stored in the ATP and the protons from the $NADPH_2$ (NADPH + $H^+$) are used to convert the $CO_2$ into organic substrate. In the Calvin-Benson Cycle, A five-carbon compound (ribulose bisphosphate, RuBP) combines with $CO_2$ to form an unstable six-carbon intermediate, that breaks down to form two molecules of the three-carbon compound glycerate 3-phosphate. This is converted to glyceraldehyde 3-phosphate, which is used to regenerate ribulose bisphosphate and to produce a glucose. The enzyme that mediates the carboxylation of RuBP is ribulose bisphosphate carboxylase/oxygenase (Rubisco). The series of carbon assimilation reactions is cyclic because the first substrate, e.g. RuBP, is regenerated at the end of the cycle and ready to fix other molecules of $CO_2$ (Falkowski and Raven 1997, Nelson and Cox 2000).

If all the products from light-dependent reactions are used in the carbon assimilation reactions, the primary production resulting is the gross amount. The most notable process that decreases primary production from the gross amount is respiration, which in order to release the energy of chemical bonds within the carbohydrates for use in metabolism, the cell consumes $O_2$ and releases $CO_2$. The reaction for respiration is the opposite of photosynthesis (Equation 2.1). Carbohydrates are oxidised and the products are $CO_2$ and $H_2O$. There are other processes that consume $O_2$, changing the ratio of $O_2$ evolved to $CO_2$ assimilated, like the Mehler Reaction (pseudocyclic electron transport) and also the photorespiration. The Mehler reaction consumes the $O_2$ from the PSII, binding it to the protons and electrons from PSI to generate ATP, re-forming $H_2O$ and leaving no net $O_2$ (Falkowski and Raven 1997). It has been linked to thermal dissipation of excess light energy absorbed (Demmig-Adams and Adams 1992). Photorespiration is a light-dependent consumption of $O_2$ and it happens because $O_2$ competes with $CO_2$ to bind to the Rubisco and $O_2$ is fixed instead of $CO_2$. It can be significant in high oxygen environments but because phytoplankton have a mechanism to concentrate $CO_2$, the ratio $O_2/CO_2$ is lower than in air. This mechanism suppresses the photorespiration in the phytoplankton (Falkowski and Raven 1997).

## 2.3 Environmental factors that affect photosynthesis

The main three environmental factors that affect phytoplankton are light, nutrients and temperature, and the time-scale of the changes in these is important for primary productivity (Marra 1995, MacIntyre *et al.* 2000). Although nutrients have a big influence in phytoplankton community structure (McCarthy 2002), their changes occur in time-scales of days to seasons and are less likely to drive short-term changes in photosynthesis (Mac-

Intyre *et al.* 2000). Temperature also changes in time-scales of days to seasons and is more predictable. Light is the factor that fluctuates most in both spectral quality and intensity, subsurface wave focusing effect, cloud cover and solar elevation (Kirk 1994). Due to its very broad time-scale (from miliseconds and minutes to seasonal), light is the factor that most affects photosynthetic rate (MacIntyre *et al.* 2000).

### 2.3.1 Light

As light is the energy source for photosynthesis, it is an essential prerequisite for phytoplankton growth. The sun is the source for energy necessary for photosynthesis in natural environment. The sunlight spectrum at the top of the atmosphere is practically constant with changes in the intensity due to change in the distance between Earth and Sun as the result of eccentricity of the Earth's orbit around the Sun (Kirk 1994). Spectral changes occur as light travels through the atmosphere, being attenuated by the variety of gases and aerosols that constitute the atmosphere (Gregg and Carder 1990). Cloud cover and types change not only the intensity and direction (Bishop and Rossow 1991) but also the spectrum of the light (Bartlett *et al.* 1998). The light remaining after atmospheric attenuation, penetrates the water column dependent on the surface roughness and waves (Gregg and Carder 1990). In the water column, the spectral attenuation is stronger mainly due to the water molecule itself, with strong absorption in the red part of the spectrum (Pope and Fry 1997). The attenuation by water is added to by that from other substances, e.g. dissolved organic matter, suspended inorganic matter, phytoplankton (Prieur and Sathyendranath 1981, Kirk 1994). The upper layer of the ocean illuminated by sunlight is the euphotic zone the depth of which is dependent on the attenuation properties and concentration of substances present in the water. The euphotic zone is usually shallower than 200 m. The *photosynthetically available radiation* (PAR), between 400 and 700 nm

of wavelength (Mobley 1994), corresponds to about half of the total solar spectrum energy and is the fraction used by plants for photosynthesis.

The phytoplankton are able to absorb light using a variety of pigments, the function of which can be photosynthetic or photoprotectant (Rowan 1989, Jeffrey *et al.* 1997). The monovinyl form of Chl*a* MVChl*a* (with absorption peaks at 440 and 662 nm) is present in all the algae apart from the prochlorophytes, which have the divinyl form DVChl*a* (with absorption peak at 436 and 661 nm) instead. Different classes and division of phytoplankton have different compositions of pigments (Rowan 1989, Jeffrey *et al.* 1997) and some species even have exclusive pigments (Garrido *et al.* 2000, Zapata *et al.* 2000). Apart from Chl*a*, phytoplankton have other chlorophyll derivatives and carotenoids to cover the light spectrum where Chl*a* has less absorption ability. Chlorophytes and chromophytes have respectively Chl*b* (peak absorption at 456 and 645 nm) and Chl*c* (Rowan 1989). Chl*c* is found in a variety of derivatives and the main peak of absorption varies between 446 and 454 nm (Jeffrey *et al.* 1997). Cyanobacteria do not have either Chl*b* or Chl*c* but have phycobiliproteins for photosynthetic light absorption (Rowan 1989). Phycobiliproteins are proteinaceous pigments with four major types (phycocyanin, phycoerythrin, allophycocyanin and phycoerythrocyanin) found in cyanobacteria, red algae and cryptomonads (Rowan 1989). Prochlorophytes also have Chl*b* (e.g. the divinyl form DVChl*b* instead of MVChl*b*) and although they are prokaryotes, they lack phycobiliproteins (Rowan 1989, Jeffrey *et al.* 1997 but see also Hess *et al.* 1996, Lokstein *et al.* 1999). Other accessory pigments are the carotenoids that cover wavelengths between 400 and 550 (Jeffrey *et al.* 1997).

Although light is essential for photosynthesis, excess light may cause damage to the photosynthetic apparatus (Demmig-Adams and Adams 1992). Plants in general have a spec-

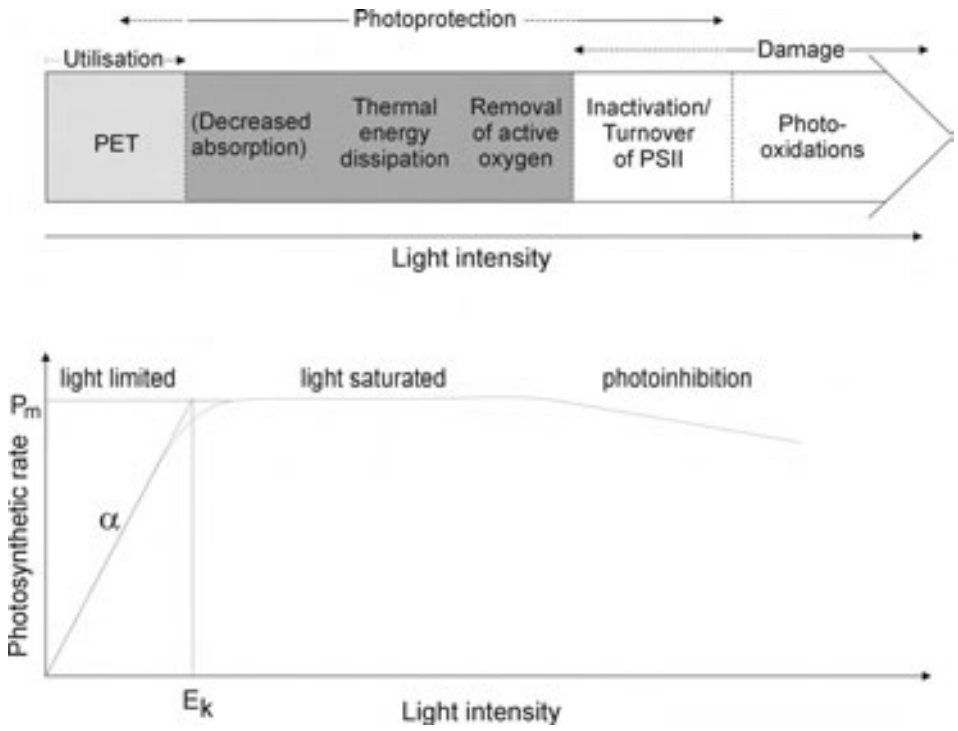


Figure 2.2: Top plot is a schematic representation of the effect of increasing light on photosynthetic apparatus and of various forms of photoprotective response and potential damage (from Demming-Adams and Adams 1992). Thermal energy dissipation happens through non-photochemical quenching (NPQ). Bottom plot is the P-E curve, showing the photosynthesis response to the light increase. The curve is divided in three parts the light limited, light saturated and photoinhibited parts. In the first portion, photosynthesis is light limited and usually occurs at low light conditions and photosynthesis is linearly related to irradiance with photosynthetic electron transport as the main process (PET). At light saturated region, photosynthesis is at maximum rate and the increase in light does not increase photosynthetic rate. When photoinhibition takes place, increase in light decreases photosynthetic rate. $P_m$ is the maximum photosynthetic rate and $E_k$ is the minimum light level that saturates photosynthesis (Jassby and Platt 1976).

trum of responses to increasing light intensity. Over a range of light intensity, an increase in the absorption of light will result in an increase in fixation of $CO_2$. This corresponds to the light limited part of the photosynthesis versus irradiance (P-E) curve (Jassby and Platt 1976) (Figure 2.2). At saturating light levels, a variety of mechanisms acts as photoprotection, to release the excessive light absorbed, with no increase in photosynthetic rate with increasing light. Photoinhibition has been treated as any damage in the PSII, but here the definition given by Long *et al.* (1994) will be adopted: *photoinhibition is the light impairment of PSII only if a decrease in the overall photosynthetic rate results.*

Since an early review proposing that photoinhibition is the consequence of a damage in the photosynthetic reaction center (Kok 1956), the decreases in maximum quantum yield for $CO_2$ (end part of the P-E curve) and $O_2$ evolution have been correlated to decreases in the variable fluorescence of PSII *in vivo*, and consequent decreases in the photochemical conversion efficiency of PSII (Long *et al.* 1994). In a prolonged exposure to excessive light, a decreased rate of light saturated photosynthesis follows decreases in maximum quantum yield for $CO_2$ and $O_2$ evolution. Photoinhibition results from energy absorbed by the pigments and channelled to PSII. In response to the light absorption in excess, the photosynthetic apparatus reacts by decreasing the absorption, thermally dissipating the excess light by non-photochemical quenching (NPQ). When light intensity is very high and the photoprotective strategies cannot cope, damage takes place with cycle of damage-repair of PSII (Figure 2.3), and decrease in photosynthetic rate with increasing light. Functional PSII may be reversibly or irreversibly inactivated due to the excess light. The first site of PSII to be affected when photoinhibition takes place involving damage is the polypeptide D1 located in the PSII reaction centre (Long *et al.* 1994). D1 has a role in donor and acceptor side of electron in the PET through PSII, with the binding sites for the phaeophytin and the $Q_B$.

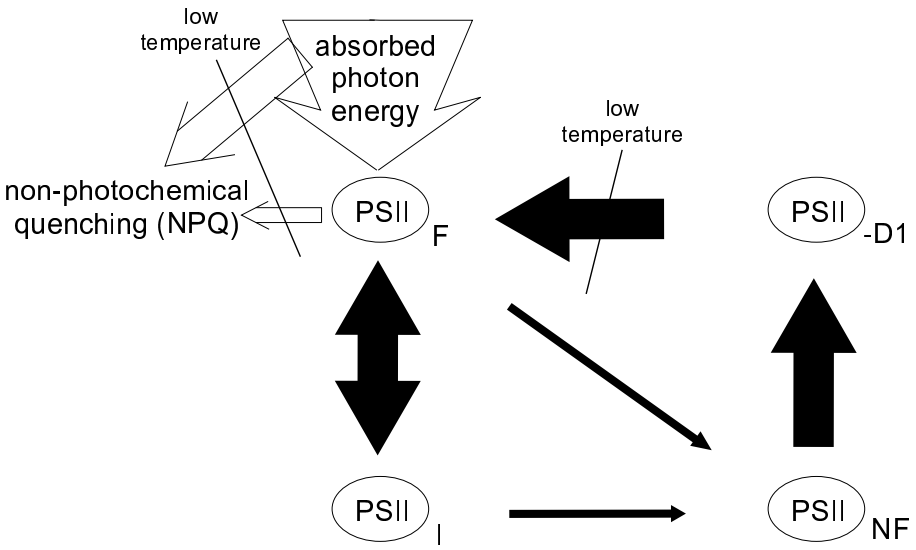


Figure 2.3: Simplified cycle of PSII damage and repair. Excess absorbed light is thermally released (NPQ) from either the antenna or the reaction centre. If over-excitation cannot be decreased harmlessly, functional PSII (F) may be reversibly inactivated (I), irreversibly inactivated or made non-functional (NF). $PSII_{NF}$ with a damaged D1 may result from $PSII_I$ or directly from $PSII_F$. $PSII_{NF}$ may be repaired by removal of damaged D1 ($PSII_{-D1}$) and insertion of a newly synthesised D1 and PSII can become functional again ($PSII_F$). Low temperature can inhibit the synthesis of D1 and also the xanthophyll cycle for NPQ (From Long *et al.* 1994).

The absorption of excess light is minimised by vertical mixing of water, or in calm conditions by vertical movement of phytoplankton by altering buoyancy of the cell or vertical migration in motile species. Phytoplankton can also reduce about 20 % of absorption by moving chloroplasts from the periphery to the inner part of the cell and/or changing orientation of chloroplasts (Long *et al.* 1994).

When excess light reaches the photosynthetic apparatus, NPQ acts to dissipate the excess excitation energy as heat (Figures 2.3). The extent of NPQ depends on the time-scale of persistence of light saturation photosynthesis (Müller *et al.* 2001). The quickest NPQ is referred as $q_E$ and acts on time-scales of less than seconds, triggered by trans-thylakoid gradient in pH, created by absorption of light energy exceeding the $CO_2$ fixation capacity (Krause and Weis 1991, Niyogi *et al.* 1997). Low pH in the lumen side of the thylakoid activates the xanthophyll synthesis via the xanthophyll cycle. Xanthophylls have a function not only in $q_E$ but also in the protection of the thylakoid membrane against photooxidative damage and an additional photoprotective role in longer-term high light. After exposure to bright light chlorophyll fluorescence yields in the dark are relatively low for an extended period, sometimes for many minutes. This lowered fluorescence yield cannot be attributed to quenching by the photochemical reduction of $Q_A$, so it must be as a consequence of NPQ. Normally, photosynthetic carotenoids transfer excitation energy to the chlorophylls. There are, however, some xanthophylls in de-epoxideted form, zeaxanthin and diatoxanthin, that tend to facilitate the loss of excitation via radiationless decay (Falkowski and Raven 1997). At high light levels most of the xanthophyll is in the de-epoxidated form, while in darkness this de-epoxidated form is converted back to its epoxidated form (Falkowski and Raven 1997). Two main types of xanthophyll cycle are observed, the violaxanthin cycle and the diadinoxanthin cycle. The former is the conversion of violaxanthin (with two epoxide group) to zeaxanthin (without epoxide

group), via antheraxanthin (one epoxide group). This has been seen in plants, green algae (Chlorophyta) and brown algae (Phaeophyceae). The latter has been documented in diatoms and most other eukaryotic algae, and consists of removing the only one epoxide group of diadinoxanthin converting it to its de-epoxidated form diatoxanthin, with no epoxide group. No xanthophyll cycle or analogue has been discovered in cyanophytes or in prochlorophytes (Falkowski and Raven 1997).

Another form of NPQ is the state transition quenching of fluorescence ($q_T$; see Müller *et al.* 2001) and occurs in time-scales of 1 to 10 min (MacIntyre *et al.* 2000). It is a migration of part of the light-harvesting complex of PSI or PSII and subsequent attachment to the other photosystem, depending on the light excitation spectrum (Falkowski and Raven 1997).

The first step of photooxidative damage seems to start in the formation of active oxygen, so their removal helps to prevent PSII damage (Demmig-Adams and Adams 1992). The Mehler reaction are reported to remove the singlet oxygen ($^1O_2^*$) resulting in the formation of triplet state Chl*a* ($^3Chl^*$, see Figure 2.4). Cyanobacteria were reported to have high activity of the Mehler reaction at saturation light levels (Kana 1992).

The damage-repair cycle of PSII is more focused on the D1 protein. It contains the electron acceptor and donor side in the PSII, hence its importance in photosynthesis. $^1O_2^*$ is linked to formation of $PSII_I$ and subsequent $PSII_{NF}$. The light prehistory determines the capacity of a plant for D1 synthesis, so those acclimated to high light levels are more able to synthesise D1 (Demmig-Adams and Adams 1992, Long *et al.* 1994), depending on the nutrient availability (Arsalane *et al.* 1994).

### 2.3.2 Nutrients

The mean chemical composition of phytoplankton is considered mostly constant for the major elements C, N and P, and was defined by the Redfield ratio as C:N:P = 106:16:1, being remarkably close to that of seawater (Redfield *et al.* 1963). This ratio can change considerably at small scales, both due to species- and group-specific differences in response to small time/spatial-scale changes in environmental conditions, but the average over larger time/spatial-scale is quite constant (Riebesell and Wolf-Gladrow 2002). However, the same authors point out that if environmental conditions change over large-scales and/or if there is a long-term shift in the phytoplankton community composition, such changes can modulate this ratio.

The products of photosynthesis are substrates for other reactions to form essential cellular components like amino and nucleic acids, lipids, enzymes, photosynthetic pigments, electron carriers, among others. These compounds require not only carbon, hydrogen and oxygen, but also macro-nutrients (N, S, P, K, Na, Ca, Mg and Cl) and micro-nutrients (Fe, Mn, Cu, Zn, Co and Mo). These elements can be limiting to the phytoplankton in terms of biomass production (N, P, also Si for diatoms) and/or the rate of primary production (N, P, Si, C and micro-nutrients).

Part of the organic matter from phytoplankton, their consumers and also fecal material can sink and be lost to the deep sea. The other part is remineralised by the microbial-loop (Cullen *et al.* 2002) in near surface waters, recycling the nutrients and thus sustaining primary production. This production dependent on the regenerated nutrient, for which ammonia is the main source of nitrogen, is known as regenerated production (Mann and Lazier 1996). The slow turnover rate of the deep sea makes it the reservoir of nutrients essential to primary production (McCarthy 2002). The density of seawater causes a

physical barrier forming a strong gradient of nutrient at the bottom of the surface mixed layer. Deep sea nutrients are brought back to the surface layer by upwelling events. The wind-driven surface circulation causes upwelling and downwelling, moving the nutricline closer to, and further from the sea surface in the Equatorial upwelling and subtropical gyres, respectively (Gargett and Marra 2002). When the nutricline gets shallow enough to be within the euphotic zone, phytoplankton can utilise the new nutrients from the deep sea reservoir for new production (Mann and Lazier 1996). Another source of new nutrients to the photic layer is atmospheric deposition. Although the regenerate process in surface layers accounts for more than 80 % of the global average nitrogen supply to phytoplankton, the processes that regulate the input of new nutrients have the largest influence on the success of different groups of phytoplankton (McCarthy 2002) and production export to higher trophic layer (Cullen *et al.* 2002).

The inorganic nutrients occur as more than one chemical species in seawater and not all of them are readily available for phytoplankton assimilation (McCarthy 2002). Selective uptake of the chemical species causes disequilibrium in the ratio between the chemical species and provokes conversion of non-utilised form(s) into that removed by algae. This applies for carbon ($CO_2$, $HCO_3^-$ and $CO_3^{-2}$), silicon ($H_4SiO_4$, $H_3SiO_4^-$ and $H_2SiO_4^{-2}$), phosphorus ($HPO_4^{-2}$, $PO_4^{-3}$ and $HPO_4^-$) and ammonia ($NH_4^+$ and $NH_4$). Other species of nitrogen ($NO_3^-$, $NH_4^+$ and $N_2$) can be converted into each other but at the expense of complex biochemical reactions. Phytoplankton can assimilate only fixed forms of nitrogen despite the fact that the most abundant form is $N_2$. Some cyanobacteria are the only phytoplankton capable of fixing $N_2$ but then the supply of phosphorus, iron or molybdenum can become limiting (McCarthy 2002).

Among the macro-nutrients, nitrogen is the most likely to limit primary production within

the surface mixed layer (Falkowski 2000). However, even in nitrate abundant waters, phytoplankton photosynthesis may be limited by iron (Falkowski 1997). Iron has been confirmed to decrease in Fv/Fm value at night in comparison to day values in the Pacific Ocean (Behrenfeld *et al.* 1996, Behrenfeld and Kolber 1999) and the Southern Ocean (Coale *et al.* 1996).

Phytoplankton taxa are characteristically linked to dynamics of the environment and nutrient availability as summarised by Margalef (1978) and recently revisited by Cullen *et al.* (2002). Different phytoplankton taxa have strategies that apply better to one environment than to others. Some phytoplankton are more adapted in terms of structure and physiology for rapid uptake of nutrients in well mixed high nutrient waters, e.g. diatoms which depend on the water mixing processes to keep them in suspension in the water column. Dinoflagellates, on the other hand, are motile, making them more adapted to low turbulent environments (Margalef 1978). The smaller the cell size, the greater ability of the phytoplankton to assimilate nutrients, so smaller cells can tolerate low nutrient environments better (Riebesell and Wolf-Gladrow 2002).

### 2.3.3 Carbon

Since $CO_2$ is the substrate for carbohydrate production in the photosynthesis, the uptake ability of the organisms affect the photosynthetic rate. The most abundant chemical species of carbon is $HCO_3^-$ and just a small fraction is $CO_2$, which is the form that diffuses passively through the cell membrane. Phytoplankton have enzymes, very catalytically active (carbonic anhydrase) that can work in the plasmalemma and as extra-cellular soluble. The intra-cellular function of these enzymes is to supply $CO_2$ to a $CO_2$-specific enzyme, decreasing the $CO_2$ within the cell and facilitate the diffusive transport of $CO_2$

into the cell whilst its extra-cellular function is to facilitate the diffusion of inorganic carbon into the cell. This mechanism avoids $CO_2$ limitation in photosynthesis in marine environments (Falkowski and Raven 1997).

### 2.3.4 Temperature

The effect of temperature on primary production rate lies in the catalytic reaction of enzymes. At low temperatures, the rate for carbon fixation is low but an increase in temperature does not yield similar increases in carbon fixation rate due mostly to nutrient depletion in high temperature zones (Falkowski and Raven 1997). Low temperature causes reduced specific activity but this can be compensated by an increase in Rubisco abundance (Geider and MacIntyre 2002). Low temperatures can also inhibit synthesis of D1 and the xanthophyll cycles and consequently the NPQ (Long *et al.* 1994). This increases the rate of damage of PSII and decreases the rate for repair. However, if the organism is acclimated to low temperatures, the observed photoinhibition is caused by inhibition of electron transport and not by loss of D1 (Long *et al.* 1994).

## 2.4 Fluorescence and photosynthesis

In the photosynthesis apparatus, light is absorbed by the antenna pigments resulting in the singlet-state excitation of a Chl*a* molecule ($^1$Chl$^*$). In order to return to the ground state the Chl*a* molecule needs to release the excitation energy (Figure 2.4), one of which is harmful (Butler 1978, Krause and Weis 1991, Müller *et al.* 2001). To avoid damage to PSII the absorbed energy is used for emission of fluorescence, delivery to the reaction centre for photochemistry or dissipation as heat. Either photosynthesis or thermal dissipation can quench fluorescence, so when the quencher is the former, process

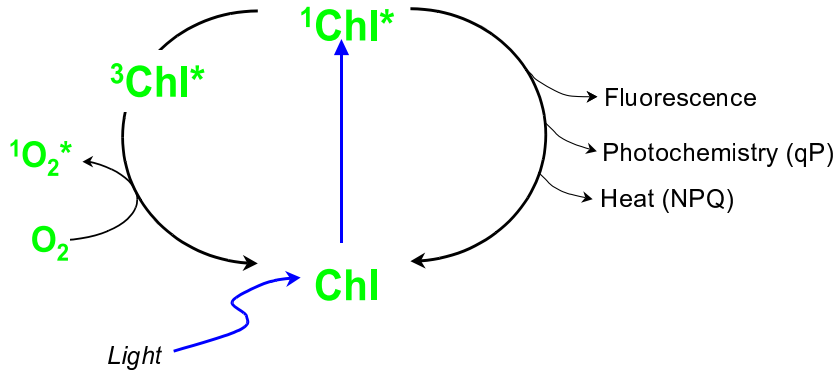


Figure 2.4: Pathways for absorbed light energy. When ground state Chl absorbs light energy it becomes excited to singlet state ($^1$Chl$^*$). $^1$Chl$^*$ can relax back to ground state through three harmless ways: emitting the absorbed energy as fluorescence; fuelling photosynthetic reactions ($q_P$); or via NPQ. It can also relax back forming the triplet state $^3$Chl$^*$, yielding singlet $O_2$ ($^1O_2^*$), a harmful species. From Müller *et al.* 2001.

termed photochemical quenching ($q_P$) and the latter non-photochemical quenching, e.g. NPQ. When these three pathways are saturated, $^1$Chl$^*$ returns to the ground state by transferring energy to ground-state $O_2$ and generating singlet oxygen ($^1O_2^*$), a chemical species extremely harmful to the photosystem (Demmig-Adams and Adams 1992). In low light and under optimal conditions, photochemical efficiency is very high, with more than 90% of absorbed light being utilised by photosynthesis. In spite of maximum fluorescence yield being only around 3% of the absorbed light, when all the reaction centres are ready for photochemistry, e.g. they are in open state, fluorescence yield is about 5 times lower. This big variation in the fluorescence yield is due to competition with photochemistry and thermal dissipation (See Figure 2.4).

The most important reactions are photochemical reaction ($k_p$) and the thermal deactivation ($k_h$) and both of them quench fluorescence emission ($k_f$). Some assumptions and several simplifications (Schreiber *et al.* 1995, Parkhill *et al.* 2001) allow the measurement of fluorescence parameters to be used as a proxy of maximum quantum yield of PSII

(Fv/Fm). The first assumption is that those competing reactions and the photochemistry are the only pathways for the total absorbed energy:

$$k_p + k_f + k_h = 1 \tag{2.4}$$

where k represents the portion of the absorbed energy to be delivered to one of the three processes: photochemistry (p), fluorescence emission (f) or thermal dissipation(h).

Second, when all the reaction centres are working for photochemistry, e.g. reaction centres are 'closed', just after saturating light pulses, or treatment with an inhibitor (e.g. DCMU[2]), the probability of photochemistry becomes zero with maximum fluorescence emission ($k_{f_m}$) and maximum heat dissipation ($k_{h_m}$):

$$k_{f_m} + k_{h_m} = 1 \tag{2.5}$$

Third and finally, the ratio between the quantum yield of fluorescence and the quantum yield of thermal deactivation is constant:

$$\frac{k_f}{k_h} = \frac{k_{f_m}}{k_{h_m}} \tag{2.6}$$

The rate of fluorescence emission, F, is a fraction of absorbed light, $E_a$, driven by the ratio between the rate constant of fluorescence, $k_f$, and the sum of rate constants, $\Sigma k_i$ of all competing reactions that return the excited, singlet chlorophyll molecule, $^1Chl^*$, back to the ground state, Chl. The fluorescence yield ($\Phi F$) can be written as following general equations:

[2]DCMU: dichlorophenyldimethyl urea, herbicide that inhibits electron transfer beyond $Q_A^-$.

$$F = \frac{E_a \times k_f}{\Sigma k_i} \tag{2.7}$$

$$\Phi F = \frac{F}{E_a} = \frac{k_f}{k_p + k_f + k_h} \tag{2.8}$$

When all reaction centres are in an active, *open* state, the fluorescence yield is minimal, $\Phi F_0$, because most of absorbed light is used for photochemistry, $k_p \gg k_f + k_h$. When $Q_A$ is fully reduced, it cannot receive the excitation energy coming from the $P_{680}$ to maintain the photochemistry ($k_p = 0$), e.g. the reaction centre is in *closed* state, and the fluorescence yield is maximum, $\Phi F_M$.

In the same way, the potential yield of the photochemical reaction of PSII, $\Phi P_0$, is given by:

$$\Phi P_0 = \frac{k_p}{k_p + k_f + k_h} = \frac{\Phi F_M - \Phi F_0}{\Phi F_M} = \frac{Fv}{Fm} \tag{2.9}$$

where Fv is the variable fluorescence given by the difference between the maximum (Fm) and minimum ($F_0$) fluorescence emission. Fv/Fm is quantitatively related to the photochemical efficiency of PSII (Butler 1972) and has become a common measurement since 1990s (Falkowski and Kolber 1990, Kolber and Falkowski 1993). Environmental stress affects PSII efficiency leading it to a characteristic decrease in Fv/Fm, that is also influenced by various NPQ mechanisms.

The application of fluorescence for photochemical studies also assume that fluorescence from PSI is negligible.

## 2.5 Fast Repetition Rate Fluorometry

The first observation of fluorescence was as early as 1646, but its description came more than 300 years later (Kautsky and Hirsch 1931), and even then the detection was by the naked eye (Govindjee 1995). It was more than 30 years after its first description that the measurement of *in vivo* fluorescence emission was achieved by Lorenzen (1966), giving a tool for indication of biomass (Kiefer and Reynolds 1992). By the mid 1970s, commercial instruments capable of measuring *in situ* fluorescence continuously became available to biological oceanographers (Falkowski and Kolber 1995, Holm-Hansen *et al.* 2000). This early technique, the so-called fluorescence induction, was based on the analysis of a transient fluorescence induced in a dark adapted sample by quick exposure to continuous light (Kolber 1997). The detection of the deep Chl*a* maximum (DCM) in the oligotrophic gyres was possible due to the continuous measurement of fluorescence in the water column, previously non-detected due to the discrete sampling (Cullen 1982). Fluorescence measurements also allowed assessment of photoinhibition in nature by application of an inhibitor to prevent re-oxidation of $Q_A^-$, e.g. DCMU (Neale 1987). However this is a sample-destructive method and cannot be applied in real time. Recent technological advances and progress in the understanding of *in vivo* fluorescence have provided more powerful tools to assess biomass and measure physiology of phytoplankton PSII in natural environments (Falkowski 1992). The first instrument built for the measurement of variable fluorescence was the pulse amplitude modulated (PAM) fluorometer applied by Schreiber *et al.* (1986) to distinguish between photochemical and non-photochemical quenching (Kolber 1997). This approach applies different wavebands and intensities of light, synchronised to obtain maximum and minimum fluorescences (van Kooten and Snel 1990). Another approach is pump and probe (P&P) fluorometry which uses a weak

probe flash before and after a pump flash, to saturate PSII and measure the fluorescence response for each probe flash to retrieve Fo and Fm, respectively. By controlling the intensity of pump flash and the time delay between the pump flash and probe flashes, more physiological information can be retrieved (Falkowski *et al.* 1986a, Falkowski and Kolber 1990, Falkowski *et al.* 1992, Kolber and Falkowski 1993).

However, both of the two methods have limitations. The PAM fluorometry provides variable fluorescence only and the P&P is too slow to follow the dynamic changes in PSII (Kolber 1997). The fast repetition rate (FRR) fluorometry has been developed to overcome these deficiencies (Kolber 1997). As the name suggests the instrument is based on high frequency emission of blue light flashes at subsaturating energy to gradually saturate PSII reaction centres, by oxidising gradually the electron acceptor $Q_A$ (Figure 2.5). The response fluorescence for the first excitation blue flash gives the minimum fluorescence (Fo) and, at the saturation point, the fluorescence is maximum (Fm). The rate required to saturate the PSII reaction centre is proportional to the effective absorption cross-section of PSII ($\sigma_{PSII}$). High values for $\sigma_{PSII}$ indicates high efficiency of the antenna to intercept photons and rapid saturation of PSII while low values for $\sigma_{PSII}$ indicates low efficiency and takes longer to saturate PSII (Falkowski and Raven 1997). After saturation, relaxation flashes, which have longer inter-flash delay, are emitted to re-open PSII reaction centre. The rate of relaxation is related to the turnover rate of photosystem II ($\tau_{QA}$). To obtain the variable fluorescence and the rate of saturation, the saturation protocol of FRR fluorometry is used. It applies a set of 50 to 100 flashes to reduce cumulatively $Q_A$, during which time the re-oxidation of $Q_A$ and subsequent reduction by a second photochemical turnover is negligible (Kolber 1997, Kolber *et al.* 1998).

For relaxation of the PSII reaction centre, another set of low energy flashes can be emitted

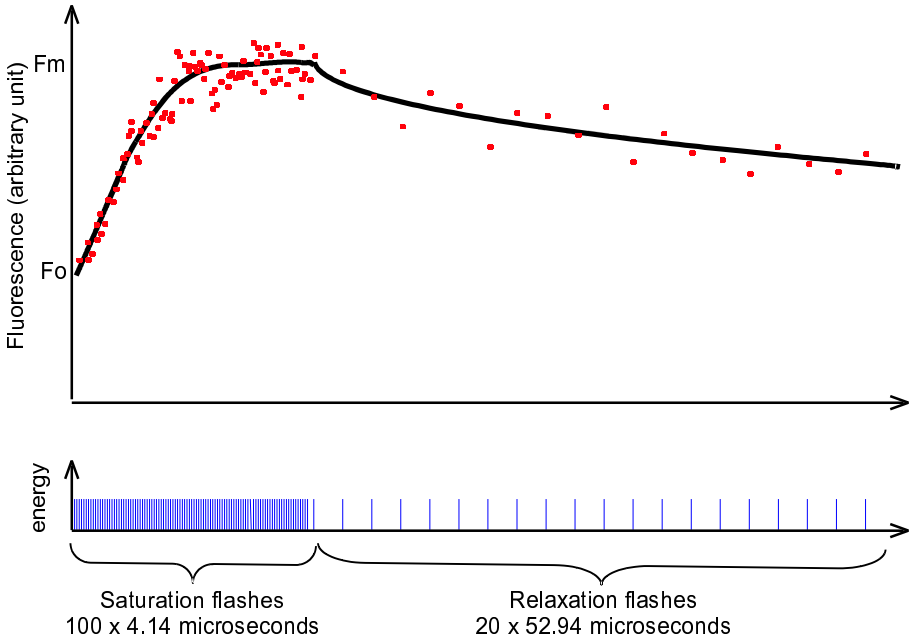


Figure 2.5: Fluorescence yields from FRR fluorometry and the estimation of physiological parameters. One hundred excitation blue flashes (bottom plot, blue vertical bars) at subsaturation intensity are emitted. For every excitation flash emitted by the FRRF, the respective phytoplankton fluorescence emission (red dots) is collected. Fluorescence yields increase gradually with successive excitation flashes until all the PSII reaction centre are closed and the fluorescence yield reaches the maximum value. The rate of saturation of PSII reaction centre is the effective absorption cross-section ($\sigma_{\mathrm{PSII}}$). After saturation, a sequence of longer-interflash-delay, relaxation flashes are emitted to allow re-opening of PSII reaction centre and decrease the fluorescence gradually. The rate for fluorescence decay is the $\tau_{\mathrm{QA}}$.

with a longer time-delay between the flashes to allow re-oxidation of $Q_A$. The rate for re-oxidation or decay in the fluorescence yields gives the turnover rate of $Q_A$ re-oxidation ($\tau_{QA}$), which means the rate electron transfer from $Q_A$ to the to the following electron carrier, $Q_B$. Literature for active, variable fluorescence measurements comes mostly from the PAM (Schreiber *et al.* 1986) and P&P (Kolber and Falkowski 1993) fluorometry, hence most of the nomenclature are specific for those methodologies and most of them do not apply to the fluorescence parameters obtained from FRR fluorometry. All nomenclature adopted here is specific for fluorescence values obtained with FRR fluorometry.

### 2.5.1 Technical information about FRR fluorometer

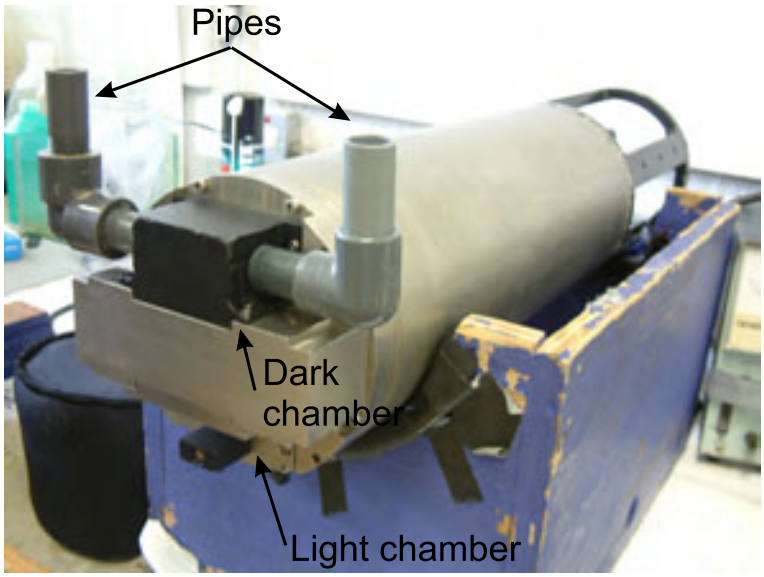


Figure 2.6: Fast repetition rate fluorometer in bench-top mode

The FRR fluorometer has light and dark chambers (Figure 2.7), the former is for sampling under environmental light and the latter for sampling without photochemical quenching caused by ambient light by holding the sample in darkness. The chambers can be activated either together or one at a time. The FRR fluorometer used for this thesis was a submersible instrument from Chelsea Technologies Group, the FAST$^{tracka}$ (Figures 2.6 and

2.7), designed initially by Kolber and Falkowski (1992), and later described by Kolber (1998). Although emission blue LED has been changed (*pers. comm.* Chelsea Technologies Group) the main characteristics are described by Kolber and Falkowski (1992), Kolber (1998) and Kolber *et al.* (1998). The excitation flashes are emitted and filtered to produce a peak at 470 nm (LED NICHIA NSPB300A). Fluorescence yields are collected perpendicular to the excitation flashes, collimated by a prism to the emission filters and photomultiplier. The collected light is filtered centred at 685 nm with a full width half maximum of 30 nm. Signals from both chambers are detected by the same photomultiplier. The photomultiplier has 5 different gains which are set manually or automatically adjusted to the fluorescence amount. The difference in excitation LED banks between the chambers are corrected internally, by measuring with the reference detector a fraction (2%) of the excitation flash at every emission (Kolber *et al.* 1998). For measurements in the laboratory, the instrument can be connected directly to a computer through RS242 to operate the data acquisition procedure via a software provided with the instrument by the Chelsea Technologies Group. In this case, the data are stored directly to the computer. The same software makes the connection between the instrument and the user, via a computer and is used to prepare the instrument and the operational protocols for data acquisition. The saturation and/or relaxation protocols can be set for fluorescence acquisition. The instrument is switched on before the deployment by swiping a magnet to connect a reed-switch on the optical head. The data are stored in an internal memory card as one set of values averaged from a pre-programmed number of flash sequences.

The data stored in the internal memory card are downloaded to a computer via RS242, using the Hyperterminal (Windows system). The physiological parameters can be retrieved using the data reducing software, FRS.exe (v1.8), provided by the Chelsea Technologies Group.

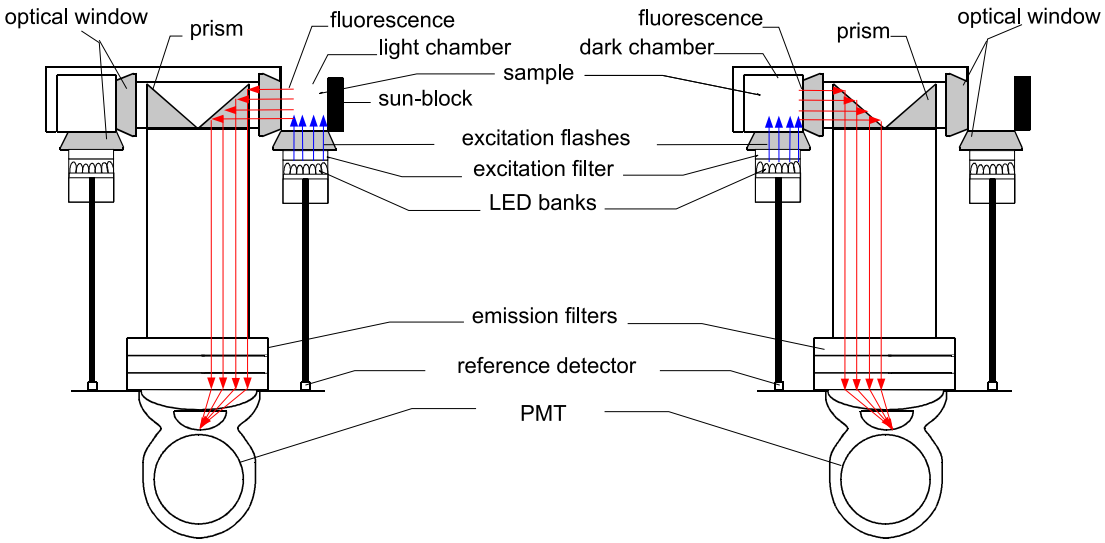


Figure 2.7: Schematic representation of optical head of FRR fluorometer and the pathways for light. The scheme on the left side shows sampling in the light chamber and that in the right side, the sampling in the dark chamber. Blue excitations flashes (blue arrows) are emitted from the blue LEDs sensitising the sample in the light or dark chamber. Then the excited Chl*a* emits the excess energy as fluorescence (red arrows). Fluorescence emitted perpendicular to the excitation flashes are collected and collimated to the photomultiplier. A small fraction of the excitation flashes are collected in the reference detector to correct for the amount of excitation energy in each chamber.

Other sensors to measure pressure and PAR are attached to the FAST$^{tracka}$ and the data acquired and stored for each flash sequence in the internal memory card.

## 2.6 Determination of primary production with FRR fluorometry

Since the introduction of the $^{14}$C method to estimate the rate of photosynthetic carbon fixation by marine phytoplankton in 1952 by Steeman Nielsen, it has been the main method applied in studies of marine primary production (Barber and Hilting 2002). The method is based on the counting of $^{14}$C incorporated in the phytoplankton (particle) after some time of incubation and the particles retained in the filter pad after filtration (Steeman Nielsen 1952). Another isotope method is the addition of water labelled with $^{18}$O for light dependent production of $^{18}$O$^{16}$O and it gives the standard estimate of gross primary production (Grande *et al.* 1989). The titration method to estimate $O_2$ evolution is difficult because the background concentration in seawater is much bigger than the change in $O_2$ (Falkowski and Raven 1997). All these methods are time consuming and with some methodological problems (Peterson 1980, Williams 1993)

Fluorescence applied to primary productivity studies can overcome the time consuming processes required for other methods. The variable fluorescence has been applied for primary production estimates since the early 1990s (Kolber and Falkowski 1993). The gross photosynthetic oxygen evolution can be obtained as described in Equation 2.10:

$$P^{B}_{O_2}(\mathrm{PAR}) = \sigma_{\mathrm{PSII}} \times \Phi_{\mathrm{RC}} \times q_{\mathrm{P}} \times \phi_{\mathrm{e}} \times f \times n_{\mathrm{PSII}} \times \mathrm{PAR} \qquad (2.10)$$

where $P^{B}_{O_2}(\mathrm{PAR})$ is the rate of gross photosynthetic oxygen evolution per unit of biomass, e.g. Chl*a*, in mol $O_2$ evolved (g Chl*a*)$^{-1}$ time$^{-1}$; $\sigma_{\mathrm{PSII}}$ is the effective absorption cross-

section of PSII; $\Phi_{RC}$ is the number of electrons transferred from $P_{680}$ to $Q_A$ per quanta absorbed and delivered to PSII reaction centre (= 1 electron quanta$^{-1}$); $q_P$ is the photochemical quenching coefficient; $\phi_e$ is the quantum yield of electron transfer by PSII (mol $O_2$ mol photon$^{-1}$); $f$ is the proportion of functional to total PSII reaction centres; $n_{PSII}$ is the number of PSII reaction centres per Chl*a* and PAR is the photosynthetically available radiation.

From all the parameters required to estimate gross photosynthetic oxygen evolution, PAR and $\sigma_{PSII}$ are the only ones that can be measured directly with the FAST$^{tracka}$. Between other parameters from Equation 2.10, $q_P$ is the most problematic when determination of primary production is the objective. This parameter had been measured using PAM (van Kooten and Snel 1990) or P&P (Kolber and Falkowski 1993) methods, in which fluorescence acquisition protocols are different from FRR fluorometry and that difference makes the estimation of $q_P$ complicated if fluorescences are induced with the FRR method. Estimation of $q_P$ requires fluorescence measurements which PAM and P&P methods can retrieve but FRR method cannot. The problem can be overcome if the sample is kept in the dark for recovery from light exposure for 15 min (Frameling and Kromkamp 1998) to 30 min (Geider *et al.* 1993). After the dark recovery time the sample can be measured with FRR method in bench-top mode. However, such sampling can be applied for some discrete depths only. Other parameters can be assumed as constant.

If $q_P$ is accounted together with $f$, as the ratio $(Fv/Fm_L)/0.65$, $q_P$ can be avoided. The ratio $(Fv/Fm_L)/0.65$ accounts for photochemical quenching ($q_P$), NPQ and also $f$. It results from $(Fv/Fm_L)/(Fv/Fm_D) \times (Fv/Fm_D)/(Fv/Fm^{\infty}) \times f$. Measurements after dark adaptation (30 min in the dark) are indicated by $^{\infty}$. The first ratio, $(Fv/Fm_L)/(Fv/Fm_D)$, is the ratio of Fv/Fm collected by the light chamber to that collected by the dark chamber

and represents the $q_P$. The second ratio, $(Fv/Fm_D)/(Fv/Fm^\infty)$, was introduced because the dark chamber measures without recovery from NPQ and accounts for NPQ. Finally the ratio $(Fv/Fm_L)/0.65$ is obtained considering $f = Fv/Fm^\infty/0.65$ (Kolber and Falkowski 1993). Babin *et al.* (1996) argue that the fraction of functional PSII reaction centres ($f$) is given by $(Fv/Fo^\infty)/1.8$, which yields a value slightly different from $(Fv/Fm^\infty)/0.65$ (Ficek *et al.* 2000b). However, if the ratio $(Fv/Fo^\infty)/1.8$ is to be applied, it would require the measurement of $Fv/Fm^\infty$, e.g. the measurement after at least 30 min of recovery, making the estimation of primary production complicated. The value of 0.65 is the maximum value of Fv/Fm measured in phytoplankton grown in laboratory cultures and it is not 1 due to the inefficiencies in energy transfer within the reaction centre (Kolber and Falkowski 1993). Although bigger values have been observed (Babin *et al.* 1996) the value of 0.65 is remarkably constant (Kolber and Falkowski 1993).

Replacing $f$ and $q_P$ by the ratio $(Fv/Fm_L)/0.65$ and introducing the photosynthetic quotient (PQ) in Equation 2.10, the rate of carbon fixation can be obtained by Equation 2.11:

$$P_B(t,\, z) = \frac{Fv/Fm_L(t,\, z)}{0.65} \times \sigma_{PSII}(t,\, z) \times PAR(t,\, z) \times \Phi_{RC} \times n_{PSII} \times \phi_e \times (PQ)^{-1} \quad (2.11)$$

where $P_B(t, z)$ is carbon fixation rate per unit of Chl*a*. Observe that some parameters are dependent on time (t) and depth (z). The D or L indexes indicates dark or light chambers respectively.

Equation 2.11 has the advantage of determining primary production from *in situ* measurements only. Other parameters can be assumed as constant, although some vary in natural environments.

**Number of reaction centres per Chl*a* ($n_{PSII}$):** From the three variables that cannot be measured with FRR fluorometry, $n_{PSII}$ is the parameter with the biggest range. It

varies depending on the species, light level and nutrient availability (Barlow and Alberte 1985, Dubinsky *et al.* 1986, Berges *et al.* 1996). The biggest difference is between the eukaryotes and prokaryotes and a value of 1/500 and 1/300 Chl*a* per PSII reaction centre, respectively, can be assumed under optimal growth (Falkowski and Kolber 1995).

**Photosynthetic quotient (PQ):** Although the process of photosynthesis is described as one mole of $CO_2$ being fixed for every mole of $O_2$ released (Equation 2.1), it does not have such a strict balance in natural environments. Plants are not made from carbohydrates only, they also synhtesis proteins, lipids and nucleic acid, so the ratio mol$O_2$ mol$CO_2^{-1}$ is higher than 1. In fact phytoplankton requires more protein than carbohydrate, hence it has a higher PQ than higher plants (Myers 1980). In phytoplankton PQ varies from 1.1 to 1.4 mol$O_2$ mol$CO_2^{-1}$ , for ammonia and nitrate as the source of nitrogen, respectively (Myers 1980, Laws 1991 but see Williams and Robertson 1991). The value of 1.3 mol$O_2$ mol$CO_2^{-1}$ will be adopted here. This will imply in some overestimation of primary productivity below the nitracline, where nitrate is replete, and underestimation above the nitracline, where nitrate is depleted.

**Quantum yield of electron transport for $O_2$ ($\phi_e$):** In the light limited part of the water column, most of the absorbed light is used for photochemistry and consequently carbon fixation. Four successive electron transfers are necessary to release one $O_2$ molecule, so $\phi_e$ is 0.25 $O_2$ photon$^{-1}$. In the photosaturated or photoinhibited photosynthesis, where all the absorbed energy cannot be used, due to the saturation of the processes in the electron transport chain after PSII, the release of one $O_2$ molecule requires more than 4 electron transfers. Although estimation of $\phi_e$ is possible, it requires knowledge of $q_P$ (Kolber and Falkowski 1993), so $\phi_e$ will be assumed to have a constant value of 0.25 $O_2$ photon$^{-1}$.

Fluorescence induction with FAST$^{tracka}$ and the following data reduction with FRS (v1.8), derives $\sigma_{\mathrm{PSII}}$ (in units of $10^{-20}$ m$^2$ photon$^{-1}$) and PAR (in $\mu$E m$^{-2}$ s$^{-1}$). The estimation of carbon fixation rate per Chl*a* is derived in mgC mgChl$^{-1}$ s$^{-1}$ if Equation 2.11 is used with parameters supplied here.

# Chapter 3

# Background for the study area

## 3.1 The Atlantic Ocean

The Atlantic Ocean is bounded to the west by the eastern shores of the American continent, to the east by the coasts of Europe and West Africa. To the south it is largely open to the Southern Ocean and to the north it is restricted by the Arctic Polar Basin (Figure 3.1). These limits form a long meridional basin with a curved meridional axis known as the Mid Atlantic Ridge (Tchernia 1980). There have been many reviews of the topography (Tchernia 1980), climatology and currents (Pickard and Emery 1990, Peterson and Stramma 1991, Tomczak and Godfrey 2001) in the Atlantic Ocean and they are the main source of information summarised in the following subsections.

### 3.1.1 Surface circulation

The general circulation in the Atlantic Ocean consists of two great anticyclonic circulations or *gyres*, a counter-clockwise one in the South Atlantic and a clockwise one in the North Atlantic, driven separately by the trade winds in each hemisphere (Pickard and Emery 1990). The main currents and the pattern of surface circulation is presented schematically

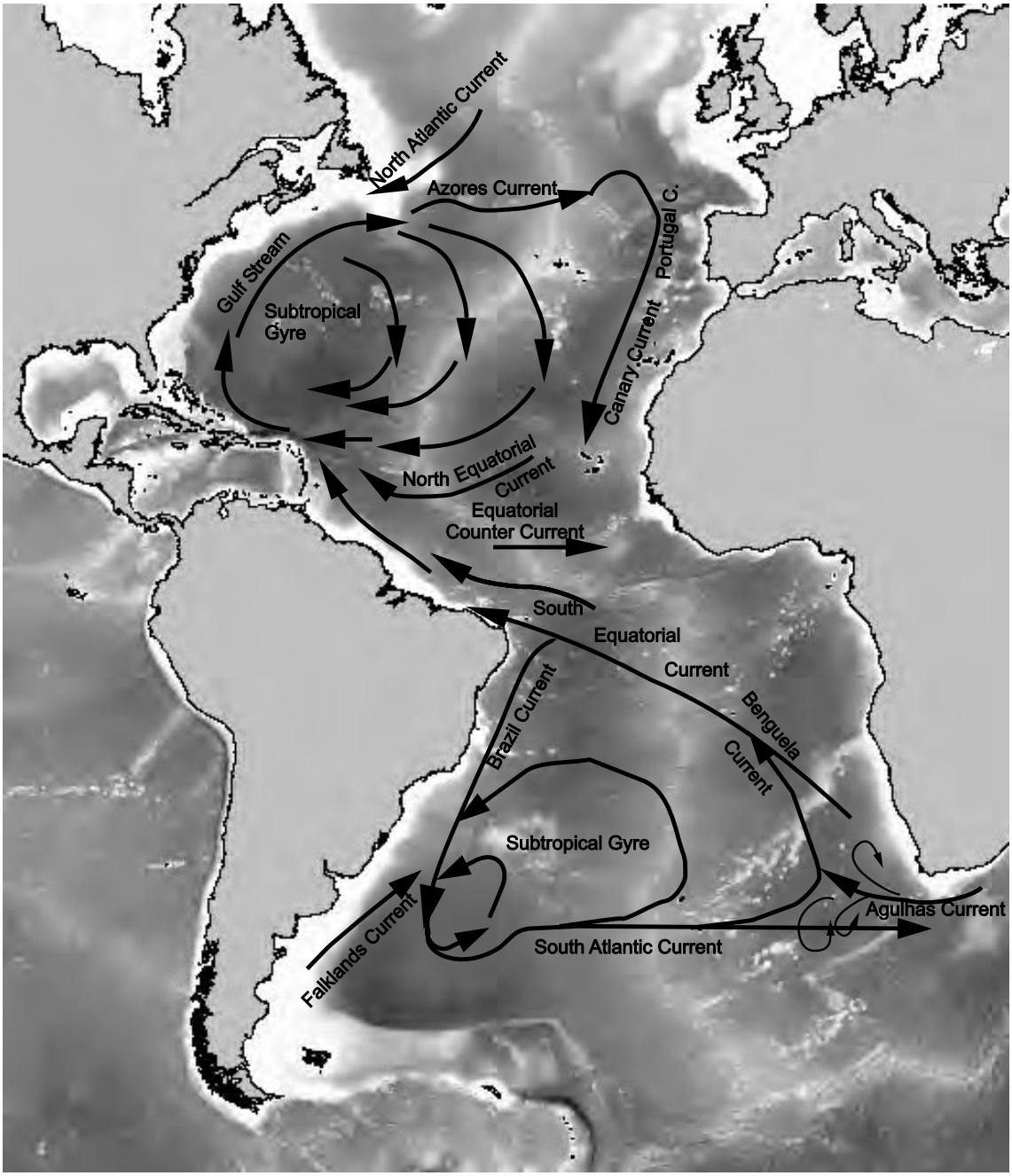


Figure 3.1: Schematic representation of major surface circulation patterns in the Atlantic Ocean adapted from Tomczak and Godfrey (2001). The background gray colour indicate local bathymetry where brighter colours are shallower regions.

in Figure 3.1.

The northern subtropical gyre consists of the North Equatorial Current as the southern limit, the Antillas Current and the Caribbean Current through the Caribbean Sea, the Gulf Stream System and its components at north-west extremes, the Azores Current, and the Portugal-Canary Current at the eastern border. The North Atlantic and the Azores Currents, which are continuations of the Gulf Stream, input warm water to the north eastern Atlantic Ocean. The Azores Current feeds the Portugal and Canary Currents and subsequently the North Equatorial Current. The Gulf Stream receives water from re-circulations of the Gulf Stream water in the Sargasso Sea, Antillas Current and the Florida Current which is fed by part of the North Equatorial Current with some possible contribution from the North Brazil Current. Another part of the water transported by the North Equatorial Current goes to the Antillas Current, closing the gyre circulation in the North Atlantic.

Between the North and South Equatorial Currents there is a weak equatorial countercurrent, which flows from west to east in the Doldrums (the Inter Tropical Convergence Zone - ITCZ).

The southern gyre is made up of the South Equatorial Current as the northern limit, the Brazil Current at the eastern border, the South Atlantic Current at the southern border and the Benguela Current at the eastern border. The South Equatorial Current, despite being centred in the southern hemisphere, extends across the Equator and it is multibanded. It flows westward and separates, around 10°S, into the North Brazil Current, which crosses the equator carrying most of the original water to the North Atlantic, and the Brazil Current, which is the weakest of the two. The Brazil Current flows southwards along the South American coast and receives waters from its re-circulation cell which

makes the current stronger. This warm water current meets the northward cold water Falklands Current resulting into the Brazil-Falklands Confluence in the western part of the Subtropical Convergence. The Brazil Current leaves the shelf somewhere around 33 and 38°S. The southernmost extent of the Brazil Current after separation from the shelf varies between 38 and 46°S, linked with eddy formations. Most of these eddies escape from the re-circulation region and are swept eastward with the South Atlantic Current, marking the southern branch of the Southern Atlantic Subtropical gyre. The main feature of eastern South Atlantic is the Benguela Current, flowing north, and the coastal upwelling system. Another significant feature is the Agulhas Current, which comes from the Indian Ocean and enters the Atlantic Ocean south of Africa as a free jet and develops instabilities with eddy sheddings by retroflection loops. Most of these eddies are incorporated into the Benguela Current and drift northwestwards, feeding one of the South Equatorial Current branches. This is the branch that bifurcates at circa 10°S - 12°S to form the North Brazil Current and the Brazil Current.

### 3.1.2 Water masses

Tomczak and Godfrey (2001) proposed that the observed variation in the temperature-salinity characteristics of central waters across the ocean basin results from environmental variability within the formation region. They called North Atlantic Central Water (NACW) the central waters in the North Atlantic. In the South Atlantic, the analysis of Sprintall and Tomczak (1993) reinforced the theory that central water in the South Atlantic is formed in the Brazil-Falklands Confluence (Gordon 1981) and that there is also a contribution of Indian Central Water from the Agulhas retroflection eddies (Gordon 1986). Following that reasoning Poole and Tomczak (1999) consider two central waters in the South Atlantic, one formed near Brazil-Falklands confluence, the Western South

Atlantic Central Water (WSACW, 6.5 - 16.3°C and 34.40 - 35.69), and another one from the Agulhas Current retroflection, the Eastern South Atlantic Central Water (ESACW 6.0 - 14.4°C and 34.41 - 35.30).

Three central water masses (ESACW, WSACW and NACW) are found in the surface waters of the Atlantic Ocean and they will be referred to as *source water masses*. They form a strong front with a gradient in water mass between North Atlantic (NACW) and South Atlantic central waters (WSACW) at about 15°N and even as far north as 20°N at the eastern boundary (Poole and Tomczak 1999). This front bends north close to Africa to follow the confluence of the northern subtropical gyre and the Guinea Dome (Tomczak and Godfrey 2001).

### 3.1.3 Biogeographical provinces

Several works have been carried out in an attempt to divide or establish the biogeography of the ocean in small-scale (Santamaría-del-Angel *et al.* 1994), basin-scale (González *et al. submitted*[1]) and global-scale (Longhurst *et al.* 1995, Longhurst 1998). In global-scale, analyses carried out by Longhurst and collegues (Longhurst *et al.* 1995, Longhurst 1998) divided the global ocean into four biomes according to the regional discontinuities in physical processes, and then those biomes were subdivided into smaller regions called provinces. Some provinces of the Atlantic Ocean are presented in Figure 3.2 and summarised in Table 3.1. Surface circulation and distribution of water masses in the upper ocean (Figure 3.1) mostly determine the biogeographical provinces. Although the provinces are well described, boundaries between the provinces change seasonally and interannually, in position and in sharpness, and they must not be taken as fixed geographically (Longhurst

[1]González *et al.* Biogeographical regions of the tropical and subtropical Atlantic Ocean off South America, submitted to Continental Shelf Research.

*et al.* 1995, Longhurst 1998).

### 3.1.4 Primary production

Primary productivity across the Atlantic has a big range of variation due either to the province characteristics or to the seasonal variation (Longhurst 1998). Although there are many primary productivity measurements reported for the Atlantic Ocean, most of them are in the Northern Hemisphere, in the Western Tropical (Sathyendranath *et al.* 1995, Morel *et al.* 1996) or Eastern Atlantic as part of the JGOFS NABE (Ducklow and Harris 1993, Joint *et al.* 1993).

A summary of primary productivity published for September or October are presented for some provinces of the Atlantic Ocean in Table 3.2.

This big difference between different regions of the ocean led to the partitioning of the ocean according to physical, nutritional and biological points of view (Santamaría-del-Angel 1995, Muller and Lange 1989, Sathyendranath *et al.* 1995, Longhurst *et al.* 1995, Longhurst 1998). Even though changes in primary production as quick as time-scales of days were observed in bloom formation (Savidge *et al.* 1995).

## 3.2 The Atlantic Meridional Transect Programme

The data analysed in this thesis were collected during the $11^{th}$ cruise of the Atlantic Meridional Transect (AMT11). The investigation focused the primary production along the AMT11 transect but some other data were acquired in support of the AMT11 data.

The AMT programme is led by the Plymouth Marine Laboratory (PML), in collaboration

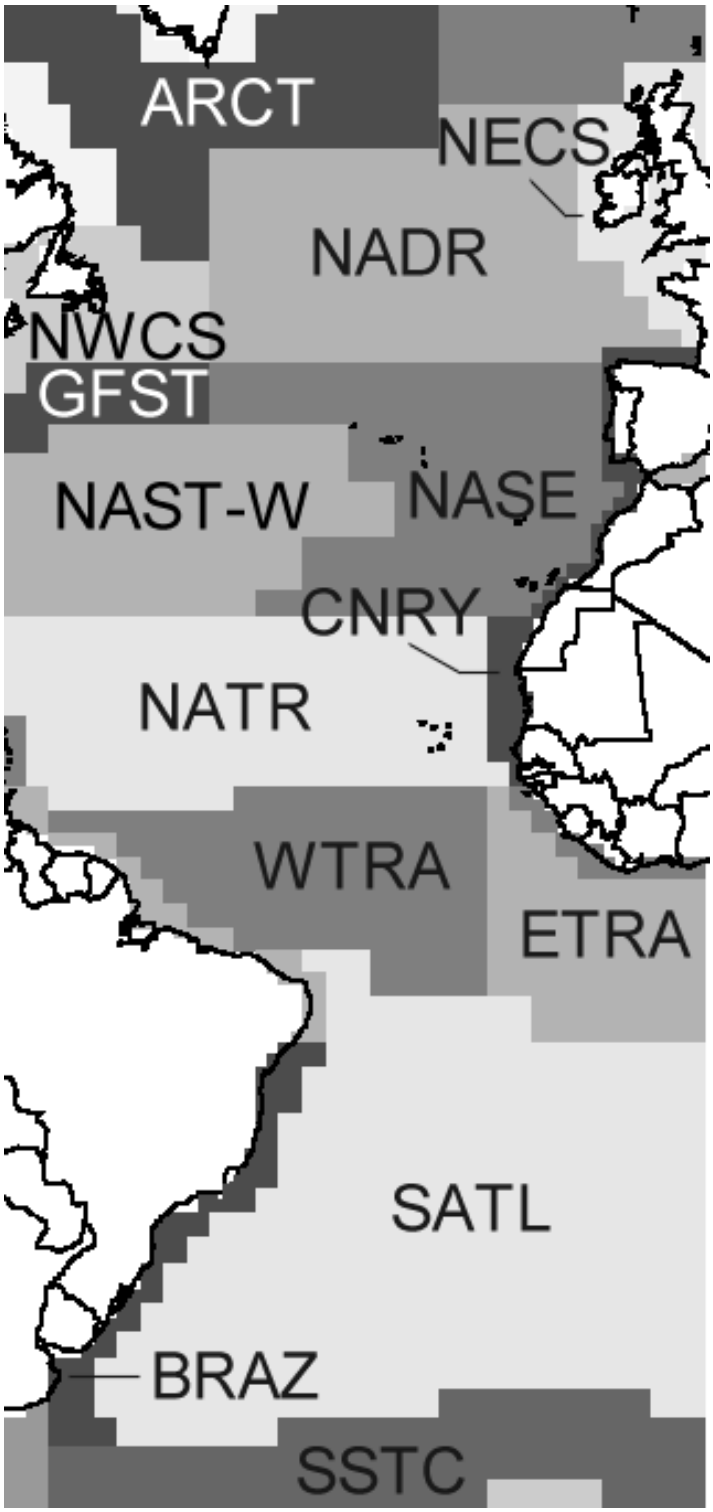


Figure 3.2: Biogeographical provinces in the Atlantic Ocean as identified by Longhurst (1998). Location of the boundaries between provinces must not be taken as fixed geographically. See Table 3.1 for main features of the provinces.

Table 3.1: Some provinces of the Atlantic Ocean and their main features (From Longhurst 1988 and Longhurst *et al.* 1995).

| Abbreviation | Name | Main features |
|---|---|---|
| Atlantic Westerly Winds Biome | | |
| GFST | Gulf Stream Province | From the Strait of Florida to the Newfoundland Basin, dominated by Gulf Stream with cold core eddies |
| NADR | North Atlantic Drift | Comprises the North Atlantic Current |
| NAST - E and W | North Atlantic Subtropical Gyre | North Atlantic central gyre polewards of the subtropical convergence, recirculation over divided in Eastern and Western provinces by the |
| Atlantic Trade Wind Biome | | |
| NATR | North Atlantic Tropical Gyre | Central gyre south of the subtropical convergence zone with southern limit around 10°N |
| WTRA | Western Tropical Atlantic | Region west of the mid-Atlantic Ridge and between 10°N and with influence of Amazon water |
| ETRA | Eastern Tropical Atlantic | The Gulf of Guinea eastwards to around 20°W of longitude |
| SATL | South Atlantic Gyral Province | Comprises the South Equatorial Current |
| Atlantic Coastal Biome | | |
| BRAZ | Brazil Current Coastal Province | Comprises the Brazil Current |
| CNRY | Eastern (Canary) Coastal Province | Comprises the seasonal upwelling from Cape Finisterre (43°N) to Cape Verde (15°N) |
| NECS | Northeast Atlantic Shelves Province | From the narrow shelf of western France to north across the British shelf |
| NWCS | Northwest Atlantic Shelves Province | Comprise Labrador Current and the Gulf of St Lawrence |
| Antarctic Westerly Winds Biome | | |
| SSTC | South Subtropical Convergence | The most northerly feature of the Southern Ocean, lots of eddy fields, and surface discontinuity fronts |

Table 3.2: Some primary productivity published recently for provinces in the Atlantic Ocean (Longhurst 1998): North Atlantic Drift (NADR), Northeastern Atlantic Sub-tropical gyre (NASE), Western Tropical Atlantic (WTRA), Eastern Tropical Atlantic (ETRA), South Atlantic Gyral Province (SATL). CC is the region influenced by the Canary Current (Aiken *et al.* 2000), RCBC is the region of recirculation cells of the Brazil Current in the Southwestern Atlantic (Tomczak and Godfrey 2001). All the data are in mgC $m^{-2}$ $d^{-1}$, average for the province unless otherwise stated and numbers in brackets are standard deviations.

| source | date | NADR | NASE | CC | WTRA | ETRA | SATL | RCBC | method |
|---|---|---|---|---|---|---|---|---|---|
| Marañón & Holligan | Sep 95 | 268 | 77 | | 111 | | 301§ | | $^{14}$C, 6-7 h incubation on deck |
| 1999 | | (75) | (28) | | (25) | | (149) | | |
| Antoine *et al.* 1996 | | 350† | 250† | 1000† | 400‡ | 800‡§ | 250‡ | 300‡ | CZCS mo Chl*a* , model |
| Longhurst 1998 | | 524* | 200* | | 438* | 515* | 259# | | CZCS, model, P-E |
| Morel *et al.* 1996 | 16 Sep 1991 | | | 525 | | | | | $^{14}$C Let-Go device, *in situ* |
| Morel *et al.* 1996 | 08 Oct 1991 | | | 521 | | | | | $^{14}$C Let-Go device, *in situ* |

Morel *et al.* 1996, EUMELI3 mesotrophic station. †seasonal mean for July, August and September; ‡seasonal mean for October, November and December; §include RCBC; Longhurst 1988: climatological montly average for *September and **October;

with British Antarctic Survey (BAS) and in association with the Southampton Oceanography Centre (SOC) and the University of Plymouth (UoP) (Robins *et al.* 1996). AMT cruises take advantage of twice-a-year meridional voyages of the Royal Research Ship James Clark Ross (RRS JCR) between the UK and Antarctica, adding only a few days to the normal transect time, to give basin-scale sampling across the Atlantic Ocean. The main objective of the AMT is to investigate basic biological processes in the open Atlantic Ocean, at broad spatial scales. The AMT allows sampling for calibration, validation, and continuing understanding of remotely sensed observations of biological oceanography (Aiken *et al.* 2000).

AMT11 started in Grimsby (UK) on September $11^{th}$ 2000 and docked in Montevideo (Uruguay) on October $13^{th}$ 2000. On this cruise there were two stations for water sampling per day, one at pre-dawn and another around local mid-day.

For the pre-dawn stations, only a conductivity, temperature and depth sensor (CTD) with a fluorometer was deployed attached to a rosette with 10 litre Niskin bottles for water collection. For the mid-day stations, there were two simultaneous deployments, one for the CTD and bottle rig and another for a rig with bio-optical sensors attached.

The pre-dawn water samples were analysed for nutrients, fluorometric Chl*a*, 24 hours $^{14}C$ incubation and phytoplankton physiology with fast repetition rate (FRR) fluorometry, amongst others.

At mid-day stations, the measurements focused on optical data for SeaWiFS calibration: downwelling spectral irradiance, FRR fluorometer profiling for *in situ* measurement, P-E curve with $^{14}C$, particulate absorption coefficient (PABS), nutrients, nitrogen production, High Performance Liquid Chromatography (HPLC) pigments and fluorometric Chl*a*. The

bio-optical rig consisted of spectral irradiance and radiance collectors, FRR fluorometer and logger system for the optical sensors. This rig also had a CTD with a fluorometer attached. The FRR fluorometer is a separate system with its own logger for fluorescence yields, photosynthetically available radiation (PAR) and pressure sensors.

# Chapter 4

# Province analysis

## 4.1 Introduction

The AMT11 transect covered around 80 degrees in latitude, crossing different regions of the ocean from oligotrophic waters in the gyres to mesotrophic upwelling regions. Due to this large scale, it was convenient to know where each station took place. Although consistent provinces could be identified throughout the year, no rigid boundaries could be established due to the seasonal or interannual variability in physical processes, changing the location and/or sharpness of the boundaries. This non-rigid boundary between provinces makes it difficult to locate where the samples were collected. This chapter attempts to identify where each of the AMT11 CTD stations took place, based on the data collected, and a summary of each province is given.

## 4.2 Data collection

### 4.2.1 Chl*a* concentration

#### Fluorometric method

Water samples were taken at 10 depths between 4 and 250 m depth (typically from above and below the 1.0 % light irradiance depth and included samples from the sub-surface chlorophyll maximum and at least three from across the thermocline). 0.250 L from each depth was filtered through Whatman GF/F (0.7 $\mu$m nominal pore size) glass fibre filters at mid-day and pre-dawn stations for determination of Chl*a* concentration using the fluorometric method described by Welschmeyer (1994). Each filter was extracted in 10 mL of 90% acetone for 24 hours in the -20°C walk in freezer. Chlorophyll-a was measured on an 10-AU Turner Design digital fluorometer calibrated against a standard chlorophyll-a stock solution previous to the cruise. The Chl*a* concentration was determined from the fluorometer reading as [Chla] = (volume acetone / volume water filtered) x fluorometer reading[1].

#### High Performance Liquid Chromatography - HPLC

Duplicate of 1.5 samples were filtered through Whatman GF/F (0.7 $\mu$m nominal pore size) glass fibre filters at mid-day stations of AMT11 for analysis by HPLC. In the oligotrophic waters of the subtropical gyre, single samples of 3.0 L were filtered for HPLC instead of duplicate 1.5 L samples. The filters were immediately frozen at -80°C during the cruise and then shipped in a dry-shipper to Vigo, Spain, where the pigments were analysed with

[1]Fluorometric Chl*a* data was analysed by Sandy Thomalla, SOC, Southmpton, UK.

HPLC[2] method described in Zapata *et al.* (2000). This method combines a $C_8$ column with an optimised mobile phase including an aqueous pyridine solution as an ion-pair reagent. This allows the separation between DVChl*a* and MVChl*a*. The method was performed using Waters Alliance HPLC equipment, with a 2690 separations module (low-pressure mixing system) and a Waters 996 diode-array detector (1.2 nm optical resolution) interfaced with a Waters 474 scanning fluorescence detector (Zapata *et al.* 2000).

### 4.2.2 CTD data

CTD measurements were conducted by profiling vertically a Sea-Bird SBE 9 attached to the bottle rig at mid-day and pre-dawn stations. Also fitted to the CTD were secondary temperature and conductivity sensors, a WETstar miniature fluorometer (Wet Labs, Inc.) and a spherical PAR sensor (Biospherical Instruments, Inc). The dual set of temperature and conductivity sensors allowed the SBE 9 instrument to self-check and nominally self-calibrate the measurements. The average difference between the primary and secondary sensors was seen to be 0.001°C in temperature and 0.005 in salinity (Aiken *et al.* 1998).

The CTD data from the cast with water-collection, normally the up-cast, were binned into 1 m depth interval for analysis of water column structure.

### 4.2.3 Chl*a* estimate from CTD fluorescence

The Chl*a* was estimated from the fluorescence measured with the Sea-Bird SBE 9 system (CTDf). The CTDf was calibrated with total Chl*a* determined by the HPLC method. For most of the water column (except the 10 to 20 m upper layer), the relationship between CTD fluorescence and fluorometric Chl*a* does not change from pre-dawn to mid-

[2]HPLC data provided by Emílio Fernández, Universidad de Vigo, Vigo, Spain.

Table 4.1: Relationship between the signal from the CTD fluorometer and Chl*a* concentration. Regression analysis results provided by Emílio Fernández.

| Method | Time | intercept | slope | $R^2$ | n |
|---|---|---|---|---|---|
| HPLC | day | -0.70 | 0.669 | 0.83 | 211 |
| Fluor | day | -0.52 | 0.542 | 0.75 | 110 |
| Fluor | night | -0.55 | 0.547 | 0.77 | 125 |
| Fluor | day & night | -0.54 | 0.546 | 0.75 | 235 |

day stations. Table 4.1 presents linear regression analysis between measured Chl*a* and voltage from the CTDf with samples collected during the day (with light influence) and night (without light influence). Chl*a* concentration was measured with HPLC method for mid-day stations only so the assessment of influence of light over the relationship between CTDf and Chl*a* was done with fluorometric estimation of Chl*a*. There was no considerable difference in values of intercept and slope for regression analysis over day & night data, day only data and night only data (Table 4.1). Based on the analyses presented in, it is assumed there is no light influence in the relationship (but see Holm-Hansen *et al.* 2000). The linear regression between the HPLC total Chl*a* (only measured during the mid-day stations) was used. The 1 m binned CTD fluorescence could be then converted into Chl*a*. This relationship had a high coefficient of correlation ($R^2 = 0.83$), but did not apply to the CTD station 01. This station was considered separately by: Chl$a = 10^{1.625317 * CTDf - 3.189663}$ (n = 6; $R^2 = 0.997$).

### 4.2.4 Nitrate

Nitrate[3] analysis was carried out using a segmented-flow, colorimetric autoanalyser (Technicon AAII). The analytical technique for the analysis of Nitrate was an adaptation of the classical Brewer and Riley method (1965). This can be found in Woodward (1994). Samples were collected in 60 mL HDPE (Nalgene) bottles and analysed within 2 hours of collection.

## 4.3 Province identification

The provinces described by Longhurst (1998) were the starting point for identification of the provinces that were likely to be found along the AMT11 transect. The sea surface temperature and Chl*a* concentration analyses (Figure 4.1) associated with rough location of provinces (Figure 3.2), helped to define those most likely to have been sampled during the AMT11.

With the location of each station and knowing the most likely provinces for each station, station data were analysed to match one of the likely province characteristics. The data analysed for province classification were isothermal layer depth (ILD) and the temperature of the ILD, the surface concentration of nitrate and the depths of the nitracline, and the concentration and the depth of the maximum Chl*a*. These parameters are summarised in Table 4.2.

The ILD was determined as the depth where *in situ* temperature ($\Delta$t) changed by >0.1°C $m^{-1}$, except for station 24 ($\Delta$t=0.2 °C $m^{-1}$). The CTD data from the up-cast corresponding to depths shallower than 200 m were analysed for each station (Appendix B Figure

[3]Nitrate data provided by Malcom Woodward (PML, Plymouth, UK).

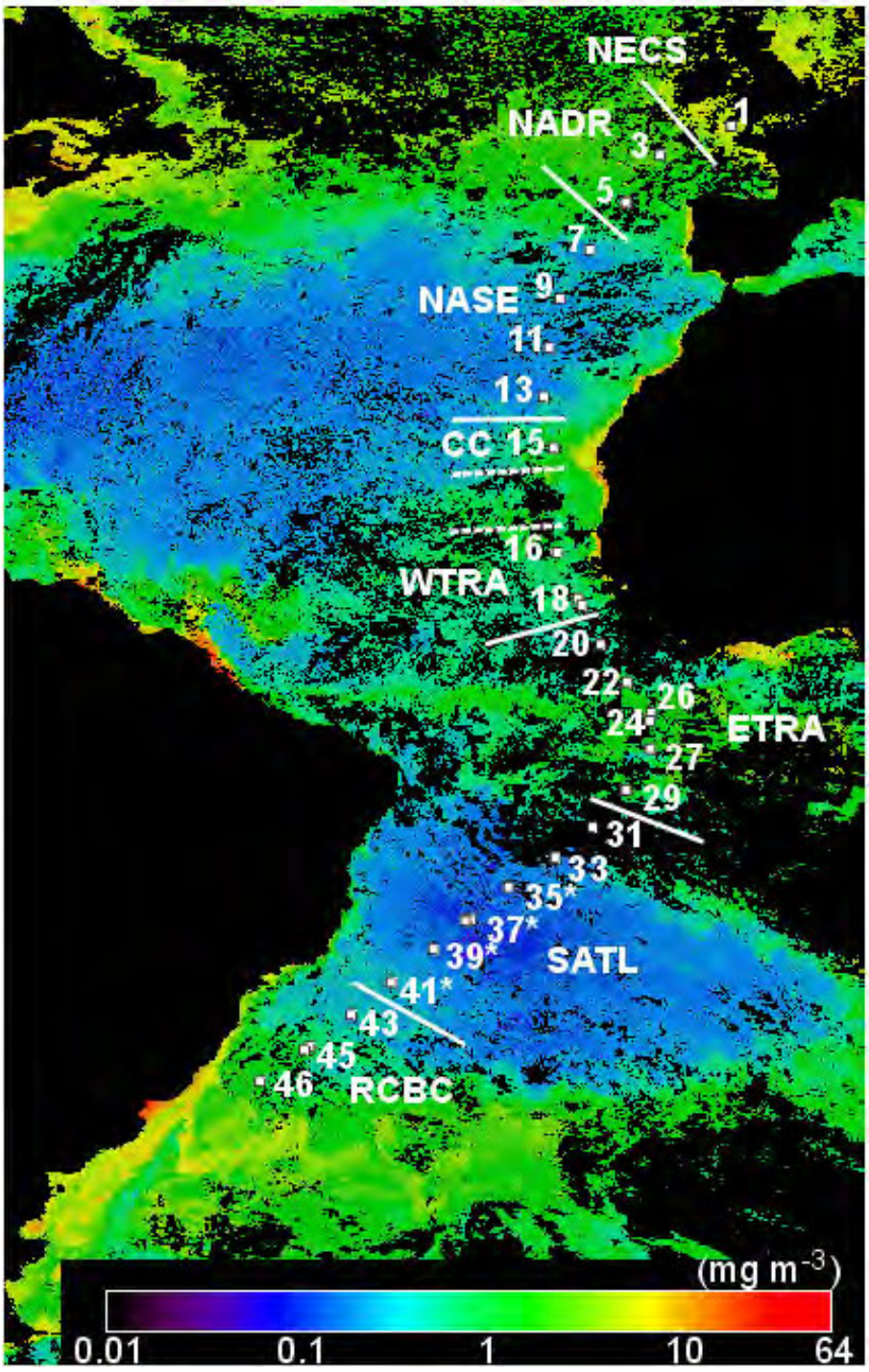


Figure 4.1: Eight-days (7-14 October 2000) composite of surface Chl*a* concentration from SeaWiFS. The mid-day stations and the provinces for AMT11 are indicated. Stations in the core of the SATL are indicated by * (see text for further details).

B.5).

Two depths of nitracline were considered: the first was the depth where the nitrate concentration changed 0.025 $\mu$M m$^{-1}$ (N025) and the second was the depth where that change was 2 $\mu$M m$^{-1}$ (N2). The closer these two depths (N025 and N2) were, the sharper was the increase in nitrate concentration with depth.

The temperature and salinity (T-S) diagram for each station was analysed to support the province classification. Usually the upper 200 m layer is not included in the water mass analyses (Emery and Meincke 1986) because contact with the atmosphere causes seasonal heating, modifying the original physical characteristics. However, this layer is where primary production occurs, hence the importance to understand the physico-chemical characteristics. The T-S analysis was carried out with the CTD data from the upper 200 m layer, station by station, to identify the water mass with unchanged physical properties, e.g the source water mass. Two of the source water masses (WSACW and NACW) were used as references for the T-S plots. However, regional environmental variability due to the seasonal heating at the surface layer also needs to be taken into account. In the eastern part of North Atlantic, the Eastern North Atlantic Central Water (ENACW) may be altered to subpolar (ENAWp, 4-12°C and 34.96-35.66) or subtropical (ENAWt, 13.15-18.5°C and 35.8-36.75) characteristics (Ríos *et al.* 1992). Around the Equator, remnant water from the Amazon discharge with temperatures higher than 25°C and salinities lower than 35 were found as far east as 15°W transported eastward by the North Equatorial Counter Current (Aiken *et al.* 2000). Such Amazon Water (AW) was registered as deep as 70 m, centred at 5°N during the Boreal-Autumn-AMT cruises by Aiken *et al.* (2000). They also described the Equatorial Surface Water (ESW), a surface South Atlantic Central Water (SACW) diluted by high precipitation in the Intertropical

Convergence Zone (ITCZ) around the Equator (Tomczak and Godfrey 2001).

## 4.4 Results

The results of province classification and the parameters analysed are summarised in Table 4.2. This analysis led to the classification of the stations into provinces (Table 4.2). The 80° of latitude covered eight oceanic provinces: Northeast Atlantic Shelves Province (NECS), North Atlantic Drift Province (NADR), North Atlantic Subtroptical Gyre - East (NASE), Canary Current Province (CC), Western Tropical Atlantic Province (WTRA) including Guinea Dome (Longhurst 1998), Eastern Tropical Atlantic Province (ETRA), South Atlantic Gyral Province (SATL) and Recirculation Cell of Brazilian Current (RCBC). These provinces are overplotted on the satellite image of surface Chl*a* concentration (Figure 4.1).

Apart from AMT8 (Apr-Jun/1999), the AMT11 cruise track was different from all other AMT cruises. The northern part of the AMT11 transect between 10°N and about 35°N was geographically close to previous AMT cruises but only AMT6 and AMT8 sampled the Eastern Tropical Atlantic (ETRA). The core of South Atlantic subtropical gyre (SATL) was sampled only at AMT8 and AMT11, although in different seasons.

### 4.4.1 Physical structure

A contour plot for temperature, salinity and potential density is presented in Figure 4.2. The original stations sampling depths and position data used for gridding are presented in Appendix A (Figure A.1). These contour plots are for visualisation of the whole transect, because individual features are smoothed in the gridding process. For detailed

Table 4.2: Hydrographic characteristics of the AMT11 CTD stations. # indicates mid-day station, ILD: isothermal layer depth (m) and the temperature (T°C) within the ILD, Chl*a* is the maximum Chl*a* (mg $m^{-3}$) and its depth (m) is indicated in brackets, N025 and N2: depth of nitracline of 0.025 and 0.2 $\mu$M $m^{-1}$ respectively, ↓S: low salinity, $N_s$: nitrate concentration at surface. The SATL* is the core of the province. The zero values for N025 means that the change in nitrate was higher than 0.025 $\mu$M $m^{-1}$ at the surface.

| Province | CTD | ILD | T°C | Chl*a* | N025 | N2 | Water mass |
|---|---|---|---|---|---|---|---|
| NECS | 1# | 11.6 | 16.7 | 6.71 (17) | 13.6 | 15.6 | |
| NADR | 2 | 13.2 | 18.5 | 0.53 (31.5) | 24.2 | 30.4 | ENAWp |
| NADR | 3# | 5.5 | 18.2 | 0.62 (34) | 36.3 | 44.3 | ENAWp, ↓S at surface |
| NADR | 4 | 17.3 | 20.5 | 0.66 (60) | 46.7 | 55.0 | ENAWp |
| NADR | 5# | 10.5 | 21.1 | 0.6 (56) | 46.5 | 52.8 | ENAWp |
| NASE | 6 | 28.4 | 21.2 | 0.33 (75) | 67.5 | 77.7 | ENAWt |
| NASE | 7# | 37.4 | 21.5 | 0.31 (88.5) | 87.9 | 102.0 | ENAWt |
| NASE | 8 | 29.5 | 22.5 | 0.3 (80) | 70.1 | 83.3 | ENAWt |
| NASE | 9# | 34.6 | 23.4 | 0.33 (84.5) | 66.4 | 79.4 | ENAWt |
| NASE | 10 | 30.5 | 23.8 | 0.3 (105) | 98.5 | 118.7 | ENAWt |
| NASE | 11# | 13.7 | 23.9 | 0.27 (118) | 105.3 | 125.1 | ENAWt |
| NASE | 12 | 44.2 | 23.8 | 0.27 (116) | 105.9 | 126.7 | ENAWt |
| NASE | 13# | 36.0 | 23.8 | 0.27 (111) | 96.7 | 115.3 | ENAWt |
| CC | 14 | 30.7 | 23.8 | 0.38 (52) | 39.9 | 53.6 | ENAWt ↓S at surface |
| CC | 15# | 23.5 | 24.3 | 0.5 (42.5) | 29.8 | 36.7 | ENAWt ↓S at surface |
| WTRA | 16# | 9.0 | 28.2 | 0.53 (47) | 29.8 | 36.7 | Guinea Dome: ESW WSACW |
| WTRA | 17 | 20.4 | 27.8 | 0.42 (47.5) | 28.3 | 36.6 | AW ESW WSACW |
| WTRA | 18# | 26.2 | 27.4 | 0.38 (47.5) | 29.0 | 39.9 | AW ESW WSACW |
| WTRA | 19 | 41.1 | 27.3 | 0.42 (62.5) | 53.6 | 61.2 | AW ESW WSACW |
| WTRA | 20# | 45.5 | 27.2 | 0.39 (74) | 38.9 | 49.1 | AW ESW WSACW |
| ETRA | 21 | 24.4 | 24.3 | 0.49 (9) | 21.5 | 56.7 | $N_s$=0.4 $\mu$M , WSACW, ESW |
| ETRA | 22# | 32.0 | 23.5 | 0.33 (84.5) | 34.0 | 62.1 | $N_s$=2.0 $\mu$M, WSACW ESW |
| ETRA | 23 | 21.4 | 23.1 | 0.59 (1) | 0 | 27.8 | $N_s$=2.0 $\mu$M, WSACW ESW |
| ETRA | 24# | 24.1 | 23.3 | 0.52 (29) | 9.1 | 43.4 | $N_s$=2.0 $\mu$M, WSACW ESW |
| ETRA | 25 | 15.9 | 23.3 | 0.54 (21) | 7.2 | 18.3 | $N_s$=2.3 $\mu$M, WSACW ESW |
| ETRA | 26# | 14.6 | 22.9 | 0.49 (19) | 0 | 18.05 | $N_s$=2.5 $\mu$M, WSACW ESW |
| ETRA | 27# | 16.7 | 23.7 | 0.38 (51) | 14.9 | 62.4 | $N_s$=1.3 $\mu$M, WSACW ESW |
| ETRA | 28 | 76.7 | 23.8 | 0.43 (1) | 58.0 | 72.5 | WSACW ESW |
| ETRA | 29# | 78.4 | 23.9 | 0.38 (66) | 65.2 | 86.2 | $N_s$=0.006 $\mu$M, SWACW ESW |
| SATL | 30 | 55.0 | 24.4 | 0.37 (100) | 89.7 | 109.4 | WSACW |
| SATL | 31# | 86.7 | 24.3 | 0.37 (97) | 80.5 | 101.0 | WSACW |
| SATL | 32 | 48.3 | 24.1 | 0.30 (128) | 115.3 | 143.4 | WSACW |
| SATL | 33# | 110.0 | 23.8 | 0.32 (127) | 123.7 | 154.5 | WSACW |
| SATL* | 34 | 146.6 | 23.1 | 0.21 (124) | 136.9 | 170.4 | WSACW |
| SATL* | 35# | 142.1 | 23.4 | 0.24 (145) | 148.8 | 188.3 | WSACW |
| SATL* | 36 | 148.0 | 23.6 | 0.25 (174) | 161.3 | 202.9 | WSACW |
| SATL* | 37# | 125.0 | 23.5 | 0.25 (144) | 146.8 | 185.8 | WSACW |
| SATL* | 38 | 140.0 | 23.0 | 0.25 (149) | 178.2 | 224.9 | WSACW |
| SATL* | 39# | 100.0 | 23.2 | 0.21 (118) | 151.9 | 192.3 | WSACW |
| SATL* | 40 | 90.0 | 23.4 | 0.23 (99) | 147.6 | 186.9 | WSACW |
| SATL* | 41# | 120.0 | 21.7 | 0.19 (92) | 140.0 | 177.2 | WSACW |
| SATL | 42 | 50.4 | 21.8 | 0.28 (84) | 89.3 | 110.5 | WSACW |
| RCBC | 43# | 55.0 | 20.5 | 0.35 (95) | 84.6 | 105.2 | WSACW |
| RCBC | 44 | 50.6 | 19.7 | 0.4 (78) | 74.2 | 92.3 | WSACW |
| RCBC | 45# | 74.9 | 18.1 | 0.34 (80) | 71.0 | 88.7 | WSACW |
| RCBC | 46# | 76.1 | 16.5 | 0.42 (56) | 79.3 | 98.7 | WSACW |

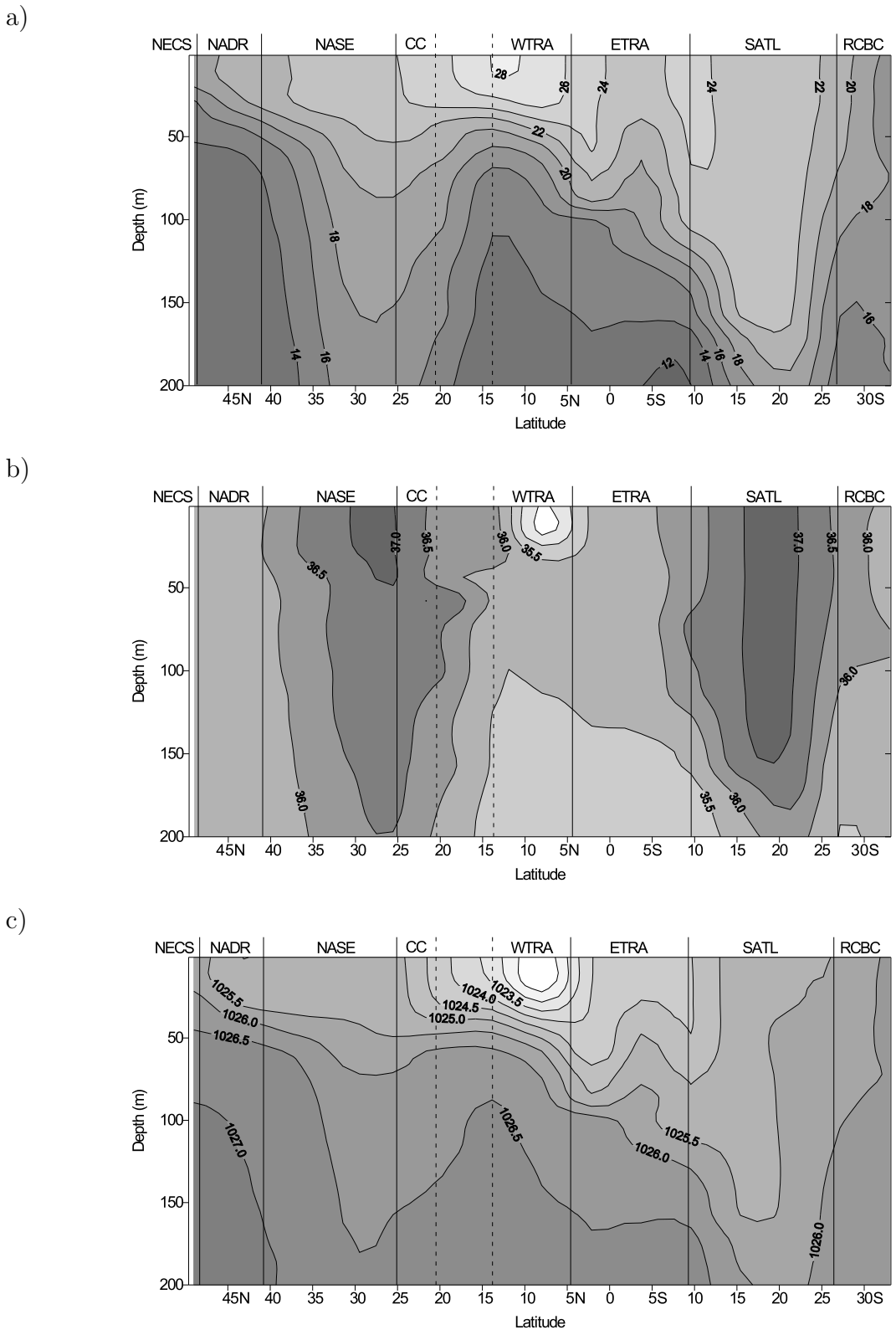


Figure 4.2: Physical structure of the surface (0 to 200 m) layer along the AMT11 transect. a) Temperature (°C), b) Salinity and c) Potential density (kg $m^{-3}$). Note that the vertical lines separate the stations from one province to another only and do not mean the location of boundary between two provinces. The dashed lines between CC and WTRA indicate there might be some other province in between. Top axis indicates the provinces and the bottom one the latitude in degrees. See Appendix A (Figure A.1) for location of the original data used for the gridding.

station profiles, see individual station profiles (Appendix B). The general temperature structure (Figure 4.2 a) shows colder surface water in the North Atlantic than previous September/October AMT cruises (González et al. 2002, Zubkov et al. 1998, Zubkov et al. 2000) but similar temperature to AMT1 surface waters (Hooker *et al.* 2000). The 24°C isothermal was found at 25°N in the AMT11 (Figure 4.2 a) whilst previously this isothermal was as far north as 32°N in the AMT3 (Zubkov *et al.* 2000) and AMT5 (González *et al.* 2002) cruises at an equivalent time of year.

Station 1 was sampled within NECS, over the European continental shelf. The temperature was lower than 17°C and constant salinity (35.4) but no characteristic structure for the province could be defined here because only one station was sampled. Stations 2 to 5 (NADR) were characterised by constant salinity (around 35.7) and temperature ranged between 12 and 22°C, as shown in T-S diagram (Figure 4.3 and B.1), with a shallow ILD (<18 m, Table 4.2). The water mass was ENAWp but the T-S relationship was altered from its original properties, increasing temperature (Figure 4.3) due to the seasonal heating or biological processes (Sathyendranath *et al.* 1991). The North Atlantic Subtropical Gyre stations (NASE, stations 6 to 13) had shallow ILD (<45 m), consistent with those reported in the literature for August-October (between 25 and 50 m, Tomczak and Godfrey 2001). The water mass changed from ENAWp in the NADR to ENAWt in the NASE. The seasonal heating in the surface was more diverse in the NASE than in the NADR surface waters, with increase in temperature not following a unique form, although all the profiles have as source water mass ENAWt (Figure 4.3 NASE). The NASE province had the highest salinity in the North Atlantic Ocean (Figure 4.2b).

Although the temperature within the isothermal layer of station 14 (CC) was very similar to those found in the NASE stations (Table 4.2 a), the density gradient was sharper in the

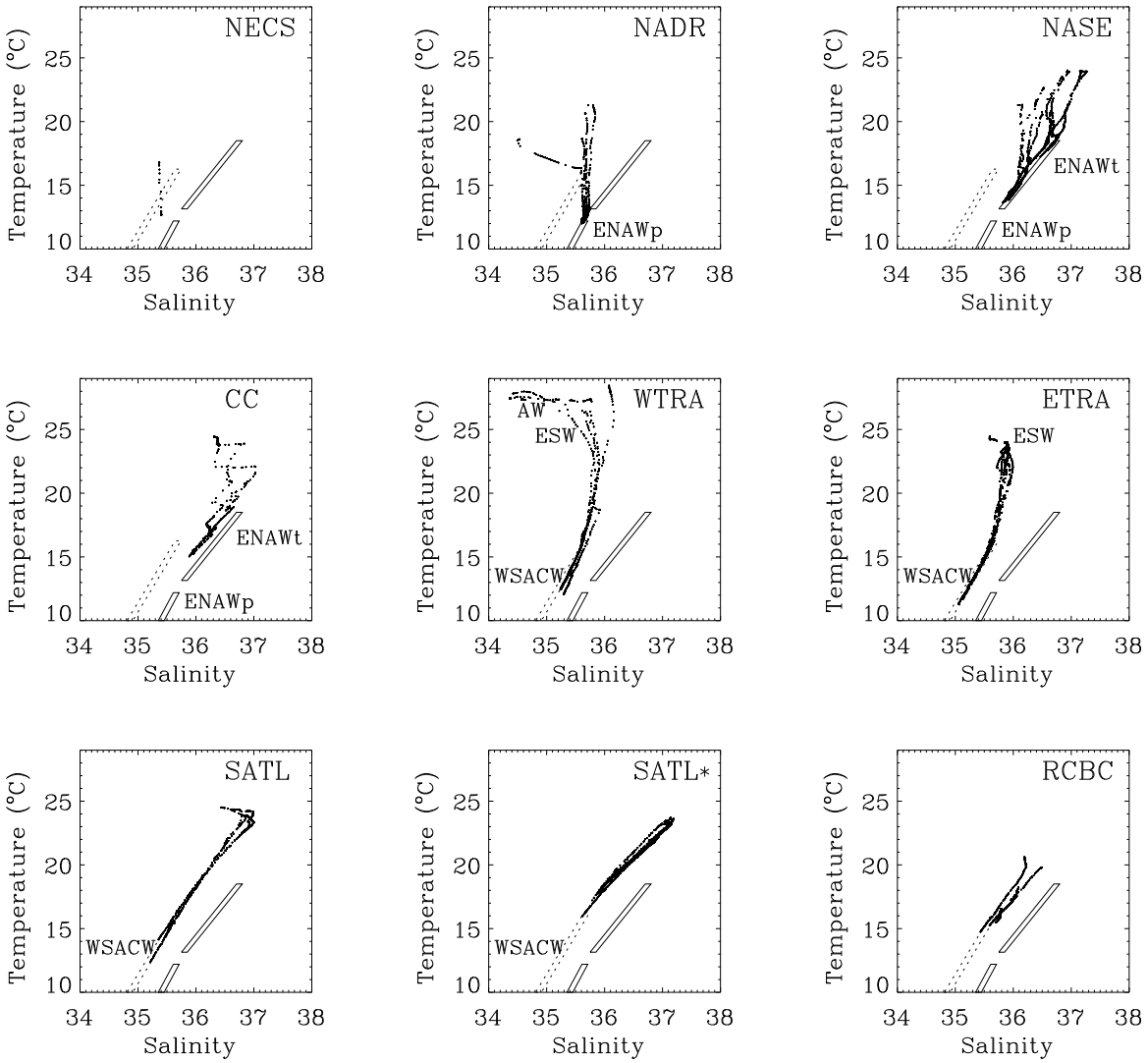


Figure 4.3: Temperature versus salinity (T-S) diagrams for the provinces along the AMT11 transect. The reference water masses are indicated by the solid parallelograms (upper is ENAWt and bottom: ENAWp) and a dotted parallelogram (WSACW) as a guide for comparison between provinces.

CC and even sharper in the WTRA (Figure 4.2 c). The T-S diagram of CC indicated a water body with salinity lower than the ENAWt (Figure 4.3 CC). These two stations did not conform to the characteristics of Canary Coastal Province (Longhurst 1988). They were not in the oligotrophic gyre because Chl*a* concentration was higher than values found in NASE, although not high enough to be from an upwelling region. These intermediate characteristics indicated that stations 14 and 15 were in the boundary between Canary Coastal Province and NASE, still receiving influence from the Canary Current but without the characteristics of upwelled water. Such water was sampled in previous AMTs and called Canary Current province, around 20 and 25°N (Aiken *et al.* 2000) in the southern extension of Canary Current, with surface density around 24 and 24.5 kg $m^{-3}$ (Hooker *et al.* 2000). The source water mass was changing from the NACW, getting less saline (Figure 4.3 CC). This conformed to the front between the North Atlantic and the South Atlantic central waters usually found around 15°N (Poole and Tomzak 1999).

Further south, the WTRA (stations 16 to 20) had the lowest salinity and the warmest surface water of the whole transect (Figure 4.2a and b), due to the remnant of Amazon discharge (Longhurst 1998, Hooker et al. 2000). The structure is formed by AW, ESW and WSACW (Figure 4.3). Note that the source water mass changed completely to the central water originating in the South Atlantic (WSACW). This province is dominated by North Equatorial Counter Current and it was so named as a province by Hooker *et al.* (2000) for AMT1 and AMT2. CTD station 16 (the highest temperature T-S plot of WTRA in Figure 4.3) had a characteristic T-S relationship from the Guinea Dome, which is a permanent, quasi-stationary feature on the eastern part of the thermal ridge system in the Tropical Atlantic (Siedler *et al.* 1992). Characteristics of this station was found during the AMT1 and AMT2 and described by Hooker *et al.* (2000) as a distinct province, the Guinea Dome province. The whole province (WTRA) had a shallower ILD

(Table 4.2) due to the colder water upwelled at the Equator, confining the warmer AW to the surface (Figure 4.2b and c).

Towards the south, Figures 4.2 a and b show equatorial upwelling bringing colder, lower salinity water to the surface. Most of the stations were stratified at the surface with very shallow ILDs (Table 4.2). The presence of only ESW and WSACW and absence of AW indicated stations 21 to 29 as ETRA province (Figure 4.3). Salinity maximum did not reach 36.0 at the ETRA.

Further south, the only source water mass identified was WSACW, indicating the SATL province. The first four stations sampled in it (Stations 30 to 33) had a structure like a '*hook*' in the T-S diagram with warmer and lower salinity water than in the subsequent stations. Probably these first four stations were under influence of high precipitation in the ITCZ, decreasing the salinity. The core of southern gyre (SATL*, stations 34 to 41) was characteristically saltier and colder (Figure 4.2 a and b) with narrower limits for temperature and salinity than the SATL (Figure 4.3) and much deeper ILD than that in the northern gyre (NASE in Table 4.2). The lower temperature (Figure 4.2 a) compared to previous cruises, may be due to the more southernly AMT11 track than previous cruises or to interannual variability.

The southern end of the transect was characterised by T-S diagram being much shorter than that at SATL (Figure 4.3). This region was identified as province R11 in the sea surface Chl*a* images (González *et al.* submitted). This province had a high latitudinal temperature gradient due to the recirculation cell of the Brazilian Current (Tomczak and Godfrey 2001), and re-named here Recirculation Cell of Brazilian Current (RCBC) province. Station 42 and 43 were sampled in the boundary between SATL* and RCBC with the former having a characteristically higher temperature as the SATL* and the later

with a temperature lower than 21°C as the RCBC (Figure 4.3). Hooker *et al.* (2000) also found a distinct province at the southern end of the transects (AMT1 and AMT2), naming it Brazil Current Province (BraC). Although the misleading name, BraC represents the recirculation cells of the Brazil Current as described by Peterson and Stramma (1991) and Tomczak and Godfrey (2001). This province was as South Atlantic Subtropical Waters detected by Poulton (2000) who applied cluster analyses in hydrographic parameters of AMT7. Another work analysing time series of satellite-derived Chl*a* also discriminated this region as a province (González *et al. submitted*). Different approaches indicated the existence of a province which was not described by Longhurst (1998) and Longhurst *et al.* (1995). This must be due to the better data set analysed by works other than that by Longhurst for this region.

The physical structure along the AMT11 transect, especially the water mass distribution and regional seasonal heating, showed clear differences between the provinces. Hydrographical data

### 4.4.2 Nitrate distribution

Nitrate vertical distribution is plotted over temperature in Figure 4.4. ETRA was the only province with nitrate concentration higher than 2 $\mu$M in the surface. Station 23 had high inputs of nitrate from the bottom due to the Equatorial upwelling so that high nitrate value in the surface with an increase of more than 0.025 $\mu$M m$^{-1}$ . In other provinces, nitrate was undetectable at $\mu$M level within the isothermal layer. Other characteristic in the AMT11 transect was the nitracline being much deeper than the ILD in NADR and NASE, in contrast to the rest of the transect, where the nitracline was more coincident to the ILD. The depth of nitracline, especially N2, was linearly correlated to the ILD in

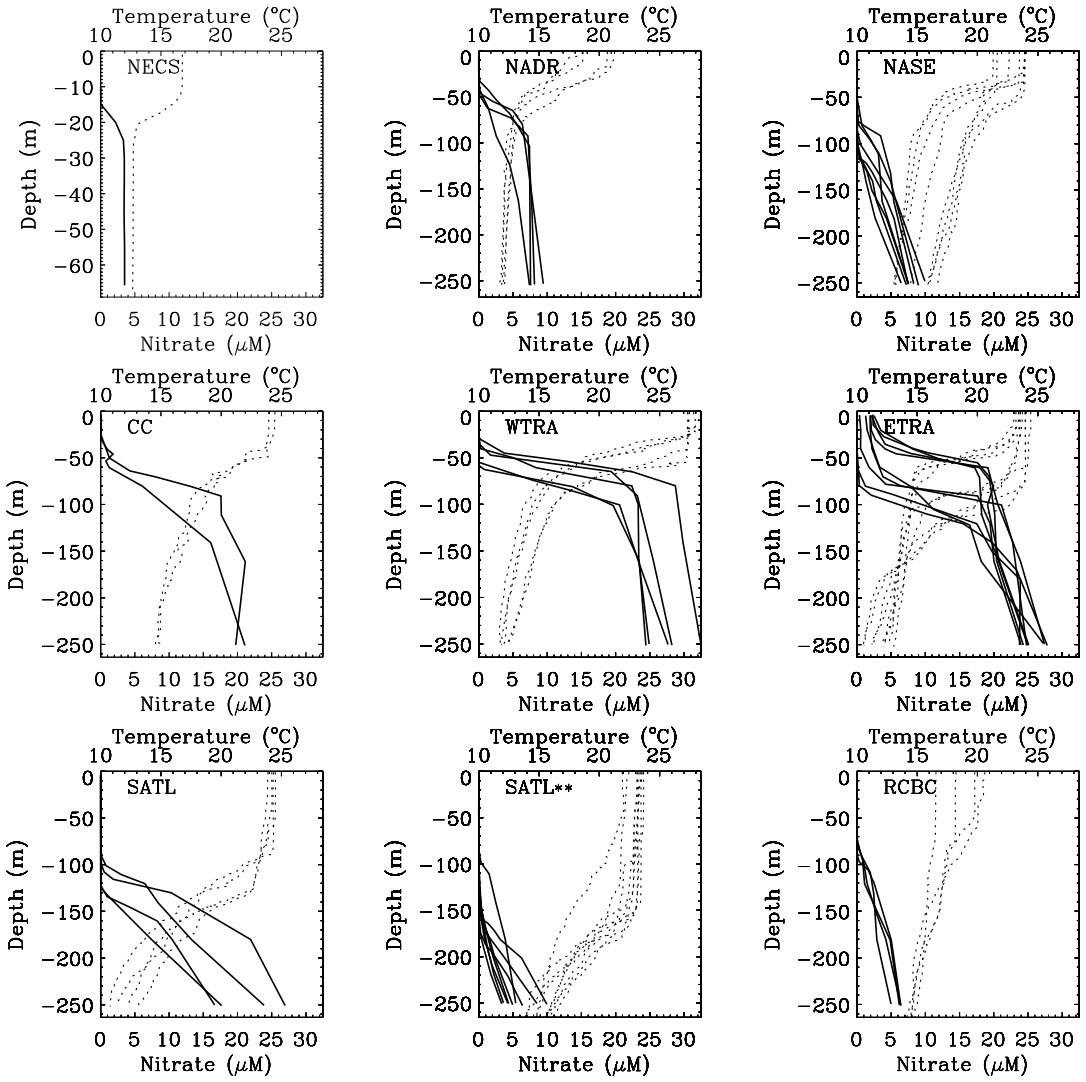


Figure 4.4: Station profiles of temperature and nitrate concentration in the provinces, indicated in the top left corner of each plot. Nitrate concentration (bottom axis in $\mu$M) in solid line and temperature (top axis, °C) in dotted line.

Table 4.3: Results from linear regression analysis between the depths of isothermal layer (ILD) and nitracline and between the depths of DCM and nitracline. D and I are respectively the dependent and independent variables analysed, * indicates the number of data (n) excluding NASE.

| D | I | n | $R^2$ | intercept | slope | F-ratio | p |
|---|---|---|---|---|---|---|---|
| N025 | ILD | 46 | 0.685 | 21.63 | 0.965 | 99.04 | $< 10^{-5}$ |
| N025 | ILD | 38* | 0.825 | 8.27 | 1.069 | 175.89 | $< 10^{-5}$ |
| N2 | ILD | 46 | 0.732 | 32.48 | 1.162 | 123.81 | $< 10^{-5}$ |
| N2 | ILD | 38* | 0.840 | 19.37 | 1.266 | 194.71 | $< 10^{-5}$ |
| DCM | N025 | 46 | 0.809 | 19.79 | 0.782 | 191.93 | $< 10^{-5}$ |
| DCM | N2 | 46 | 0.779 | 14.82 | 0.657 | 159.13 | $< 10^{-5}$ |

the whole transect (Table 4.3), and the relationship had significant improvement when data of NASE stations were excluded. The poorer relationship between N025 and ILD was due to the negative N025 in some provinces (Table 4.2).

Nitrate and temperature profiles were characteristic features for a province (Figure 4.4). The temperature decrease from the surface to the bottom was followed by an increase in nitrate, and the stronger the temperature gradient was, the stronger the nitrate gradient was. A linear regression analysis showed better correlation between nitrate and temperature. The vertical distribution of nitrate could be described as a function of temperature within a province, and the strength of the relationship was dependent on the province (Table 4.4). These functions applied over a small temperature range, as indicated for each province. In CC and ETRA, where upwelled water was reaching the surface, nitrate vertical distribution was explained by temperature in the whole water column (250 m). The gradient in temperature was caused more by upwelling of nitrate richer water from the bottom. In other provinces, within the upper-warmer layer, the temperature did not explain the nitrate concentration. In the WTRA, the presence of lighter density

Table 4.4: Best results from linear and non-linear regression analyses to predict vertical distribution of nitrate ($NO_3$) from temperature. For each province (P), the equation applied (Eq) and the parameters estimated (a, b, c), $R^2$, the number of data (n), F-ratio (F) and probability (p) are presented. Equations applied were simple linear regression (S): $NO_3 = a + b\mathrm{T}$, log-linear (L): $\log_{10} NO_3 = a + b\mathrm{T}$, non-linear (NL): $NO_3 = 10^{(a+b\mathrm{T})}$ or second-order non-linear (2NL): $NO_3 = 10^{(a+b\mathrm{T}+c\mathrm{T}^2)}$. The temperature ([T], in °C) and the corresponding nitrate ([N], in $\mu$M) ranges from which the equations were generated are also indicated. Stations 6, 7 and 8 were accounted in the NADR' instead of in the NASE (see text for explanation).

| P | Eq | a | b | c | $R^2$ | n | F | p | [T] | [N] |
|---|---|---|---|---|---|---|---|---|---|---|
| NECS | L | 2.82 | -0.17 | - | 0.985 | 9 | 513.1 | $\ll 10^{-5}$ | 10 to 16.4 | 1.0 to 12.7 |
| NADR' | S | 30.9 | -1.92 | - | 0.635 | 39 | 67.0 | $\ll 10^{-5}$ | 11 to 16 | 1.2 to 9.7 |
| NASE' | NL | 3.73 | -0.19 | - | 0.738 | 48 | - | - | 14 to 19.6 | 1.0 to 12.1 |
| CC | L | 3.79 | -0.15 | - | 0.919 | 19 | 205.5 | $\ll 10^{-5}$ | 15 to 24.6 | 1.0 to 31.0 |
| WTRA | 2NL | -0.71 | 0.33 | 0.013 | 0.969 | 38 | - | - | 12 to 23.4 | 1.0 to 27.3 |
| ETRA | S | 49.5 | -2.01 | - | 0.980 | 85 | 4030.5 | $\ll 10^{-5}$ | 10 to 25 | 1.6 to 29.4 |
| SATL | L | 2.73 | -0.12 | - | 0.890 | 123 | 986.2 | $\ll 10^{-5}$ | 10 to 23.1 | 1.0 to 35.4 |
| RCBC | L | 2.93 | -0.15 | - | 0.614 | 37 | 58.3 | $\ll 10^{-5}$ | 10 to 19.1 | 1.0 to 25.2 |

AW in the surface, with depleted nutrient, impeded nitrate-rich WSACW from reaching the surface. In the northern hemisphere, within the ILD and part of the thermocline, temperature did not explain the nitrate vertical distribution. In the southern gyre, the upper layer where temperature did not explain nitrate (T > 23.1 °C) was equivalent to the hook-like structure in the T-S diagram (Figure 4.3). Within this upper layer, the temperature gradient results probably from local seasonal heating and is not due to the upwelling of cooler water. The temperature-nitrate relationship was detected at that part of the water column where the seasonal heating was minimum.

This temperature-nitrate relationship was not exclusively characteristic of a province. An inter-province relationship for nitrate and temperature was detected. Stations 6, 7 and 8

(north of NASE) were analysed alongside NADR stations yielded better relationship than when those north NASE stations were considered with other NASE stations, although the water masses were different between NADR and NASE provinces (Figure 4.3). The water mass analysis had shown clear difference in the physical structure between these two provinces. Probably local conditions were more similar between NADR and northern NASE than between the northern NASE and other NASE stations.

The water mass analysis showed the province characteristic was highly driven by the physical structure of the water column. The nitrate analysis complemented that analysis, showing that the local conditions also strongly affect some provinces. The nitrate profile also could be characterised at province bases . The water mass distribution and regional seasonal heating were decisive in province characterisation and detection.

### 4.4.3 Chl*a*

Chl*a* distribution along the AMT11 transect is presented in Figure 4.5 with the depth of the nitracline overplotted. In general, the depth of maximum Chl*a* concentration matched to the depth of the nitracline, with a statistically significant coefficient of determination between them (Table 4.3).

The total Chl*a* concentration ranged from 0.02 mg $m^{-3}$ to 6.7 mg $m^{-3}$ across the AMT11 transect (Figure 4.5). To avoid mis-interpolation due to the large gradient in concentration between the first and second CTD stations, CTD station 1 is not considered for grid interpolation, so the highest Chl*a* concentration (6.7 mg $m^{-3}$, see Table 4.2) is not shown in Figure 4.5. The second highest Chl*a* concentration along the transect occurred at surface waters of ETRA with 0.5 mg $m^{-3}$. At NADR, CC and WTRA the maximum (0.3 mg $m^{-3}$) were found at the subsurface (50 m depth). The Chl*a* concentration follows the

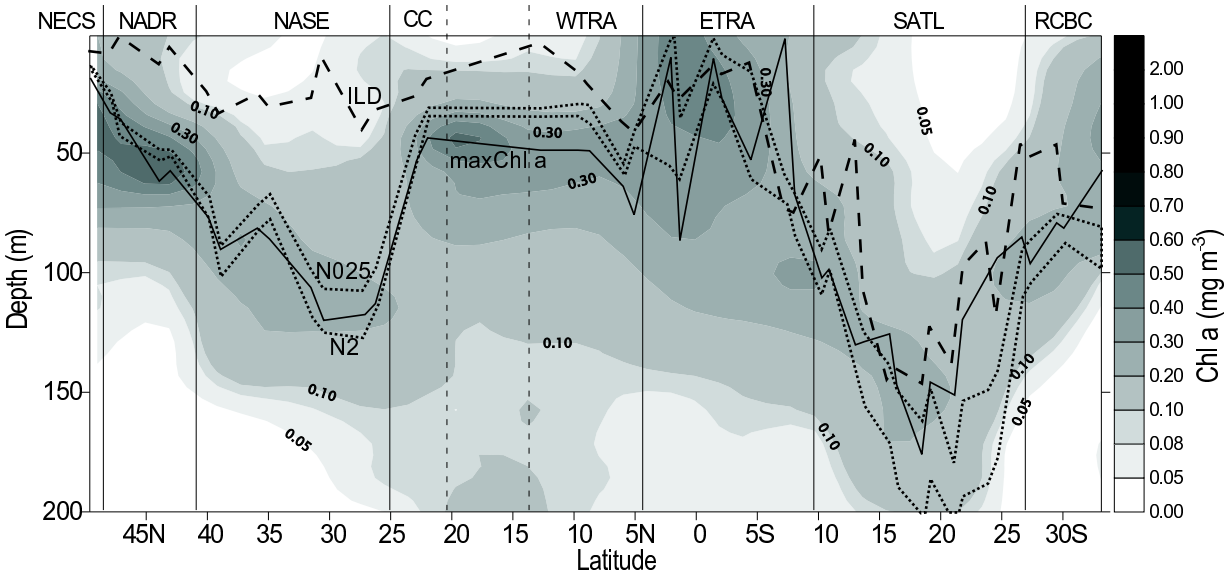


Figure 4.5: Total Chl*a* distribution along AMT11 transect. Depths of nitracline (dotted line, N025 and N2), isothermal layer depth (dashed line, ILD) and maximum Chl*a* (solid line) are indicated. Chl*a* was estimated from CTD fluorescence calibrated with HPLC total Chl*a*. The depth of maximum Chl*a* was taken from station profile, so it may not match with the background Chl*a* from gridding.

vertical distribution of nitrate and again, any doubts about whether the station 14 was sampled in NASE or CC, e.g. not clear from the physical structure analysis, could be removed by the depth of the maximum Chl*a* and its concentration. In CC the maximum Chl*a* concentration was much higher than in the gyre (Table 4.2 and Figure 4.5) reinforcing the results of province identification with physical structure. At the northern margin of SATL (station 30-33), the DCM is still shallower than 110 m and the maximum Chl*a* concentration is higher than 0.3 mg $m^{-3}$. At SATL*, the DCM is much deeper (maximum DCM at 150 m) and with lower concentrations of Chl*a* ($< 0.25$ mg $m^{-3}$) than in the NASE (DCM $< 120$ m and Chl*a* $> 0.27$ mg $m^{-3}$). The depth of DCM and the maximum Chl*a* concentration are presented in Table 4.2. Surface waters of the gyres have their Chl*a* around 0.03 mg $m^{-3}$. The general trend is that the depth of maximum Chl*a* is coincident with the depth of nitracline rather than the ILD, since at the North Atlantic the ILD is

much shallower than the DCM and nitracline (Figure 4.5 and Table 4.2).

## 4.5 Final considerations and conclusions

In this chapter, a set of station data were analysed for identification of the province where the station took place. Isothermal layer depth (ILD) and the temperature within the ILD, the depth of the nitracline, the depth of maximum Chl*a* and its concentration were analysed first, by summarising these parameters in a table. Then temperature and salinity of upper 200 m were analysed by temperature-salinity diagram, detecting of the source water mass and alterations. The source water mass and the alterations on it were similar within a province and of easy visualisation, supporting province analysis presented in Table 4.2. Although this sequence of analyses, worked well, it was time consuming and subjective and the data for each province were very diverse even within a province (Table 4.2). On the other hand the temperature and salinity diagram and the nitrate vertical profile showed very consistent features within a province (Figure 4.3). Even though surface waters are altered by environmental influence (seasonal heating), the upper layer water column down to 200 m still had characteristics of the source water masses. Although physical characteristic changes in the shallowest part of the water column, these changes and the source water mass characterise the provinces very clearly. The results of the analyses indicated that the T-S diagram analysis with water mass identification gives quicker and more reliable evidence about the province and that the other data can support or remove any doubts in case of small distinction in the T-S plots between adjacent provinces. Although only one cruise was analysed in this work, the T-S diagrams showed clear distinction between adjacent provinces, proving that this method is worth consideration for application in other cruises. The T-S diagrams obtained in this

work can be used as a reference for subsequent cruises, making it easier to identify the province in *real time* just after the CTD data processing.

Normally nitrate was depleted within the ILD, but deeper nitrate could be described as a function of temperature within a province. Because nitrate was depleted within the ILD in most of the provinces, the use of sea surface temperature images to predict nitrate is questionable. Estimation of nitrate from sea surface temperature imagery can be applied only in provinces where there is upwelling occurring and the water upwelled is reaching the surface. In provinces where nitrate was deplete in the upper layer, the detection of the depth of isothermal layer or mixed layer are important because below that depth, the vertical distribution of nitrate was strongly related to the vertical distribution of temperature for the whole transect. These simple nitrate-temperature relationships were derived from only one transect, so they might not be a final description of nitrate distribution in a province. More analyses are required.

The depth of maximum Chl*a* concentration was strongly related to the nitracline, so the physical processes were indirectly driving the Chl*a* distribution.

# Chapter 5

# Phytoplankton community structure

## 5.1 Introduction

The development of High Performance Liquid Chromatography (HPLC) and its application to determine plant pigments (Jeffrey *et al.* 1997 and references there in) has improved our knowledge about phytoplankton pigment distributions across the ocean. The HPLC method can separate all the main chlorophylls and carotenoids (Mantoura and Llewellyn 1983, Jeffrey *et al.* 1997, Barlow *et al.* 1997a, Garrido *et al.* 2000, Zapatta *et al.* 2001), which are used to identify different phytoplankton taxa.

This chapter analyses the structure of the phytoplankton community across the Atlantic Ocean and gives background for the phytoplankton primary production. Due to the variety of provinces sampled in the AMT11 (Chapter 4), a pattern in the phytoplankton community is expected that can be linked to the provinces.

## 5.2 Data collection

AMT11 crossed the Atlantic Ocean mostly through oligotrophic regions (Chapter 4), with mainly low biomass. To give a bigger range in the phytoplankton taxa and more contrast, another set of data collected during the BENEFIT-L1 cruise is combined with the AMT11 data for the phytoplankton community structure analysis. In this chapter the pigments sampled during the AMT11 (Chapter 3) and BENEFIT-L1 cruises are analysed to characterise phytoplankton community structure in the Atlantic Ocean.

### 5.2.1 Benguela Environment Fisheries Interaction and Training

The Benguela Environment Fisheries Interaction and Training (BENEFIT) Programme is a regional partnership between Namibia, Angola and South Africa focused on fisheries and the marine resources of the Benguela Current ecosystem off southwest Africa. The cruises are for training purposes but high quality hydrographic data was possible during the first leg (BENEFIT-L1) of the February 2002 cruise, on board Fisheries Research Ship Africana. The BENEFIT-L1 started in Cape Town (South Africa) on the February 15$^{th}$ and ended seven days later in Walvis Bay (Namibia) (Figure 5.1). Sampling took place at about every other hour from pre-dawn till dusk. At each station CTD/rosette rig was deployed before or after bio-optical rig deployment. The bio-optical rig consisted of spectral irradiance and radiance sensors (attached to a logger), FRR fluorometer with PAR and pressure sensors. Station numbers used in this document refer to the bio-optical station numbers.

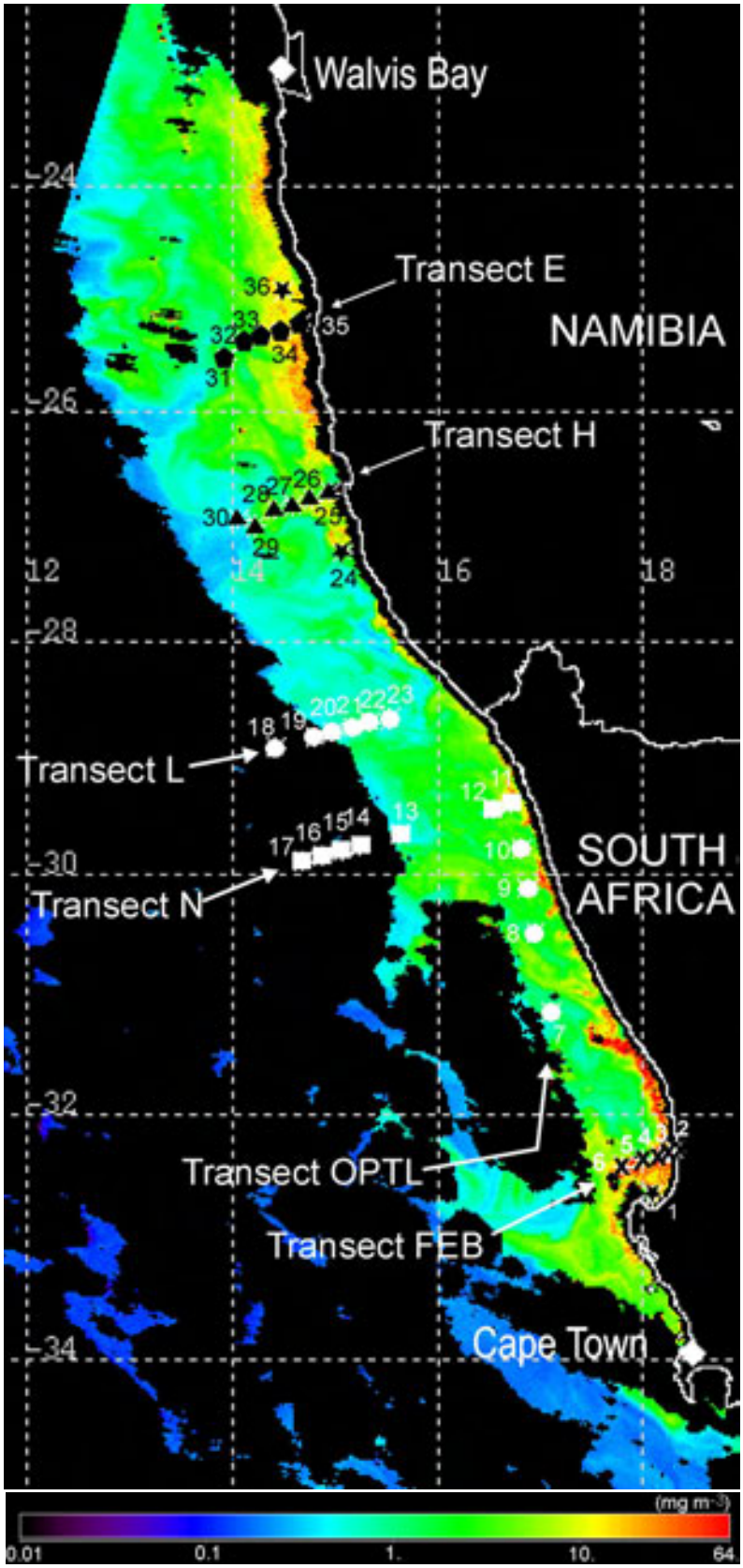


Figure 5.1: BENEFIT-L1 bio-optical stations and the surface Chl*a* distribution from SeaWiFS (24 February 2002). Different transects are indicated by different symbols. Stations indicated by star were not included in any of the transects.

### 5.2.2 High Performance Liquid Chromatography

HPLC pigments for AMT11 were determined as explained in Chapter 4.

During the BENEFIT-L1, 0.3 to 2.0 L of water were filtered onto 25 mm GF/F glass fibre filters (Whatman). The filters were kept frozen in liquid nitrogen and analysed in the Marine & Coastal Management (MCM), Cape Town, South Africa[1]. The sample was extracted in 2.0 to 5.0 mL of 90 % acetone by ultrasonication and centrifugation and then the extract loaded into a Thermo Separations AS3000 autosampler following the method described by Barlow *et al.* (1997a). The equipment used for analysis of the BENEFIT-L1 data was a Varian ProStar tertiary pump and Thermo Separations UV6000 diode array detector. The procedure detects the pigment at 440 nm and the chlorophyllide *a* at 665 nm, and the pigment confirmation spectral data was from 400 to 700 nm with 1 nm intervals. The internal standard was 8-apo-carotenal. Apart from the Chl*a* standard from Sigma and the carotenal from Fluka, all the standards were from DHI Water and Environment (formerly VKI Insitute). Chromatographic data were processed using the ChromQuest Chromatography Software.

### 5.2.3 Particulate absorption coefficient

The total particulate matter absorption spectra for the AMT11 were measured with GF/F Millipore filters fitted with an opal glass on a single beam Beckman DU650 scanning (350-750 nm) spectrophotometer. The light absorption by particulate detritus was estimated numerically following the method of Bricaud and Stramski (1990) improved for low detritus content (Varela *et al.* 1998).

[1]HPLC data from BENEFIT-L1 were provided by Ray Barlow (MCM, Cape Town, South Africa)

For both cruises, 0.3 to 3.0 L of water were filtered onto 25 mm GF/F glass fibre filters. The filters from the BENEFIT-L1 (Whatman) were kept frozen in liquid nitrogen and analysed in the laboratory following Tassan and Ferrari (1995) and Roesler (1998). The spectral absorption was scanned on whole cells on the filters, then bleached with sodium hypochlorite, scanned again for detritus absorption to correct for phytoplankton absorption.

## 5.3 Phytoplankton groups

The phytoplankton can be roughly grouped into five major taxa: cyanobacteria, prochlorophytes, nanoflagellates, dinoflagellates and diatoms. The nanoflagellates included prymnesiophytes, chrysophytes, cryptomonads and green algae (Chlorophyceae and Prasinophyceae). These phytoplankton taxa can be represented by their marker pigments (Barlow *et al.* 1997b, Gibb *et al.* 2000, Gibb *et al.* 2001): zeaxanthin (ZEA) for prokaryotes (cyanobacteria and prochlorophytes), DVChl*a* for prochlorophytes, fucoxanthin (FUC) for diatoms, peridinin (PER) for dinoflagellates, 19'-hexanoyloxyfucoxanthin (HEX) for prymnesiophytes, 19'-butanoyloxyfucoxanthin (BUT) for chrysophytes, alloxanthin (ALL) for cryptomonads, Chl*b* for green algae, prochlorophytes and some dinoflagellates with endosymbionts. The latter four pigments were used as an indicator for nanoflagellates as a whole, with extra care taken for Chl*b*, since its presence could be due to non-green algae, as explained in detail in Appendix C. Some dinoflagellates lack PER and have endosymbionts instead, which makes this dinoflagellates to have pigments typical of these endosymbionts (e.g. prymnesiophytes, crysophytes, cryptomonads and chlorophytes. Although extra care was taken for Chl*b* (chlorophytes), the effect of other three endosmbionts are not considered. Prochlorophytes were accounted twice by these marker pigments, once

as prokaryotes in ZEA and again as prochlorophytes in DVChl*a* because none of these pigments alone could give all the information provided together, so none of them were discarded. Cyanobacteria was only taken into account in ZEA, since no phycobilins were analysed. At deeper depths in the water column, where photoprotection is not required, there is no ZEA. Thus DVChl*a* is the unique representative pigment of the prochlorophytes at these depths. FUC is assumed to represent diatoms only but this pigment can be found also in prymnesiophytes (Jeffrey *et al.* 1997).

## 5.4 Pigment ratios

The HPLC analysis quantified a large number of pigments that were considered marker pigments of phytoplankton groups. However because most of the pigments can be present in different groups of phytoplankton, a straight analysis over these pigments cannot provide a reasonable representation of phytoplankton group presence/absence. As a test, a preliminary study has been conducted analysing 19 HPLC pigments, joining all the Chl*c*-like pigments as totChl*c*. All the Chl*a*-like pigments epimer Chl*a* and allomeric Chl*a* were accounted together with MVChl*a* as totMVChl*a* (MVA), following the Mackey *et al.* (1997) method (DVChl*a* separated from MVChl*a*). The Chlorophyllide a was considered as MVChl*a* because of their similar absorption spectra (Jeffrey *et al.* 1997). The cluster and subsequent non-metric multi-dimensional scaling (MDS) ordination analyses did not give good discrimination, even with standardised data (MDS stress = 0.12). As an attempt to improve the overall analysis, the starting point for the statistical analysis was based on the biological knowledge of phytoplankton pigments, analysing the pigment ratios as variables instead of the pigments themselves.

### 5.4.1 MVChl*a*-ratios

Many chemotaxonomy analyses apply ratios of the marker pigments to Chl*a* concentration (Barlow *et al.* 1997b, Mackey *et al.* 1997) to assess the phytoplankton community structure. The HPLC method used, separated the DVChl*a* from the MVChl*a* allowing better discrimination of the phytoplankton groups, so the MVChl*a*-ratio was more certain. Following these reasonings, the five phytoplankton groups (prokaryotes, prochlorophytes, nanoflagellates, dinoflagellates and diatoms) were represented by their marker pigments normalised by totMVChl*a*, hence named MVChl*a*-ratios. The MVChl*a*-ratios represented the prokaryotes (PROK = ZEA/MVA), the prochlorophytes (PROC = DVChl*a*/MVA), the nanoflagellates (NANO = marker pigments for nanoflagellates/MVA), the dinoflagellates (DINO = marker pigments for dinoflagellates/MVA) and the diatoms (DIAT = FUC/MVA). The marker pigments for the nanoflagellates and dinoflagellates are discussed in the Appendix C.

### 5.4.2 Optical-ratios

To consider the adaptation level of the phytoplankton community to light exposure, all the pigments (PIG) detected by the HPLC method were split into four groups: total Chl*a* (totChl*a*= MVChl*a* + epimerChl*a* + allomericChl*a* + DVChl*a*), all the Chl*b* and Chl*c* (all the Chl*b* and Chl*c*-like pigments: Chl*b*, Chl$c_3$, MVChl$c_3$, MgDVP, Chl$c_2$, Chl$c_2$-*Eh* and Chl$c_2$-*Cp*[2]), total photosynthetic carotenoids (totPSC) and total photoprotectant (non-photosynthetic) carotenoids (totPPC).

[2]Chl$c_2$-*Eh* and Chl$c_2$-*Cp* are the pigments Chl$c_2$-moiety esterified to a monogalactosyldiacylglyceride (Chl$c_2$-MGDG) found in *Emiliania huxleyi* (Garrido *et al.* 2000) and in *Chrysochromulina polylepis* (Zapata *et al.* 2001), respectively.

For the AMT11 data, where the $\beta$,$\varepsilon$-CAR and $\beta$,$\beta$-CAR were separated, the former was included in the totPSC besides FUC, HEX, BUT, PRA and PER (Bricaud *et al.* 1995, Babin *et al.* 1996 and Stón *et al.* 2000). For the BENEFIT-L1 data, these two carotenes were not separated. In this case, the total CAR ($\beta$,$\varepsilon$-CAR + $\beta$,$\beta$-CAR) was included in the totPPC with VIO, ZEA, ALL, DIAD, DIAT, LUT and NEO (Bricaud et al. 1995, Babin et al. 1996, Stón et al. 2000, Trees et al. 2000).

The optical ratios were the ratios of each of these four pigment groups to the total pigments: CHA = totChl*a*/PIG; CHBC = (Chl*b* + totChl*c*)/PIG; PSC = (totPSC)/PIG and PPC = (totPPC)/PIG. They were named simply by their numerator acronyms as were the MVChl*a*-ratios.

## 5.5 Statistical analysis

The nature of multivariate data set leads to analytical method as it has been done frequently in environmental and species composition data analysis (Clarke and Warwick 2001). Recently, analytical methods have been applied to plankton data (Latasa and Bidigare 1998, Widdicombe *et al.* 2002) and a similar approach was adopted here.

The 176 samples with nine ratios were $4^{\text{th}}$-root transformed[3] to allow better detection of the MVChl*a*-ratios. For example, the presence/absence of DVChl*a* have as much meaning as the difference in the quantity of DVChl*a*, so the $4^{\text{th}}$-root transformation maximises the difference between presence and absence of marker pigments while minimising the difference between quantities when the pigments are present (Clarke and Warwick 2001). The similarity matrix was calculated throught Bray-Curtis coefficient and then clustered

[3] $4^{\text{th}}$-root transformation is to take the square root twice, e.g., $\sqrt{\sqrt{ratio}}$.

through group average cluster analysis.

The similarity analysis (SIMPER analysis in PRIMER-E v5) was applied to assess which ratios contributed more for the clustering: how similar were the samples within a cluster and how dissimilar were the samples between two clusters.

## 5.6 Results and Discussion

### 5.6.1 Cluster analysis

The dendrogram resulting from the group average linkage cluster analysis is presented in Figure 5.2. An arbitrary level was chosen for clustering (similarity level of 90 %), resulting in seven clusters: A, B, C, D, E, F and G (Figure 5.2) with one outlier (B24-9.5). The distribution of pigments and the Clusters along the AMT11 (Figures 5.3, 5.4 and 5.5) and along the six BENEFIT-L1 temperature transects (Figures 5.6 and 5.7) are presented.

Three of the Clusters were exclusive from one of the cruises and the other four originated mainly from waters of one of the cruises. The two cruises were of extreme characteristics, the AMT11 crossed oligotrophic ocean gyres, while BENEFIT-L1 sampled the eutrophic waters of an coastal upwelling. Cluster B was formed exclusively of water samples collected at the deep chlorophyll maximum (DCM) along the AMT11 transect. Cluster D was the smallest, with only three samples from red[4] tide, in the Benguela upwelling. Cluster F was another BENEFIT-L1 group from exclusively green water, off Namibian coast.

Other clusters were formed mostly of samples from one of the cruises but with a few samples from the other cruise. Cluster A consisted of samples collected at the surface of

[4]Red tide, green water and blue water: the colours refer to that perceived by naked eyes at the time of sampling.

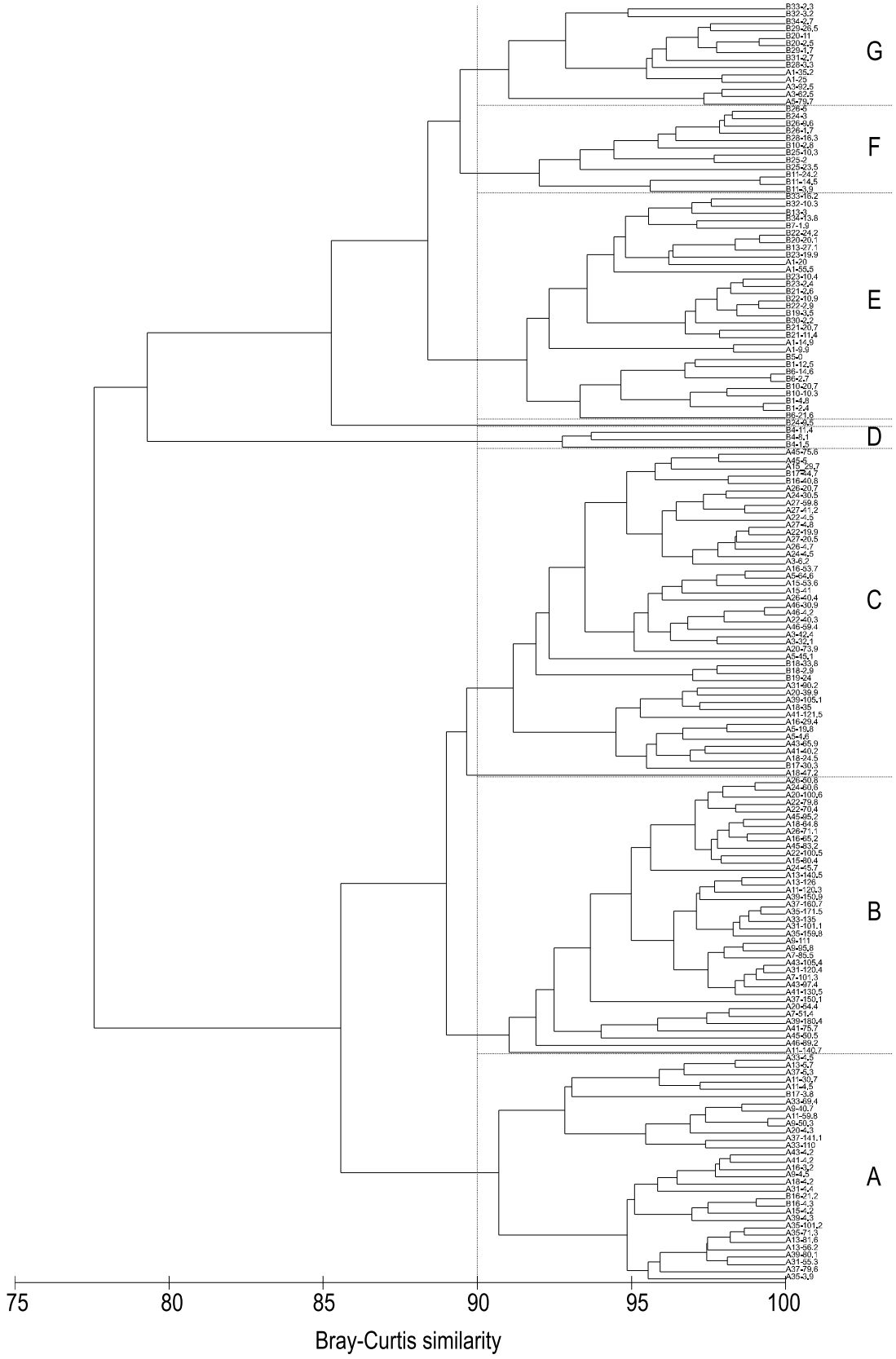


Figure 5.2: Dendrogram of cluster analysis of HPLC pigment ratios. The samples are labeled as Cxx-zz.z where C is the cruise label (A for AMT11 or B for BENEFIT-L1), xx is the cruise station number (bio-optical station number for the BENEFIT-L1) and zz.z is the sampling depth (m).

a) totChl*a*

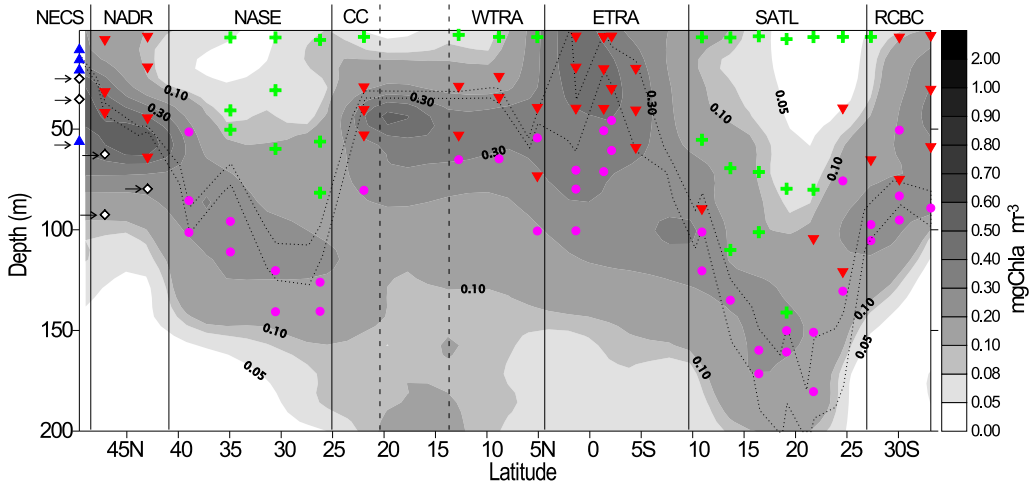


b) zeaxanthin

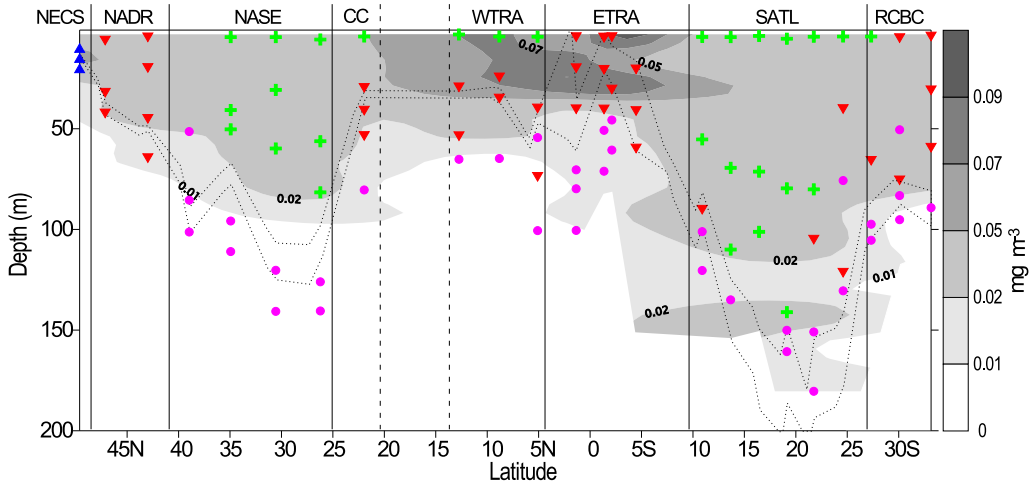


c) peridinin

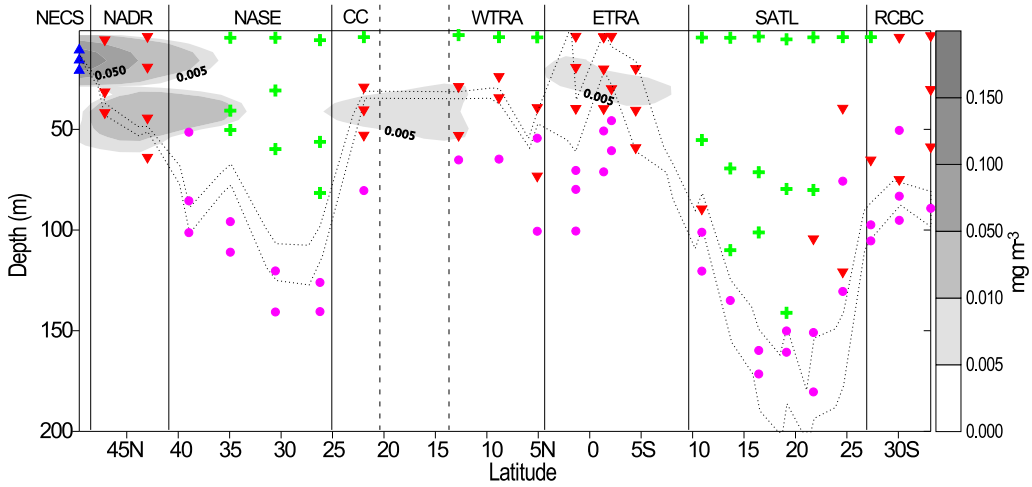


Figure 5.3: Distribution of the pigment clusters and a) totChl*a*, b) zeaxanthin and c) peridinin along the AMT11 transect. Arrows indicate senescent samples. Dotted lines are the depth of nitracline N025 and N2. The Clusters are: A (green plus sign), B (pink circle), C (red down triangle) and E (blue up triangle).

a) DVChl*a*

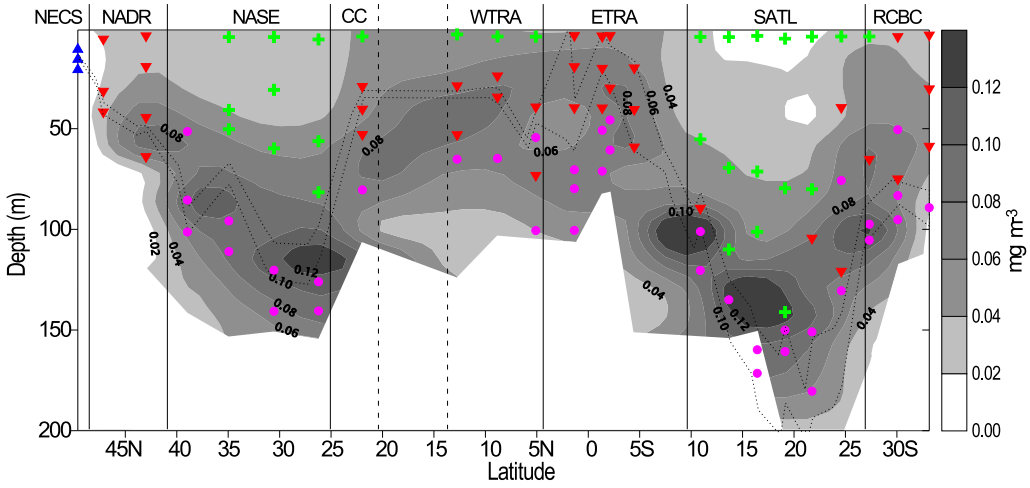


b) fucoxanthin

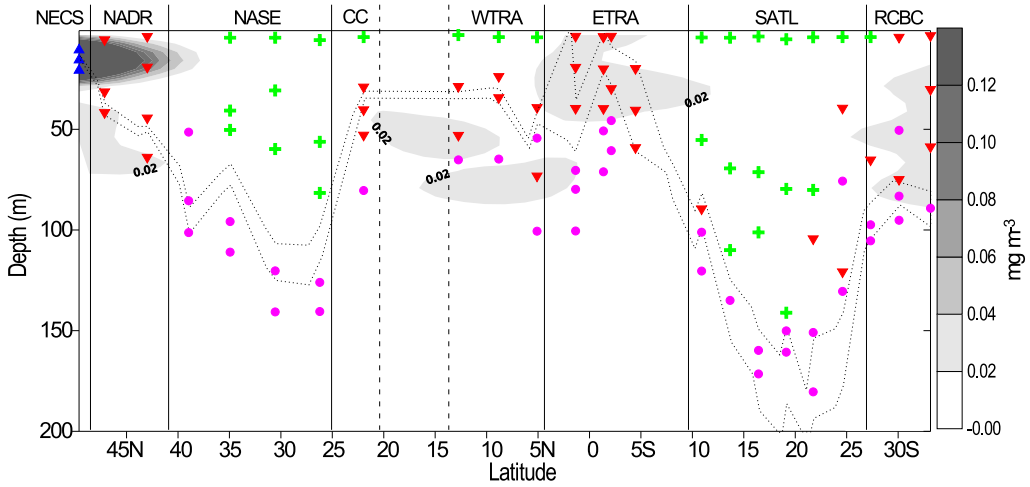


Figure 5.4: Distribution of the pigment clusters and a) DVChl*a* and b) fucoxanthin along the AMT11 transect. Dotted lines are the depth of nitracline N025 and N2. The Clusters are: A (green plus sign), B (pink circle), C (red down triangle) and E (blue up triangle).

a) 19'-hexanoyloxyfucoxanthin

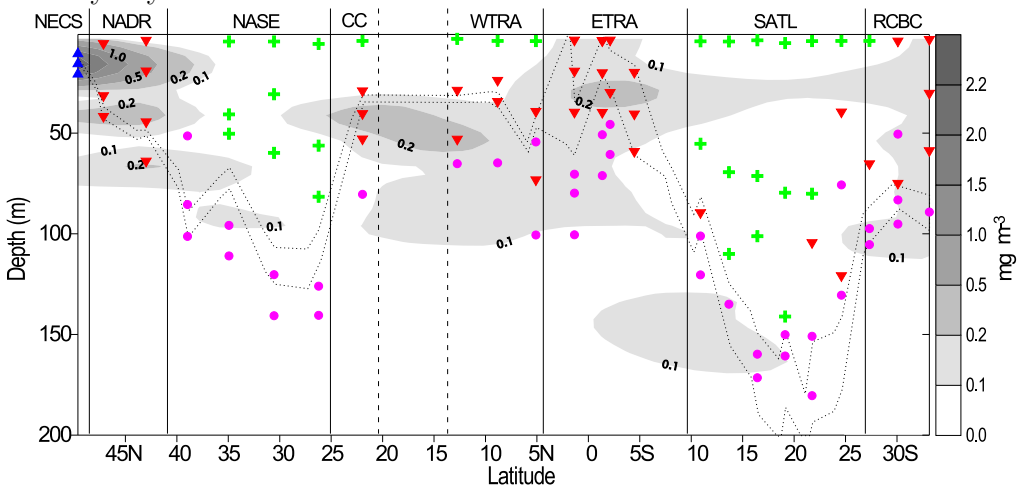


b) alloxanthin + 19'-butanoyloxyfucoxanthin

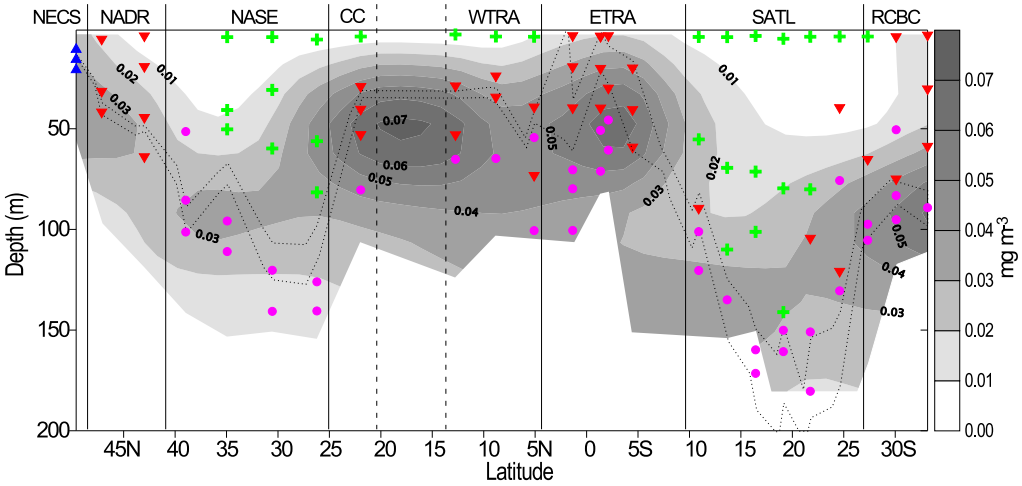


c) totChl*b*

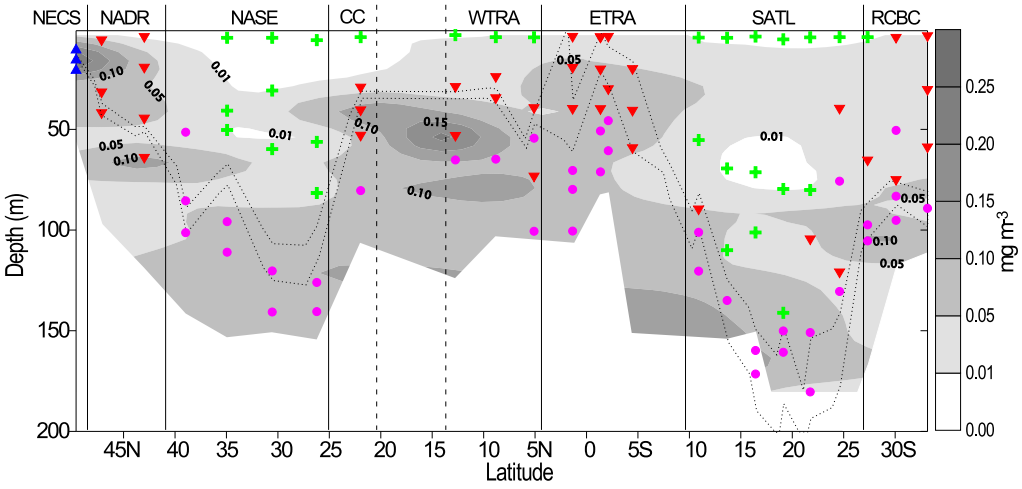


Figure 5.5: Distribution of the pigment clusters and a) HEX, b) ALL + BUT and c) totChl*b* along the AMT11 transect. Dotted lines are the depth of nitracline N025 and N2. The Clusters are: A (green plus sign), B (pink circle), C (red down triangle) and E (blue up triangle).

a) Transect FEB

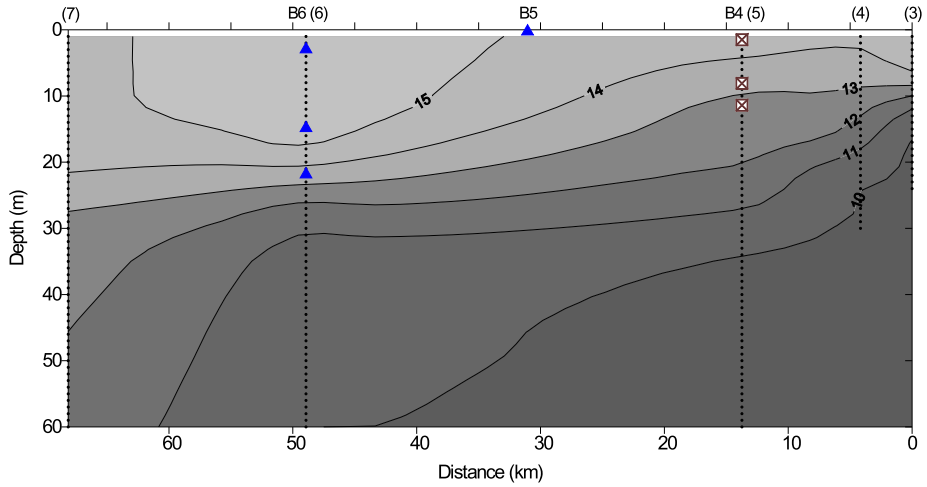


b) Line OPTL

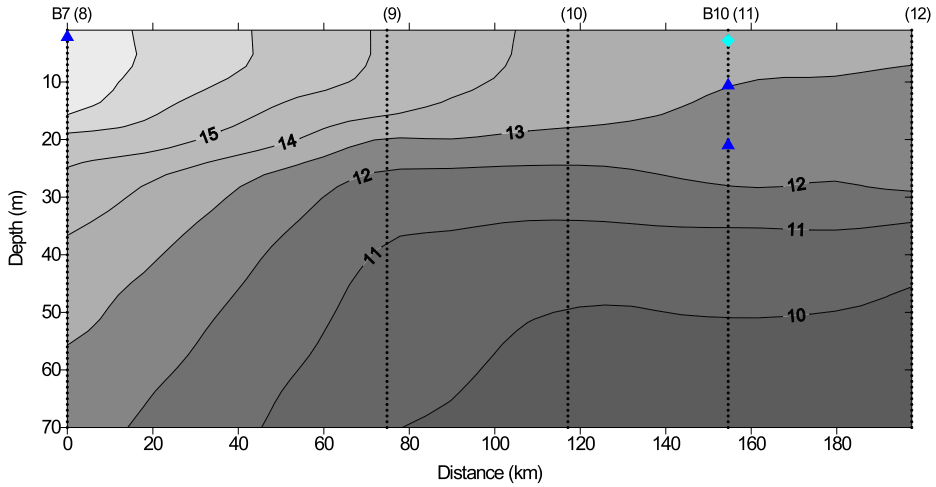


c) Line N

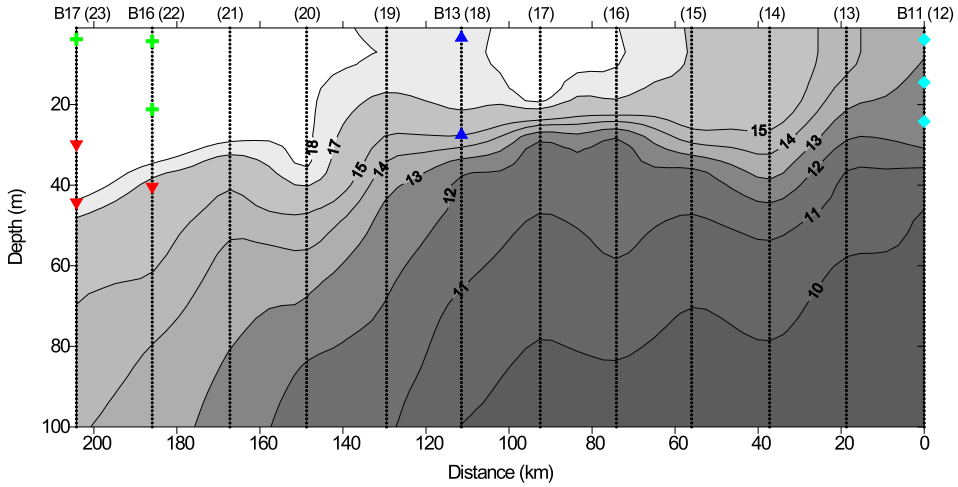


Figure 5.6: BENEFIT-L1 temperature contours and pigment clusters for Transect FEB, Line OPTL and Line N. The Clusters are indicated: A (green cross), C (red down triangle), D (brown crossed square), E (blue up triangle), F (cyan filled diamond) and G (black open diamond).

a) Line L

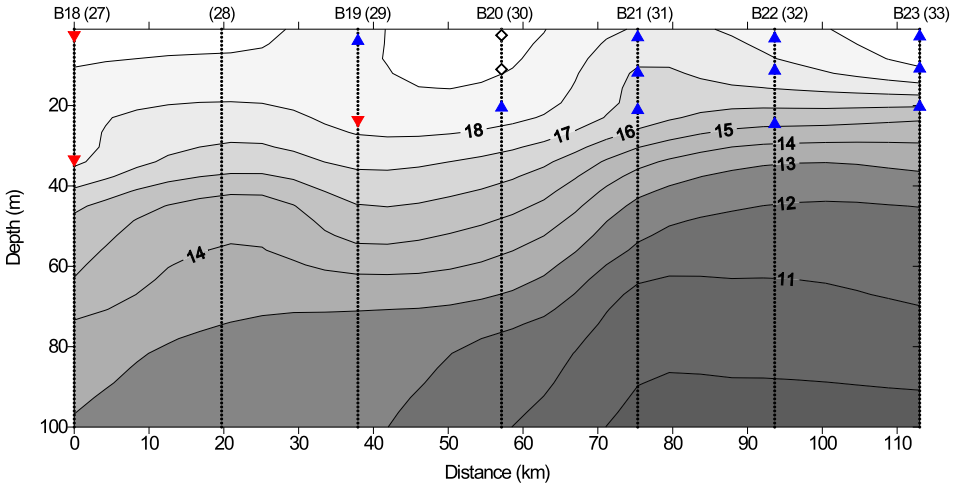


b) Line H

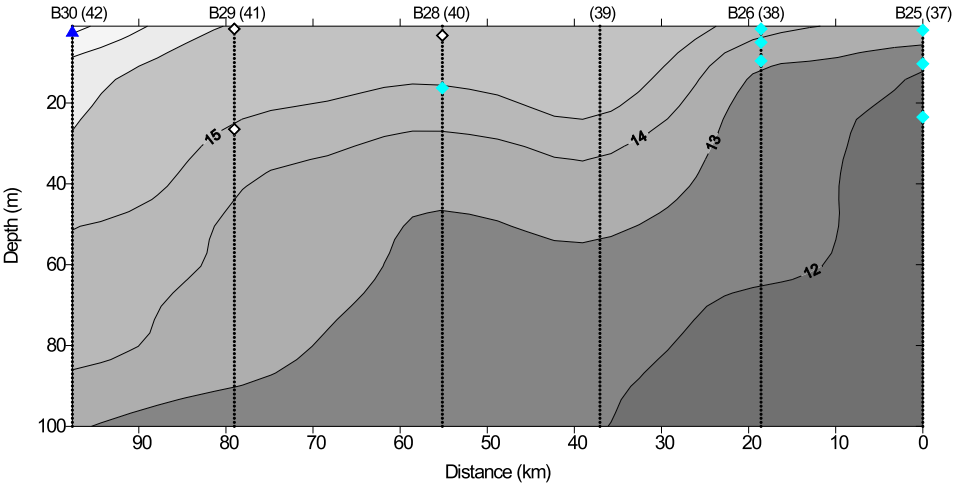


c) Line E

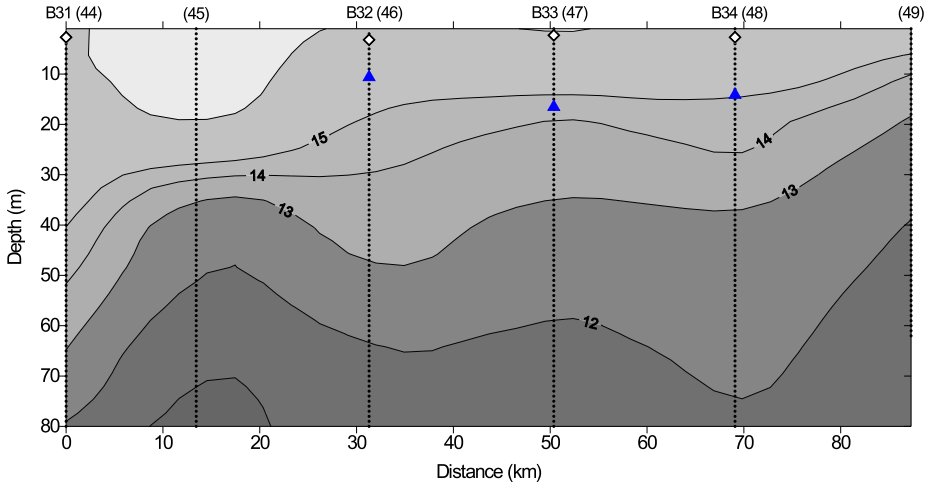


Figure 5.7: BENEFIT-L1 temperature contours and pigment clusters for Lines L, H and E. The Clusters are indicated: A (green cross), C (red down triangle), D (brown crossed square), E (blue up triangle), F (cyan filled diamond) and G (black open diamond).

the oligotrophic gyres and at the surface of blue waters adjacent to the Benguela upwelling. Cluster C was formed by waters from the Equatorial upwelling of the Eastern Tropical Atlantic Province (ETRA), surface waters of North Atlantic Drift Province (NADR), Recirculation Cells of Brazil Current (RCBC) and from the DCM of the BENEFIT-L1 blue waters. Cluster E comprised Station 1 of AMT11, situated on the continental shelf (NECS), with others from the BENEFIT-L1 cruise. The Cluster G had representatives from the AMT11 transect and also from the surface along BENEFIT-L1 cruise.

Applying again the $4^{th}$-root transformed ratios and Bray-Curtis similarity, the resulting Clusters were ordered in two dimensions (no scale) through MDS ordination (Figure 5.8a). This allows the visualisation of samples distribution in between each other, based on the pigment ratio values. If the results of cluster analysis does not match to that of MDS ordination, e.g. samples of distinct clusters are mixed in the MDS ordination, that is because the samples are not distinct from each other based in the pigment ratios. The MDS ordination presented a stress considered good[5] (Clarke and Warwick 2002) Figure 5.8. The bubble size of each sample is related to the Chl*a* concentration[6], the biggest the bubble, the highest the Chl*a* concentration. The lowest Chl*a* samples were grouped as Cluster A (A37-5.3 with 0.018 mg $m^{-3}$) and the most concentrated ones as Cluster D (B4-8.1 with 43.27 mg $m^{-3}$). Although Chl*a* concentration was not included as a variable for the cluster analysis, the resulting Clusters reflected it very well, confirming the nine input ratios were connected to the Chl*a* concentration (Figure 5.8a). It can be observed that Chl*a* concentration increased from the Clusters on the left to those on the right side of the graphic, minding that the difference in bubble sizes was minimised by the square root transformation. Summarising all the pigments into these nine ratios gave better

[5]Stress values <0.05 (excellent representation), < 0.1 (good), < 0.2 (still useful), > 0.3 (the samples are close to being arbitrarily placed) (Clarke and Warwick 2002)

[6]The bubble size corresponds to the root square of respective Chl*a* concentration.

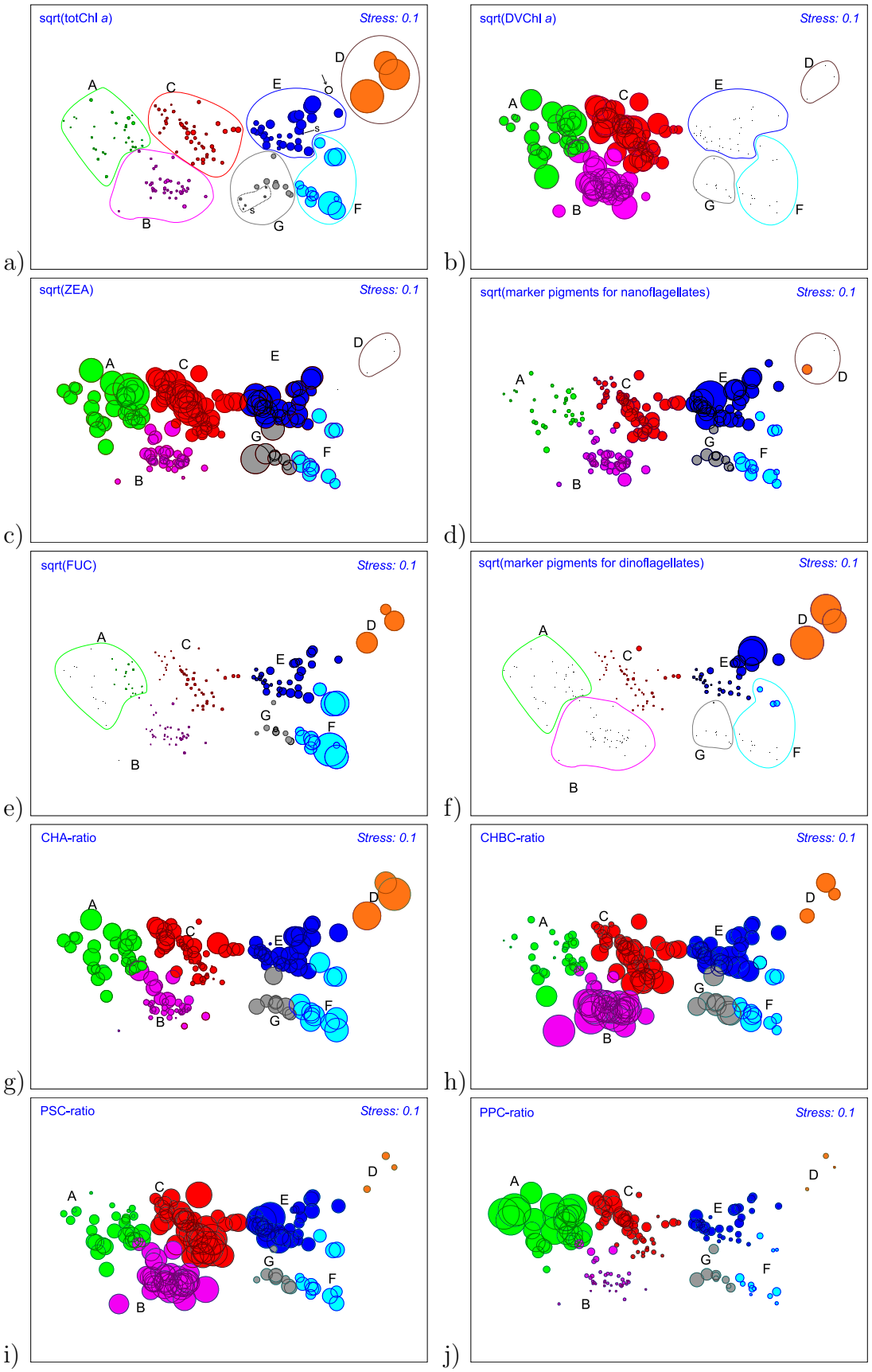


Figure 5.8: MDS of pigment ratios overplotted with pigment cluster analysis. The bubble size of the samples is proportional to the square root of concentration of a) totChl*a* with senescent (s) and outlier (arrow) samples, b) DVChl*a*, c) zeaxanthin, d) nanoflagellates pigments, e) fucoxanthin, f) dinoflagellates pigments, or to its ratio values of g) CHA-ratio, h) CHBC-ratio, i) PSC-ratio and j) PPC-ratio. See text and Table C.1 for nanoflagellates and dinoflagellates marker pigments.

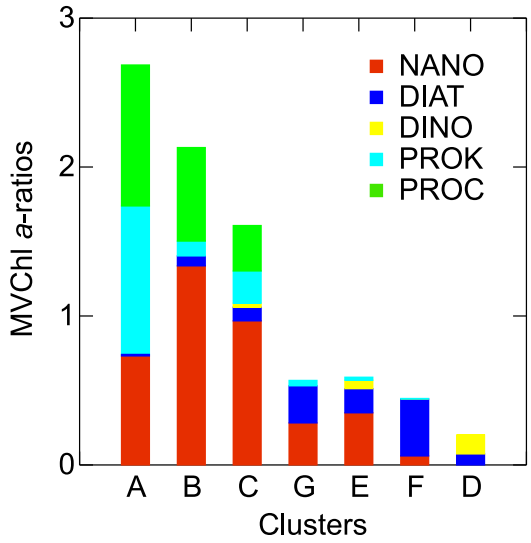


Figure 5.9: Average MVChl*a*-ratios for each pigment cluster. NANO-ratio is plotted from zero to its highest value, then DIAT-ratio is plotted on the top of NANO-ratio and so on. Chl*a* concentration incrases from the left to the right Clusters.

understanding (Figure 5.8a, MDS stress=0.10) than the standardised raw pigment data (MDS stress=0.12, not shown), analysed previously as a test.

### 5.6.2 Clusters and the phytoplankton groups

The average values of MVChl*a*-ratios are schematically represented in Figure 5.9 for easy visualisation of phytoplankton group composition in each Cluster. The average values of the ratios (presented later with analysis of similarity in Table 5.1) were not directly comparable to the MVChl*a*-ratios for monospecific samples (e.g. Mackey *et al.* 1996) because the field data had different phytoplankton groups contributing to the totMVChl*a* concentration while their marker pigments did not increase in same proportion, decreasing the MVChl*a*-ratio.

All the seven Clusters had very characteristic combination of MVChl*a*-ratios (Figure 5.9). The three Clusters with lowest Chl*a* concentration (A, B and C) were composed by very

distinct proportions of NANO-, PROC- and PROK-ratios. The following Clusters (D, E, F and G) had no PROC-ratio, low NANO-ratio and higher DIAT- and DINO-ratios. The sum of all the MVChl*a*-ratios for each of the oligotrophic Clusters were higher than 1.5, whilst other Clusters (D, E, F and G, $\overline{\text{Chla}}$>0.57 mg m$^{-3}$) had the sum of MVChl*a*-ratios less than 1. The linear regression analysis showed that the highest biomass (totChl*a*) had the smallest sum of MVChl*a*-ratios ($R^2_{adj}$=0.76, Figure 5.10). Five samples from the Cluster G and one from the Cluster E (reproduced in the left bottom corner of the graphic in Figure 5.9) were displaced with much lower totChl*a* concentration than expected by the relationship. Those samples were from waters deeper than the DCM of the AMT11 CTD stations 1, 3 and 5 (Figure 5.3, totChl*a*), so they were possibly ageing phytoplankton pigments, which had lost the normal pigment proportion. Assuming that the relationship presented in Figure 5.9 represents phytoplankton pigment relationship for not-ageing cells. These ageing samples could not be detected by analysing just the relationship between the accessory pigments and Chl*a* (Trees *et al.* 2000). Eliminating these samples, Cluster G became exclusive to BENEFIT-L1 and the re-clustering linked it to Cluster F at a similarity level higher than 90 %. Although the similarity between Clusters G and F became higher than the limit first applied, the latter Cluster had samples with much higher concentrations than those in Cluster G (Figure 5.8 totChl*a*, letter *s* indicates the senescent samples), which justified considering them as separate Clusters. The regression line was derived without these senescent data (Figure 5.10). The senescent samples are shown in Figure 5.8a only (indicated by letter *s*) and excluded from the subsequent analyses and figures. Even after the elimination of these ageing samples, Cluster G had a lower sum of MVChl*a*-ratios. These remaining samples had an amount of Chlorophyllide between 0.4 to 1.5 times that of Chl*a*, suggesting that the low sum of MVChl*a*-ratios of Cluster G could be due to the senescent phytoplankton. Cluster D also

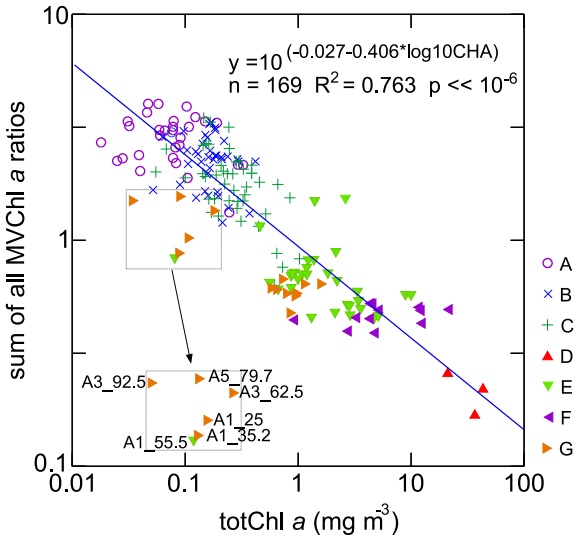


Figure 5.10: Relationship between sum of all MVChl*a*-ratios and the total Chl*a*. The Clusters are indicated by symbols and colours. The subset on the left bottom corner is the six samples identified as senescent samples. The linear regression line from the data without those six senescent samples is indicated by blue solid line.

had high amounts of Chlorophyllide a, which was about 2 to 3 times more than Chl*a*. Probably this cluster was also in a ageing state. In general, Chlorophyllide a in found at concentrations around 2 to 5 % of Chl*a* in most pigment samples because it is precursor molecule for Chl*a*. When Chlorophyllide a accounts for more than 20 % of totChl*a*, it is regarded as an indicator of senescent diatoms (Latasa and Bigigare 1998). This pigment has absorption characteristics very similar to Chl*a*, and chromatography (e.g. HPLC) is the only technique able to separate them (Jeffrey *et al.* 1997). Here, the ratios were analysed with Chlorophyllide a accounted for MVChl*a*, assuming that Chlorophyllide a resulted from degradation of MVChl*a*. Thus the sum between these two would be the MVChl*a* values expected when phytoplankton was before ageing. If Chlorophyllide a is not accounted for MVChl*a*, the MVChl*a*-ratios would increase for Cluster D and G.

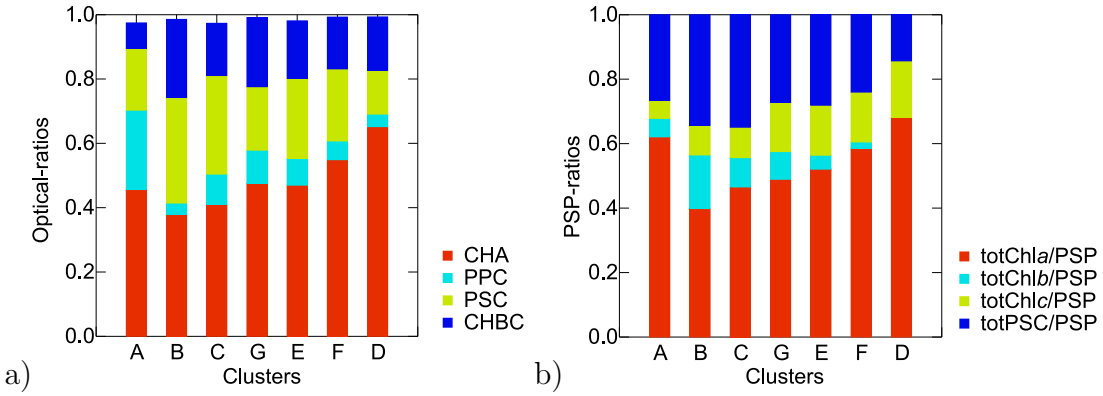


Figure 5.11: Average optical-ratios (a) and PSP-ratios (b) for each pigment cluster, without ageing samples. Chl*a* concentration increases from the left to the right Clusters. The sum of all four optical-ratios is smaller than 1 due to the $4^{th}$-root transformation procedure (see text).

### 5.6.3 Optical-ratios

The optical-ratios (Figure 5.11a) were not as characteristic as the MVChl*a*-ratios. The gap between the sum of all optical-ratios and 1 was due to the $4^{th}$-root transformation applied in the cluster analysis. The average value for the graphic was calculated by back-transforming the average of $4^{th}$-root transformed ratios per cluster, so most of the variability within a cluster was minimised, creating the gap. This gap resulted from the statistics applied to the cluster analysis, so Figure 5.11a is the most realistic representation of the method.

Comparing the Clusters dominated by eukaryotes (all except Cluster A) CHA-ratio tended to increase with totChl*a* concentration and decreasing PSC-ratio, showing the main photosynthetic pigment changed from photosynthetic carotenoids to Chl*a* with increase of Chl*a* concentration along the Clusters (Figure 5.11a). Cluster A did not follow this trend, probably due to a high presence of prochlorophytes. This phytoplankton has DVChl*a* as its main photosynthetic pigment, which was accounted for in the numerator of CHA-ratio.

If Chlorophyllide a was discarded from MVChl*a*, Clusters D, F and G would change considerably. CHA-ratio of Cluster D would drop down from 0.652 to 0.165 and the totChl*a* from 32.6 to 8.38 mg $m^{-3}$; Cluster F CHA-ratio from 0.549 to 0.503 and the totChl*a* from 5.79 to 5.33 mg $m^{-3}$; and Cluster G CHA-ratio from 0.475 to 0.348 and the totChl*a* from 0.91 to 0.63 mg $m^{-3}$.

**Photosynthetic pigments:** Breaking down the total photosynthetic pigments (totPSP) into chlorophylls and carotenoids per Cluster (Figure 5.11b), again Cluster A apart, the ratios totChl*b*/totPSP and totPSC/totPSP decreased with increasing Chl*a* concentration while, as expected, the opposite happened to the totChl*c*/totPSP, since the bigger cells (diatoms and dinoflagellates) have Chl*c* instead of Chl*b*, whilst smaller cells (nanoflagellates and prochlorophytes) have Chl*b* instead of Chl*c* (Rowan 1989).

### 5.6.4 Similarity within a Cluster

In general, the bigger the ratio value was, the more the ratio contributed to the similarity, but not always, because the consistency of that ratio value was also important. Table 5.1 presents the average similarity between the samples in a Cluster, the average value of the ratios, the contribution of the ratio to the Cluster similarity and also the totChl*a* concentration for each Cluster. The three oligotrophic Clusters (A, B and C) had the MVChl*a*-ratios as the highest contributors to the similarity, characterising first the phytoplankton group, followed by the CHA-ratio. The other Clusters, with higher totChl*a* concentration (D, E, F and G), had the CHA-ratio as the main contributor to their similarity. The optical-ratios were more important to the similarity than the phytoplankton taxa in communities dominated by bigger cells (diatom and dinoflagellates).

Table 5.1: Similarity within pigment clusters. The ratios are listed in decreasing order of their contribution in percentage (cont%) to the cluster's average similarity ($\overline{sim}$). For each cluster, the average ratio (M) and its mean lower (M-sd) and upper limits (M+sd) are presented; $\overline{\text{Chl}a}$ is the Cluster's average totChl$a$ in mg m$^{-3}$.

| Cluster A (n=31): $\overline{sim}$=92.89 | | | | | | | | | | |
|---|---|---|---|---|---|---|---|---|---|---|
| ratios | PROK | PROC | NANO | CHA | PPC | PSC | CHBC | DIAT | DINO | $\overline{\text{Chl}a}$ |
| M-sd | 0.685 | 0.654 | 0.472 | 0.418 | 0.175 | 0.134 | 0.046 | 0.000 | | 0.036 |
| M | 0.997 | 0.946 | 0.732 | 0.456 | 0.247 | 0.192 | 0.079 | 0.010 | | 0.078 |
| M+sd | 1.404 | 1.327 | 1.087 | 0.498 | 0.338 | 0.268 | 0.127 | 0.132 | | 0.152 |
| cont% | 17.16 | 16.94 | 15.74 | 14.72 | 12.18 | 11.41 | 8.97 | 2.88 | 0.00 | |

| Cluster B - AMT11 DCM (n=38): $\overline{sim}$=94.66 | | | | | | | | | | |
|---|---|---|---|---|---|---|---|---|---|---|
| ratios | NANO | PROC | CHA | PSC | CHBC | PROK | DIAT | PPC | DINO | $\overline{\text{Chl}a}$ |
| M-sd | 1.027 | 0.325 | 0.328 | 0.287 | 0.182 | 0.043 | 0.026 | 0.021 | | 0.11 |
| M | 1.337 | 0.628 | 0.379 | 0.328 | 0.243 | 0.099 | 0.067 | 0.035 | | 0.17 |
| M+sd | 1.711 | 1.107 | 0.436 | 0.374 | 0.317 | 0.199 | 0.144 | 0.055 | | 0.25 |
| cont% | 19.18 | 15.01 | 14.25 | 13.75 | 12.51 | 9.29 | 8.50 | 7.51 | 0.00 | |

| Cluster C (n=45): $\overline{sim}$=92.82 | | | | | | | | | | |
|---|---|---|---|---|---|---|---|---|---|---|
| ratios | NANO | CHA | PSC | PROC | CHBC | PROK | DIAT | PPC | DINO | $\overline{\text{Chl}a}$ |
| M-sd | 0.671 | 0.347 | 0.235 | 0.092 | 0.121 | 0.078 | 0.057 | 0.052 | 0.012 | 0.14 |
| M | 0.968 | 0.410 | 0.307 | 0.306 | 0.162 | 0.215 | 0.092 | 0.094 | 0.028 | 0.28 |
| M+sd | 1.353 | 0.481 | 0.394 | 0.767 | 0.213 | 0.484 | 0.140 | 0.158 | 0.056 | 0.49 |
| cont% | 16.63 | 13.81 | 12.66 | 11.14 | 10.78 | 10.40 | 9.10 | 8.98 | 6.50 | |

| Cluster D - BENEFIT-L1 red tide (n=3): $\overline{sim}$=93.07 | | | | | | | | | | |
|---|---|---|---|---|---|---|---|---|---|---|
| ratios | CHA | CHBC | PSC | DINO | DIAT | PPC | NANO | PROC | PROK | $\overline{\text{Chl}a}$ |
| M-sd | 0.582 | 0.131 | 0.123 | 0.073 | 0.049 | 0.023 | | | | 22.2 |
| M | 0.652 | 0.165 | 0.137 | 0.128 | 0.074 | 0.039 | | | | 32.6 |
| M+sd | 0.728 | 0.207 | 0.151 | 0.208 | 0.107 | 0.062 | | | | 46.3 |
| cont% | 24.94 | 17.34 | 16.89 | 15.42 | 13.89 | 11.53 | 0.00 | 0.00 | 0.00 | |

| Cluster E (n=30): $\overline{sim}$=93.27 | | | | | | | | | | |
|---|---|---|---|---|---|---|---|---|---|---|
| ratios | CHA | NANO | PSC | CHBC | DIAT | PPC | DINO | PROK | PROC | $\overline{\text{Chl}a}$ |
| M-sd | 0.411 | 0.161 | 0.188 | 0.155 | 0.099 | 0.054 | 0.017 | 0.005 | | 0.79 |
| M | 0.470 | 0.350 | 0.249 | 0.179 | 0.162 | 0.083 | 0.057 | 0.020 | | 1.94 |
| M+sd | 0.534 | 0.671 | 0.324 | 0.205 | 0.251 | 0.123 | 0.142 | 0.058 | | 4.02 |
| cont% | 17.49 | 14.83 | 14.60 | 13.69 | 12.72 | 10.85 | 9.04 | 6.78 | 0.00 | |

| Cluster F - BENEFIT-L1 green water (n=12): $\overline{sim}$=94.01 | | | | | | | | | | |
|---|---|---|---|---|---|---|---|---|---|---|
| ratios | CHA | DIAT | PSC | CHBC | PPC | NANO | PROK | DINO | PROC | $\overline{\text{Chl}a}$ |
| M-sd | 0.521 | 0.312 | 0.197 | 0.130 | 0.038 | 0.030 | 0.001 | 0.000 | | 2.30 |
| M | 0.549 | 0.382 | 0.224 | 0.161 | 0.058 | 0.060 | 0.003 | 0.000 | | 5.79 |
| M+sd | 0.579 | 0.464 | 0.255 | 0.197 | 0.086 | 0.109 | 0.012 | 0.004 | | 12.25 |
| cont% | 21.22 | 18.98 | 16.78 | 15.24 | 11.45 | 11.13 | 4.83 | 0.36 | 0.00 | |

| Cluster G (n=9): $\overline{sim}$=95.30 | | | | | | | | | | |
|---|---|---|---|---|---|---|---|---|---|---|
| ratios | CHA | NANO | CHBC | PSC | DIAT | PPC | PROK | PROC | DINO | $\overline{\text{Chl}a}$ |
| M-sd | 0.446 | 0.197 | 0.193 | 0.156 | 0.183 | 0.072 | 0.013 | | | 0.65 |
| M | 0.475 | 0.282 | 0.215 | 0.197 | 0.249 | 0.103 | 0.037 | | | 0.91 |
| M+sd | 0.507 | 0.393 | 0.239 | 0.246 | 0.331 | 0.144 | 0.085 | | | 1.22 |
| cont% | 18.59 | 15.68 | 15.30 | 15.15 | 14.58 | 12.15 | 8.56 | 0.00 | 0.00 | |

Cluster A had half of its similarity due to the MVChl*a*-ratios (PROK-, PROC- and NANO-ratios), which suggested that the phytoplankton taxa were more important to the similarity than the functional pigments (represented by optical-ratios). It also had the highest contribution from the PPC-ratio (12% to the similarity), a very low contribution from the DIAT-ratio and none from the DINO-ratio.

Cluster B had the highest NANO-ratio, which was the main contributor, with 19%, to the similarity of this Cluster. Other main contributors to Cluster B similarity were the high PROC-ratio, the lowest CHA-ratio, the highest PSC-ratio and CHBC-ratio, low PROK-ratio and DIAT-ratio. From all the Clusters, this was the most adapted to the low light regime.

Cluster C was the most heterogeneous with all the phytoplankton taxa present. The contribution to the similarity was well distributed between the nine ratios, with the highest contributor (NANO-ratio) adding only 16% and the lowest one (DINO-ratio), 6.5%.

The high Chl*a* samples from red tide formed Cluster D. It had CHA-ratio as the highest contributor (25%) to the average similarity, with CHBC-ratio and PSC-ratio together adding another 34%. The MVChl*a*-ratios appeared only as fourth and fifth contributors, as DINO-ratio and DIAT-ratio, to characterise the phytoplankton taxa. Although PPC-ratio value was very low and comparable to that found in the DCM (Cluster B), its contribution to the similarity was high (11.53%). Contrary to the previous three Clusters, the optical-ratios were more important to the similarity of Cluster D than the MVChl*a*-ratios.

Cluster E had CHA-ratio as the major contributor to the similarity, followed by NANO-ratio and photosynthetic pigment ratios (PSC-ratio and CHBC-ratio), with DIAT-ratio,

DINO-ratio and PROK-ratio present with low photoprotection.

Cluster F was formed of high Chl*a* samples, from green waters of the Benguela upwelling. As the other high Chl*a* cluster (D), Cluster F had very high value for CHA-ratio, accounting 21% to the average similarity, followed by DIAT-ratio (19%). Again the optical-ratios were more important to the similarity than the MVChl*a*-ratios.

The Cluster G had 18% of similarity characterised by CHA-ratio and then 15% by NANO-ratio.

### 5.6.5 Dissimilarity between two adjacent Clusters

The totChl*a* concentration was a good indication of the differences between the Clusters although it was not included in the cluster analysis (Table 5.1). The gradual difference in marker pigments and optical-ratios between the Clusters is presented in Figure 5.8b-f and the results of the dissimilarity analysis (SIMPER) are presented in Table 5.2.

The MVChl*a*-ratios were stronger discriminators than the optical-ratios because the former can be present in one Cluster and absent in another, increasing the difference and contributing more to the dissimilarity between those two Clusters. On the contrary, all the four groups of functional pigments are always present, causing less contrast due to the optical-ratios. The CHA-ratio contributed more to the similarity within a Cluster, but it contributed less than 5% to the dissimilarity between Clusters because Chl*a* is ubiquitous and its proportion to the total pigments varied little in comparison to the MVChl*a*-ratios.

The main dissimilarity between the oligotrophic Clusters (A, B and C) and the Clusters with higher totChl*a* (D, E, F and G) was due to the PROC-ratio (Table 5.2 Clusters B-G, C-G, C-E, Figure 5.8b). DINO-ratio separated the Clusters A, B, G and F from

Table 5.2: Dissimilarity between two adjacent clusters. List of ratios that together account to 90% of the dissimilarity ($\overline{dis}$).

| Clusters A and B: $\overline{dis}$=13.80 | | | |
|---|---|---|---|
| ratios | Av.Diss | Diss/sd | contrib% |
| PROK | 3.77 | 3.13 | 27.28 |
| DIAT | 2.35 | 1.15 | 17.01 |
| PPC | 2.34 | 3.48 | 16.97 |
| CHBC | 1.49 | 2.15 | 10.77 |
| NANO | 1.38 | 1.51 | 9.96 |
| PROC | 1.28 | 1.33 | 9.30 |

| Clusters A and C: $\overline{dis}$=14.95 | | | |
|---|---|---|---|
| ratios | Av.Diss | Diss/sd | contrib% |
| DINO | 3.38 | 5.18 | 22.61 |
| PROK | 2.68 | 1.82 | 17.95 |
| DIAT | 2.35 | 1.13 | 15.69 |
| PROC | 2.30 | 1.62 | 15.35 |
| PPC | 1.30 | 1.72 | 8.70 |
| NANO | 0.97 | 1.32 | 6.47 |
| CHBC | 0.92 | 1.53 | 6.18 |

| Clusters B and C: $\overline{dis}$=11.01 | | | |
|---|---|---|---|
| ratios | Av.Diss | Diss/sd | contrib% |
| DINO | 3.45 | 5.23 | 31.32 |
| PROC | 1.93 | 1.43 | 17.52 |
| PROK | 1.50 | 1.40 | 13.61 |
| PPC | 1.09 | 1.67 | 9.89 |
| NANO | 0.95 | 1.36 | 8.60 |
| DIAT | 0.75 | 0.92 | 6.80 |
| CHBC | 0.67 | 1.66 | 6.09 |

| Clusters B and G: $\overline{dis}$=18.75 | | | |
|---|---|---|---|
| ratios | Av.Diss | Diss/sd | contrib% |
| PROC | 8.58 | 7.40 | 45.76 |
| NANO | 3.35 | 3.83 | 17.84 |
| DIAT | 1.92 | 1.68 | 10.25 |
| PROK | 1.53 | 1.58 | 8.16 |
| PPC | 1.33 | 2.21 | 7.09 |
| PSC | 0.88 | 2.12 | 4.67 |

| Clusters C and G: $\overline{dis}$=18.36 | | | |
|---|---|---|---|
| ratios | Av.Diss | Diss/sd | contrib% |
| PROC | 6.88 | 4.30 | 36.14 |
| DINO | 3.55 | 3.54 | 18.67 |
| NANO | 2.44 | 2.50 | 12.84 |
| PROK | 2.38 | 1.69 | 12.51 |
| DIAT | 1.35 | 1.70 | 7.38 |
| PSC | 0.77 | 1.56 | 4.04 |

| Clusters C and E: $\overline{dis}$=15.57 | | | |
|---|---|---|---|
| ratios | Av.Diss | Diss/sd | contrib% |
| PROC | 6.66 | 4.29 | 42.80 |
| PROK | 2.75 | 1.73 | 17.66 |
| NANO | 2.13 | 1.69 | 13.71 |
| DINO | 1.09 | 1.02 | 7.01 |
| DIAT | 0.92 | 1.37 | 5.91 |
| PPC | 0.70 | 1.46 | 4.49 |

| Clusters G and E: $\overline{dis}$=10.79 | | | |
|---|---|---|---|
| ratios | Av.Diss | Diss/sd | contrib% |
| DINO | 4.81 | 3.12 | 47.46 |
| NANO | 1.29 | 1.47 | 12.75 |
| PROK | 1.25 | 1.16 | 12.32 |
| DIAT | 0.97 | 1.43 | 9.54 |
| PPC | 0.65 | 1.38 | 6.39 |
| PSC | 0.57 | 1.27 | 5.64 |

| Clusters G and F: $\overline{dis}$=10.56 | | | |
|---|---|---|---|
| ratios | Av.Diss | Diss/sd | contrib% |
| NANO | 2.62 | 2.44 | 28.43 |
| PROK | 2.21 | 1.53 | 24.00 |
| DINO | 1.14 | 0.57 | 12.36 |
| DIAT | 0.97 | 1.74 | 10.59 |
| PPC | 0.95 | 1.53 | 10.29 |
| CHBC | 0.57 | 1.53 | 6.19 |

| Clusters E and F: $\overline{dis}$=12.58 | | | |
|---|---|---|---|
| ratios | Av.Diss | Diss/sd | contrib% |
| DINO | 4.33 | 1.99 | 34.45 |
| NANO | 2.95 | 1.84 | 23.45 |
| PROK | 1.70 | 1.35 | 13.54 |
| DIAT | 1.66 | 1.97 | 13.17 |
| PPC | 0.76 | 1.43 | 6.06 |

| Clusters E and D: $\overline{dis}$=18.51 | | | |
|---|---|---|---|
| ratios | Av.Diss | Diss/sd | contrib% |
| NANO | 7.68 | 3.54 | 41.51 |
| PROK | 4.29 | 3.49 | 23.15 |
| DINO | 1.78 | 1.89 | 9.64 |
| DIAT | 1.33 | 1.49 | 7.18 |
| PPC | 1.14 | 1.61 | 6.14 |
| PSC | 1.12 | 2.06 | 6.04 |

| Clusters F and D: $\overline{dis}$=20.26 | | | |
|---|---|---|---|
| ratios | Av.Diss | Diss/sd | contrib% |
| DINO | 6.29 | 2.87 | 31.06 |
| NANO | 4.99 | 2.50 | 24.64 |
| DIAT | 3.28 | 4.71 | 16.19 |
| PROK | 2.96 | 2.85 | 14.60 |
| PSC | 0.99 | 3.07 | 4.91 |

the Clusters C, E and D (Table 5.2 Clusters A-C, B-C, C-G and E-F and Figure 5.8f). PROK-ratio discriminated Cluster B from A (Figure 5.8c) and NANO-ratio discriminated Clusters G and E from Clusters D and F (Figure 5.8d).

### 5.6.6 Phytoplankton commnunity structure

The comparison of phytoplankton pigments within a large range in Chl*a* concentration showed that the gradient in Chl*a* concentration is related to change in phytoplankton dominant group (Figure 5.8). Low Chl*a* concentrations were dominated by the prochlorophytes and nanoflagellates, with high or low levels of photoprotection. High Chl*a* concentrations samples had more contribution from bigger cells like diatoms and dinoflagellates.

**PROK-ratio and Cyanobacteria:** It is recognised that the pigment information by its own can lead to a mis-interpretation of the data (Latasa and Bidigare 1998) and support from other data are needed. Cluster A and C had high PROK-ratio value. The first Cluster was in a oligotrophic region whilst the second was over a higher nutrient region (Figure 5.3 b). *Synechococcus* can be expected to contribute to the high PROK-ratio value in high nitrate and high light waters (Blanchot *et al.* 1992), however most of the ZEA detected in the Cluster A and C seemed to be due to the prochlorophytes or green algae. The chlorophyll-specific absorption spectra showed that there were very few *Synechococcus* in these samples (Figure 5.12). The two shallowest samples from the CC province in Figure 5.3 a and from the surface waters of the ETRA (Cluster C) were the only ones with phycobilin absorption (a shoulder at 550 nm; Jeffrey *et al.* 1997), suggesting a contribution from the *Synechococcus* (Figure 5.12). However, the absorption ratio between 550 and 440 nm (the minimum absorption and the maximum absorption, respectively, of phycobilin, Jeffrey *et al.* 1997) was lower than 0.2 in the CC province and

Table 5.3: Ratio of minimum (550 nm) to maximum (440 nm) absorption of phycoerythrobilin.

| A15-4.2 | A15-29.7 | A15-41 | A15-53.6 | A22-4.5 | A22-40.3 | A24-4.5 | A24-20 | A24-30.5 |
|---|---|---|---|---|---|---|---|---|
| 0.135 | 0.192 | 0.129 | 0.125 | 0.095 | 0.121 | 0.095 | 0.109 | 0.112 |

even lower in the ETRA ($< 0.13$, Table 5.3), so the phycobiliprotein absorption was less than 20% of the chlorophyll absorption. The absorption at 550 nm was not as evident in these samples (Figure 5.12) as those found at the mesotrophic site of the EUMELI3 cruise (Bricaud *et al.* 1995), when the absorption ratio between 550 nm and 440 was higher than 0.4 in the vicinity of the CC province. The phycoerythrin absorption may not be that significant even in regions where cyanobacteria are abundant. Barlow *et al.* (2002) found no sign of *Synechococcus* in the absorption spectra while Zubkov *et al.* (1998) detected higher abundance of *Synechococcus* by flow cytometric analysis around the 20°N in the AMT3 transect, where Chl*a* was 0.8 mg $m^{-3}$ and ZEA, 0.07 mg $m^{-3}$. Around the same latitude in the AMT11, the concentration of these pigments were much lower than that (Figure 5.3 b). The higher ZEA concentration in the equatorial region may have resulted more from prochlorophytes and green algae than cyanobacteria.

Cluster A dominated in the surface waters of oligotrophic gyres with very low nutrient and high light regime. The high value of PROK-ratio in the Cluster A was due to the prochlorophytes and nanoflagellates (green algae), with the exception of sample A15-4.2. The prochlorophytes and nanoflagellates with high photoprotection dominated the low nutrients waters at the surface of the oligotrophic gyres while *Synechococcus* were found, according to the analysis of particulate absorption coefficient, only at the region influenced by the upwelling water off northwest Africa. The Cluster A sample with the highest Chl*a*

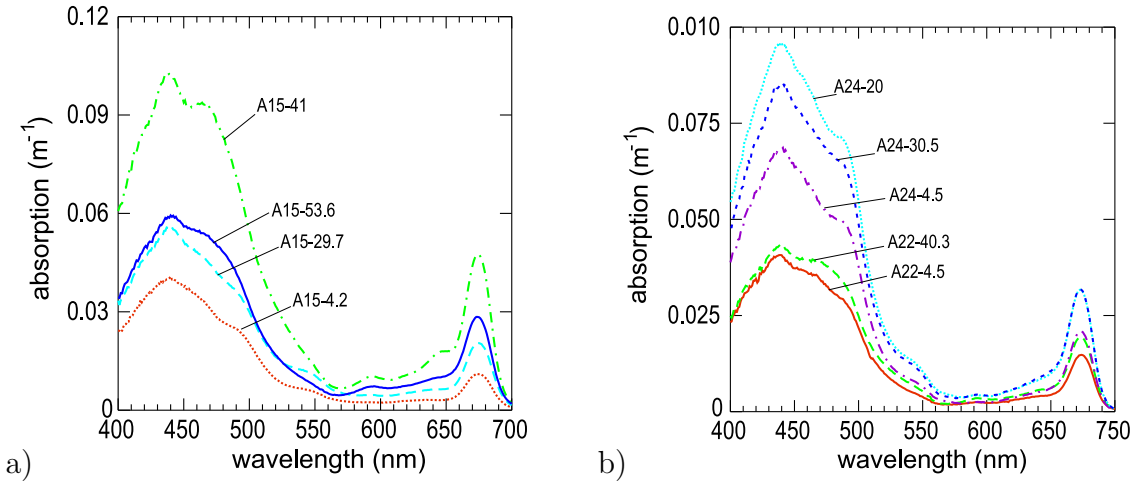


Figure 5.12: Particulate absorption coefficient - Clusters A and C. a) AMT11 CTD15, A15-4.2 is the only Cluster A sample, others are Cluster C. b) AMT11 ETRA: all Cluster C.

concentration was found at the surface of blue waters in the BENEFIT-L1 cruise (B16).

Cluster B dominated at the DCM of the oligotrophic gyres, waters deeper than the Cluster A domain. Low light and increasing nutrients allowed the development of more nanoflagellates, and decreased the relative contribution from the prochlorophytes. Nanoflagellates and prochlorophytes with high Chl*b* content were the most abundant phytoplankton groups (Figure 5.11b).

The DCM of BENEFIT-L1 blue waters had a higher value for and a lower contribution from the PROC-ratio than the DCM waters of the oligotrophic gyres, so these samples were classified as Cluster C alongside samples collected at the ETRA and RCBC provinces, where nitrate nutricline was shallower than in the gyres. The PROC-ratio and DIAT-ratio were very low, indicating that nanoflagellates was dominating over the prochlorophytes, diatoms. The diagnostic pigment for dinoflagellates (PER) may be only in trace amounts when compared to the total MVChl*a* concentration of the whole sample. For the Equatorial Pacific, Mackey *et al.* (1996) found 0.462 for the ratio peridinin to

MVChl*a* (ratio for a cell), which is bigger than the DINO-ratio (= 0.028) for Cluster C. Although NANO-ratio for this Cluster was very high (= 0.968), cell counts showed that 40 to 70 % of the cells were dinoflagellates and 15 to 44 % were nanoflagellates cells. These cell count results, associated to the fact that peridinin concentration may be in trace small fractions only, suggest presence of dinoflagellates as well. This water was a mixed population with flagellates (nanoflagellates and dinoflagellates) dominating over Prochlorophytes and diatoms.

Unfortunately, no nutrient data were available for the BENEFIT-L1 cruise. From the low temperature, it can be speculated that there was high availability of nutrients (Waldron and Probyn 1992). For the BENEFIT-L1 data, the Clusters are overploted on the temperature contours in the six transects (Figures 5.6 and 5.7), indicated in Figure 5.1. Samples that formed the Cluster D were collected in red tide waters with very high totChl*a* concentration (Figure 5.1, stations 2 to 4), the coldest and lowest salinity water of the whole data (Figure 5.13a and b), with very high totChl*a* concentration (Table 5.1). DIAT-ratio and DINO-ratio were within the limits for FUC/MVChl*a* and PER/MVChl*a* suggested in the literature (Mackey *et al.* 1996) respectively for diatoms and dinoflagellates. Previous works carried out in the same region (Lambert's Bay) in February 1996, registered red tide formed by a dinoflagellate (*Ceratium furca*), in a narrow temperature range of 12 to 15°C (Pitcher *et al.* 1998). The three samples of Cluster D had temperature raging between 12.7 and 14.5 °C. Such similarities leads to the conclusion that dinoflagellates was dominating in these waters. The following shift from dinoflagellates to diatom dominating population was accompanied by increase in temperature to higher than 15°C (Pitcher *et al.* 1998). This fact helps to support the dinoflagellates domination in Cluster D.

About half of the BENEFIT-L1 samples were grouped as Cluster E, with high Chl*a*

a)

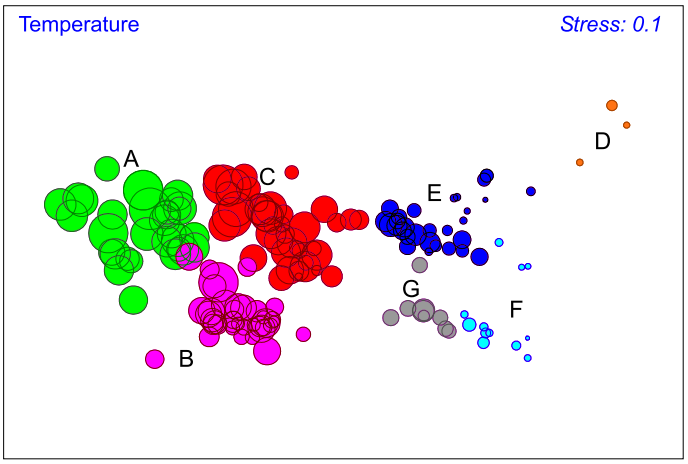


b)

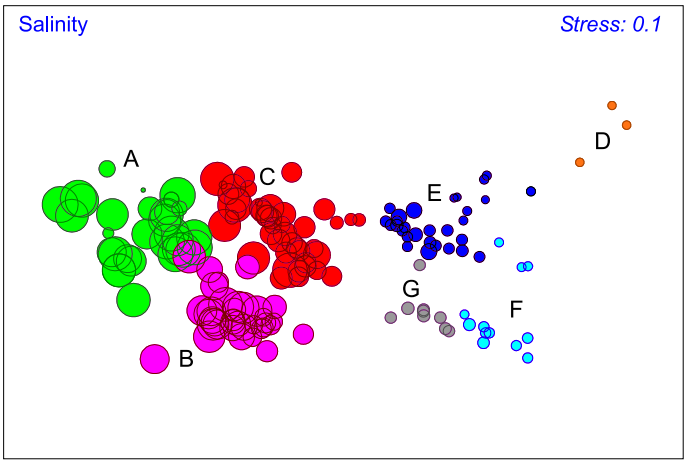


Figure 5.13: Temperature and salinity superimposed over MDS scaling and pigment clusters. The size of the bubbles indicates a) Temperature (in the range 10 to 30°C) and b) Salinity (in the range 34.0 to 37.0).

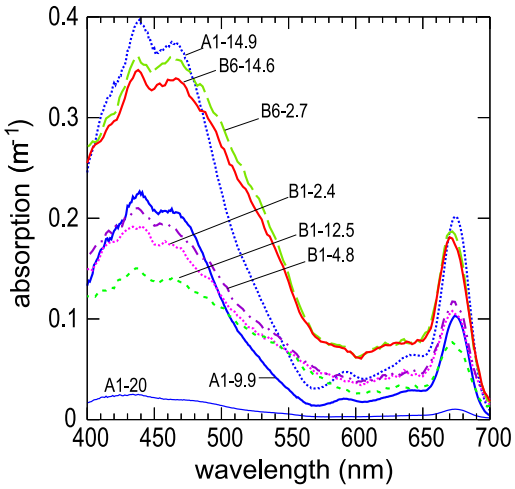


Figure 5.14: Particulate absorption coefficient - Cluster E. Observe the narrower spectra for the AMT11 CTD1 (blue lines) in comparison to the BENEFIT-L1 samples.

concentration (Table 5.1). NANO-ratio was the MVChl*a*-ratio that most contributed to the Cluster E similarity, but its ratio value was about a quarter of the NANO-ratio of Cluster B (dominated by nanoflagellates). However DIAT-ratio value was found within FUC/MVChl*a* limits (Mackey *et al.* 1996). This Cluster must be diatom dominated with presence of nanoflagellates. The chlorophyll-specific absorption spectra support this with a spectra characteristic of diatoms with a peak for FUC absorption around 470 nm (Figure 5.14). The AMT11 samples have lower values for DINO-ratio than the samples from the BENEFIT-L1, suggesting less dinoflagellates in the first cruise. The absorption spectra for the Cluster E (Figure 5.14) shows a narrower peak at wavelengths shorter than 550 nm for the AMT11 samples (A1-9.9 and A1-14.9 in Figure 5.14), indicating less peridinin than in the BENEFIT-L1 samples.

BENEFIT-L1 stations B11, B25 and B26 were sampled in green water with very high Chl*a* concentration (Figure 5.1) were grouped with some other samples as Cluster F. A closer look at the transects showed that these green water samples occurred in moderate temperature (15°C) observed in the Transects OPTL and N (Figure 5.6 b and c) and H

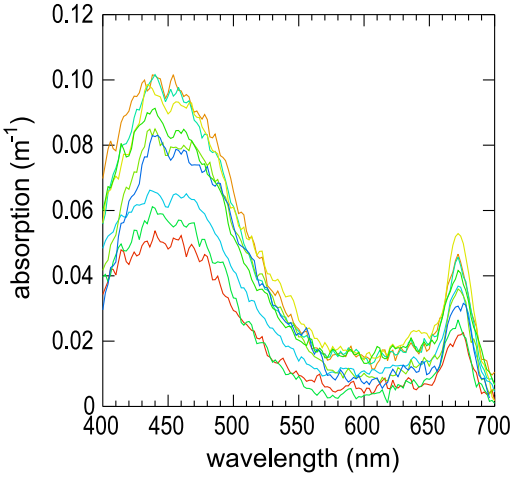


Figure 5.15: Particulate absorption coefficient - Cluster G. Observe the absorption lowering around 570 nm.

(Figure 5.7 b). The DIAT-ratio value (0.38) was the highest between the Clusters and it was within the range proposed by Mackey *et al.* (1996) for the diatoms. Diatoms were the main phytoplankton taxa with very small presence of nanoflagellates.

Along the BENEFIT-L1 transects north of 29°S, Cluster G was found above the Cluster E and adjacent to the Cluster F (Figure 5.1 and Figure 5.7 a, b and c), with no dinoflagellates and lower Chl*a* concentration than the Cluster E (Figure 5.6 a). This is supported by the absorption spectra with narrower absorption for carotenoids, due to lack of peridinin (Figure 5.15), than the Cluster E absorption spectra (Figure 5.14). NANO-ratio value was less than a third of the NANO-ratio of Cluster B while the DIAT-ratio value lay between the limits proposed by Mackey *et al.* (1996) for the diatoms, suggesting dominance over the nanoflagellates.

## 5.7 Summary and conclusions

Phytoplankton community structure were analysed by combining statistics and biological knowledge about phytoplankton pigments. Five phytoplankton taxa were analysed, represented by the ratios between their marker pigment to the MVChl*a* concentration, coupled with four optical ratios to account for the degree of photoacclimation.

These nine ratios were based on biological knowledge of phytoplankton pigments which assisted the cluster analysis, resulting in a good understanding of phytoplankton pigment distributions across oligotrophic and eutrophic waters in the Atlantic Ocean. This approach separated the samples according to the phytoplankton taxa and level of photoacclimation, resulting in grouping of depth and latitude limits. A summary of phytoplankton community structure and the cluster are presented in Table 5.4.

The nine ratios represented the gradient in totChl*a* and also the change in phytoplankton taxa (Table 5.4), although Chl*a* concentration was not included in the analysis. The increase in totChl*a* was followed by the change of phytoplankton groups, with prochlorophytes dominating the Clusters with lowest concentrations, followed by the domination shift to nanoflagellates. Diatoms were present in every Cluster, but in higher proportion in samples/Clusters with higher concentrations of Chl*a* . Dinoflagellates were present in surface waters especially at lower temperatures and salinities, mostly in upwelling regions.

Along the AMT11 transect, the approximate community structure was: 1) Surface waters of oligotrophic gyres with nitrate depletion and abundant light which were dominated by prochlorophytes and nanoflagellates, with high photoprotection, and the lowest Chl*a* concentration of the whole transect (Cluster A); 2) Deeper depths with abundant nitrate and low light which were dominated by nanoflagellates and prochlorophytes with high Chl*b*

Table 5.4: Summary of phytoplankton clusters obtained from cluster and MDS analyses. Clusters (Cl), number of samples (n), main feature of sample and location are indicated. DVChl*a* (DVA) and marker pigments for dinoflagellates (Din) are presented as present (+) or absent (-). The +/- means present in some samples and absent in others. The average values of Chl*a* (mg $m^{-3}$), depth (m), temperature (T°C) and salinity are presented with minimum and maximum values in italic. Note that the Clusters are listed obeying the increase in Chl*a* concentration, thus Cluster D and G are interchanged.

| Cl | n | Feature | Chl*a* | DVA | Din | depth | T°C | Sal | Suggested main phytoplankton taxa |
|---|---|---|---|---|---|---|---|---|---|
| A | 31 | Surface of oligotrophic gyres, high light, low nutrient | 0.078 *0.03, 0.15* | + | - | 36.1 *3.2, 141.1* | 23.1 *20.2, 28.3* | 36.55 *34.37, 37.19* | Prochlorophytes and nanoflagellates, with high photoprotection |
| B | 38 | DCM of oligotrophic gyres, low light | 0.17 *0.11, 0.25* | + | - | 101.9 *45.7, 180.4* | 19.0 *14.9, 27.3* | 36.19 *35.52, 36.97* | Nanoflagellates and prochlorophytes with high Chl*b* content |
| C | 45 | high nutrient, hight light (ETRA) | 0.14 *0.28, 0.49* | + | + | 38.0 *2.9, 121.5* | 20.8 *13.4, 27.5* | 35.86 *34.60, 37.02* | Mixed population, with dinoflagellates and nanoflagellates domination |
| G | 9 | surface water, off Namibian coast | 0.91 *0.65-1.22* | - | - | 6.2 *1.7, 26.5* | 17.2 *15.0, 19.6* | 35.03 *34.99, 35.10* | Diatom domination over nanoflagellates |
| E | 30 | Over the shelf, NECS and South African Western coast | 1.94 *0.79, 4.02* | - | + | 11.3 *1.9, 27.1* | 15.6 *12.1, 20.1* | 34.96 *34.70, 35.40* | Diatom and nanoflagellates domination |
| F | 12 | Green water, Namibian coast | 5.79 *2.30, 12.25* | - | +/- | 9.7 *1.7, 24.2* | 13.5 *11.7, 15.8* | 34.89 *34.78, 35.06* | Diatom domination, nanoflagellates present |
| D | 3 | red tide samples, Lambert's Bay | 32.6 *22.2, 46.3* | - | +/- | 7.0 *1.5, 11.4* | 13.3 *12.7, 14.5* | 34.73 *34.72, 34,73* | Dinoflagellate domination |

content and very low photoprotection (Cluster B); and 3) Shallow or intermediate depth waters with abundant nitrate and light which were dominated by flagellates (nanoflagellates and dinoflagellates) and with the presence of all other phytoplankton taxa (Cluster C). These three clusters are characteristically of low Chl*a* concentration and high temperature with very variable depth.

The light penetration in the water column cannot be taken as constant even within a province nor a cluster. Results from this analysis draw the limits in a set of data to divide it into smaller sets by analysing the similarity between samples. This analysis provides the main characteristics and the dominating phytoplankton taxa of a sample but it cannot give further information like amount of Chl*a* each taxa is contributing to the total Chl*a* of the sample, as does CHEMTAX software (Mackey *et al.* 1996). CHEMTAX applies statistical methods to iteratively seek for a convergence and derive fractions that each taxa is contributing to the total Chl*a* of a sample, by analysing a group of samples with similar community structure and light history. Working with natural environment, however, is difficult to generate a dataset with similar community structure and light history. Cluster analysis with MDS plot may give the conditions required by CHEMTAX. However, latitudinal or regional differences should still be taken into account, since these pigment analyses did not assess species composition, which can make pigment proportions different.

These analyses were based on one cruise along a longitudinal transect (AMT11) and one cruise in the coastal upwelling region (BENEFIT-L1). The contrast between these two cruises, allowed to conclude that the gradient in Chl*a* concentration, temperature and change in phytoplankton community structure are all related (Table 5.4). The temperature must be due to the good correlation with nutrient (Chapter 4). The phytoplankton

community structure found in the AMT11 (Clusters A, B and C) is very likely to be representative of the region since the range in temperature and salinity are bigger than in the coastal upwelling (Clusters D, E, F and G). The ranges of temperature and salinity for the former clusters are much wider than that for the latter clusters. The wider that range the more the phytoplankton community structure can stand environmental changes. There may be a difference in species, but the phytoplankton taxa should not change much in the AMT11 clusters. In the other extreme, clusters found in coastal regions had narrower range of temperature and salinity, so the phytoplankton community structure is more affected by environmental changes. In fact, in coastal regions phytoplankton groups changes quicker and more dramatically because the community structure is more sensitive to smaller changes in environmental conditions. Thus small changes in environmental conditions can cause not only change in species but also in taxa, causing dramatic alteration in the community structure.

# Chapter 6

# Phytoplankton physiology

## 6.1 Introduction

Previous chapters have provided knowledge about the environment that the phytoplankton were exposed to at the time of sampling (Chapter 4) and the structure of the phytoplankton community (Chapter 5) along the AMT11 transect. In this Chapter, phytoplankton physiology is assessed using fast repetition rate fluorometry, seeking for a pattern along the AMT11 transect.

Active fluorometry such as fast repetition rate (FRR) fluorometry method has been proposed as a method to assess phytoplankton physiology in the natural environment directly (Falkowski *et al.* 1992, Kolber *et al.* 1998), with minimum manipulation of the sample, minimising artefacts associated with bottle incubations. Methods based on variable fluorescence provide real-time, nondestructive and noninvasive measurements of phytoplankton physiology (Kolber and Falkowski 1993). Moreover, because the sample is free of manipulation, it is expected that the physiology assessed reflects the environment the phytoplankton were exposed to, including the light history, nutrient availability and tem-

perature.

Recent investigations of phytoplankton physiology either with $CO_2$ (Marañón *et al.* 2000) or active fluorescence methods (Falkowski 1992, Geider *et al.* 1993, Babin *et al.* 1996, Behrenfeld *et al.* 1996, Behrenfeld and Kolber 1999) have indicated that macro- or micro-nutrients are a primary factor likely to affect the performance of photosystem photochemistry.

## 6.2 Methods and data

The data were collected during the AMT11 cruise (Chapter 3). Eight provinces were sampled along the AMT11 transect and in each province (except NECS), measurements from at least a pair of pre-dawn and mid-day stations were acquired. A CTD/rosette rig consisting of a Seabird CTD and 12 Niskin bottles was deployed vertically at every station. Discrete water samples were collected at selected depths for on-board, bench-top mode analysis of fluorescence with FRR fluorometry, as explained later (Section 6.2.1). At mid-day stations the bio-optical rig with spectral light sensors, FRR fluorometer with PAR (photosynthetically available radiation) and pressure sensors, was deployed from the starboard quarter crane at the same time as the CTD/rosette rig deployment with the main crane.

Potential density ($\sigma_\theta$) was estimated (Emery and Thomson 2001) from potential temperature and salinity from the CTD. Chl*a* concentration was estimated from the signal of fluorometer attached to the CTD, calibrated with HPLC totChl*a* as described previously (Chapter 4).

### 6.2.1 Fast repetition rate fluorometry

The physiological data analysed in this thesis was obtained using a FAST$^{tracka}$, Chelsea Technologies Group, fluorometer serial number 182018.

**Pre-dawn stations:** Variable fluorescence of discrete water samples collected with rosette bottles was measured with bench-top mode FRR fluorometer (Figure 2.6). The water sample was poured into the pipes mounted on the dark chamber of the fluorometer, taking care to avoid bubble formation, and then covered with black felt during the fluorescence data acquisition to prevent interference from room lights. A minimum of 20 acquisitions were taken for each sample. At most of the stations, water samples from the deep chlorophyll maximum (DCM) were analysed with two or three different gains to test whether the gain setting affects the measurements ('*Gain Test*') and to check which of them had the best performance. When the gain is not correspondent to the fluorescence yields, the very first fluorescence yield (see Figure 2.5) is much higher than the subsequent fluorescence yields. Figure 2.5 presents a set of fluorescence yields obtained with the right gain, thus the first fluorescence yield is not discrepant from the following yields.

**Mid-day stations:** Took place approximately 4 to 5 hours after pre-dawn station, around 115 km distant. The FRR fluorometer was deployed vertically attached to the bio-optical rig (Figure 6.1) for *in situ*, continuous measurement with the gain fixed for the best performed in the DCM of the previous pre-dawn station.

**Blank measurement:** MilliQ water was measured to check the background fluorescence caused by the instrument at the pre-dawn stations (Behrenfeld and Kolber 1999). The fluorescence yields from this measurements were very small, so no correction was adopted for sample measurements.

### Data processing

All the FRR fluorescence data were processed using the FRS v1.8 software (Chelsea Instrument). Some parts of the water column (surface layer or around the DCM) were averaged into 3 m bins whilst other parts were averaged into 8 m bins, always attempting to minimise the noise, by seeking smoother profile. The data that resulted from only one value or with a coefficient of variation (cv) bigger than the threshold (cv = 0.2) were discarded by the quality assurance test. In the case of the cv being bigger than the threshold, but the averaged value agreeing with the values above and below, that averaged value was quality controlled visually and analysed further. For discrete bench-top mode data, the biggest and the smallest acquisitions in a sample were deleted before binning. Again the cv was analysed for quality control but with a higher threshold (cv = 0.4).

### Chamber and methods correction

The difference in the methods used for the pre-dawn and mid-day stations may mean that the measurements are not comparable. An experiment was carried out to compare the light and dark chambers of the FRR fluorometer and also to compare the bench-top mode and *in situ* profiling methods (Appendix D). The data from pre-dawn stations were corrected to match the light chamber of *in situ* profiling method, according to the results of chamber comparison and methods comparison (Appendix D), since dark chamber measurements were the only ones performed for discrete bench-top mode. The mid-day measurements with dark chamber (*in situ* profiling method) were corrected for chambers difference only to match the light chamber.

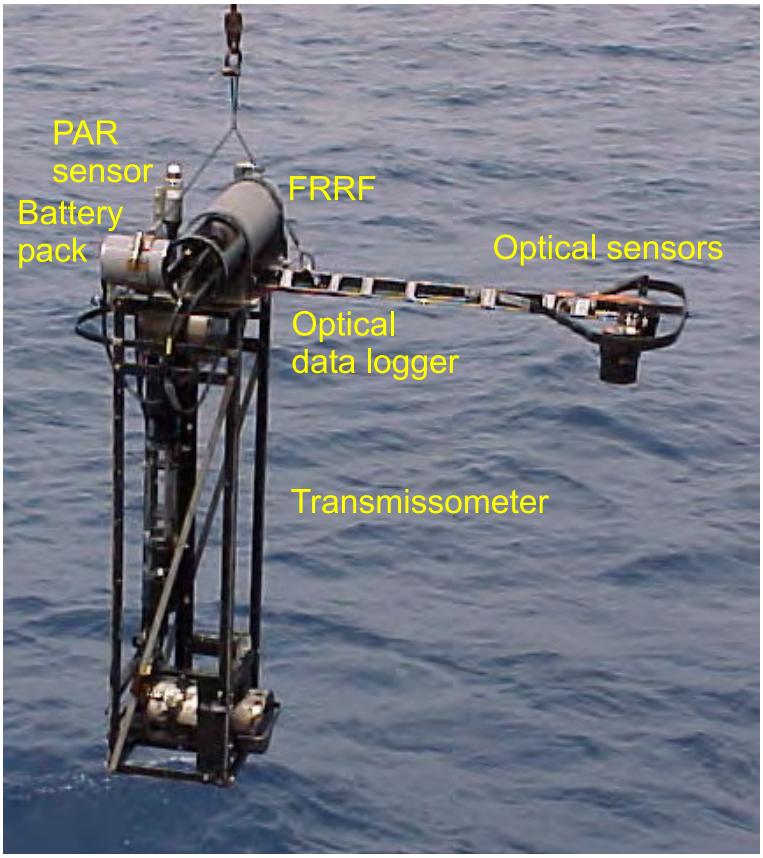


Figure 6.1: Bio-optical rig with fast repetition rate fluorometer (FRRF) attached for *in situ* vertical profiling. The rig frame measures 1 m in height and a top of 0.3 m × 0.3 m, with an arm of 1.3 m long, carrying optical sensors. The optical arm carries a pair of 7-channel irradiance and radiance sensors. FRRF is a cylindrical instrument, 0.16 m in diameter and 0.65 m in length, with a small external battery pack. PAR sensor and a pressure sensor (attached 10 cm below the FRRF) are connected to the FRRF.

### 6.2.2 Depth correction

The FRR fluorometer was attached to the bio-optical rig which was deployed independently from the CTD/rosette rig. A major concern of simultaneous/separate deployments of the CTD and the bio-optical rigs was possible differences in depth of particular features in the profiles when the data from these two deployments were analysed together. The water column can be more or less 'stretched' in one rig deployment compared to another due to internal waves. The depth of a feature, e.g. like the DCM, sampled by

one deployment may not be the same as in another. Depth matching-up was carried out by comparing the fluorescence profiles from the FRR fluorometer and CTD taking the depth from the CTD as the reference. The most characteristic features in the fluorescence profile from the CTD were determined graphically. The depth of the (DCM), its 'neck', the local fluorescence maxima and minima were taken as *reference depths*. These features were identified in the FRR fluorescence profile, and their depths replaced by the corresponding reference depth from the CTD. Depths of FRR fluorescence between those reference depths were corrected through linear interpolation. In general, AMT11 stations northern than 16°N needed correction in depth. The extreme case was difference in 9 m depth (around DCM of station 13) but usually the difference was around 2 to 3 m, and just in some parts of the water column. Some parts of some stations in the ETRA had differeces between 2 to 5 m. Stations 39, 41 and 45 also needed depth correction between 0.3 to 5 m.

## 6.3 Results

The FRR fluorometer was set to the fixed gain mode, with the gain selected for the Chl*a* concentration at the DCM of the previous pre-dawn station. Setting the instrument to a fixed gain made the fluorescence measurements in the less concentrated parts of the water column, usually 10 to 30 m upper layer was very noisy, so they were discarded in the quality control procedure.

### 6.3.1 Overview

Large differences in phytoplankton physiology at local mid-day were observed across the Atlantic Ocean during the AMT11 (Figure 6.2). Such differences were expected since three contrasting phytoplankton communities were observed (Chapter 5) in eight provinces along the AMT11 transect (Chapter 4). The gradient in Fv/Fm showed higher values towards deeper part of the water column.

ETRA presented the lowest Fv/Fm in the surface of the whole transect, although nitrate was the highest in the surface of the whole transect. Highest values of Fv/Fm were, in general, deeper than the depth of Chl*a* maximum. This gradient in physiology matched to the gradient of phytoplankton community structure (Table 5.4). Above the nitracline, non-photochemical quenching prevented $Fv/Fm_L$ from reaching higher values. The highest Fv/Fm in the water column was found in general deeper than the nitracline and the depth of DCM, where nitrate was replete. What was unexpected were the small values of Fv/Fm in the surface of ETRA because nitrate was higher than 2 $\mu$M in the surface. The effective absorption cross-section ($\sigma_{PSII}$) was also increasing towards deeper part of the water column with higher values found around the depth of maximum Chl*a*. The higher values in the surface waters were found in the ETRA.

More details are presented later, exploring selected pairs of pre-dawn and following mid-day stations for each of the provinces (except NECS), where both stations had measurements acquired with the same gain from the FRR fluorometry.

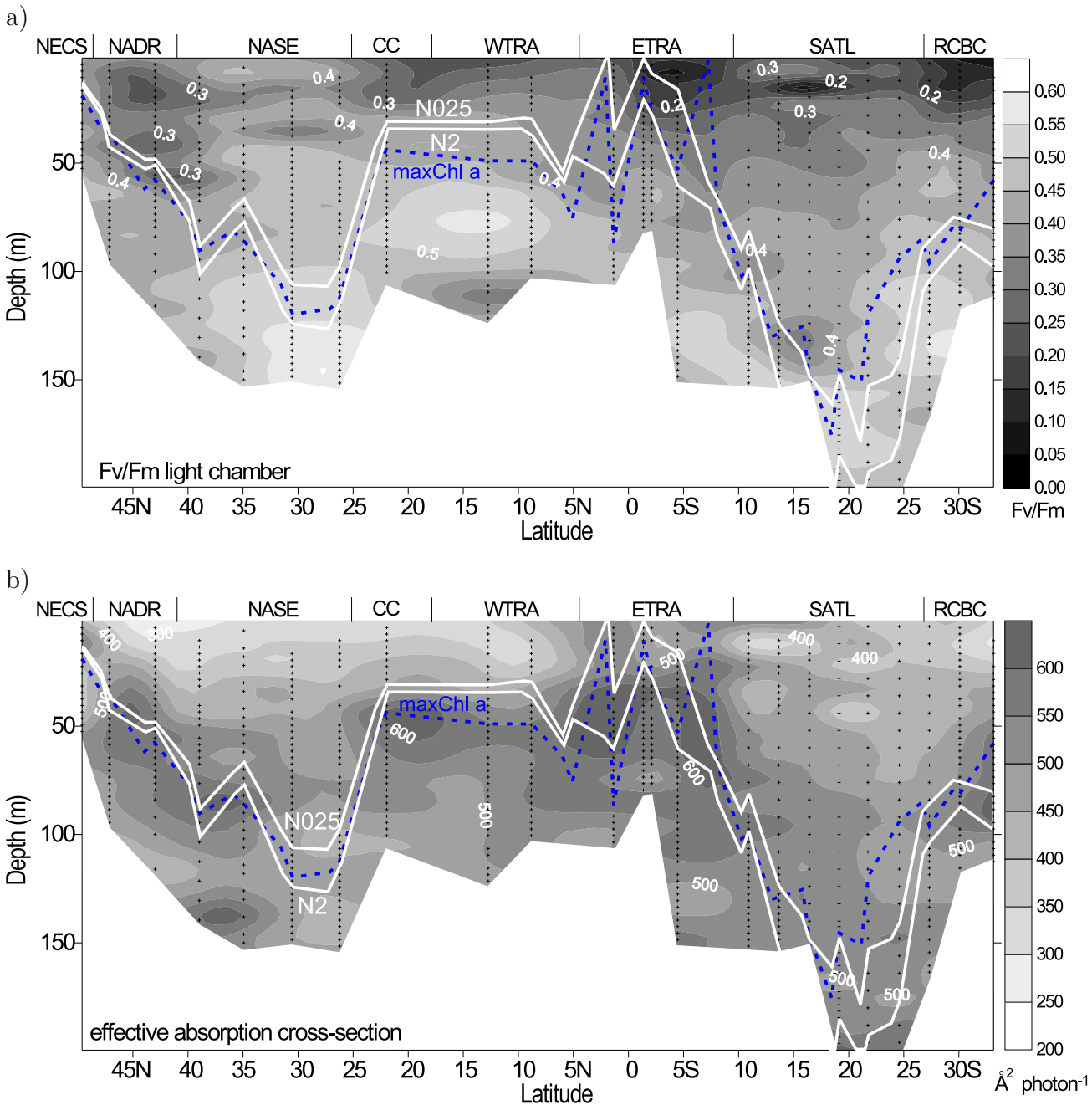


Figure 6.2: Phytoplankton physiological parameters at local mid-day across the AMT11 transect. Top graphic is quantum efficiency of photochemistry ($Fv/Fm_L$) and bottom graphic is effective absorption cross-section of photosystem II ($\sigma_{PSII}$). The solid white lines define the nitracline where nitrate concentration changes 0.025 $\mu$M m$^{-1}$ (N025) and 0.2 $\mu$M m$^{-1}$ (N2). Dashed blue line indicates the depth of maximum Chl*a* (maxChl a) Provinces and latitudes are indicated respectively in the top and bottom axes. Note that the most of the surface samples discarded in the quality control procedure are kept for gridding purposes.

### 6.3.2 Quantum yield of photochemistry - Fv/Fm

For each station analysed, potential density ($\sigma_\theta$), Chl*a* concentration and PAR are presented (Figure 6.3, 6.4 and 6.5, left side graphics). Because of the pre-dawn and the following mid-day station were not at the same position (e.g. 115 km distant from each other), the water sampled from these paired stations can be different. This explained the difference in Chl*a* and $\sigma_\theta$ profiles in either magnitude or profile shape between the pre-dawn and the following mid-day stations in ETRA, SATL, CC and RCBC (Figures 6.3, 6.4 and 6.5, left side graphics). In provinces where there were changes in the Chl*a* vertical profile between the pre-dawn and the following mid-day stations, photosynthetic parameters from above, at and below the depth of chlorophyll maximum at the respective stations were compared. Changes in the ambient light due to cloud cover were one of the most significant factors affecting Fv/Fm during the day and these changes can mask any real diel variation in the phytoplankton physiology. All the AMT11 stations took place at well defined illumination condition. At pre-dawn, the phytoplankton had recovered (overnight) from both photochemical and non-photochemical quenching processes. All the measurements under ambient light took place at local 11 am, and any effect of light variation due to clouds could be recognised by comparing the PAR and FRR fluorescence measurements.

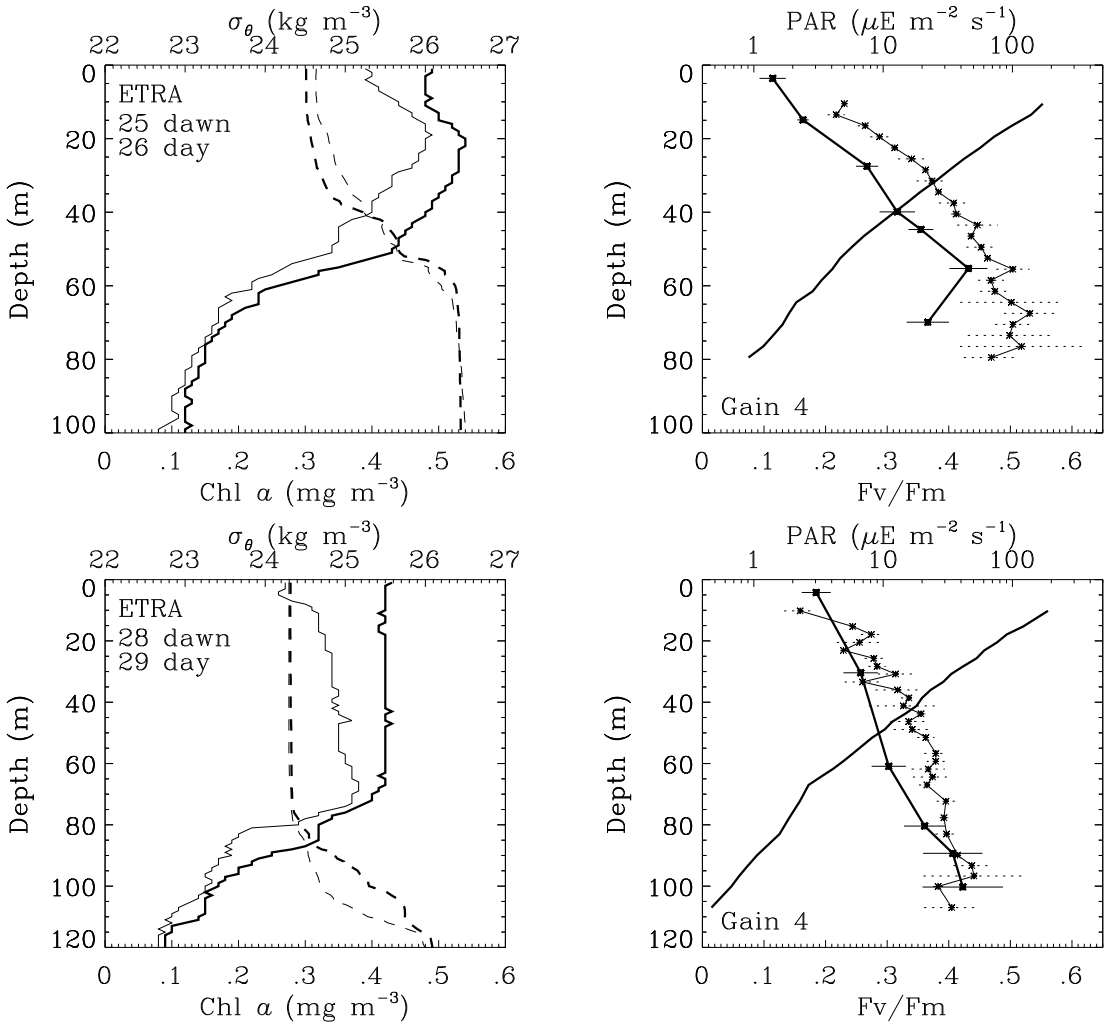


Figure 6.3: Fv/Fm in the high nutrient province (ETRA). Left side graphics show profiles of potential density ($\sigma_\theta$, dashed lines) and Chl*a* concentration (solid lines). Pre-dawn station in thick line and mid-day station in thin line. Right side graphics show PAR (solid line), $\mathrm{Fv/Fm_{dawn}}$ (solid thick line with *) and mid-day $\mathrm{Fv/Fm_L}$ (solid thin line with *) with standard deviation as error bars. Station, province and the gain used for FRR fluorescence measurements are indicated.

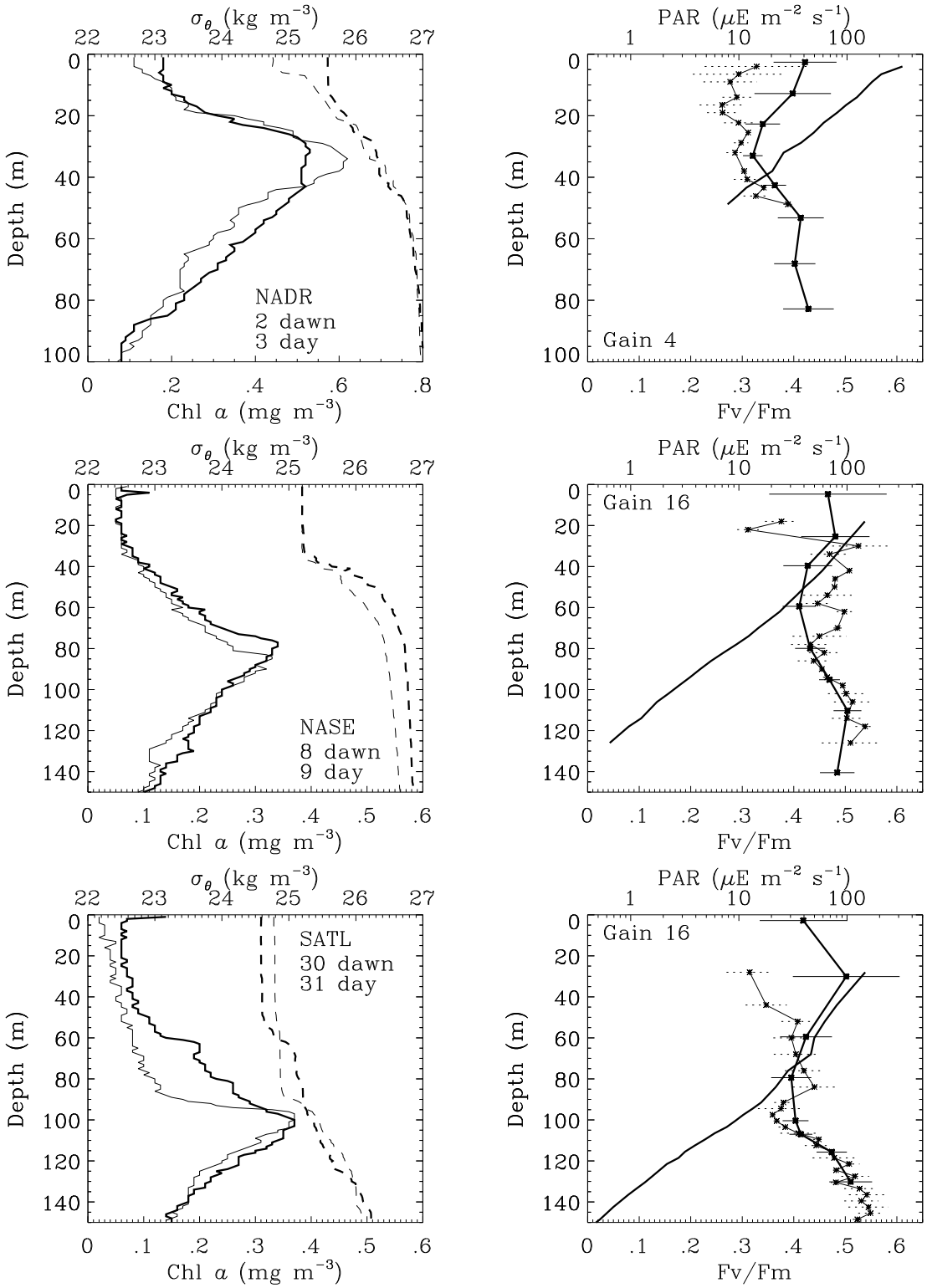


Figure 6.4: Provinces with minimum Fv/Fm at the depth of Chl*a* maximum (NADR, NASE and SATL). Left side graphics show profiles of potential density ($\sigma_\theta$, dashed lines) and Chl*a* concentration (solid lines). Pre-dawn station in thick line and mid-day station in thin line. Right side graphics show PAR (solid line), $\mathrm{Fv/Fm_{dawn}}$ (solid thick line with *) and mid-day $\mathrm{Fv/Fm_L}$ (solid thin line with *) with standard deviation as error bars. Station, province and the gain used for FRR fluorescence measurements are indicated.

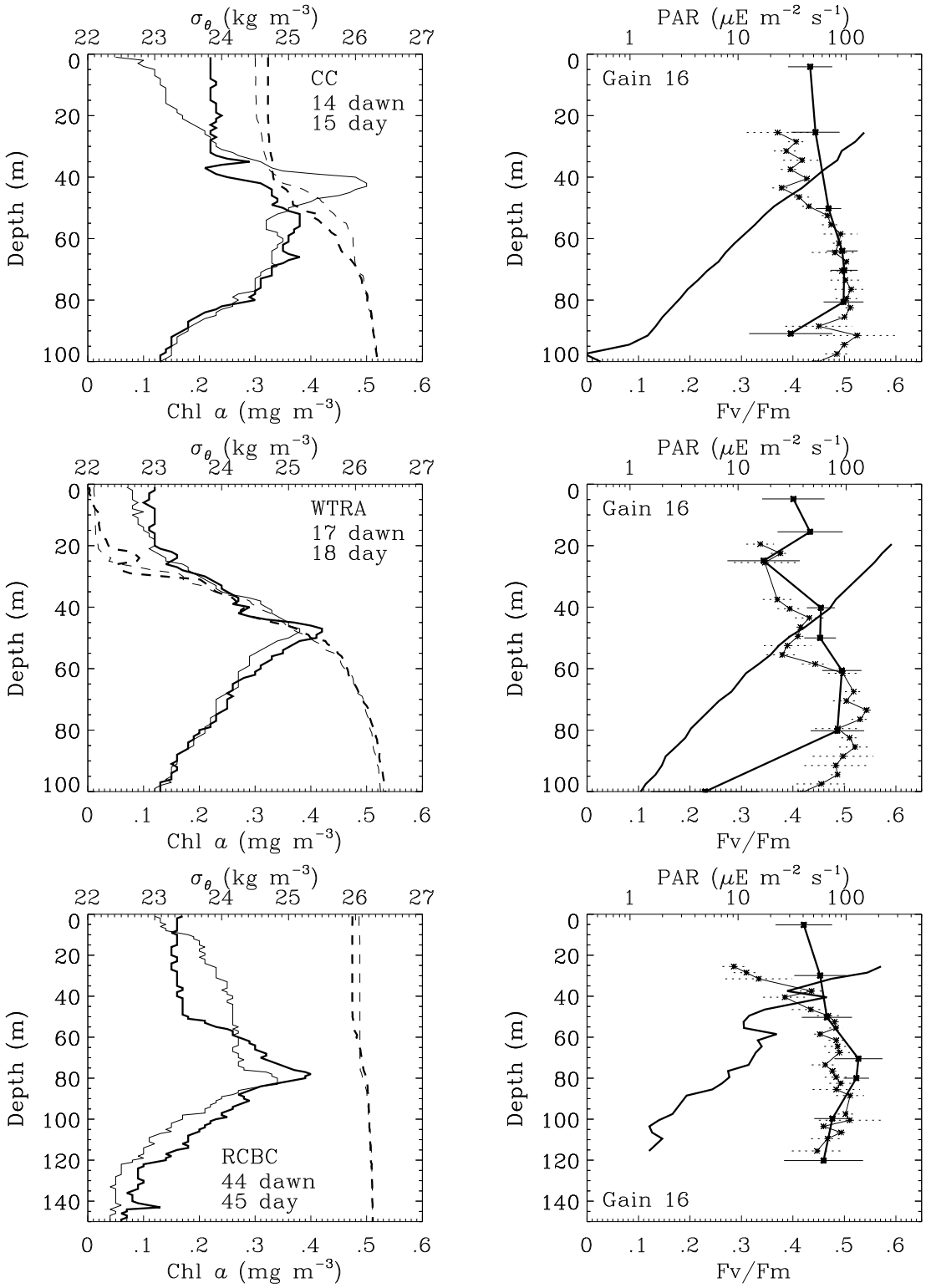


Figure 6.5: Provinces with maximum Fv/Fm at the depth of Chl*a* maximum (CC, WTRA and RCBC). Left side graphics show potential density ($\sigma_\theta$ in dashed lines) and Chl*a* profiles (solid lines). Pre-dawn station in thick line and mid-day station in thin line. Right side graphics show PAR (solid line), $Fv/Fm_{dawn}$ (solid thick line with *) and mid-day $Fv/Fm_L$ (solid thin line with *) with standard deviation as error bars. Station, province and the gain used for FRR fluorescence measurements are indicated.

### Pre-dawn Fv/Fm

After an overnight darkness, the phytoplankton is expected to have recovered from the supra-optimal-light exposure on the day before, e.g. relaxation of photochemical and non-photochemical quenching is expected, so a constant value of Fv/Fm is expected at dawn ($Fv/Fm_{dawn}$) in the vertical profile within the mixed layer depth. However during the AMT11, several variations in $Fv/Fm_{dawn}$ profiles were detected with values ranging from 0.1 to 0.53 (Figures 6.3, 6.4 and 6.5). The lowest value was found at the surface water of ETRA, and the highest value around the DCM of RCBC. NADR and ETRA had the station highest value lower than 0.45 for $Fv/Fm_{dawn}$.

In the only province with high nutrient ($> 0.2$ $\mu$M) in the surface layer (ETRA), the lowest $Fv/Fm_{dawn}$ was in the surface, increasing with depth and reaching the maximum value (0.4) in the bottom of chlorophyll maximum layer (Figure 6.3). This province had a mixed community with flagellates dominating (Figure 5.3 and Table 5.4, Cluster C), with maximum Chl*a* in the surface. Phytoplankton did not recover the photosynthetic efficiency even after an overnight darkness recovery, and the same quenching structure measured at mid-day (lower Fv/Fm in the surface and higher value in deeper water) persisted at pre-dawn measurements, with lower values in the whole water column in comparison to mid-day Fv/Fm (Figure 6.3).

In NADR, NASE and SATL, e.g. provinces with a well developed DCM, $Fv/Fm_{dawn}$ ranged from 0.32 to 0.51. The minimum $Fv/Fm_{dawn}$ of the water column was coincident to the depth of maximum chlorophyll and about 0.1 lower than in the rest of the water column (Figure 6.4). In the surface water of the gyres (NASE and SATL), the phytoplankton community was dominated by prochlorophytes and nanoflagellates with high levels ofphotoprotectant pigments (Figure 5.3 and Table 5.4, Cluster A) whilst in

the DCM, nanoflagellates were more significant than the prochlorophytes, with high Chl*b* content (Figure 5.3 and Table 5.4, Cluster B).

In CC, WTRA and RCBC, $Fv/Fm_{dawn}$ ranged between 0.34 and 0.53 (Figure 6.5), with minimum $Fv/Fm_{dawn}$ measured at the surface and the maximum at the DCM. The DCM of these provinces had a mixed phytoplankton community with flagellates dominating (Figure 5.3 and Table 5.4, Cluster C) and below the DCM nanoflagellates was dominating over prochlorophytes with high Chl*b* content (Figure 5.3 and Table 5.4, Cluster B). In the low biomass, surface layer of CC and WTRA, prochlorophytes and nanoflagellates with high levels of photoprotective pigments were dominating (Figure 5.3 and Table 5.4, Cluster A).

**Mid-day Fv/Fm**

In general, Fv/Fm measured at mid-day stations with the light chamber ($Fv/Fm_L$) was quenched at the surface, and Fv/Fm increased as it deepened (decreasing light) until the maximum value, which was deeper than the depth of the chlorophyll maximum. In the ETRA $Fv/Fm_L$ profile had the same shape as in the pre-dawn but with higher values.

In the SATL, where a DCM was the characteristic feature, the vertical profile had double quenching-recovering pattern in the $Fv/Fm_L$: quenching-recovering for the phytoplankton community above the DCM and another quenching-recovering pattern for the phytoplankton community at the DCM (Figure 6.4, station 31). This double quenching-recovery pattern was not evident in the Northern Gyre where the isothermal layer depth (ILD) was shallower than the depth of nitracline (Table 4.2).

**Diel variation in Fv/Fm**

The diel variation in Fv/Fm was characteristically dependent on the province and depth. At CC, WTRA and RCBC, $Fv/Fm_L$ was lower than $Fv/Fm_{dawn}$ for the surface phytoplankton community, whilst there was no difference between $Fv/Fm_{dawn}$ and $Fv/Fm_L$ for the phytoplankton community at and below the chlorophyll maximum, except for RCBC where $Fv/Fm_{dawn}$ was higher than $Fv/Fm_L$ (Figure 6.5). In provinces with DCM (NADR, NASE and SATL) the surface community had $Fv/Fm_{dawn}$ higher than $Fv/Fm_L$ but no significant difference was detected at and below the DCM (Figure 6.4). In the ETRA the $Fv/Fm_{dawn}$ was lower than $Fv/Fm_L$ in the whole water column (Figure 6.3).

### 6.3.3 Effective absorption cross-section: $\sigma_{PSII}$

The effective absorption cross-section ($\sigma_{PSII}$) measured by light and dark chambers should be the same regardless the ambient light because the time interval that the phytoplankton was held in the darkness of the dark chamber was shorter ($< 0.4$ s) than that required for recovery from non-photochemical quenching. The minimum time necessary for the phytoplankton to recover from pH triggered non-photochemical quenching, the quickest of them, has been documented as few seconds (Müller *et al.* 2001). Therefore, measurements of $\sigma_{PSII}$ from the two chambers must be the same. In this work dark chamber measurements of effective absorption cross-section were analysed ($\sigma_{PSII}$ and $\sigma_{PSIIdawn}$ for the pre-dawn measurement).

The depth of maximum $\sigma_{PSII}$ was related to the depth of nitracline (N2, see Chapter 4) with stations 16 and 18 as outliers (Figure 6.6).

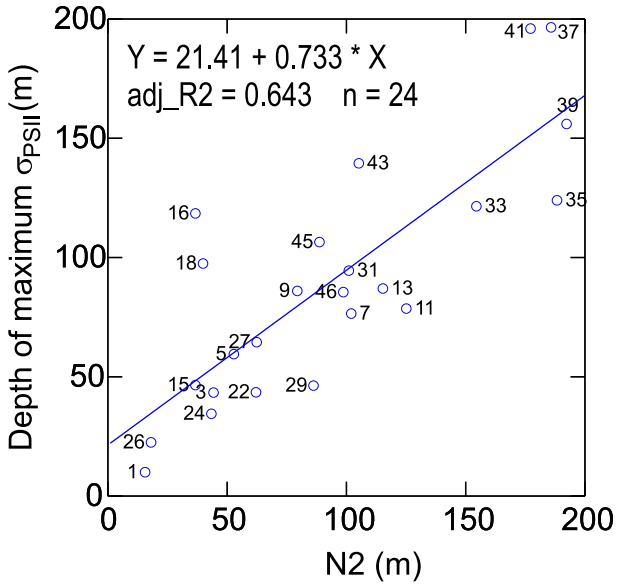


Figure 6.6: Relationship between the depth of maximum $\sigma_{\mathrm{PSII}}$ and the depth of nitracline (N2).

### Vertical profile of $\sigma_{\mathrm{PSII}}$

The vertical profile of $\sigma_{\mathrm{PSII}}$ are shown in Figures 6.7, 6.8 and 6.9. The $\sigma_{\mathrm{PSII}}$ along AMT11 transect varied from 277.6 to 729.4 $\times 10^{-20}$ m$^2$ photon$^{-1}$.

There was not a clear pattern in the $\sigma_{\mathrm{PSIIdawn}}$ (Figures 6.7, 6.8 and 6.9) following the Fv/Fm pattern detected at pre-dawn. The vertical profile of $\sigma_{\mathrm{PSIIdawn}}$ showed two distinct characteristic shapes. In the oligotrophic gyres (NASE and SATL) and RCBC, the maximum Chl*a* was deep, $\sigma_{\mathrm{PSIIdawn}}$ was almost constant in the water column (Figures 6.8 and 6.9). In NADR, CC, WTRA and ETRA, where the depth of maximum Chl*a* was shallower than 60 m, $\sigma_{\mathrm{PSIIdawn}}$ was small in the surface and maximum at the depth of maximum Chl*a* (Figure 6.7 and 6.8).

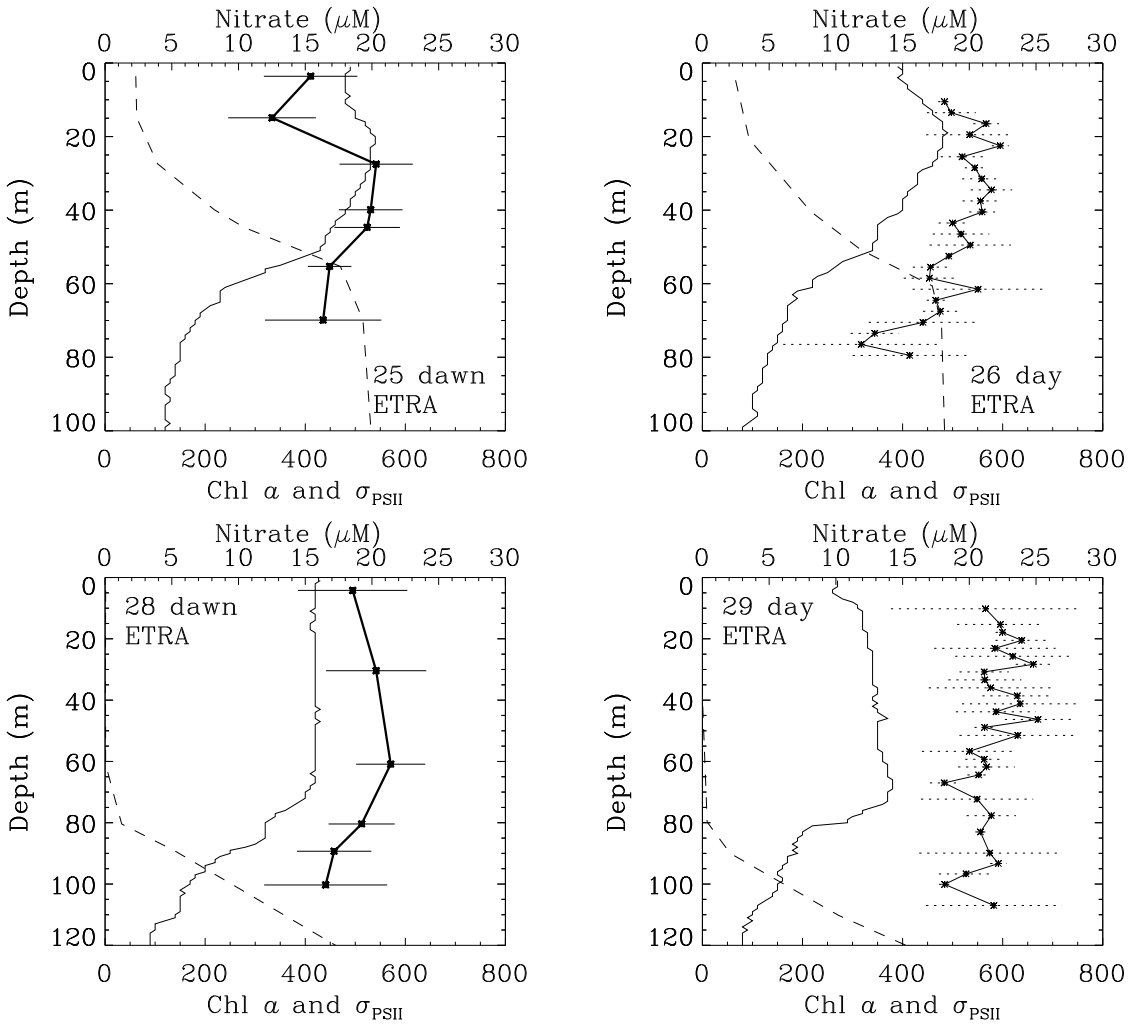


Figure 6.7: Effective absorption cross-section ($\sigma_{\mathrm{PSII}}$) for the high nutrient province (ETRA). Station profiles of nitrate (dashed line), Chl$a$ (in $\mu$g m$^{-3}$, solid line) and $\sigma_{\mathrm{PSII}}$ (in $10^{-20}$ m$^2$ photon$^{-1}$, $\sigma_{\mathrm{PSIIdawn}}$ in solid thick line with * and mid-day $\sigma_{\mathrm{PSII}}$ in dotted line with *) with standard deviation as error bars are presented. Left side graphics are pre-dawn stations (dawn) and right side graphics are the following mid-day stations (day).

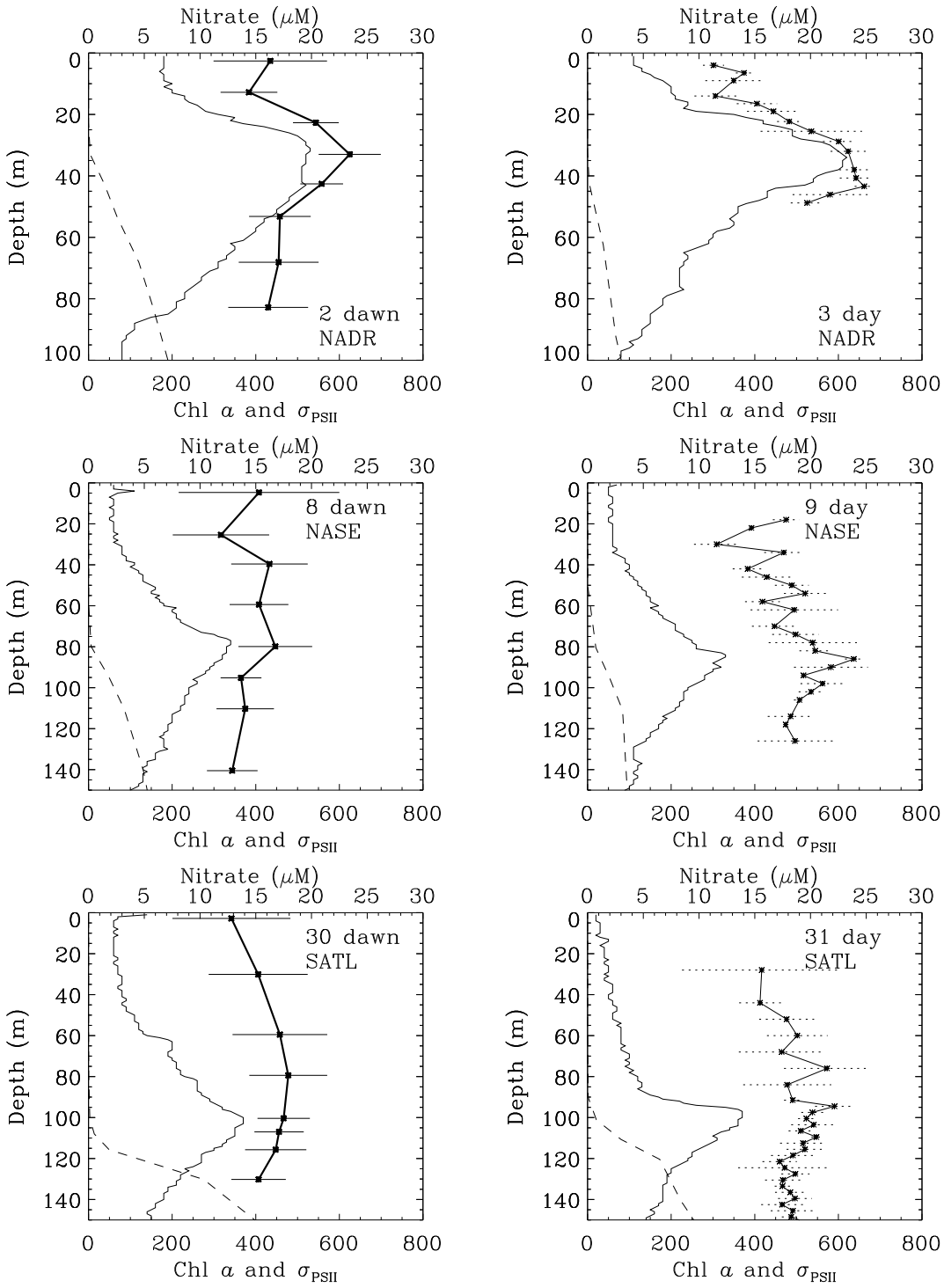


Figure 6.8: Effective absorption cross-section ($\sigma_{\mathrm{PSII}}$) for the provinces with minimum Fv/Fm at the depth of Chl$a$ maximum (NADR, NASE and SATL). Station profiles of nitrate (dashed line), Chl$a$ (solid line, in $\mu$g m$^{-3}$) and $\sigma_{\mathrm{PSII}}$ (in $10^{-20}$ m$^2$ photon$^{-1}$, $\sigma_{\mathrm{PSIIdawn}}$ in solid thick line with * and mid-day $\sigma_{\mathrm{PSII}}$ in dotted line with *) with standard deviation as error bars are presented. Left side graphics are pre-dawn stations (dawn) and right side graphics are the following mid-day stations (day).

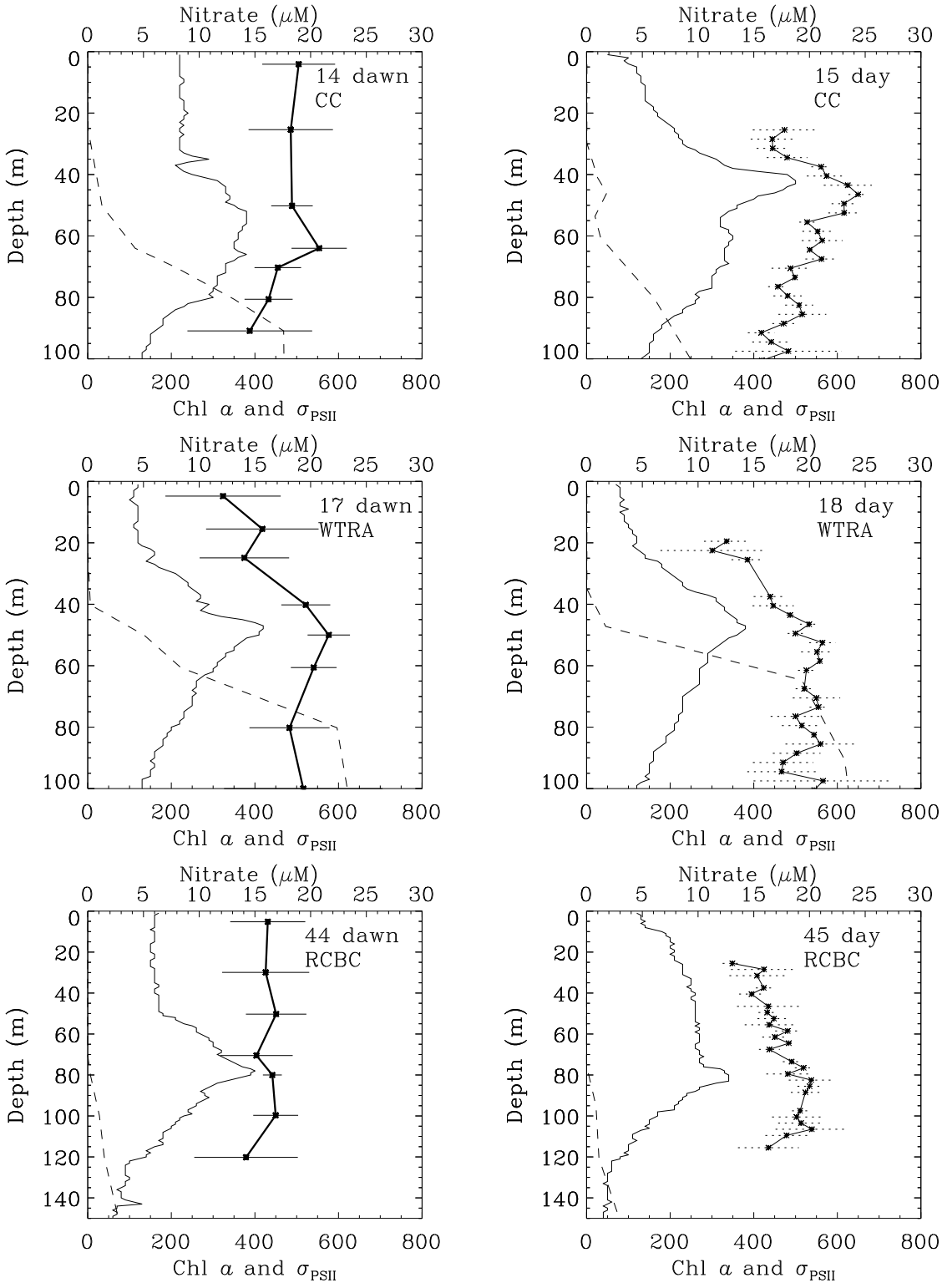


Figure 6.9: Effective absorption cross-section ($\sigma_{\mathrm{PSII}}$) for the provinces with maximum Fv/Fm at the depth of Chl$a$ maximum (CC, WTRA and RCBC). Station profiles of nitrate (dashed line), Chl$a$ (solid line, in $\mu$g m$^{-3}$) and $\sigma_{\mathrm{PSII}}$ (in $\times 10^{-20}$ m$^2$ photon$^{-1}$, $\sigma_{\mathrm{PSIIdawn}}$ in solid thick line with * and mid-day $\sigma_{\mathrm{PSII}}$ in dotted line with *) with standard deviation as error bars are presented. Left side graphics are pre-dawn stations (dawn) and right side graphics are the following mid-day stations (day).

**Diel variation in $\sigma_{PSII}$**

In provinces where $Fv/Fm_{dawn}$ was minimum at the DCM (NADR, NASE, ETRA and SATL) $\sigma_{PSII}$ was maximum around the DCM, except in NASE, with lower value at pre-dawn (Figures 6.7 and 6.8). Surface values were in general lower at pre-dawn, except for NADR. In provinces where $Fv/Fm_{dawn}$ was maximum at the DCM (Figure 6.9), $\sigma_{PSIIdawn}$ was lower than mid-day value around the DCM (CC and RCBC) or at least similar (WTRA). Above the DCM there was no difference between the $\sigma_{PSIIdawn}$ and $\sigma_{PSII}$ values.

## 6.4 Discussion

### 6.4.1 Nutrient replete region with $Fv/Fm_{dawn} < Fv/Fm_{L}$

The most unexpected feature was detected in the ETRA where surface nitrate concentration was the highest in the whole AMT11 transect. $Fv/Fm_{dawn}$ was about 0.1 smaller than $Fv/Fm_{L}$. It was expected a diel variation in which pre-dawn measurement was higher than the mid-day because there was plenty of nutrient available even at the surface and the phytoplankton would recover the photochemical efficiency after overnight recovery from photochemical and non-photochemical quenchings and repair of PSII. It did not happen in the ETRA. The pattern of $Fv/Fm_{dawn}$ smaller than $Fv/Fm_{L}$ was detected in the surface of Equatorial Pacific (Behrenfeld *et al.* 1996), which is a well known *high nutrient and low chlorophyll* (HNLC) region and also in the South Pacific gyre where nutrient was depleted and the dominant phytoplankton were prokaryotes (Behrenfeld and Kolber 1999). Despite deficiency in nitrate in the South Pacific gyre, Behrenfeld and Kolber (1999) attributed that diel variation to iron deficiency. They argued that in prokaryotes darkness leads to state II transition which causes a detachment of chlorophyll-protein

complex of PSII, decreasing the $\sigma_{\mathrm{PSII}}$. Fv/Fm measured in environments with lack of iron has shown an increase in the background fluorescence, which affects Fo and decreases Fv/Fm. When State II transition occurs, the phosphorylation caused by reduction of platoquinone pool and some pigment protein complex detaches from the PSII, decreasing the $\sigma_{\mathrm{PSII}}$. Normally that detached part of chlorophyll-protein complex attaches to the PSI (Falkowski and Raven 1997), increasing the PSI antenna size. In iron deficiency, however, the relative abundance of PSI lessens, decreasing the probability of that detached chlorophyll-protein complex to attach to a PSI. Then the absorbed light of that portion is re-emitted as fluorescence, increasing the background fluorescence and enhancing the decrease in Fv/Fm. Some parts of the Atlantic Ocean have shown deficiency in iron. Dissolved iron measurements carried out along AMT3 and AMT6 (Bowie *et al.* 2002) indicated ETRA alongside the oligotrophic gyres, as the lowest dissolved iron region of the Atlantic Ocean. Although differences between the phytoplankton community in ETRA (mainly eukaryotes) and in the South Pacific gyre (mainly prokaryotes) and also that the former was nutrient replete and the later nutrient deficient, iron seems to be the limiting factor in ETRA. The same nocturnal reduction of the plastoquinone pool under iron deficiency was observed in eukaryotic cells, increasing the background fluorescence (Belkhodja *et al.* 1998). Iron deficiency also caused a decrease in nocturnal $\sigma_{\mathrm{PSII}}$ in relation to the day value (Behrenfeld and Kolber 1999) and similar variation was observed in ETRA (Figure 6.7). Sosik *et al.* (2002) analysed the PSII turnover time ($\tau_{\mathrm{QA}}$) to discriminate between the physiological effects of nitrogen and iron deficiency (Falkowski *et al.* 1992). A systematic increase in $\tau_{\mathrm{QA}}$ has been documented with increasing iron deficiency (Greene *et al.* 1992) whilst nitrogen limitation caused no apparent variation in $\tau_{\mathrm{QA}}$ (Kolber *et al.* 1988). Such patterns have not, however, been found in the iron deficient Antarctic waters, so suggesting that the interpretation of measurement of $\tau_{\mathrm{QA}}$ in the environment

needs more laboratory work for adequate interpretation (Sosik *et al.* 2002). In ETRA $\tau_{QA}$ was higher in the surface waters (top 20 to 30 m only), supporting the theory of iron deficiency in the region (Figure 6.10). More discussion about iron limitation is presented later.

### 6.4.2 Vertical profile of $Fv/Fm_{dawn}$

In previous AMT transects, two characteristic vertical profiles of dissolved iron have been documented (Bowie *et al.* 2002). Profiles with minimum dissolved iron coincident with depth of maximum Chl*a* were found in regions with DCM of Chl*a* concentration $< 0.5$ mg $m^{-3}$ and low macronutrient concentration in the euphotic zone. Such iron depletion was more closely associated with higher rate for iron removal than iron supply. Another set of vertical profiles had the maximum dissolved iron at the depth of maximum Chl*a*, and it was found in the vicinity of sub-tropical convergence zone in the Southwest Atlantic, in the northwest African upwelling regions and in a region influenced by river outflow. These regions match respectively to RCBC, CC and WTRA of AMT11.

Iron addition was shown to cause an increase in Fv/Fm in HNLC regions (Kolber *et al.* 1994, Behrenfeld *et al.* 1996) and the response of Fv/Fm was more rapid than either the increase in biomass or the change in community structure during the iron release experiment in the Southern Ocean (Boyd and Abraham 2001).

Considering that iron limitation causes decrease in Fv/Fm, the depression in $Fv/Fm_{dawn}$ at the depth of maximum Chl*a* along the AMT11 transect (NADR, NASE and SATL, Figure 6.4) could an effect of iron deficiency over phytoplankton physiology. This proposition of iron deficiency can be reinforced by dissolved iron measurements during the AMT3 and AMT6 (Bowie *et al.* 2002). They found the lowest dissolved iron around the DCM

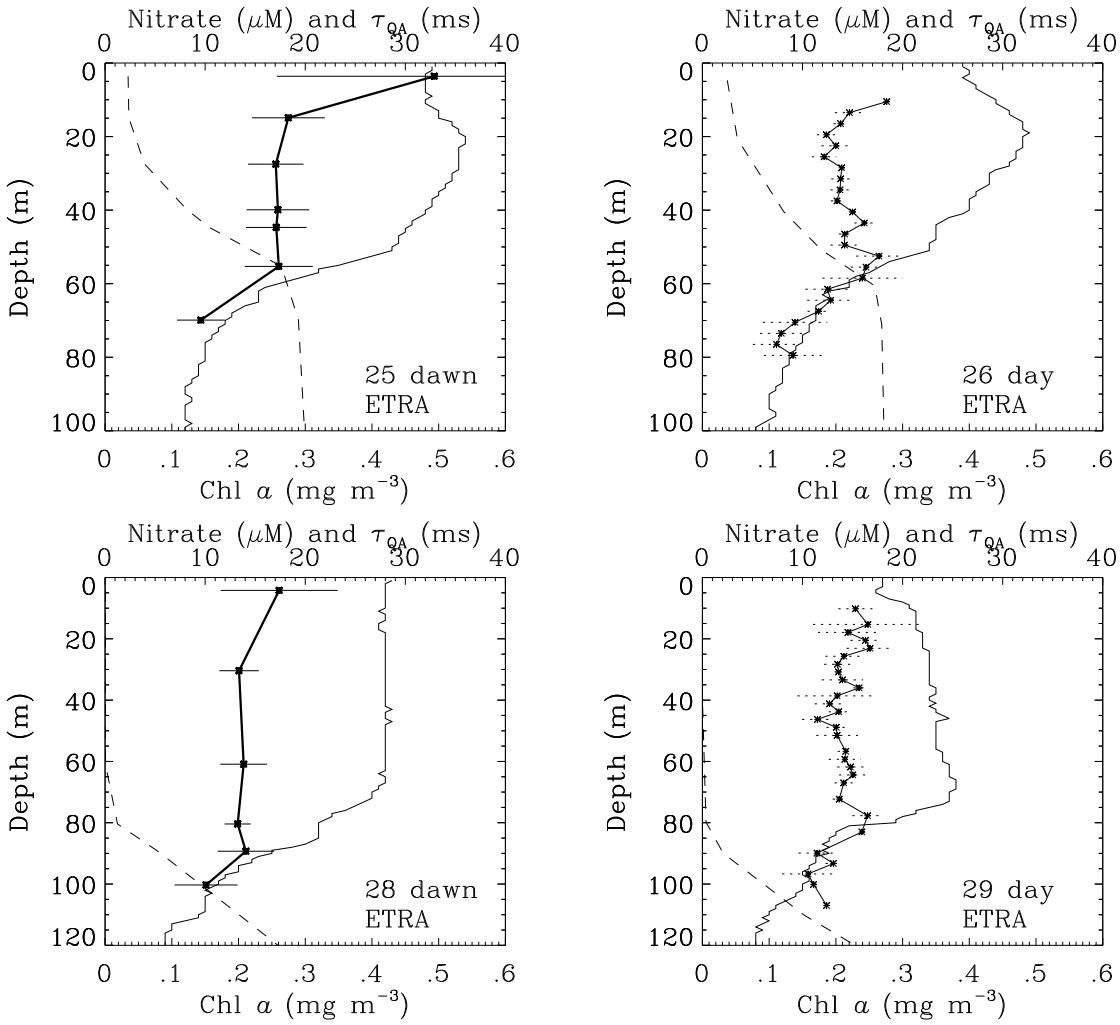


Figure 6.10: PSII turnover time ($\tau_{\mathrm{QA}}$) for the high nutrient province (ETRA). Profiles of $\tau_{\mathrm{QA}}$ (dawn value in solid thick line with *, mid-day value in dotted line with *, in ms) with standard deviation as error bars, Chl$a$ concentration (solid line) and nitrate (dashed line) are shown. Left side graphics are pre-dawn stations (dawn) and right side graphics are the following mid-day stations (day).

of the gyres. If this feature of minimum iron around the DCM of gyres frequent, it might be the cause for lower Fv/Fm. The lack of iron led to decrease in Fv/Fm around the maximum Chl*a*. Although there was a difference in the Chl*a* concentration and phytoplankton community structure between ETRA and the gyres (NADR, NASE and SATL), the depression in $Fv/Fm_{dawn}$ in these four provinces seems to have the same cause, the iron supply was lower than the iron consumption by the phytoplankton which led to the iron limitation. The major cause of reduction in Fv/Fo[1] under iron or nitrate limitation has been considered due to the reduction in the efficiency to transfer excitation energy to the reaction centres (Greene *et al.* 1991, Falkowski 1992). Iron deficiency causes a reduction in photosytem II proteins D1, D2, CP43 and CP47. The loss of D1 was consistent with a reduction in functional reaction centre II content (Greene *et al.* 1991). CP43 and CP47 are important proteins that mediate excitation energy transfer from the antenna to the reaction centre (Bassi *et al.* 1987) and their damage was being reflected in the proportional decrease in $Fv/Fm_{dawn}$. Other studies have indicated iron as the limiting factor for fixation of nitrogen by marine phytoplankton (Falkowski 1997, Falkowski 2000). Iron is required in the enzyme nitrogenase, necessary to catalyse the reaction and it requires iron. Iron is also highly required in the PSI (see Figure 2.1).

Bowie *et al.* (2002) argue that the lower dissolved iron around the DCM in the gyres is due to higher iron consumption by the phytoplankton at DCM than in the other part of the water column due to higher biomass (Chl*a*), so higher requirement and consumption of iron, decreasing the dissolved iron in the water. Lower dissolved iron in the water causes decrease in the proteins for energy transfer (Greene *et al.* 1991, Falkowski 1992). The lack of those proteins leads to the excess excitation energy being dissipated as fluorescence

[1]Fv/Fo is related to Fv/Fm through Fv/Fo = (Fv/Fm)/(1-Fv/Fm) and the theoretical maximum value is 1.8.

and decreasing Fv/Fm (Kolber *et al.* 1988).

The stratification in the $Fv/Fm_{dawn}$, inclusive in ETRA, can be explained by the same reason. If the iron requirement is dependent on the biomass, the higher the biomass, the higher the iron consumption, the lower the dissolved iron available in the water, so the lower would be Fv/Fm. $Fv/Fm_{dawn}$ was responding proportionally to the dissolved iron in the water with minimum around the DCM (Figures 6.3, 6.5, 6.4).

Stratification in $\tau_{QA}$ with opposite pattern to $Fv/Fm_{dawn}$, e.g. higher $\tau_{QA}$ around the DCM, was observed in the provinces with minimum $Fv/Fm_{dawn}$ around the DCM (Figure 6.11). Iron limitation has been recognised to increase $\tau_{QA}$ (Greene *et al.* 1992, Sosik and Olson 2002), supporting the proposition that there was iron limitation around the depth of maximum Chl*a* in NADR, NASE and SATL. The increase in $\tau_{QA}$ (Figure 6.10) in the surface waters of ETRA was not as evident as observed in the DCM of NADR, NASE and SATL (Figure 6.11). Sosik and Olson (2002) anlysing iron limitation in the Southern Ocean did not found bigger $\tau_{QA}$ where iron was deficient. They concluded more research was still needed.

The AMT11 provinces with maximum $Fv/Fm_{dawn}$ around the DCM (Figure 6.9, CC, WTRA and RCBC) were coincident with regions where dissolved iron was higher in the DCM during the AMT3 and AMT6 (Bowie *et al.* 2002). They explained that increase in terms of regeneration through degradation of organic matter or grazing by zooplankton and subsequent release increased dissolved iron. $Fv/Fm_{dawn}$ profiles in these provinces reinforce that this phytoplankton physiological parameter can be a direct indicator of relative availability of iron in the water column.

Adopting the proposition that iron was replete around the depth of maximum Chl*a*,

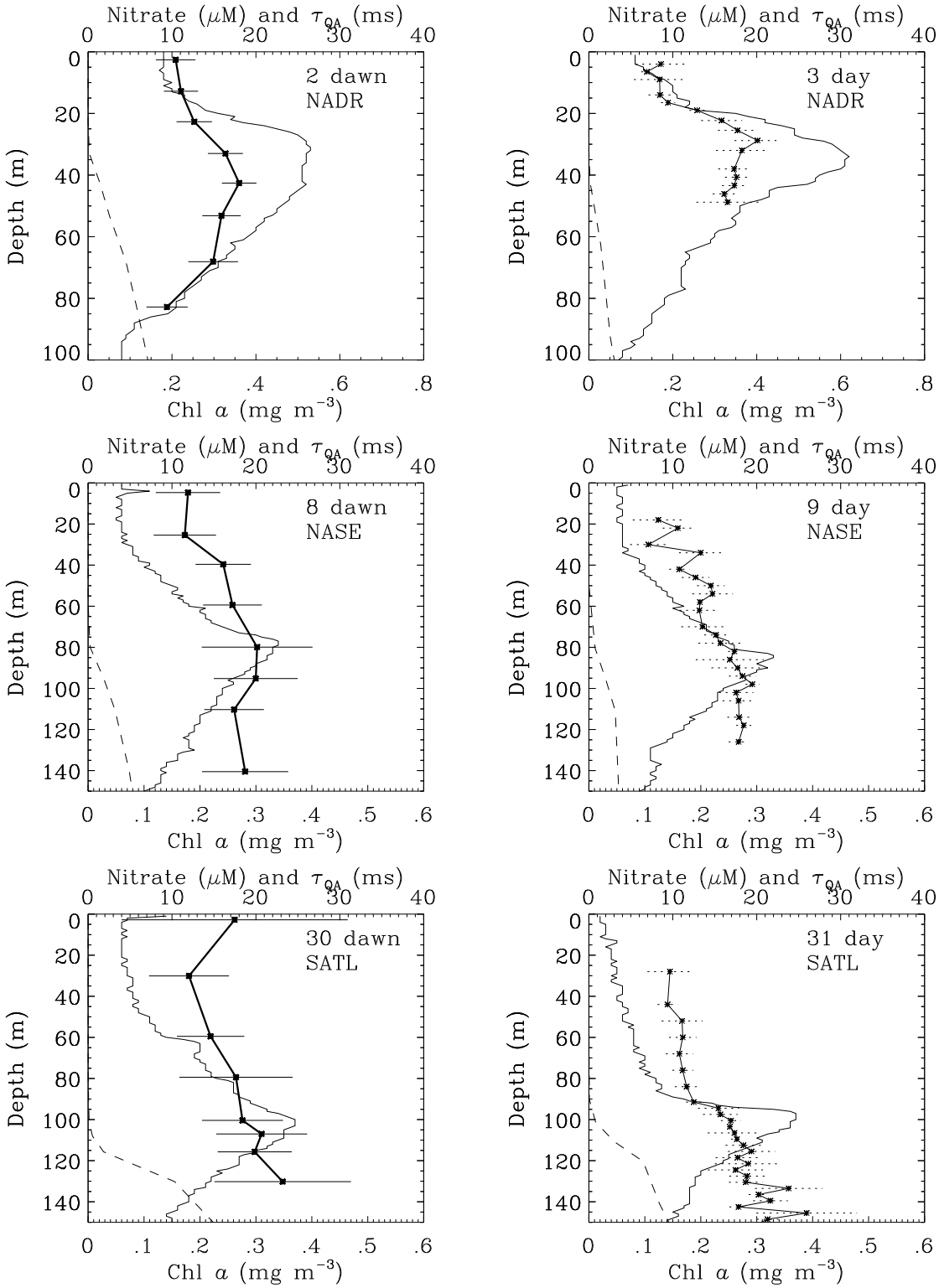


Figure 6.11: PSII turnover time ($\tau_{\mathrm{QA}}$) for the provinces with the minimum Fv/Fm at the depth of Chl*a* maximum (NADR, NASE and SATL). Profiles of $\tau_{\mathrm{QA}}$ (dawn value in solid thick line with *, mid-day value in dotted line with *, in ms) with standard deviation as error bars, Chl*a* concentration (solid line) and nitrate (dashed line) are shown. Left side graphics are the pre-dawn stations (dawn) and right side graphics are the following mid-day stations (day).

higher value of $\tau_{QA}$ is not expected around these depths as observed during the AMT11 in the CC, WTRA and RCBC (Figure 6.12). Unfortunately, the surface layer could not be sampled properly but there might be iron deficiency at surface of RCBC as hinted because $Fv/Fm_{dawn}$ is lower than Fv/Fm at mid-day value above the depth of maximum Chl*a* (Figure 6.4) and mid-day $\tau_{QA}$ is higher at surface than around the depth of maximum Chl*a* (Figure 6.12). These results do not mean, however, that the phytoplankton are growing at maximum limit in CC, WTRA and RCBC despite higher $Fv/Fm_{dawn}$ around the DCM. Although there is an increase in $Fv/Fm_{dawn}$ around the DCM, they did not recover totally and the maximum value was still far lower than the theoretical maximum of 0.65. The phytoplankton growth may be limited by either iron even with recycling of iron around the DCM or by some other nutrient.

**Diel variation of Fv/Fm**: The above findings also support the proposition that surface waters of the Atlantic Ocean were not iron limited (Behrenfeld and Kolber 1999). In the surface of NADR, NASE and SATL, nitrate was lower than 0.01 $\mu$M and $Fv/Fm_{dawn}$ was higher than $Fv/Fm_L$ (Figures 6.3 and 6.4). Non-photochemical quenching was probably acting in the surface waters of the oligotrophic gyres, so an overnight recovery allowed the phytoplankton to regain the photochemical efficiency. Either nitrogen or iron limitation provokes decrease in Fv/Fm, due to the loss of PSII proteins (Kolber *et al.* 1988, Greene *et al.* 1992). Iron deficiency, however, leads to a decrease of the ratio of number of PSI in relation to PSII. In the ETRA (Figure 6.7), there was indeed a night decrease in $\sigma_{PSII}$ though it was not as enhanced as the diel variation observed in the South Pacific gyre (Behrenfeld and Kolber 1999). The dominant phytoplankton in ETRA were eukaryotes which nocturnal reduction of plastoquinone pool was attributed to chlororespiration (Belkhodja *et al.* 1998) and it may not be enough to cause big difference in $\sigma_{PSII}$, as observed for prokaryotes in the South Pacific gyre.

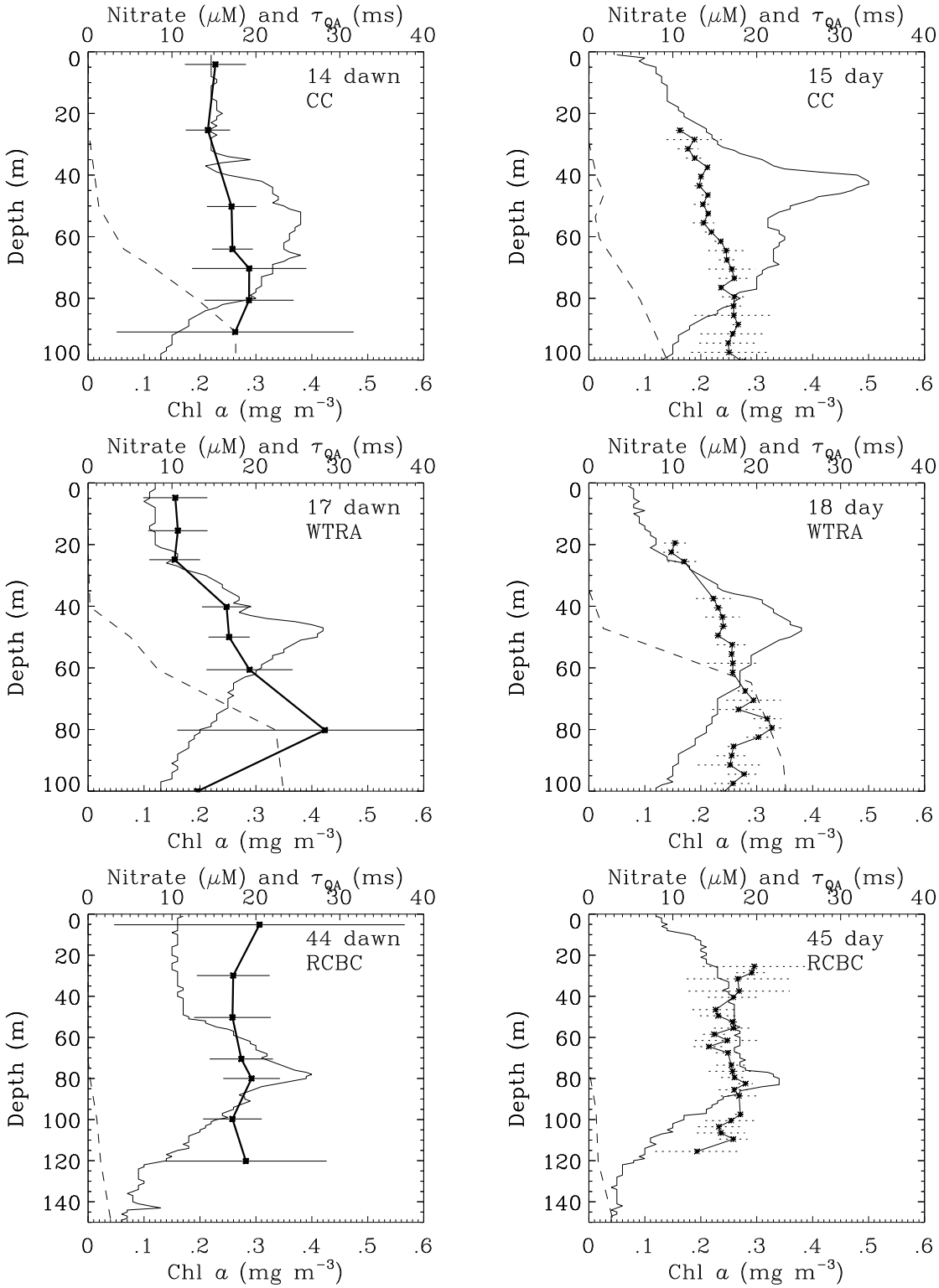


Figure 6.12: PSII turnover time ($\tau_{\mathrm{QA}}$) for the provinces with the maximum Fv/Fm at the depth of Chl*a* maximum (CC, WTRA and RCBC). Profiles of $\tau_{\mathrm{QA}}$ (dawn value in solid thick line with *, mid-day value in dotted line with *, in ms) with standard deviation as error bars, Chl*a* concentration (solid line) and nitrate (dashed line) are shown. Left side graphics are the pre-dawn stations (dawn) and right side graphics are the following mid-day stations (day).

### 6.4.3 DCM of oligotrophic gyres

In the DCM of oligotrophic gyres, $Fv/Fm_{dawn}$ and $Fv/Fm_{L}$ were similar (Figure 6.4) but $\sigma_{PSIIdawn}$ values were lower than mid-day $\sigma_{PSII}$ values (Figure 6.8). Change in $\sigma_{PSII}$ without change in Fv/Fm has been attributed to the non-photochemical quenching in the antenna only (Falkowski and Raven 1997). The results presented so far suggest iron deficiency, causing decrease in $Fv/Fm_{dawn}$ around the DCM, causing stress to the phytoplankton. Both non-photochemical quenching and iron limitation were acting over Fv/Fm. The vertical variation was caused by vertical distribution of dissolved iron while diel variation in physiology was due to the non-photochemical quenching. Do phytoplankton in such deep water with light at mid-day less than 10 $\mu$E $m^{-2}$ $s^{-1}$ still need photoprotection that cause diel variation in the physiology? This is a question that needs to be investigated further with fluorescence technique since it cannot be resolved with $^{14}C$ methods which are not sensitive enough at such low light.

The phytoplankton community found at this depth can tolerate more shortage in iron, nutrient and light despite damaged physiology. This kind of ecology are documented for saltmarsh plants, found in a stressful environment of broad range of salinity although they grow better in more stable conditions where most of the plants are found (Adam 1993). They are found in stressful environments to avoid competition with other species. Maybe the phytoplankton community found in the DCM of oligotrophic gyre of Atlantic Ocean, although stressed by deficiency of iron and with limited growth rate, can survive in such situation.

### 6.4.4 Oligotrophic gyres in the Atlantic Ocean

Phytoplankton community above and around the DCM of oligotrophic gyres are physiologically limited due to nutrient deficiency. Nitrate may be limiting phytoplankton growth in the top layer of water column, since there was no evidence of iron limitation in diel variation of either Fv/Fm or $\tau_{QA}$. The iron supply in the Atlantic Ocean must be barely enough for the phytoplankton development, regulating the species composition (Geider and La Roche 1994). Around the thermocline the supply of iron and macronutrients are enough for phytoplankton growth but the re-supply of iron is not enough to allow the phytoplankton to grow healthily despite the formation of DCMs. The regulation of phytoplankton growth is physiologically limited by deficiency of iron (bottom up). Deeper, light availability is the limiting factor for the phytoplankton.

## 6.5 Summary and conclusions

Phytoplankton physiology was assessed with fast repetition rate fluorometry through the Atlantic Ocean. This method allows real-time, *in situ* measurements under ambient light conditions, with no manipulation of the sample. It measures dynamic parameters of phytoplankton physiology that reacted to diel change and even quicker fluctuations of light intensities due to cloud cover. This advantage of the method may be a hindrance if the measurement light conditions are not stable and standardised. The rapid adjustments of the phytoplankton physiology to environmental fluctuations make the interpretation difficult. To minimise the effect of these rapid changes, sampling took place at fixed times of the day with ambient light monitored.

Diel variations in the surface of the gyres in the Atlantic Atlantic Ocean was evidenc-

ing nitrate limitation, reinforcing the results of Behrenfeld and Kolber (1999). However around the DCM, the physiological parameters showed strong evidence of impairment in phytoplankton physiology, due probably to iron deficiency, not only in the gyres but also in ETRA. The DCM in the oligotrophic gyres and ETRA had higher nitrate, similar nutrient condition to high nutrient low chlorophyll regions in the Pacific Ocean where iron is limiting physiology as confirmed in iron enrichment experiments. Iron limitation provokes lower Fv/Fm during the night than during the night. Even in provinces where there was a physiological recovery after an overnight period in darkness (CC, WTRA and RCBC), there was not a total recovery and that may be due to limitation of iron or some other nutrient.

Although this hypothesis of iron limitation is speculation, it is supported by dissolved iron measurements carried out during the AMT3 and AMT6 by Bowie *et al.* (2000). According to their measurements, ETRA and the oligotrophic gyres had the lowest concentration of dissolved iron with even lower values around the DCM of the oligotrophic gyres. Such measurements are coincident with the hypothesis based in the analysis of FRRF physiological data: iron deficiency in the ETRA and around the DCM of oligotrophic gyres. The FRRF physiological data of AMT11 also suggest that around the depth of maximum Chl*a* of CC, WTRA and RCBC, iron is more available than in the rest of the water column. During the AMT3 and AMT6, Bowie *et al.* (2000) measured higher values of dissolved iron around the depth of maximum Chl*a* in regions with coastal upwelling influences in the Western African coast, in regions of river discharge and in the subtropical convergence zone in the southwest of Atlantic Ocean, which hydrographical description are similar to CC, WTRA and RCBC of AMT11, respectively. A concomitant measurement of dissolved iron and phytoplankton physiology are still required for confirmation of these conclusions.

Active fluorescence technique can cover wide range of light intensity, from surface waters with light higher than 500 $\mu$E m$^{-2}$ s$^{-1}$ to very deep waters with light as low as 0.5 $\mu$E m$^{-2}$ s$^{-1}$. Although upper layer of the water column was undersampled, it could be improved if gain is set to auto-ranging mode with slower deployment.

# Chapter 7

# Primary productivity

## 7.1 Introduction

Traditionally primary production in the oceans has been determined with a time consuming method, counting the radiation of $^{14}C$ incorporated into the phytoplankton biomass. Despite the long history of the $^{14}C$ method, not only the measurement is on discrete samples but also there are still uncertainties associated with the method, such as the significance of differences between light and dark bottle incubations (Harris *et al.* 1989, Grande *et al.* 1989), no sensitivity for low light (Steeman Nielsen 1952 in Søndergaard 2002), the uncertainty of $^{14}C$ measurement if it measures gross primary production, net primary production or something between them (Peterson 1980). Differences in duration of incubation does not affect as much as does the inclusion of dark period to the $^{14}C$ incubation (Woods 2003). Loss of carbon during the dark period is due to respiration of assimilated carbon by phytoplankton, grazing and respiration by heterotrophs (Harris *et al.* 1989).

Estimates of phytoplankton physiological parameters by measurements of variable fluo-

rescence with some assumptions and parameterisation using Equation 2.11 may allow an easier and quicker way for determination of carbon fixation rates. If this method can give a confident determination of carbon fixation rates, it overcomes the need for an incubation over a period of time and bottle effects. The determination of carbon fixation rates through fluorescence method can be applied also continuously and at lower light than the $^{14}$C methods.

This chapter will cover the fast repetition rate measurements applied to the determination of carbon fixation in the Atlantic Ocean and the limitations of the methods.

All the data were collected during the AMT11 (Chapter 3) and all the analyses and conclusions from this chapter applies to the transect of this cruise.

## 7.2 Methodology

### 7.2.1 Carbon fixation rate using FRR fluorometry parameters

As seen in the Chapter 2 section 2.6, primary production can be determined from physiological parameters derived from the FRR fluorescence measurements ($Fv/Fm_L$, $\sigma_{PSII}$), photosynthetically available radiation (PAR) and some assumptions:

$$P_B = \frac{Fv/Fm_L}{0.65} \times \sigma_{PSII} \times PAR \times n_{PSII} \times \phi_e \times (PQ)^{-1} \tag{7.1}$$

where $P_B(z)$ is the biomass specific productivity in mgC mgChl$^{-1}$ h$^{-1}$, $n_{PSII}$, $\phi_e$ and PQ were assumed to be constant as seen in Chapter 2. The $n_{PSII}$ is dependent on whether the phytoplankton are eukaryotic or prokaryotic as discussed later (Section 7.2.1). PAR changes throughout the day and with depth, as do $Fv/Fm_L$ and $\sigma_{PSII}$, so these parameters

accounted for variations in the primary productivity of a water parcel, P(t, z) in mgC $m^{-3}$ $s^{-1}$:

$$P(t, z) = P_B(t, z) \times \text{Chl a}(t, z) \tag{7.2}$$

where t represents the time and z the depth. The day integration, from sunrise to sunset, of the Equation 7.2 gave the primary productivity of a water parcel in a day, P(z) in mgC $m^{-3}$ $d^{-1}$:

$$P(z) = \int_{t=t_0}^{t=t_n} P(t, z)dt \tag{7.3}$$

To obtain the primary productivity of the water column, $P_{col}$ in mgC $m^{-2}$ $d^{-1}$, Equation 7.3 was integrated in the depth:

$$P_{col} = \int_{z=z_0}^{z=z_{max}} P(z)dz \tag{7.4}$$

**Phytoplankton physiology parameters**

FRR fluorescence measurements from the mid-day station was used to derive $Fv/Fm_L$ and $\sigma_{PSII}$. It was assumed that there was no change in these two parameters during the day for the stations. The data were processed and binned as previously described (Chapter 6 Section 6.2.1).

No quality control was applied here, so errors was calculated. The error of the primary productivity was calculated from the standard deviation of $Fv/Fm_L$ and $\sigma_{PSII}$ from depth-binned data only. The software (FRS v1.8, Chelsea Technologies Group) used to fit the curve to retrieve Fo, Fm, so $Fv/Fm_L$, and $\sigma_{PSII}$, from the FRR fluorescences, does not give the errors due to the fitting.

**Eukaryotes and Prokaryotes**

In oligotrophic waters, prokaryotic phytoplankton have been recognised as contributing significantly to the phytoplankton biomass and production (Zubkov *et al.* 1998, Partensky *et al.* 1999) and significant amounts of marker pigment for prochlorophytes (DVChl*a*) were found along the AMT11 transect, indicating their contribution to the totChl*a* was varying between 30 to 55 % (Chapter 5). Research carried out to measure the size of the photosystem units gave mean values of 1/500 PSII reaction centre per Chl*a* ($n_{PSII}$) for eukaryotic cells ($n_{euk}$) and 1/300 PSII reaction centre per Chl*a* in prokaryotes ($n_{prok}$) under optimal conditions (Falkowski and Kolber 1995). $n_{PSII}$ varies depending on the species, nutrient availability and light. The big difference in $n_{PSII}$ between prokaryotes and eukaryotes led to the attempt to determine the fractionated carbon fixation rate for these two groups of phytoplankton using Equation 7.1, so as to obtain the group fractionated $P_B$ for prokaryotes ($P_{Bprok}$) and eukaryotes ($P_{Beuk}$). The HPLC method allowed the fractionation of the Chl*a* into DVChl*a* and MVChl*a* (Barlow *et al.* 1997a, Zapata *et al.* 2000) for prochlorophytes and eukaryotes respectively (Jeffrey *et al.* 1997). The group fractionated Chl*a* was used in the Equations 7.2 and 7.3 to determine the group fractionated carbon fixation rate for prochlorophytes, $P_{proc}(z)$, and eukaryotes, $P_{euk}(z)$.

The total carbon fixation rate ($P_{col}$) of the water column in a day was determined as a sum of the group fractionated $P_{col}$ for prochlorophytes, $P_{col_{proc}}$, and eukaryotes, $P_{col_{euk}}$ (Equation 7.5):

$$P_{col} = P_{col_{proc}} + P_{col_{euk}} \tag{7.5}$$

DVChl*a*, however, represented prochlorophytes only and not other prokaryotes like *Synechococcus*, which were more abundant around the upwelling region of the Canary Cur-

rent (Bricaud *et al.* 1995, Zubkov *et al.* 1998). The main photosynthetic pigments of *Synechococcus* are phycobiliproteins and MVChl*a*, whilst its photoprotectant pigment is zeaxanthin (Rowan 1989). During the AMT11, MVChl*a* and zeaxanthin were measured but no phycobiliproteins were analysed. MVChl*a* is a ubiquitous pigment for every eukaryotic phytoplankton and zeaxanthin is present in many of the eukaryotes and also in prochlorophytes (Jeffrey *et al.* 1997). The pigment data available were not enough to assess the presence of *Synechococcus*, and the particle absorption spectra that could pick up the presence of *Synechococcus* (Bricaud *et al.* 1995) failed for the AMT3 cruise. The higher cell concentration of *Synechococcus* around 20°N by flow cytometry in AMT3 cruise (Zubkov *et al.* 1998) was not detected by particle absorption spectra (Barlow *et al.* 2002). The amount of MVChl*a* due to the *Synechococcus* could be calculated if flow cytometry had been performed (Barlow *et al.* 1997b) but there was none during the AMT11. In this work, the carbon fixation rate was fractionated for prochlorophytes and eukaryotes only because there was neither direct nor indirect quantification of *Synechococcus*. Since $n_{PSII}$ for *Synechococcus* is bigger than that for eukaryotes and all the MVChl*a* was accounted as being due to the eukaryotes, it is likely that the primary production due to *Synechococcus* was underestimated.

The size of the photosystem changes greatly, depending on species and its regulation or acclimation to the nutrient availability and growth light. Species specific measurements of $n_{PSII}$ has shown this as a very variable parameter (Table 7.1). In general the number of Chl*a* per RCII ($n_{PSII}{}^{-1}$) decreased with increasing light (Falkowski *et al.* 1981, Dubinsky *et al.* 1986, Sukenik *et al.* 1990, Neale and Melis 1986) and it also decreased with decreasing nutrient (Berges *et al.* 1996) or iron (Greene *et al.* 1991). Nanoflagellates have the biggest range of $n_{PSII}$ (Table 7.1) and that was dominant phytoplankton taxa found along the AMT11 transect (Chapter 5). In a nutrient replete condition ($< 250$ $\mu$M)

at growth light of 150 $\mu$E m$^{-2}$ s$^{-1}$ the chlorophyceae *Dunaliella tertiolecta* had 350 Chl*a* per RCII against 500 Chl*a* per RCII assumed for the eukaryotes in the present work. There might be some underestimation in the $P_{Beuk}$ in the upper layer due to the chlorophyceae. On the other hand considering light as the only factor to change $n_{PSII}$, phytoplankton at deeper than 20 m in the ETRA were receiving less than 70 $\mu$E m$^{-2}$ s$^{-1}$, and at this light diatoms, chlorophyceae and dinoflagellates had more than 613 Chl*a* per RCII (Dubinsky *et al.* 1986, Sukenik *et al.* 1990), which means the value 500 for eukaryotes overestimates production. The prymnesiophytes were another abundant phytoplankton, detected by high concentration of its marker pigment along the AMT11 transect (Chapter 5, Figure 5.5) and the number of Chl*a* per RCII found in the literature ranged from 463 to 366 from 70 to 320 $\mu$E m$^{-2}$ s$^{-1}$ as documented for *Isochrysis galbana* (Dubinsky *et al.* 1986). In this case, there might be underestimation of $P_B$ in the upper layer. At lower light $P_B$ for prymnesiophytes might be underestimated since 637 Chl*a* per RCII were found at 30 $\mu$E m$^{-2}$ s$^{-1}$ (Dubinsky *et al.* 1986). The numbers presented in Table 7.1 were based on cultures with controlled light and nutrient conditions, so it is difficult to extrapolate to natural ecosystems, especially because according to the literature increase in light has the same effect as increase in nutrient, e.g. both decrease Chl*a* per RCII, while in the nature light decreases with depth and in open ocean, nitrate increases with depth (see Chapter 4). The better knowledge of how $n_{PSII}$ changes in the natural environment is one of the keys for improving the determination of primary productivity using variable fluorescence techniques such as FRR fluorometry.

**Chl*a* profile**

Total Chl*a* concentration was estimated from the CTD fluorometer voltage (CTDf). It was recognised the high light causes disturbance in the fluorescence measurement due to

Table 7.1: Number of Chl*a* per RCII as found in the literature: 1 - Barlow and Alberte 1985, 2 - Berges *et al.* 1996, 3 - Dubinsky *et al.* 1986, 4 - Falkowski *et al.* 1981, 5 - Greene *et al.* 1991, 6 - Jursinic and Dennenberg 1985, 7 - Kawamura *et al.* 1979, 8 - Manodori *et al.* 1984, 9 - Neale and Melis 1986, 10 - Sukenik *et al.* 1990.

| Taxa | minimum | maximum | Reference |
|---|---|---|---|
| Cyanophytes | 133 | 384 | 1, 7, 8 |
| Nanoflagellates | 220 | 830 | 2, 3, 4, 6, 9, 10 |
| Diatoms | 280 | 770 | 2, 3, 4, 5 |
| Dinoflagellates | 514 | 725 | 3 |

quenching, making the totChl*a* estimate from the fluorescence non-linear down the water column. The relationship between the Chl*a* concentration and CTDf was recently revisited and concluded that that relationship is light and region dependent (Holm-Hansen *et al.* 2000). To overcome the light effect on the fluorescence, results of phytoplankton community structure (Chapter 5) were used. The phytoplankton community structure in the AMT11 transect was dominated by three characteristically different assemblages identified as Clusters[1]. In the surface waters of the oligotrophic gyres, highly photoprotected phytoplankton dominated by prochlorophytes and nanoflagellates (Cluster A) were found. At the deep chlorophyll maximum (DCM) where nutrient was more abundant but light was lower, phytoplankton assemblage with high Chl*b* content was identified with the nanoflagellates dominating over the prochlorophytes (Cluster B). At depths where nutrient was more abundant with more light, a mixed phytoplankton community with intermediate level of photoprotection (Cluster C) was found. Knowing the different phytoplankton assemblages, the relationship between the totChl*a* and CTDf was estimated separately for each of the three Clusters. The totChl*a* for the regression analysis was

[1]See Chapter 5 for explanation about the Clusters and the phytoplankton community structure.

determined by HPLC technique (Chapter 5 Section 5.2.2). A detailed explanation about the regression analysis between the HPLC totChl*a* and the CTDf and the determination of Chl*a* from CTDf is presented in Appendix E.

The ratio DVChl*a*/totChl*a*, from the pigment analysis on discrete samples, was interpolated to match the depths where FRR physiology data was available and applied to the CTDf to obtain the DVChl*a* concentration. The difference between DVChl*a* and totChl*a* gave the Chl*a* due to the Eukaryotes (MVChl*a*).

**Photosynthetically available radiation - PAR**

**PAR in the water column for hourly primary production**: Hourly biomass specific carbon estimation rate was determined using PAR in the water column measured with the PAR sensor attached to the FRR fluorometer for every cast at the mid-day stations.

**Measured PAR**: To determine daily carbon estimation rate, information about diel variation of PAR above the water is necessary. Total irradiance (W $m^{-2}$) was recorded on board at every 5 min of the day, with a Kipp & Zonen CM-5 pyranometer covering the wavelenghts between 300 and 2800 nm. Half of that irradiance was assumed to be the PAR. A conversion factor (4.74) derived during the AMT1 (Robins *et al.* 1996) was applied to get quantal irradiance, $PAR_m(t, 0^+)$ in $\mu$E $m^{-2}$ $s^{-1}$.

**PAR in the water column for daily $\mathbf{P}_{col}$**: A lookup table with the fraction $F(\lambda, z)$, of PAR above the sea surface for clear sky condition, $PAR(t, 0^+)$, due to the spectral irradiance at depth z, $Ed(\lambda, z)$, was built. The atmospheric condition was considered constant along the day using Gregg and Carder (1990) model implemented with ECMWF cloud fields, EPTOMS ozone and NCEP meteorological fields for the nearest grid point

to the station. The transmission from the air to the water column was assumed to be a constant of 0.97. The attenuation in the water column was calculated empirically for the totChl*a* concentration (DVChl*a* + MVChl*a*), following the method described in Morel (1988). It was assumed that there was no change in the coefficient of attenuation in the water column, $K_{tot}$, throughout the day, so only one lookup table was needed. The spectral irradiance at time t, at depth z was dependent on the incident light, $PAR_m$(t, $0^+$), only:

$$\mathrm{Ed}(\lambda, \mathrm{t}, \mathrm{z}) = \mathrm{F}(\lambda,\ \mathrm{z})\ \times \mathrm{PAR_m}(\mathrm{t},\ 0^+). \tag{7.6}$$

PAR(t, z), required for determination of carbon fixation rate, was obtained by integrating the Equation 7.6 for wavelengths between 400 and 700 nm (Equation 7.7):

$$\mathrm{PAR}(\mathrm{t},\ \mathrm{z})\ =\ \int_{400}^{700} \mathrm{Ed}(\lambda, \mathrm{t}, \mathrm{z}). \tag{7.7}$$

**Other measurements**

Size-fractionated Chl*a* concentration, size-fractionated $^{14}$C uptake[2] and also P-E curve experiments[3] were carried out and some of these data were analysed in this Chapter. The methods for their analysis are presented in the Appendix E Section E.3.

[2]Size-fractionated Chl*a* concentration and size-fractionated $^{14}$C uptake data were provided by Emílio Fernández, Universidad de Vigo, Spain

[3]P-E curve data provided by Ramiro Varela, Universidad de Vigo, Spain

## 7.3 Results and Discussion

### 7.3.1 Overview on the primary productivity

The carbon fixation rate determined from Equation 7.5 integrated over the water column is presented in Figure 7.1. The term *euphotic zone* is used hereafter as the layer from the surface down to the depth where PAR was 0.1 % of PAR($0^-$). In general, the value 1 % is used to determine the euphotic zone (Kirk 1994) but in some provinces the 1 % depth was shallower than the DCM.

In provinces where the depth of Chl*a* maximum was in the surface layer, the depth of 1 % of surface PAR contributed to at least 95 % of the daily production of the whole water column ($P_{col}$). However, in the gyres, specially the southern gyre, where the depth of 1 % PAR was shallower than the DCM, that part of the water column deeper than the depth of 1 % PAR contributed from 8 to 10 % of the $P_{col}$. Figure 7.1 a shows the difference between the DCM and the depth of 0.1 % of PAR($0^-$). To avoid underestimation of $P_{col}$, the depth was integrated from the shallowest depth where there was physiology measurement from the FRR fluorometry and the depth of 0.1 % of PAR($0^-$) or the deepest FRR fluorometry measurement, in either cases the deepest P(z) was nearly zero. Apart from the station 1 (NECS), which had 66 mg $m^{-2}$ of depth integrated Chl*a*, the depth integrated Chl*a* varied across the Atlantic Ocean, between 15 and 27 mg $m^{-2}$. The contribution of DVChl*a* to the totChl*a* was more than 50 % in the gyre provinces (except station 37) indicating high contribution of prochlorophytes to the total phytoplankton community (Figure 7.1b and Chapter 5). Although small change in depth integrated Chl*a*, the $P_{col}$ changed from 240 to 890 mgC $m^{-2}$ $d^{-1}$, nearly four times, across the Atlantic Ocean (Figure 7.1c). It was high over the European Shelf (NECS), as expected due to the highest Chl*a* concentration,

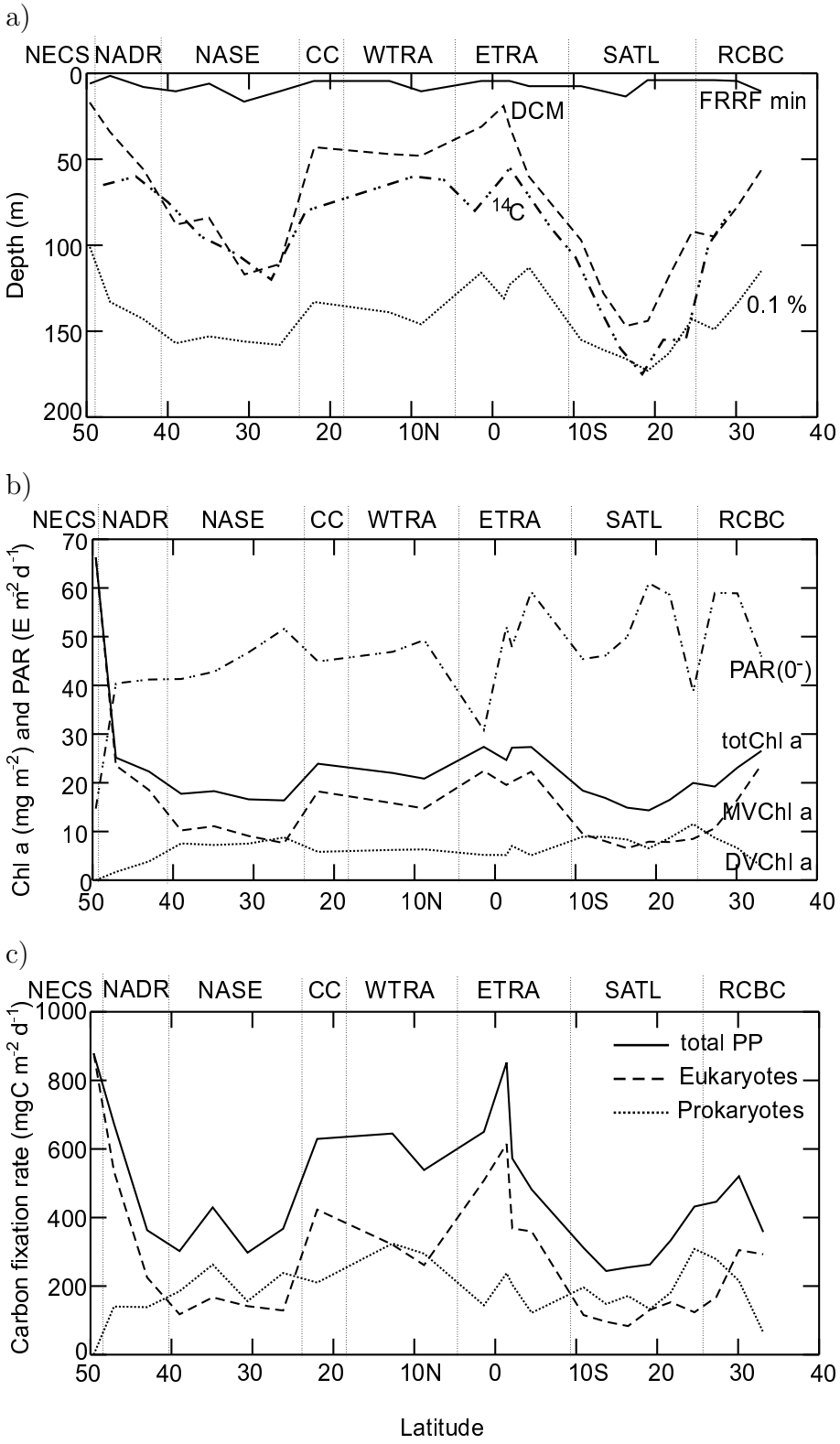


Figure 7.1: AMT11 transect with a) depth of the shallowest FRRF measurement (FRRF min), depth of Chl*a* maximum (DCM), depth of the deepest $^{14}$C 24 h sampling and the euphotic zone (depth with 0.1 % of surface PAR). b) day integrated subsurface PAR and Chl*a* concentration integrated from the shallowest depth with FRRF measurement to the bottom of the euphotic zone. c) Primary productivity determined by FRRF method within the euphotic zone for all the phytoplankton for prochlorophytes and eukaryotes.

and also in the ETRA. The $P_{col}$ in the ETRA did not seem to be affected by the iron limitation which decreased $Fv/Fm_L$ in the surface (Chapter 6 and Figure 7.4) and that will be analysed thoroughly later in this Chapter. The Equatorial and coastal upwelling provinces (ETRA, WTRA and CC) had the highest values of carbon fixation rate of the transect. The contribution of prochlorophytes to the total production was higher in the gyres and the WTRA and that can be due to the higher abundance of DVChl*a* in relation to MVChl*a*. NASE and WTRA had more amount of depth integrated MVChl*a* than DVChl*a* so the production due to the eukaryotes (represented by MVChl*a*) was expected to be higher instead of the opposite as observed (Figure 7.1).

### 7.3.2 Biomass specific production

Of the parameters required to determine production, light had the biggest range. It varied from 0.1 to nearly 1000 $\mu$E m$^{-2}$ s$^{-1}$ either in depth or time, covering 4 orders of magnitude. Physiological variability was tiny in comparison to the light range (0.01 to 0.6 for the $Fv/Fm_L$ and 170 $\times 10^{-20}$ to 730 $\times 10^{-20}$ m$^2$ photon$^{-1}$ for $\sigma_{PSII}$). The $P_B$, determined through Equation 2.11 assuming the physiology and measured PAR have not changed in one hour, was strongly related to the light in nearly linear relationship in the log-log space for most of the stations (Figure 7.2). At light lower than 50 $\mu$E m$^{-2}$ s$^{-1}$, a strong linear relationship was found between log of PAR and log of $P_B$ (Figure 7.3). The linear regression line diverges from the FRRF $P_B$ above the threshold of 50 $\mu$E m$^{-2}$ s$^{-1}$. This change in the relationship may have been caused by the gradual shift in the light spectrum from red to blue with increasing depth in natural environments. In the top layer of water column there is red light whilst in deeper part only blue light is remaining. FAST$^{tracka}$ has a excitation spectra centred in 465 nm (blue light) which is similar to

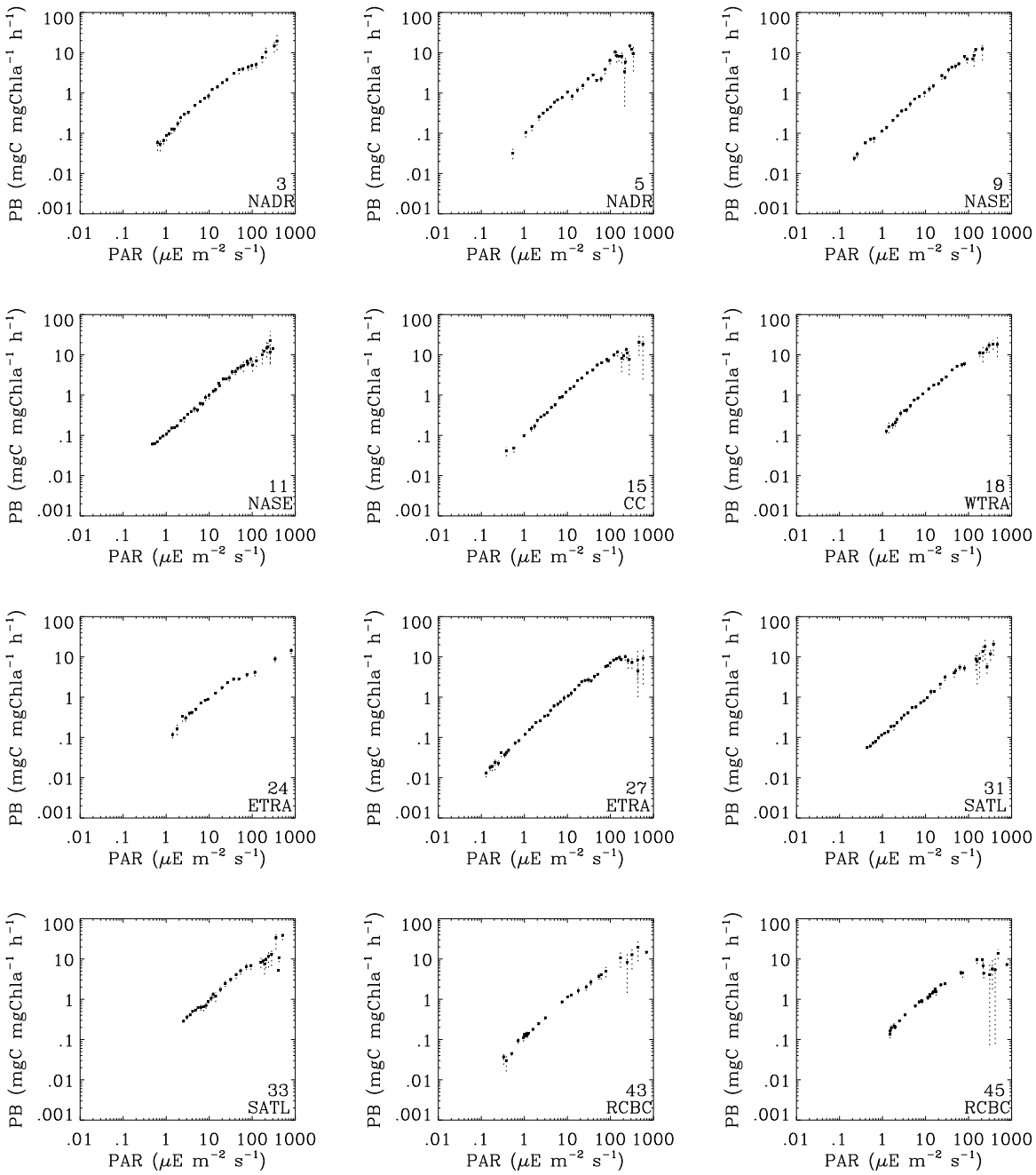


Figure 7.2: Chl*a*-specific primary production determined from FRRF against PAR. Stations with bigger errors (in vertical dotted line) are shown. The scales are the same for all the stations. Same data plotted in normal scale are presented in Appendix E, Figure E.3.

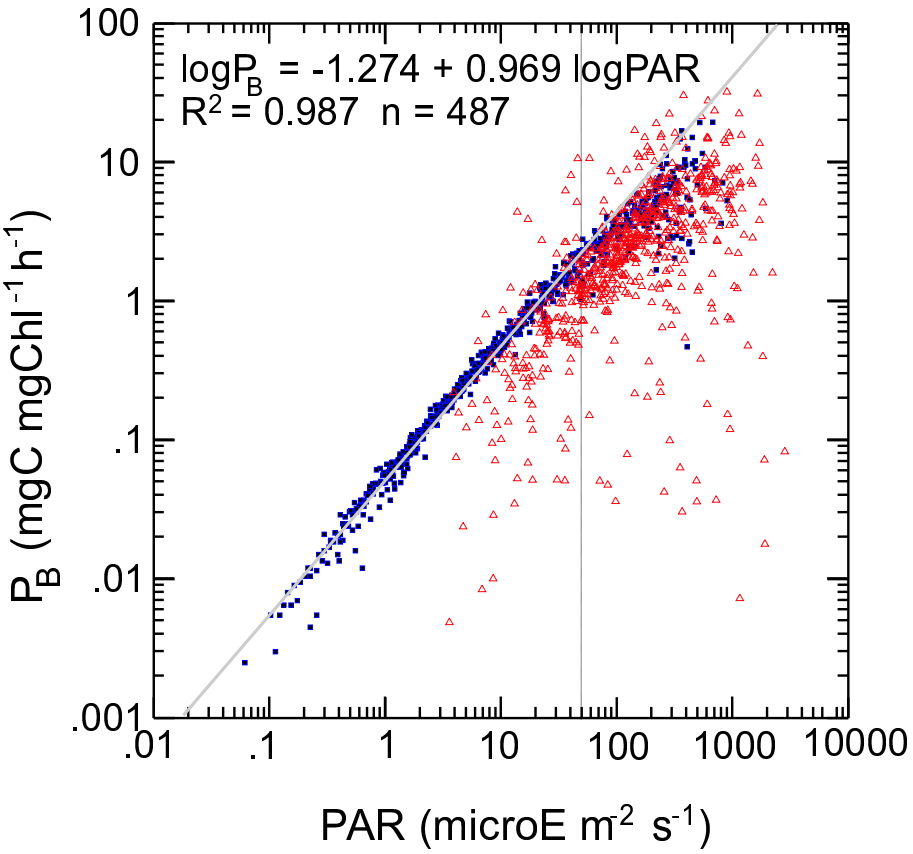


Figure 7.3: Chl*a*-specific production ($P_B$) against light from all the AMT11 stations. $P_B$ was determined with FRR fluorometry and measured light (black circles). $P_B$ was an average between $P_{Bproc}$ and $P_{Beuk}$, e.g. $n_{PSII} = 1/400$. Linear regression lines in gray for PAR $< 50$ $\mu$E m$^{-2}$ s$^{-1}$ is shown. The vertical dotted line indicates the threshold of 50 $\mu$E m$^{-2}$ s$^{-1}$ (see text). Red triangles are $P_B$ from $^{14}$C P-E experiments ($^{14}$C $P_B$). See error bars for FRRF $P_B$ for stations with bigger error bars in Figure 7.2.

the light spectrum at deeper part of the water column only. Therefor there might be underestimation in the $\sigma_{PSII}$ from FRRF method by undersampling in the surface, due to the narrower spectrum of excitation of the instrument in comparison to the ambient light and decreasing $P_B$, changing the $P_B$ versus PAR relationship. Above that light threshold the relationship between PAR and $P_B$ changed and the physiology had more importance than at lower light, causing more scattering in $P_B$ (Figure 7.3). The equation 2.11 assumed constant values for $n_{PSII}$, $\phi_e$, PQ and also a value of maximum Fv/Fm as 0.65. As already discussed all the other parameters that were assumed to be constant,

$n_{PSII}$ had the biggest range which was 6.4 times from the 130 to 830 Chl*a* per RCII (Table 7.1). The $^{14}$C P-E data, although more scattered than FRRF $P_B$, show the same trend in the relationship between $P_B$ and light (Figure 7.3), so those assumptions for single values of $n_{PSII}$ for eukaryotes and prokaryotes does not seem the cause for the strong relationship between $P_B$ and PAR. It indicates that oceanic phytoplankton in natural environments are well acclimated to the ambient light, being able to use most of the available light to fix carbon. Phytoplankton physiology was sampled in different physical structure and conditions of nutrient from eight provinces, even though $P_B$ was driven by light.

$P_B$ from $^{14}$C P v E curve ($^{14}$C $P_B$) sampled at mid-day stations were much more scattered and mainly lower than $P_B$ from FRR fluorometry. The $^{14}$C $P_B$ was a result of incubation of the standing stock Chl*a* in containers exposed to a series of light levels for 2 hours without natural changes in the light field or mixing processes and, some times, at higher temperature than from the environment where they were sampled. That decrease of $^{14}$C $P_B$ in the photoinhibited part of P-E method may be not only photoinhibition but also *hysteresis* (Long *et al.* 1994). The exposure of phytoplankton to irradiance levels higher than that to which they were acclimated makes them synthesise more carbohydrate, and because they are mainly protein producers (Myers 1980), they need to convert that carbohydrate into proteins (Long *et al.* 1994). Thus the cells increase the mithocondrial respiration to utilise the carbohydrates (Grande *et al.* 1989). These changes in respiration slow the changes in carbon fixation. When cells are exposed to lower irradiance levels than they were acclimated to, the ratio respiration/photosyntheis is higher than they need for the new condition, e.g. lower light level. This can cause hysteresis in P-E experiments, decreasing $P_B$ although such decrease is not actually resulted from photoinhibition (Falkowski *et al.* 1994). Another difference between the incubation method and the nature is the fixed light level the phytoplankton receive in each bottle. This fixed light

level can cause photoinhibition. Marra (1978) showed little or no-photoinhibition in the incubation bottle in the experiment where the bottle was cycled in the water column, so changing the light level the sample was receiving. When light is fluctuating, photochemistry is adjusted to the highest light level, since the activation time-scale is quicker than the deactivation time-scale (MacIntyre *et al.* 2000), and in so doing phytoplankton can be light limited at lower light but not photoinhibited. The $^{14}$C P-E experiment exposes each sample at one fixed light level and the constant exposure can lead to photoacclimation and eventually to photoinhibition. The light gradient for P-E experiment should be around the light experienced by the sample in the natural environment. If that light gradient is too high, phytoplankton is photoinhibited. Most of the scattered values of $^{14}$C P-E must be samples photoinhibited by exposure to too high light. The incubation temperature was also significant for the DCM populations in the oligotrophic gyres because they were incubated in surface waters and that could have increased the temperature by more than 7 °C (Falkowski and Raven 1997). The $^{14}$C $P_B$ presented high scattering with increasing light, and that may be due to the increase in photoinhibition due to the 2 hours duration of incubation. P-E experiments with incubations from 20 min to 240 min showed that increasing the duration of incubation can increase photoinhibition (Macedo *et al.* 2002), decreasing $P_B$ at higher light levels. P-E experiments incubated for 120 min resulted in photoinhibition and lower $P_B$ than results from 45 min incubation whilst no significant change occurred in the light limited part of the curve. Macedo *et al.* (2002) also suggest that if the sample is incubated at light gradient similar to the light level they were experiencing in the environment the incubation duration does not affect as much as it does when the light gradient is much higher.

The FRR fluorometric method for $P_B$ determination was based on the *in situ* phytoplankton physiology and PAR and was free from manipulations. The phytoplankton sampled

with FRR fluorometry was receiving changing light levels, in an open water parcel at ambient temperature, so the measured physiology was reflecting the ambient conditions. $P_B$ from which regression lines have been originated was an average between $P_{Bproc}$ and $P_{Beuk}$, where DVChl*a* was detected otherwise $P_B$ was $P_{Beuk}$ only. This average $P_B$ was very similar to the upper limit of the $^{14}C$ $P_B$ general trend. It does not mean that the value 400 (average between 500 and 300) Chl*a* per RCII was more realistic than the conditions created in the $^{14}C$ P-E experiment. The general physiological state resulting from all the assumptions taken must be closer to the conditions generated by the $^{14}C$ P-E experiment.

The high scattering in higher light in the FRR fluorometry $P_B$ may be because of high light fluctuations associated with the lower Chl*a* found in the surface water, making the sampling itself more difficult. Nevertheless the scattering was predominantly decreasing $P_B$ (Figure 7.3), which reinforces the view that the decrease in $P_B$ was caused by damages in the photosystems (Figures 7.4, 7.5 and 7.6). In the whole transect, $P_B$ was departing from the light profile shape in the upper layer where $Fv/Fm_L$ was decreased due to the limitation of nutrient (Figure 7.5) or iron[4] (Figure 7.4), and the increase in $\sigma_{PSII}$ for nutrient limitation was not enough to counterbalance the lost in photochemical efficiency, decreasing $P_B$. The relationship $P_B$ versus PAR was linear for nutrient replete condition (iron inclusive) but it did not apply for nutrient limited condition. Analyses of physiological parameters derived from FRRF suggest iron deficiency in the upper 30 to 60 m of ETRA (Chapter 6), where photosynthesis was light saturated (Figure 7.4). In the case of oligotrophic gyres, there was limitation by nitrate in the surface and to small extent by iron in the DCM (Figure 7.5). For the provinces where iron was replete around the DCM (CC, WTRA and RCBC), nitrate limitation was leading to light saturation in the upper layer (Figure 7.6). The relationship $P_B$ versus PAR (Figure 7.3) fails within the upper

[4]See Chapter 6 for more discussion about iron limitation and phytoplankton physiology.

layer where photosaturation is bigger.

FRRF $P_B$ was calculated with an intermediate PQ of 1.3 $molO_2$ $molCO_2^{-1}$ in the euphotic zone although nitrate was depleted in the upper layer of most of the AMT11 transect. This PQ may have underestimated P(z) above and overestimated below the nitracline. Probably the underestimation above the nitracline was bigger than the overestimation below it because of higher light in the surface layer and the bigger difference in PQ between 1.3 $molO_2$ $molCO_2^{-1}$, the value used here, and 1.1 $molO_2$ $molCO_2^{-1}$ for ammonium uptake. The $P_{col}$ may be underestimated due to the PQ value assumed.

The phytoplankton is acclimated to the light condition they are exposed to in natural environments and the general trend is to fix carbon according to the light availability and physiology accommodates to allow almost total photochemical efficiency. $P_B$ can be determined from PAR using the relationship presented (Figure 7.3), and if biomass is known, primary production can be derived, without knowledge of the *in situ* physiology. However, the log-log plot is evidencing the part of the water column with lower light level and the regression line was derived for PAR $< 50$ $\mu$E $m^{-2}$ $s^{-1}$ (Figure 7.3). There was a strong linear relationship between $P_B$ and PAR. However, constant $P_B$ occurred with increasing PAR in individual station analyses. For example in the Station 3 (Figures 7.2 and E.3), $P_B$ does not increase at PAR between 40 and 130 $\mu$E $m^{-2}$ $s^{-1}$, corresponding to the layer between 14 and 30 m. The phytoplankton population found in that layer was unable to utilise all the light available for photosynthesis, saturating the photosynthesis and causing the constant $P_B$ with increasing light (Figure 7.5). This corresponds to the well established photosynthesis versus irradiance method using the $^{14}C$ incubation to determine the saturating light ($E_k$) and the maximum level of primary production ($P_{max}$) of a phytoplankton sample (Platt *et al.* 1980). The fluorescence method can provide the

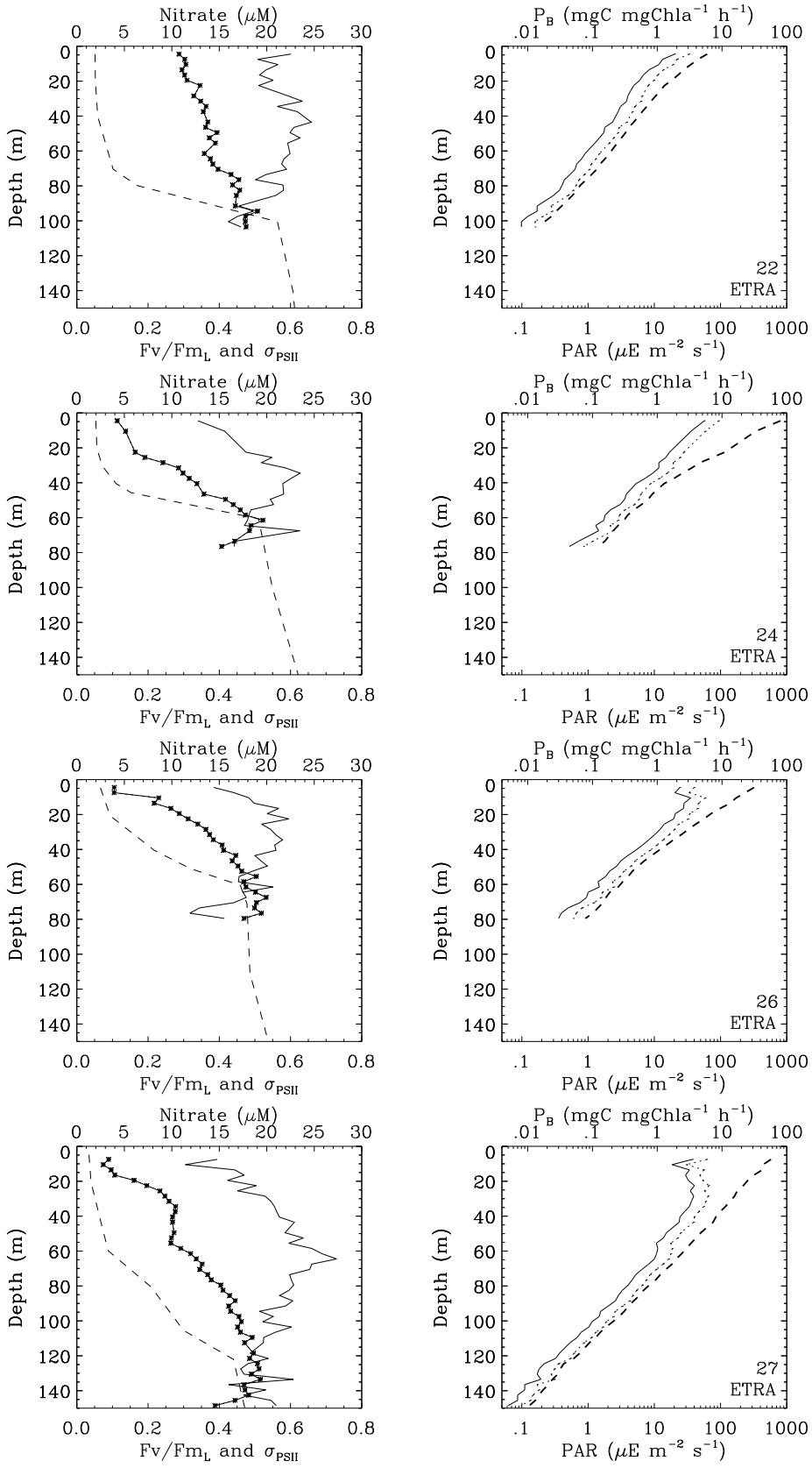


Figure 7.4: Chl*a*-specific primary production determined from the FRRF in the ETRA. Left column shows $Fv/Fm_L$ (solid line with *), $\sigma_{PSII}$ (in ($10^{-20}$ m$^2$ photon$^{-1}$)/100, solid line) and the nitrate (dashed line). Right column shows PAR (dashed line), the Chl*a* specific primary production for prochlorophytes (dotted line) and eukaryotes (solid line).

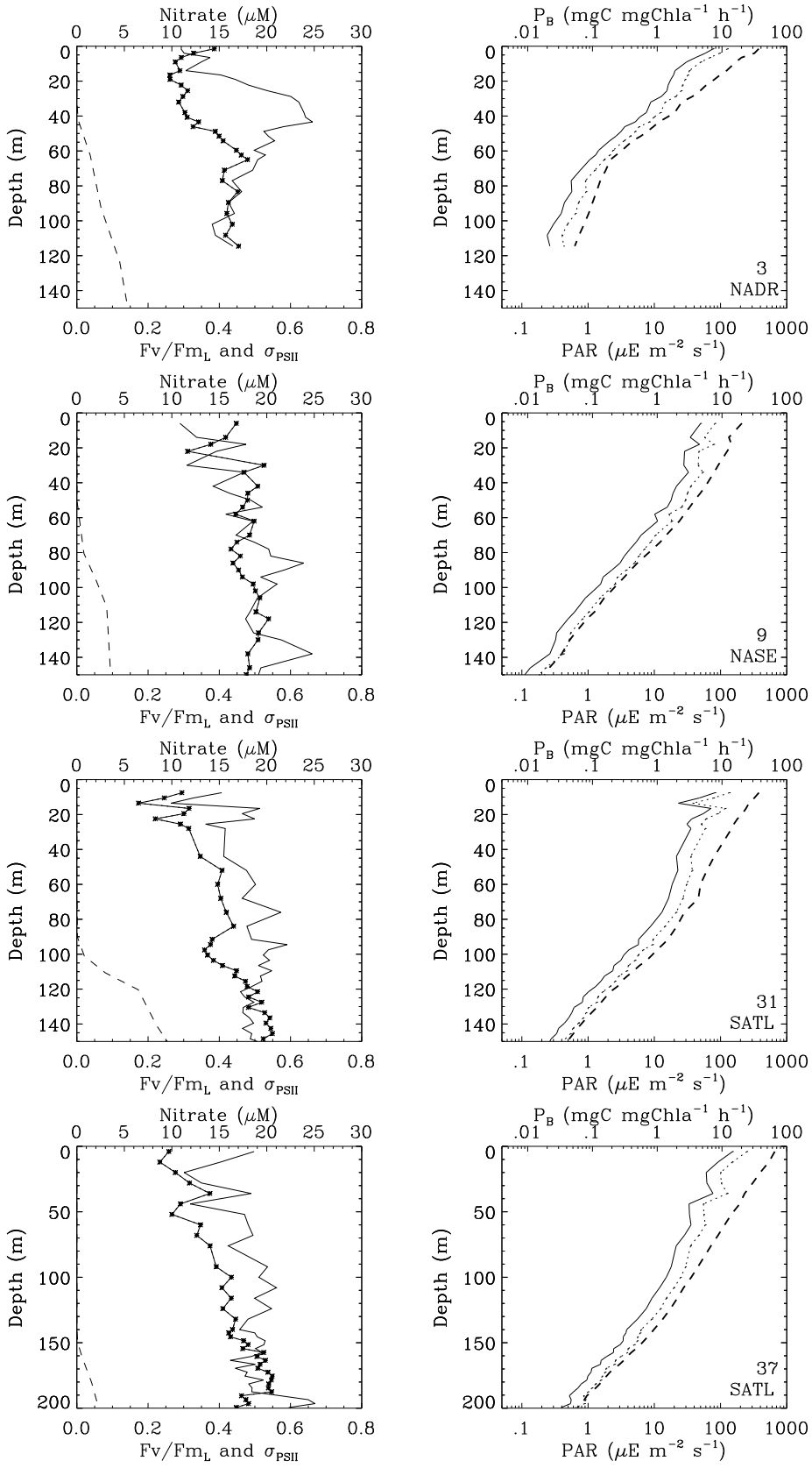


Figure 7.5: Chl*a*-specific primary production determined from the FRRF in the NADR, NASE and SATL. Left column shows $Fv/Fm_L$ (solid line with *), $\sigma_{PSII}$ (in ($10^{-20}$ m$^2$ photon$^{-1}$)/100, solid line) and the nitrate concentration (dashed line). Right column shows PAR (dashed line), the Chl*a* specific primary production for prochlorophytes (dotted line) and eukaryotes (solid line).

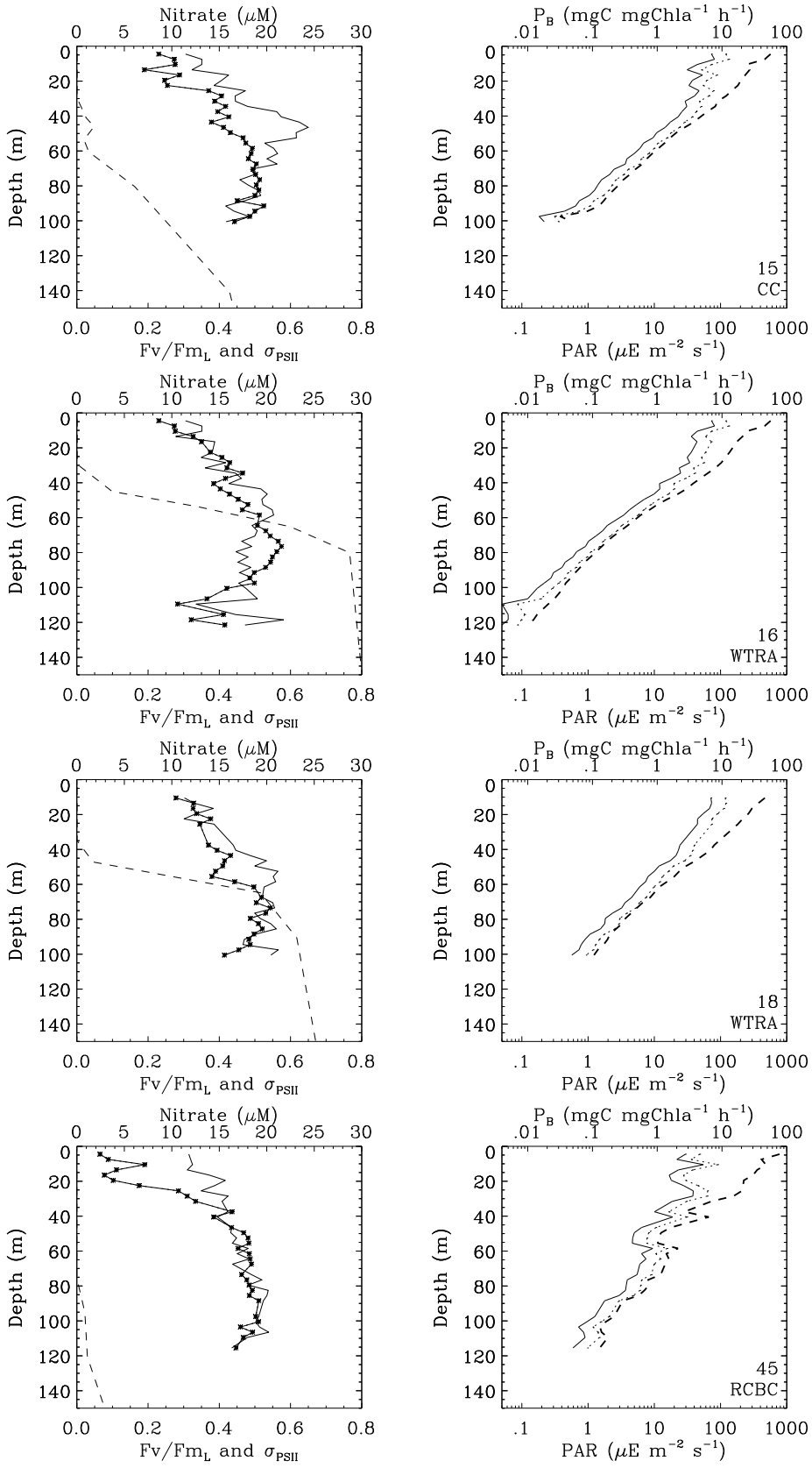


Figure 7.6: Chl*a*-specific primary production determined from the FRRF in the CC, WTRA and RCBC. Left column shows $Fv/Fm_L$ (solid line with *), $\sigma_{PSII}$ (in ($10^{-20}$ m$^2$ photon$^{-1}$)/100, solid line) and the nitrate concentration (dashed line). Right column shows PAR (dashed line), the Chl*a* specific primary production for prochlorophytes (dotted line) and eukaryotes (solid line).

same analysis avoiding the long time incubation associated with the radioactive incubation method. The constant $P_B$ with increasing light observed at these stations indicated photosaturation in some parts of the water column. For the same example of station 3, the phytoplankton within the layer 14 to 30 m depth was in a photosaturating condition with an $E_k$ of 40 $\mu$E $m^{-2}$ $s^{-1}$ (Figures 7.2 station 3). Photosaturation was detected along the water column, for example, around 2 $\mu$E $m^{-2}$ $s^{-1}$ in the same station 3, and also around 8.0 to 10.0 $\mu$E $m^{-2}$ $s^{-1}$ in stations 24 and 45, proving photosaturation occurs in natural environments (Figure 7.3). At the base of the water column light was a limiting factor and even in the saturated parts, $E_k$ was dependent on the ambient light. Falkowski *et al.* (1994) had documented that when phytoplankton were exposed to light higher than that they were previously acclimated to, non-photochemical quenching in the pigment bed increases within a half-time of 5 to 15 min (Falkowski 1992), dynamically altering the functional P-E relationship and preserving almost total photochemical efficiency.

Micro- and macro-nutrient limitations were causing damage in the photosystems and they prevented them from regulating or acclimating to the higher light by decreasing $Fv/Fm_L$ and causing saturation in the photosynthesis. Consequently the upper layer of the water column was light saturated and in the case of oligotrophic gyres, it could be as deep as 144 m as in station 37 (Figure 7.5). The upper layer of ETRA was also in a light saturated situation caused by iron limitation (Figure 7.4). The first attempt to interpret AMT11 data was by estimating $E_k$ from FRRF physiological data using the methods applied by Suggett *et al.* 2001 and Wood 2003. They applied the relationship between Fv/Fm and PAR of the water column to estimate $E_k$, taking the inflection point of this relationship as $E_k$. This method could not be applied because in the AMT11 data, Fv/Fm was depressed in most of the water column and no inflection point was evident. $E_k$ could not be determined from Fv/Fm values because most of the water column was photosaturated

and the depth of $E_k$ was not reached by the sampling.

This interpretation agrees with previous findings that there may be parts of the water column exposed to light in excess of the phytoplankton photosynthetic capacity, however, in terms of production of the water column, light is more limiting than in excess (Falkowski *et al.* 1994). The upper layer of the water column was light saturated whilst the deeper layer was light limited, according to the AMT11 data.

Figure 7.3 presents $P_B$ versus light in the log-log space and it is masking the proportion of the water column where there was photosaturation. If light is limiting, the change in $P_B$ with depth should be similar to the change in light with depth. All the stations sampled during the AMT11 showed $P_B$ departing from that trend in the upper layer and that departure was stronger in provinces where Fv/Fm was lower around the chlorophyll maximum, e.g. ETRA, NADR, NASE and SATL (Figures 7.4 and 7.5) in comparison to the provinces where Fv/Fm was higher around the chlorophyll maximum (Figure 7.5). Some stations had that departure as deep as 150 m depth (Figure 7.5, Station 37), which means most of the water column was light saturated. Regulation and acclimation of phytoplankton must be quick enough to cope with light change or long enough to cope with persistent high light (Falkowski *et al.* 1994, Müller *et al.* 2001). The time-scale that activates photoprotection mechanisms is shorter than the time-scale to deactivate the same mechanism (MacIntyre *et al.* 2000), hence phytoplankton should be photoacclimated or regulated to the maximum light they are exposed, even if that maximum light is an ephemeral increase and they regulate and acclimate for the more sudden light oscillations with non-photochemical quenchings. The regulation/acclimation only takes place, however, if micro- and macro-nutrients are replete. Consequently, in the upper layer along AMT11 transect, nutrients were limiting physiology and light was in excess.

This results reinforces what was deduced from the physiological parameters in Chapter 6.

### 7.3.3 Group fractionation

The difference between the eukaryotes and prochlorophytes was noticed in the biomass specific primary production, $P_B$ (Figures 7.4, 7.5 and 7.6). The $P_B$ due to the prochlorophytes was about 1.7 times $P_B$ due to the eukaryotes because the $n_{PSII}$ was assumed 1/300 and 1/500 for prokaryotes and eukaryotes, respectively. The $n_{prok}$ was taken from cyanobacteria (Falkowski and Kolber 1995) measurements assuming that all the prokaryotes have similar values, including prochlorophytes. However, there was differences in $n_{PSII}$ even within the *Synechococcus* (Table 7.1). The $n_{prok}$ changed with growth light and also with species. The $n_{prok}$ applied here for determination of primary productivity due to the prochlorophytes may be unreal. The thermocline found along the AMT11 transect (Chapter 4) was an indicator of the presence of two distinct populations of prochlorophytes (Moore *et al.* 1995) and very likely with different $n_{PSII}$. The lack of better knowledge about this parameter forced the use of one constant value for the euphotic zone and no documented values were found to analyse whether the value of 300 Chl*a* per RCII would underestimate or overestimate prochlorophytes production.

Primary productivity in the WTRA was an interesting case, where the areal Chl*a* had more than 50 % due to the eukaryotes whilst $P_{col}$ had more contribution from prochlorophytes. That was explained by prochlorophytes distribution along the water column in that province. Prochlorophytes were more abundant above the DCM so they were fixing more carbon than the eukaryotes above the DCM (Figure 7.6).

Unfortunately cell counts for picoplankton were not available for this cruise, so it was not possible to determine the amount of Chl*a* due to the cyanophytes (e.g. Synechococcus)

and the contribution of that organism was unknown. The fractionation of phytoplankton production into prochlorophytes and eukaryotes allowed better understanding of primary production and contribution of prochlorophytes to the total production.

If Chl*a* concentrations could be fractionated into the phytoplankton taxa like diatoms, dinoflagellates, cyanobacteria, prymnesiophytes and chorophytes, finer fractionation could be applied for determination of primary production with FRR fluorometry. The procedure would be the same as applied in this work for eukaryotes and prokaryotes. The determination of primary productivity fractionated per taxa was possible using the FRRF parameters using Equations 7.1 and 7.5 applying $n_{PSII}$ specific for each group and the amount of Chl*a* due to each group. The size of PSII ($n_{PSII}$) specific for each group can be taken from the literature (Table 7.1). Mackey *et al.* (1996) suggested statistical analysis (CHEMTAX) to estimate iteratively the fraction which each group contributes to the total MVChl*a* of the sample. However CHEMTAX did not work for AMT11 pigments due to small size of the data relative to difference in phytoplankton community and photoacclimation levels. As it was seen in Chapters 4 and 5, the depth of the nitracline and DCM changes across the transect so that the fixed-depth method as applied by Gibb *et al.* (2001) did not work. An extension of Chapter 5 may provide homogeneity (more similarity within a dataset) of pigment data necessary as input for CHEMTAX and it may allow determination of group fractionated Chl*a* concentration.

FRR fluorescence provides an average physiology for the whole community even though it is known that phytoplankton taxa may have different physiological states in the same water parcel. It can be overcome if variable fluorescence can be measured from cells isolated and classified as in flow cytometry. This has been tried in the Southern Ocean and it already provided Fv/Fm for different types of phytoplankton, specially chryptophytes

and pennate diatoms (Sosik and Olson 2002).

The advance in methodologies will allow finer group fractionation for determination of primary productivity if informations are coupled adequately.

### 7.3.4 The contrasting provinces along the AMT11 transect

The second highest $P_{col}$ (station 26) in the AMT11 transect occurred in the ETRA (Figure 7.1) although $P_B$ in that station was lower than 10 mgC mgChl$^{-1}$ h$^{-1}$ for prochlorophytes and lower than 6 mgC mgChl$^{-1}$ h$^{-1}$ for eukaryotes (Figure 7.4). $Fv/Fm_L$ was damaged at light higher than 50 $\mu$E m$^{-2}$ s$^{-1}$ due to the lack of iron which, on the other hand, increased $\sigma_{PSII}$ (Chapter 6), but such increase was not enough to prevent the decrease in $P_B$. However the amount of Chl*a* was still high enough to give high production despite of low $P_B$ in the water column (Figure 7.7) and the carbon fixation rate of the water column was one of the highest of the transect. Stations 24 and 27 had similar values of $P_B$ (Figure 7.4) but the former had higher Chl*a* concentration so fixed more carbon than the latter station (Figure 7.7). Below 60 m, primary production was insignificant to the water column.

Primary productivity in the oligotrophic gyres (NASE and SATL) was more evenly distributed throughout the water column and although it was lower than 5.0 mgC m$^{-3}$ d$^{-1}$ in the surface it was still higher than 1.0 mgC m$^{-3}$ d$^{-1}$ even as deep as 100 m (Figure 7.8 station 37). $P_B$ was in general higher in the gyres than in the ETRA, respectively $> 5$ and $< 4$ mgC mgChl$^{-1}$ h$^{-1}$ in the surface waters for eukaryotes. $P_{Bproc}$ was 1.7 times higher than $P_{Beuk}$. Chl*a* concentration was decisive for primary production. Phytoplankton in the surface waters of oligotrophic gyres, were physiologically damaged and low Chl*a* was found in such tough condition of high light and nutrient limitation. At DCM where lack

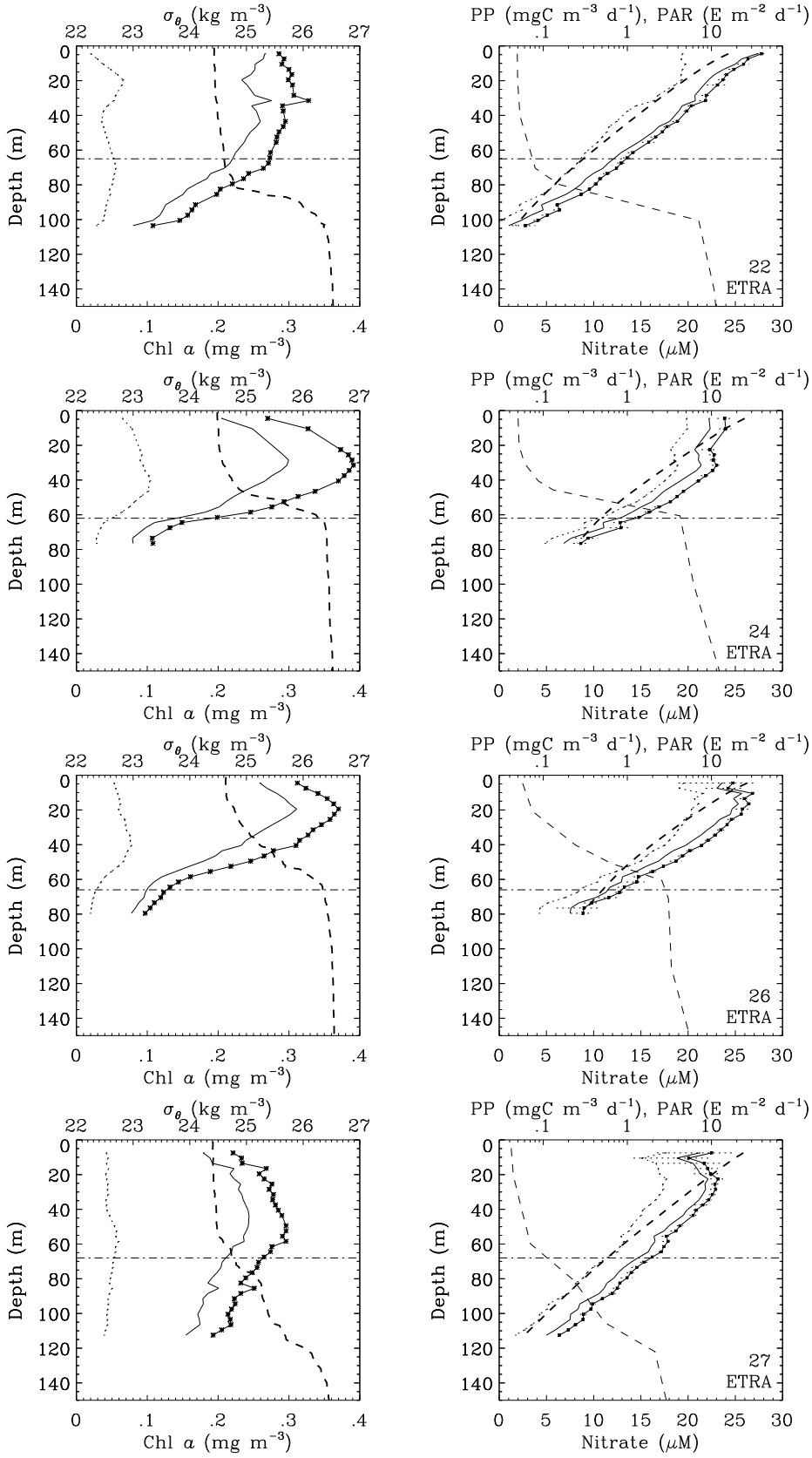


Figure 7.7: Daily primary production determined from the FRRF in the ETRA. Left column shows totChl*a* (solid line with *), MVChl*a* (solid line), DVChl*a* (dotted line) and potential density (dashed line). Right column shows the primary production for total phytoplankton (solid line with error bars), prochlorophytes (dotted line), eukaryotes (solid line), nitrate (dashed line) and PAR (thick dashed line). Station, province and euphotic zone (horizontal dashed dot line) are indicated.

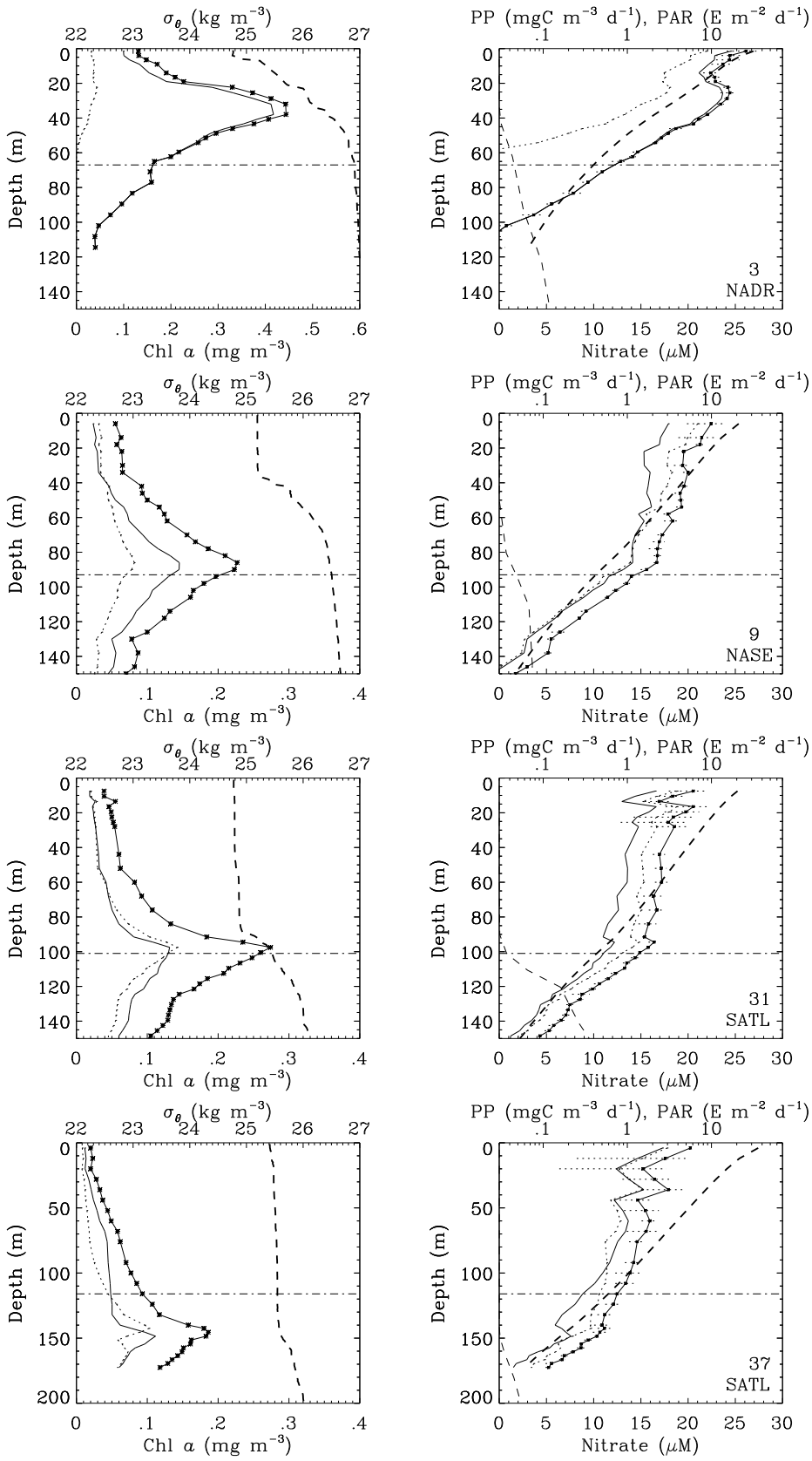


Figure 7.8: Daily primary production determined from the FRRF in the NADR, NASE and SATL. Left column shows totChl*a* (solid line with *), MVChl*a* (solid line), DVChl*a* (dotted line) and potential density (dashed line). Right column shows the primary production for total phytoplankton (solid line with error bars), prochlorophytes (dotted line), eukaryotes (solid line), nitrate (dashed line) and PAR (dashed line). Station, province and euphotic zone (horizontal dashed dot line) are indicated.

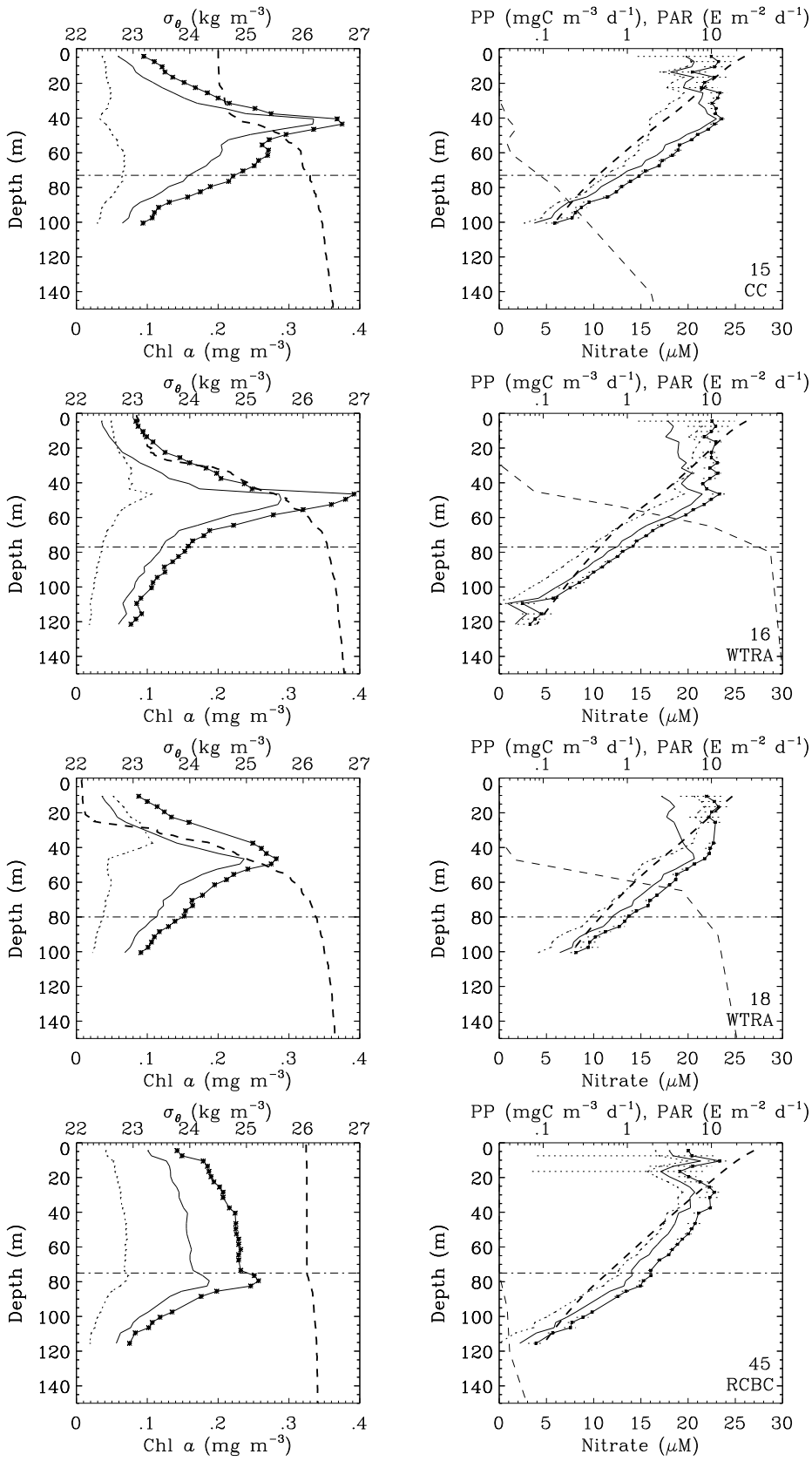


Figure 7.9: Daily primary production determined from the FRRF in the CC, WTRA and RCBC. Left column shows totChl*a* (solid line with *), MVChl*a* (solid line), DVChl*a* (dotted line) and potential density (dashed line). Right column shows the primary production for total phytoplankton (solid line with error bars), prochlorophytes (dotted line), eukaryotes (solid line), nitrate (dashed line) and PAR (dashed line). Station, province and euphotic zone (horizontal dashed dot line) are indicated.

of iron was decreasing $Fv/Fm_L$, there was too little light for photochemistry and the higher amount of Chl*a* was not a big contribution to the production. These results agree with the change in the ratio C:Chl from the surface with 79.9 to the DCM with 39.6 (Marañón and Holligan 1999). The DCM in the oligotrophic gyres in the Atlantic Ocean is a typical case of chlorophyll that does not represent phytoplankton total biomass and it is just an increase in Chl*a* per cell as an adaptation for low light. Other regions of the ocean were already recognised as such, like North Pacific Central Gyre (Cullen 1982). The chlorophyll in the DCM represents a physiological adaptation to the lower irradiance and to the increase in nutrient in that layer, and decrease in the ratio C:Chl from the surface to the depth of DCM.

### 7.3.5 Comparing to the 24 h $^{14}$C incubation

Samples inoculated with $^{14}$C were incubated for 24 h at pre-dawn stations in the same provinces where FRR fluorometry was used to determine primary production. The size fractionated $^{14}$C water column integrated primary production is presented in Figure 7.10. In general, the depth integrated primary production from $^{14}$C 24 h incubation was higher than that obtained from FRRF method (Figure 7.1) in the ETRA and CC and the opposite for the rest of the transect. Three points should be considered to compare $^{14}$C and FRRF methods: 1) the water analysed by the two methods were different ($^{14}$C at pre-dawn and FRRF at mid-day); 2) the depth of integration are different because the deepest measured with $^{14}$C was at the depth of the DCM whilst the FRRF was deployed deeper than the depth of the DCM in the gyres (Figure 7.1); 3) the standing stock (fluorometric Chl*a*) in the beginning of $^{14}$C incubation was higher than the Chl*a* retrieved from CTDf (CTDf Chl*a*), which was used for the mid-day determination of FRRF primary productivity.

Although much deeper depth was considered for FRRF production than for $^{14}$C (Figure 7.1a), $^{14}$C had higher depth integrated primary production in ETRA and CC. This can be due to the underestimation in Chl*a* used for FRRF method. It is difficult to compare FRRF and $^{14}$C methods analysing depth integrated primary production because of these three points apart from the difference in what each method measures. More detailed analysis is presented comparing vertical profiles of carbon fixation rate measured with each method.

Because of the time delay and spatial shift between the pre-dawn ($^{14}$C incubation) and the mid-day (FRR fluorometry) stations, the water sampled was different, so it was difficult to find similar Chl*a* profiles for a pair of pre-dawn (Figures 7.11, 7.12 and 7.13) and mid-day (Figures 7.7, 7.8 and 7.9) stations. The closest Chl*a* profiles were between stations 8 and 9, 12 and 13 (NASE), 21 and 22 (ETRA) and 36 and 37 (SATL).

The vertical profiles of $^{14}$C P(z) (Figures 7.11, 7.12 and 7.13) showed lower dependence on the PAR when compared with FRRF derived P(z) (Figures 7.7, 7.8 and 7.9), especially the surface sample of the $^{14}$C P(z) was lower than deeper in the water column. In general, the lower values of the $^{14}$C method for the water column integrated production ($^{14}$C $P_{col}$) in comparison to the FRRF happened because the $^{14}$C method yielded lower values throughout the whole water column, especially in the upper layer. ETRA apart, the $^{14}$C measurement (Figure 7.12) was much lower than primary productivity retrieved from FRRF (Figure 7.8). For example, Station 8 had maximum value around 2.0 mgC m$^{-3}$ d$^{-1}$, while the corresponding station, e.g. the station 9, with FRRF method had P(z) higher than 2.0 mgC m$^{-3}$ d$^{-1}$ with maximum in the surface with 10.0 mgC m$^{-3}$ d$^{-1}$. In the oligotrophic gyres, the deepest sampled with $^{14}$C method was the depth of the DCM while the FRR fluorescence went down to 0.1 % of PAR($0^-$) (Figure 7.1). In the ETRA,

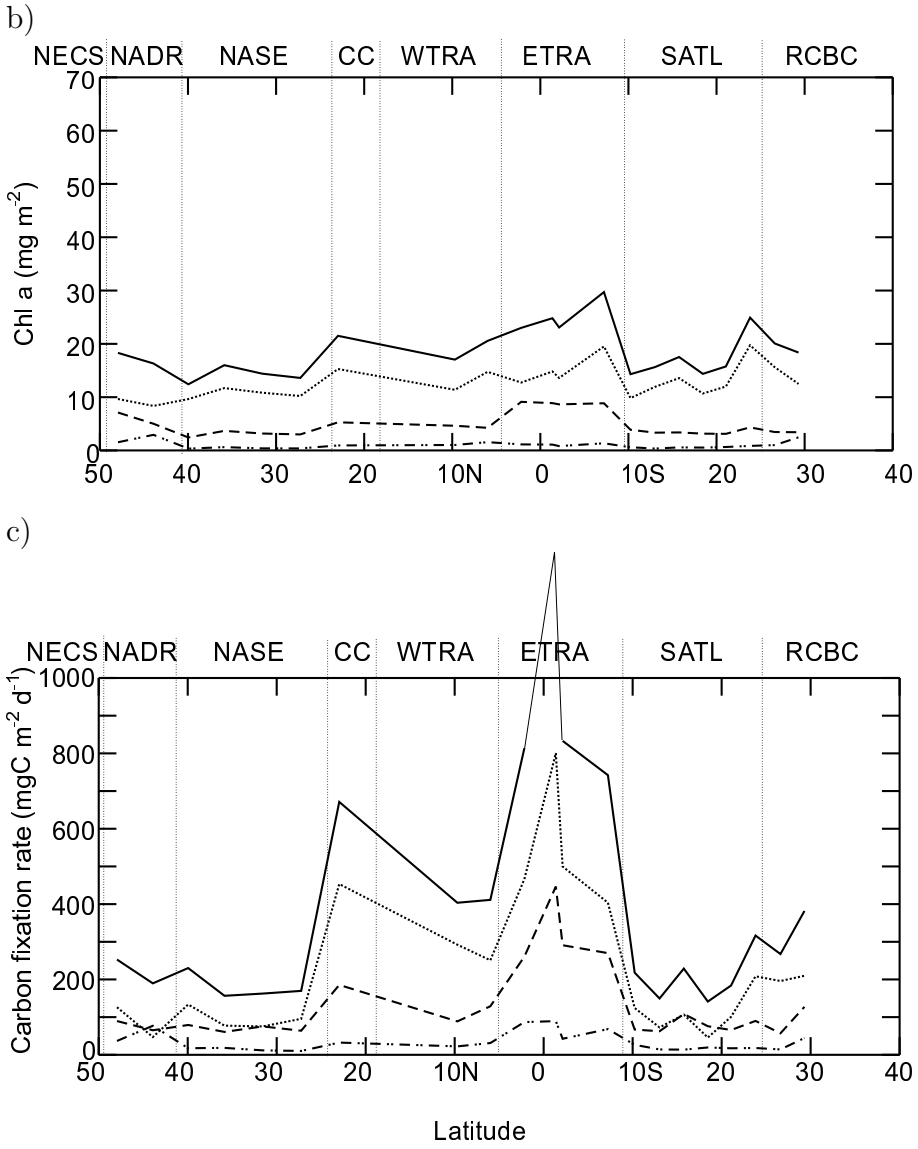


Figure 7.10: AMT11 transect for a) size fractionated Chl*a* for the samples incubated for $^{14}$C uptake. b) Primary productivity as determined with the $^{14}$C 24 h incubation (PP). The highest total PP (ETRA station 23 with 1336.6 mgC m$^{-2}$ d$^{-1}$) is off the scale. The size fractions were total (solid line), 0.2 to 2.0 $\mu$m (dashed line), 2.0 to 20.0 $\mu$m (dashed line) and $>$ 20 $\mu$m (dash dot dot line) for either Chl*a* or PP. NECS was not sampled.

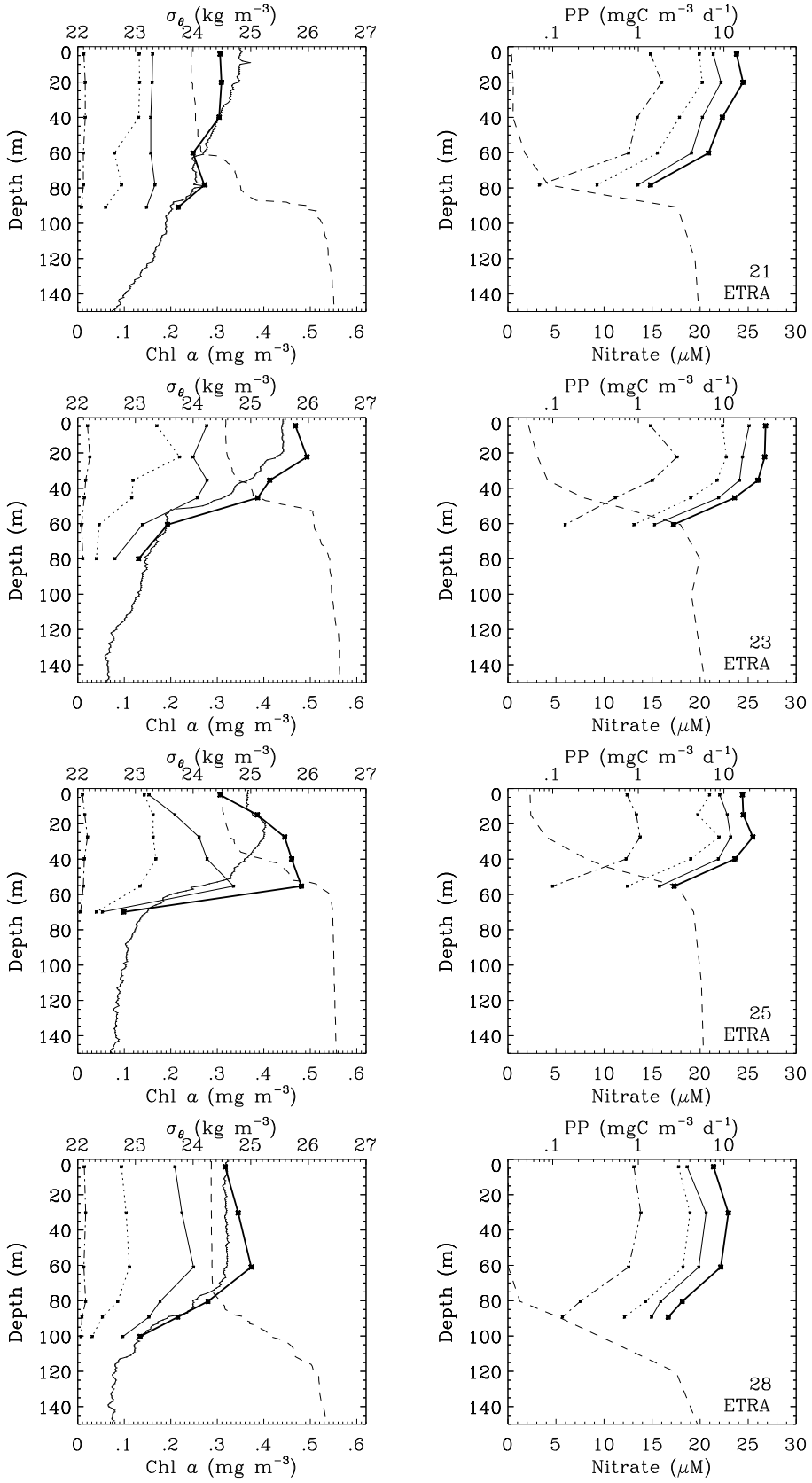


Figure 7.11: Daily primary production from 24 h $^{14}$C incubation in the ETRA. Left hand side graphics present size fractionated Chl*a* (lines with *), Chl*a* from CTD fluoremeter (solid line) and density ($\sigma_\theta$, dashed line). Right hand side graphics present size fractionated 24 h $^{14}$C uptake (PP, lines with *) and nitrate (dashed line). Size fractionations (lines with *) are: total (thick solid line), 0.2 to 2.0 $\mu$m (solid line), 2 to 20 $\mu$m (dotted line) and >20 $\mu$m (dashed dot line).

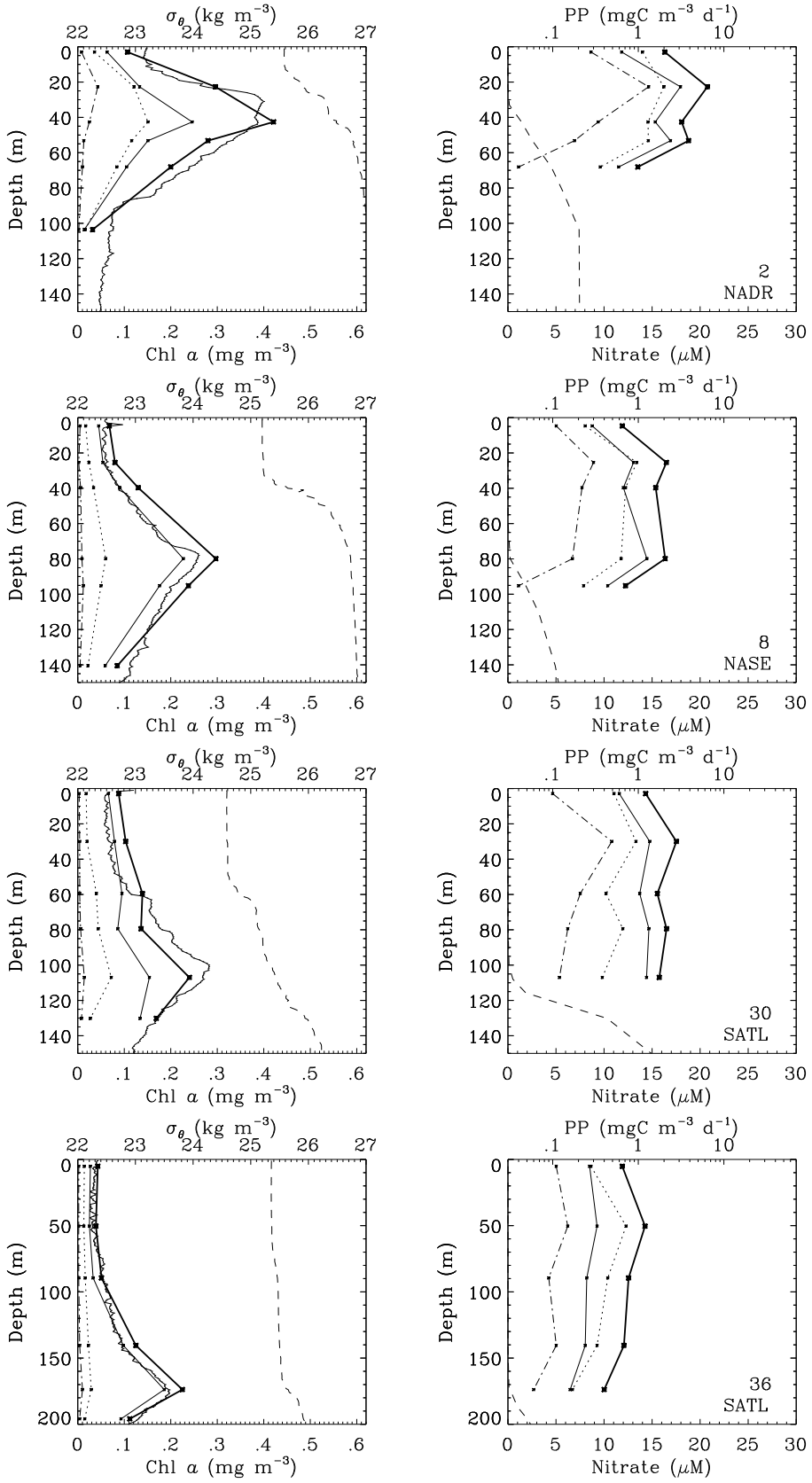


Figure 7.12: Daily primary production from 24 h $^{14}$C incubation in the provinces with minimum Fv/Fm around chlorophyll maximum (NADR, NASE, SATL). Left hand side graphics present size fractionated Chl*a* (lines with *), Chl*a* from CTD fluoremeter (solid line) and density ($\sigma_\theta$, dashed line). Right hand side graphics present size fractionated 24 h $^{14}$C uptake (PP, lines with *) and nitrate (dashed line). Size fractionations (lines with *) are: total (thick solid line), 0.2 to 2.0 $\mu$m (solid line), 2 to 20 $\mu$m (dotted line) and >20 $\mu$m (dashed dot line).

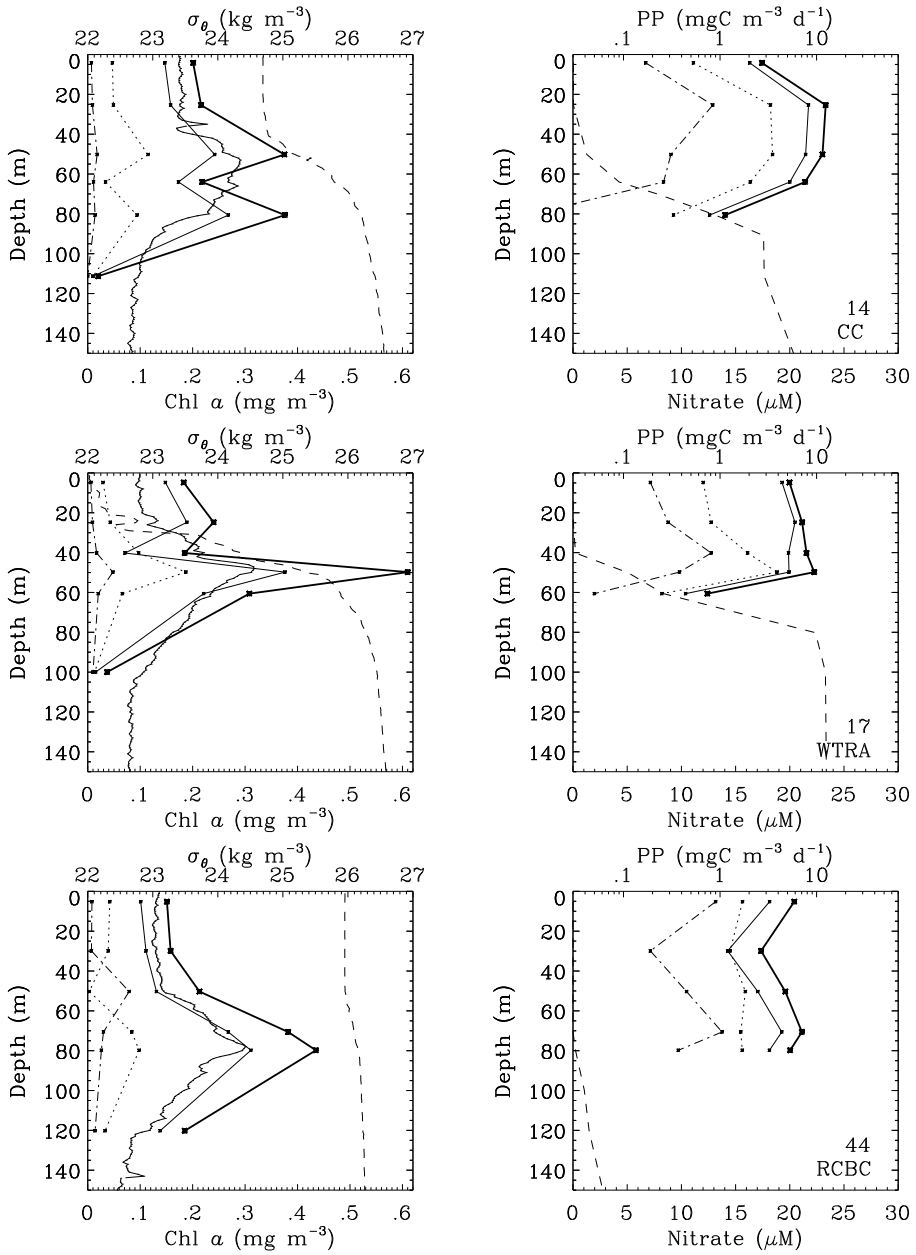


Figure 7.13: Daily primary production from 24 h $^{14}$C incubation in the provinces with maximum Fv/Fm around chlorophyll maximum (CC, WTRA and RCBC). Left hand side graphics present size fractionated Chl*a* (lines with *), Chl*a* from CTD fluoremeter (solid line) and density ($\sigma_\theta$, dashed line). Right hand side graphics present size fractionated 24 h $^{14}$C uptake (PP, lines with *) and nitrate (dashed line). Size fractionations (lines with *) are: total (thick solid line), 0.2 to 2.0 $\mu$m (solid line), 2 to 20 $\mu$m (dotted line) and >20 $\mu$m (dashed dot line).

although the $^{14}$C method yielded carbon fixation rates lower than the FRRF method in the surface, the decrease with depth was not as strong as the decrease the FRRF method yielded (Figure 7.7). Within the mixed layer, $^{14}$C P(z) decrease with depth was more associated to the decrease in Chl*a*, while the FRRF P(z) decrease was following the light decay.

Compared to the 24 h $^{14}$C incubation method, the FRR fluorescence determinations of primary production were higher for most of the provinces (NADR, NASE, WTRA, SATL and RCBC) and lower for CC and ETRA. The $^{14}$C method quantifies the radioactivity incorporated into organic carbon, $(CH_2O)_n$, at the end of the electron transport chain whilst the FRR fluorescence method used the variation of fluorescence emission from PSII, at the beginning of the electron transport chain (Figure 2.1). The 24 h $^{14}$C incubation is assumed to represent net carbon fixation. The FRR fluorometry measures the rate of electron transfer through RCII, which should be proportional to gross rate of oxygen evolution, so it was used an assumed value of constant PQ to convert released oxygen to fixed carbon. The electron taken from the water molecule in the photosystem II may not get to the end of the electron transport chain for a number of reasons, so the FRR fluorescence method is expected to overestimate photosynthesis. Dark respiration, photo-respiration and Mehler reaction are among the processes that can cause discrepancy between the two methods (Suggett *et al.* 2001). In ETRA, where nitrate was higher than 2 $\mu$M in the surface and DVChl*a* was about 30 % of the totChl*a*, carbon fixation from eukaryotes was more important. Berges *et al.* (1996) counted 350 Chl*a* per RCII in *Dunaliella tertiolecta* (chlorophyceae, eukaryotes) when grown in nitrate replete condition ($< 250$ $\mu$M). If that number is closer to the value in the ETRA (although the nitrate was never higher than 25 $\mu$M in the upper 150 m), the FRRF P(z) determined here would be an underestimation of photosynthesis. That difference in $n_{PSII}$ would increase primary

production in a factor of 1.4 which would not be enough to equal the $^{14}C$ determination. The PQ applied was 1.1 $molO_2$ $molCO_2^{-1}$ and not 1.4 $molO_2$ $molCO_2^{-1}$ as reported for nitrate as source of nitrogen (Laws 1991). That change would also decrease P(z) even more.

## 7.4 Summary and Conclusions

Fast repetition rate fluorometry was used to determine primary productivity of phytoplankton in the open ocean along the Atlantic Meridional Transect, covering 83 degrees of latitude. The strength of this method was that the *in situ* assessment of the physiology, allowed primary productivity to be derived in real time in natural ecosystems. Assumptions for some parameters and determination of light in the water column provided the means to determine the daily rate of carbon fixation from $Fv/Fm_L$ and $\sigma_{PSII}$.

There are uncertainties still regarding the assumptions used. One of the biggest concerns is the size of photosystem II, $n_{PSII}$. This parameter changes with light and nutrient availability, although it was considered constant for the analysis presented here, with values of 1/300 and 1/500 PSII reaction centres per Chl*a* for prochlorophytes and eukaryotes respectively. The assessment of this parameter in the environment will give more confidence in using FRR derived physiology data to determine primary productivity.

Phytoplankton are adapted to regulate and/or to acclimate to the ambient light conditions dependent on the nutrient availability. If either micro- or macro-nutrients are limiting, the phytoplankton are unable to repair the damage caused by high light on their photosystems and cannot exploit the light available. Consequently in the mixed layer, or in the case of North Atlantic Ocean, in even deeper layers, where nutrients were limiting,

the phytoplankton were physiologically impaired, the photosynthesis was photosaturated and the carbon fixation rate was nutrient limited.

In light limited part of the water column, biomass specific primary productivity was proportional to the light intensity and a analysis of all the stations together resulted in a linear relationship for log-transformed data. Above the light limited part, the upper layer was photosaturated due to the physiological impairment caused by high light and the nutrient limitation, prevented the repair of photosystem II. The thickness of the photosaturated layer was dependent on the province. In NADR, NASE and SATL the photosaturated layer was from the surface down to the depth of the DCM, because above this depth nitrate was depleted and at the DCM iron was deficient preventing the repair of PSII. Even so, this photosaturation was not as significant as suggested by the $^{14}$C P-E experiment.

Equatorial and coastal upwelling provinces were nutrient limited at the time of measurement, but the primary production was still high in comparison to the other provinces along the transect due to the higher biomass, e.g. Chl*a* concentration. The opposite occurred in the oligotrophic gyres, where the biomass specific production was in general higher than that in ETRA, and the low Chl*a* counterbalanced yielding primary productivity lower than that in ETRA.

Photosaturation was detected not only in the surface but also in other parts of the water column where $^{14}$C P-E experiment was insensitive, e.g. at light levels as low as 10 $\mu$E m$^{-2}$ s$^{-1}$ in natural ecosystems. It can be concluded that the phytoplankton living deep in the water column, adapted to very low light, intensities of 10 $\mu$E m$^{-2}$ s$^{-1}$ were sufficient to saturate the photosystem impaired by nutrient limitation. Such light level was found at the depth of DCM of oligotrophic gyres where although nitrate was increasing, iron was

deficient and causing decrease in Fv/Fm (Chapter 6).

Most of the primary production of the water column was due to the photosaturated photosynthesis rather than the light limited photosynthesis.

# Chapter 8

# Summary and general conclusions

The general objective of this thesis was to investigate primary productivity along the Atlantic Meridional Transect carried out during the cruise 11 (AMT11). In order to develop a comprehensive understanding, I have conducted a step by step analyses of the factors that can affect primary production.

## 8.1 Provinces in the Atlantic Ocean

One of the objectives was to develop a method to define the provinces sampled, not in terms of geography (latitude and longitude) but in terms of their characteristic oceanographic properties (Chapter 4). Simple analysis was derived based on temperature and salinity from the CTD casts. This method allowed easy determination of the province's physical characteristics and can be applied just after each CTD cast, speeding up the province characterisation. The upper layer of the oceans is normally excluded from water mass analyses because it is regionally modified by contact with the atmosphere and/or by heating processes. This regional alterations make the water mass loose its original physical properties. However, this layer with water parcel altered from the source water mass

is where phytoplankton can growth hence the importance of its knowledge in primary productivity studies. The temperature versus salinity analysis could detect these alterations, distinguishing between provinces along the AMT11 transect. This method proved to be an efficient and objective way to characterise provinces from the data collected on the station. The subsequent analysis of nitrate and Chl*a* data can give further support for the characterisation of the province.

Eight provinces were found along the AMT11 transect using the method above described: Northeast Atlantic Shelves Province (NECS), North Atlantic Drift Region (NADR), North Atlantic Subtropical Gyral Province - East (NASE), Province influenced by the Canary Current (CC), Western Tropical Atlantic Province (WTRA), Eastern Tropical Atlantic Province (ETRA), South Atlantic Gyral Province (SATL) and Recirculation Cells of Brazilian Current Province (RCBC). The nitracline was coincident with the thermocline except in NASE province where the former was much deeper than the latter. Nitrate was depleted within the isothermal layer depth. Below it, temperature could be used to derive an estimate of the nitrate concentration except for NASE province.

Although the depth of deep chlorophyll maximum was associated with the thermocline, that was due to the coincidence of depths of the thermocline and nitracline. In the NASE, however, the nitracline was much deeper than the thermocline, and so was the depth of Chl*a* maximum. This finding in the NASE indicated that better knowledge of the interaction between physical oceanography and nutrient supply was required and perhaps an application of numerical 3-D circulation model could provide it.

**Main conclusion**: Differentiation between provinces was strongly defined by regional alteration by heating or other processes of the water mass in the upper 200 m layer. This alteration was detected easily and speedily by temperature and salinity analysis which

provided strong background for definition of provinces. Further analyses of nitrate and chlorophyll gave support for province definition.

## 8.2 Phytoplankton community structure

Phytoplankton community structure was determined from HPLC pigments by applying a analytical method to establish the compositional structure of the phytoplankton. Samples from the AMT11 (oligotrophic and mesotrophic waters) and from the Benguela upwelling (mesotrophic and eutrophic waters) were summarised into groups, defined by five MVChl*a*-ratios representing five taxa of phytoplankton and another four ratios representing the physiological state of the phytoplankton, e.g. photoprotective and photosynthetic pigments contribution. The nine ratios were analysed statistically.

The phytoplankton community structure was patchy with some stratification in the Benguela upwelling whilst it was clearly stratified along the AMT11 transect. The phytoplankton community of AMT11 were found in a bigger range of temperature and salinity than those from the coastal upwelling (Table 5.4). This shows that the AMT11 phytoplankton community stands bigger variation in environmental conditions than that from upwelling regions. The phytoplankton species/group change depending on the environmental conditions driven by hydrodynamic processes affecting the nutrient availability as proposed by Margalef (1978) and Cullen *et al.* (2002). Changes not only in species composition but also in group are expected in a dynamic system, like a coastal upwelling, whilst in the open ocean the main change is in the species.

Taxa and physiological state of phytoplankton were the characteristic properties describing the distribution of phytoplankton across the Atlantic Ocean. Phytoplankton taxa

showed a gradual change following the increase in totChl*a*. Phytoplankton communities characterised by diatoms or dinoflagellates had higher concentrations of Chl*a* and a high Chl*c* content (found in the Benguella upwelling), while communities dominated by smaller cells (prokaryotes and nanoflagellates) had lower concentrations of Chl*a* (open ocean), with a high Chl*b* content in the deeper community.

The lowest Chl*a* was found in the surface of oligotrophic gyres, where nitrate was depleted. Prochlorophytes and nanoflagellates with high levels of photoprotectant pigments were dominating there. At higher nitrate and low light, normally coincident to the depth of maximum chlorophyll, nanoflagellates and prochlorophytes with high Chl*b* content and low levels of photoprotectant pigments were dominating. Where nitrate was more abundant with higher light, the phytoplankton community had a mixed composition but was dominated by flagellates (nanoflagellates and dinoflagellates).

**Main conclusion**: the phytoplankton along the AMT11 transect had a stratified structure with three main communities as indicated by pigment ratio analysis: in the surface of oligotrophic gyres a community highly photoprotected, with characteristically low Chl*a* (biomass) was dominated by prochlorophytes and nanoflagellates; in the nitracline with low light (depth of deep Chl*a* maximum) nanoflagellates and prochlorophytes with high Chl*b* content were dominating; and at higher nutrient with high light levels a mixed community dominated by nanoflagellates was present.

## 8.3 Phytoplankton physiology

Phytoplankton physiology was assessed twice a day during the AMT11 cruise, at pre-dawn and at mid-day stations using the fast repetition rate (FRR) fluorometry. The efficiency

of photochemistry of photosystem II (Fv/Fm), effective absorption cross-section ($\sigma_{\mathrm{PSII}}$) and turn over time of $Q_A$ ($\tau_{\mathrm{QA}}$) were derived from the FRR fluorescence. This method has the advantage of *in situ*, near real time, non-invasive and non-destructive characteristics, allowing sampling representative of phytoplankton reaction to the environmental conditions only and, theoretically, free of methodological manipulation.

In the surface waters along the AMT11 transect, the diel variation in the Fv/Fm suggested micro- or macro-nutrient limitation causing damage in the photosystem II of the phytoplankton. In the ETRA where nitrate was more available, there was a pronounced decrease in $\mathrm{Fv/Fm_L}$ which persisted after a night recovery from light stress. Iron limitation was previously detected in the high nutrient low chlorophyll (HNLC) region in the Pacific (Behrenfeld *et al.* 1996) and Southern Ocean (Boyd and Abraham 2001). The higher values of $\sigma_{\mathrm{PSII}}$ and $\tau_{\mathrm{QA}}$ measured in the ETRA during the AMT11 support the evidence of a deficiency of iron as suggested. In the surface waters of oligotrophic gyres, Fv/Fm at dawn had recovered from light exposure and was higher than the mid-day Fv/Fm value. This pattern has been attributed to nitrate limitation rather than iron limitation (Behrenfeld and Kolber 1999) leading to the conclusion that nitrate was the limiting factor in the upper layer of the oligotrophic gyres in the Atlantic Ocean.

Around the depth of Chl*a* maximum in the gyral provinces (e.g. NADR, NASE and SATL), the vertical profile of Fv/Fm showed depression around the depth of Chl*a* maximum despite higher concentration of nitrate brought up to the surface by the Equatorial upwelling process. The higher nitrate availability around the depth of maximum Chl*a* should provoke recovery in the photosystem II, though that was not observed. Coincidentally, iron decrease around the depth of maximum Chl*a* in the same provinces had previously reported for AMT3 and AMT6 (Bowie *et al.* 2002), leading to the speculation

of iron limitation in the depths of Chl*a* maximum in these provinces.

**Main conclusion**: Most of the upper, productive layer of the Atlantic Ocean was nitrate or iron limited causing impairment in the physiology of photosystem II of the phytoplankton.

## 8.4 Primary production

Phytoplankton primary production was determined from the FRRF physiology ($Fv/Fm_L$ and $\sigma_{PSII}$) with some assumptions, parameterisation and the photosynthetically available radiation (PAR), as described in Chapters 2 and 7. The strength of assessing primary production with FRR fluorometry lies in the calculation of primary production as it happens in natural environment, since the physiology is assessed free of manipulation, so it reflects the ambient condition the phytoplankton were experiencing. This thesis exploited the strength of the FRRF method rather than attempted to reconcile it with the traditional radioisotope method (although some comparisons were carried out). Good quality data are essential for the determination of primary productivity, so error propagation due to the high noise to signal ratio of the FRRF physiological data was calculated.

The advantage of the FRRF method is that the determination of primary productivity is more realistic to what happens in natural environment but, because it does not need estimation of light saturation parameter ($E_k$), as methods previously applied by other authors using FRR fluorometry (e.g. Boyd *et al.* 1997, Suggett *et al.* 2001, Wood 2003), a comparison with them was not possible. The inflection point of the relationship between Fv/Fm and PAR of the water column is $E_k$. This method could not be applied to the AMT11 data because Fv/Fm was depressed in most of the water column and no inflection

point was evident.

The biggest uncertainty concerned the size of the photosystem II, represented by the number of reaction centres per Chl*a* ($n_{PSII}$). The values 1/300 and 1/500 PSII reaction centre per chlorophyll were used for prochlorophytes and eukaryotes, respectively. The documented values of $n_{PSII}$ were determined in phytoplankton from cultures, and it is recommended that $n_{PSII}$ measurements in natural phytoplankton are needed for confident determination of primary production through FRRF method.

Determination of group fractionated primary production is desirable and that was attempted in this thesis by parametrising for prochlorophytes and eukaryotes (although *Synechococcus* could not be distinguished) and using the fractionated Chl*a* (DVChl*a* and MVChl*a*). Although the physiology retrieved from FRR fluorescence gives a mean value for the whole phytoplankton community, these procedures minimised the effect of assumption of a constant $n_{PSII}$ in the water column. Of all the parameters assumed to be constant for primary production estimate, $n_{PSII}$ has the most complex variation, depending on the light and nutrient, and has the biggest variability. The group fractionation showed that the prochlorophytes contributed to more than 50 % of the total primary production in the oligotrophic gyres. The minimum contribution of prochlorophytes to the total primary production occurred in the ETRA, where the DVChl*a* was contributing about 30 % of the total Chl*a*.

Hourly determination of primary productivity from mid-day measurements (assuming PAR was the same during one hour) showed lower depression at high light intensity, compared to the standard method of P-E experiment with radioisotope carbon. Photosaturation could be detected with the FRR fluorescence applied to determination of primary production in different layers of the water column, proving that photosaturation

happens in the nature throughout the water column and at light levels as low as 10 $\mu$E $m^{-2}$ $s^{-1}$. Photosaturation of photosynthesis was detected in most of the surface layer of the Atlantic Ocean due to the nutrient limitation, firstly nitrate (surface of oligotrophic gyres) and secondly iron (ETRA and around the deep Chl*a* maximum of oligotrophic gyres). The thickness of this photosaturated layer in the water column depended in the depth of nitracline. The bottom of the photosaturated layer coincided with the depth of the nitracline, so in the oligotrophic gyres, it could be as deep as the depth of DCM. This is supported by the fact that $E_k$ of the water column in the AMT11 could not be determined from methods applied by Suggett *et al.* (2001) and Woods (2003). Although photosaturation was detected, it could not be distinguished from photoinhibition.

Daily primary productivity could be determined from the mid-day measurement of FRR fluorescence, assuming the physiological parameters were constant throughout the day and modelling the diel variation in PAR. The ETRA had the highest production (apart from the NECS) in the whole AMT11 transect. In the ETRA the biomass specific production was low whilst in the gyral provinces, it was higher than in the ETRA. The standing stock Chl*a* of ETRA was the highest of the transect (apart from the NECS), so it counterbalanced the physiological impairment giving high primary production. The opposite occurred in the gyres where the standing stock Chl*a* was very low and that reduced the carbon fixation rate to low values in the whole water column.

In comparison to the 24 h $^{14}C$ incubation, the novel FRR fluorescence method for primary production determination yielded lower carbon fixation rate in the ETRA but higher in the other provinces. There was difficulties to compare primary production determined from the FRRF physiology to the $^{14}C$ method. The traditional radiocarbon method was applied in the pre-dawn stations and the novel fluorescence technique in the mid-day

stations, so the water parcel sampled was different. For the pair pre-dawn and mid-day stations sampled in the same province in the same day, with similar Chl*a* profiles, the higher primary production from the 24 h $^{14}$C incubation could be due to the value for $n_{PSII}$ used with the FRRF method for eukaryotes. Although a value of 1/300 was measured in laboratory culture the $n_{PSII}$ used was 1/500 PSII reaction centre per chlorophyll and that could be unrealistically low value.

In the whole AMT11 transect, the layer of the water column with photosaturation was thicker than or similar to the layer with light limitation. The photosaturated layer contributed more to the primary production of the water column than the light limited layer.

In general the 24 h $^{14}$C incubation showed depression in the surface carbon uptake while it was higher down to greater depths in the water column. The 24 h $^{14}$C includes dark perid and it can make the interpretation of data more complicated (Woods 2003). The $^{14}$C methods in general can give varied results depending on the methodology applied. Better controlled and quantified light levels, correction for light spectrum used and exclusion of dark periods for incubation can give better results for $^{14}$C (Woods 2003) and that can improve the comparison to FRRF method for carbon fixation rate.

**Main conclusion**: The biggest contribution to the water column primary productivity resulted from the zone with photosaturated photosynthesis rather than from light limited zone in the Atlantic Ocean. Better understanding of primary production in natural environment can be achieved if the strengths of different methods are exploited rather than attempting to reconcile between the results from different methods.

# List of References

Abraham ER, CS Law, PW Boyd, SJ Lavender, MT Maldonado and AR Bowle. 2000. Importance of stirring in the development of an iron-fertilized phytoplankton bloom. *Nature* 407(6805): 727-730.

Adam P. 1993. *Saltmarsh Ecology*. Cambridge University Press. Cambridge, UK.

Aiken J and SB Hooker. 1997. The Atlantic Meridional Transect: Spatially extensive calibration and validation of optical properties and remotely-sensed measurements of ocean color. *Backscatter*. 8: 8-11.

Aiken J, GF Moore and PM Holligan. 1992. Remote sensing of oceanic biology in relation to global climate change. *Journal of Phycology*. 28: 579-590.

Aiken J, GF Moore, CC Trees, SB Hooker and DK Clark. 1995. The SeaWiFS CZCS-type pigment algorithm. *NASA Technical Memorandum 104566*, Vol. 35, SB Hooker and ER Firestone, Eds. NASA Goddard Space Flight Center, Greenbelt, Maryland, EUA.

Aiken J, DG Cummings, SW Gibb, NW Rees, R Woodd-Walker, EMS Woodward, J Woolfenden, SB Hooker, J-F Berthon, CD Dempsey, DJ Suggett, P Wood, C Donlon, N González-Benítez, I Huskin, M Quevedo, R Barciela Fernandez, C de Vargas and C McKee. 1998. AMT-5 Cruise Report. *NASA Technical Memorandum 206892*, Vol. 2, SB Hooker and ER Firestone, Eds. NASA Goddard Space Flight Center, Greenbelt, Maryland, EUA.

Aiken J, N Rees, S Hooker, P Holligan, A Bale, D Robins, G Moore, R Harris and D Pilgrim. 2000. The Atlantic Meridional Transect: Overview and synthesis of data. *Progress in Oceanography*. 45(3-4): 257-312.

Antoine D, J-M André and A Morel. 1996. Oceanic primary production 2. Estimation at global scale from satellite (Coastal Zone Color Scanner) chlorophyll. *Global Biogeochemical Cycles*. 10(1): 57-69.

Arsalane W, B Rousseau and JC Duval. 1994. Influence of the pool size of the xanthophyll cycle on the effects of light stress in a diatom - competition between photoprotection and photoinhibition. *Photochemistry and Photobiology*. 60(3): 237-243.

Babin M, J-C Therriault, L Legendre, B Nieke, R Reuter and A Condal. 1995. Relationship between the maximum quantum yield of carbon fixation and the minimum quantum yield of chlorophyll a *in vivo* fluorescence in the Gulf of St. Lawrence. *Limnology and Oceanography*. 40(5): 956-968.

Babin M, A Morel, H Claustre, A Bricaud, Z Kolber and PG Falkowski. 1996. Nitrogen- and irradiance-dependent variations of the maximum quantum yield of carbon fixation in eutrophic, mesotrophic and oligotrophic marine systems. *Deep-Sea Research I*. 43(8): 1241-1272.

Barber RT and AK Hilting. 2002. History of the study of plankton productivity. In. *Phytoplankton productivity: carbon assimilation in marine and freshwater ecosystems*, Williams PJ le B, DN Thomas and CS Reynolds, Eds. Blackwell Science Ltd. Oxford, UK. pp. 16-43.

Barlow RG, J Aiken, PM Holligan, DG Cummings, S Maritorena and S Hooker. 2002. Phytoplankton pigment and absorption characteristics along meridional transects in the Atlantic Ocean. *Deep-Sea Research I.* 47(4): 637-660.

Barlow RG and RS Alberte. 1985. Photosynthetic characteristics of phycoerythrin-containing marine *Synechococcus* spp. *Marine Biology.* 86(1): 63-74.

Barlow RG, DG Cummings and SW Gibb. 1997a. Improved resolution of mono- and divinyl chlorophyll *a* and *b* and zeaxanthin and lutein in phytoplankton extracts using reverse phase C-8 HPLC. *Marine Ecology Progress Series.* 161: 303-307.

Barlow RG, RFC Mantoura, DG Cumming and TW Fileman. 1997b. Pigment chemotaxonomic distributions of phytoplankton during summer in the western Mediterranean. *Deep-Sea Research II.* 44(3-4): 833-850.

Bartlett JS, ÁM Ciotti, RF Davis and JJ Cullen. 1998. The spectral effects of clouds on solar irradiance. *Journal of Geophysical Research.* 103(C13): 31017-31031.

Bassi R, G Hoyer-Hansen, R Barbato, GM Giacometti and DJ Simpson. 1987. Chlorophyll-proteins of the photosystem-II antenna system. *Journal of Biological Chemistry.* 262(27): 13333-13341.

Bates TS, RJ Charlson and RH Gammon. 1987. Evidence for the climatic role of marine biogenic sulphur. *Nature.* 329: 319-321.

Behrenfeld MJ, AJ Bale, ZS Kolber, J Aiken and PG Falkowski. 1996. Confirmation of iron limitation of phytoplankton photosynthesis in the equatorial Pacific Ocean. *Nature.* 383: 508-511.

Behrenfeld MJ and ZS Kolber. 1999. Widespread iron limitation of phytoplankton in the south Pacific Ocean. *Science.* 283: 840-843.

Belkhodja R, F Morales, R Quílez, AF López-Millán, A Abadía and J Abadía. 1998. Iron deficiency causes changes in chlorophyll fluorescence due to the reduction in the dark of the photosystem II acceptor side. *Photosynthesis Research.* 56(3): 265-276.

Berges JA, DO Charlebois, DC Mauzerall and PG Falkowski. 1996. Differential effects of nitrogen limitation on photosynthetic efficiency of photosystems I and II in microalgae. *Plant Physiology.* 110: 689-696.

Bishop JKB and WB Rossow. 1991. Spatial and temporal variability of global surface solar irradiance. *Journal of Geophysical Research.* 96(C9): 16839-16858.

Blanchot J, M Rodier and A le Bouteiller. 1992. Effect of El Niño Southern Oscillation events on the distribution and abundance of phytoplankton in the western Pacific Tropical Ocean along 165 degree E. *Journal of Plankton Research.* 14(1): 137-156

Bland JM and DG Altman. 1986. Statistical methods for assessing agreement between two methods of clinical measurement. *The Lancet.* 1(8476): 307-310.

Bowie AR, DJ Whitworth, EP Achterberg, RFC Mantoura and PJ Worsfold. 2002. Biogeochemistry of Fe and other trace elements (Al, Co, Ni) in the upper Atlantic Ocean. *Deep-Sea Research I.* 49(4): 605-636.

Boyd PW and ER Abraham. 2001. Iron-mediated changes in phytoplankton photosynthetic competence during SOIREE. *Deep-Sea Research II*. 48(11-12): 2529-2550.

Bricaud A, M Babin, A Morel and H Claustre. 1995. Variability in the chlorophyll-specific absorption coefficients of natural phytoplankton: analysis and parameterization. *Journal of Geophysical Research*. 100(C7): 13321-13332.

Butler WL. 1978. Energy distribution in the photochemical apparatus of photosynthesis. *Annual Review of Plant Physiology*. 29: 345-378.

Clarke GL, GC Ewing and CJ Lorenzen. 1970. Spectra of backscattered light from the sea obtained from aircraft as a measure of chlorophyll concentration. *Science*. 167: 1119-1121.

Clarke KR and RM Warwick. 2001. *Changes in marine communities: an approach to statistical analysis and interpretation*. Plymouth, UK. PRIMER-E.

Charlson RJ, JE Lovelock, MO Andreae and SG Warren. 1987. Oceanic phytoplankton, atmospheric sulphur, cloud albedo and climate. *Nature*. 326: 655-661.

Coale KH, KS Johnson, SE Fitzwater, RM Gordon, S Tanner, FP Chavez, L Ferioli, C Sakamoto, P Rogers, F Millero, P Steinberg, P Nightingale, D Cooper, WP Cochlan, MR Landry, J Constantinou, G Rollwagen, A Trasvina and R Kudela. 1996. A massive phytoplankton bloom induced by an ecosystem-scale iron fertilization experiment in the equatorial Pacific Ocean. *Nature*. 383(6600): 495-501.

Cullen JJ. 1982. The deep chlorophyll maximum: comparing vertical profiles of chlorophyll *a*. *Canadian Journal of Fisheries and Aquatic Sciences*. 39: 791-803.

Cullen JJ, PJS Franks, DM Karl and A Longhurst. 2002. Physical influences on marine ecosystem dynamics. In. *The Sea*, Volume 12, AR Robinson, JJ McCarthy and BJ Rothschild, eds. John Wiley & Sons, Inc., New York, USA. pp. 297-336.

Demmig-Adams B and WW Adams III. 1992. Photoprotection and other responses of plants to high light stress. *Annual Review of Plant Physiology and Plant Molecular Biology*. 43: 599-626.

Dubinsky Z, PG Falkowski and K Wyman. 1986. Light harvesting and utilization by phytoplankton. *Plant Cell Physiology*. 27(7): 1335-1349.

Ducklow HW and RP Harris. 1993. Introduction to the JGOFS North Atlantic Bloom Experiment. *Deep-Sea Research II*. 40(1/2): 1-8.

Emery WJ and J Meincke. 1986. Global water masses: summary and review. *Oceanologica Acta*. 9(4): 383-391.

Falkowski PG. 1992. Molecular ecology of phytoplankton photosynthesis. Primary productivity and biogeochemical cycles in the sea. In. *Primary productivity and biogeochemical cycles in the sea*, PG Falkowski and AD Woodhead, Eds. Plenum Press. New York, USA. pp. 47-67.

Falkowski PG. 1994. The role of phytoplankton photosynthesis in global biogeochemical cycles. *Photosynthesis Research*. 39(3): 235-258.

Falkowski PG. 1997. Evolution of the nitrogen cycle and its influence on the biological sequestration of $CO_2$ in the ocean. *Nature*. 387: 272-275.

Falkowski PG. 2000. Rationalizing elemental ratios in unicellular algae. *Journal of Phycology*. 36(1): 3-6.

Falkowski PG, Y Fujita, A Ley and D Mauzerall. 1986a. Evidence for cyclic electron flow around photosystem II in Chlorella pyrenoidosa. *Plant Physiology.* 81: 310-312.

Falkowski PG, R Greene and Z Kolber. 1994. Light utilization and photoinhibition of photosynthesis in marine phytoplankton. In *Photoinhibition of photosynthesis: from molecular mechanisms to the field*, NR Baker and JR Bowyer Eds. Bios Scientific Publishers. Oxford, UK. pp. 407-432.

Falkowski PG, RM Greene and RJ Geider. 1992. Physiological limitations on phytoplankton productivity in the ocean. *Oceanography.* 5(2): 84-91.

Falkowski PG and Z Kolber. 1990. Phytoplankton photosynthesis in the Atlantic Ocean as measured from a submersible pump and probe fluorometer *in situ*. In: *Current Research in Photosynthesis*. Ed. M Baltscheffsky, Kluwer Academic Publishers. IV: 923-926.

Falkowski PG and Z Kolber. 1995. Variations in chlorophyll fluorescence yields in phytoplankton in the world oceans. *Australian Journal of Plant Physiology.* 22: 341-55.

Falkowski PG, Z Kolber and Y Fujita. 1988. Effect of redox state on the dynamics photosystem II during steady-state photosynthesis in eucaryotic algae. *Biochimica et Biophysica Acta.* 933(3): 432-443.

Falkowski PG, TG Owens, AC Ley and DC Mauzerall. 1981. Effects of growth irradiance levels on the ratio of reaction centers in two species of marine phytoplankton. *Plant Physiology.* 68(4): 969-973.

Falkowski PG and JA Raven. 1997. *Aquatic Photosynthesis.* Blackwell Science. Oxford, UK.

Falkowski PG, K Wyman, AC Ley and DC Mauzerall. 1986b. Relationship of steady-state photosynthesis to fluorescence in eucaryotic algae. *Biochimica et Biophyisica Acta.* 849: 183-192.

Ficek D, R Majchrowski, M Ostrowska and B Wozniak. 2000a. Influence of non-photosynthetic pigments on the measured quantum yield of photosynthesis. *Oceanologia.* 42(2): 231-242.

Ficek D, M Ostrowska, M Kuzio and Si Pogosyan. 2000b. Variability of the portion of functional PS2 reaction centres in the light of a fluorometric study. *Oceanologia.* 42(2): 243-250.

Flameling IA and J Kromkamp. 1998. Light dependence of quantum yields for PSII charge separation and oxygen evolution in eucaryotic algae. *Limnology and Oceanography.* 43(2): 284-297.

Gargett A and J Marra. 2002. Effects of upper ocean physical processes (turbulence, advection and air-sea interaction) on oceanic primary production. In. *The Sea*, Volume 12, AR Robinson, JJ McCarthy and BJ Rothschild, eds. John Wiley & Sons, Inc., New York, USA. pp. 19-49.

Garrido JL, Otero J, Maestro MA. 2000. The main nonpolar chlorophyll *c* from *Emiliania huxleyi* (Prymnesiophyceae) is a chlorophyll $c_2$-monogalactosyldiacylglyceride ester: a mass spectrometry study. *Journal of Phycology.* 36(3):497-505.

Geider RJ, RM Greene, Z Kolber, HL Macintyre and PG Falkowski. 1993. Fluorescence assessment of the maximum quantum efficiency of photosynthesis in the western North Atlantic. *Deep-Sea Research I.* 40(6): 1205-1224.

Geider RJ and HL MacIntyre. 2002. Physiology and biochemistry of photosynthesis and al-

gal carbon acquisition. In. *Phytoplankton productivity: carbon assimilation in marine and freshwater ecosystems*, Williams PJ le B, DN Thomas and CS Reynolds, Eds. Blackwell Science Ltd. Oxford, UK. pp. 44-77.

Geider RJ and J la Roche. 1994. The role of iron in phytoplankton photosynthesis, and the potential for iron-limitation of primary productivity in the sea. *Photosynthesis Research.* 39(3): 275-301.

Gibb SW, RG Barlow, DG Cummings, NW Rees, CC Trees, P Holligan and D Suggett. 2000. Surface phytoplankton pigment distributins in the Atlantic Ocean: an assessment of basin scale variability between 50°N and 50°S. *Progress in Oceanography.* 45: 339-368.

Gibb SW, DG Cummings, X Irigoien, RG Barlow and RFC Mantoura. 2001. Phytoplankton pigment chemotaxonomy of the northeastern Atlantic. *Deep-Sea Research II.* 48: 795-823.

González N, R Anadon and E Marañón. 2002. Large-scale variability of planktonic net community metabolism in the Atlantic Ocean: importance of temporal changes in oligotrophic subtropical waters. *Marine Ecology Progress Series.* 233: 21-20.

Gordon AL. 1981. South Atlantic thermocline ventilation. *Deep-Sea Research.* 28: 1239-1264.

Gordon AL. 1986. Interocean exchange of thermocline water. *Journal of Geophysical Research.* 91: 5037-5046.

Gordon HR, DK Clark, JL Mueller and WA Hovis. 1980. Phytoplankton pigments from the Nimbus-7 Coastal Zone Color Scanner: Comparisons with surface measurements. *Science.* 210: 63-66.

Govindjee. 1995. Sixty-three years since Kautsky: Chlorophyll *a* fluorescence. *Australian Journal of Plant Physiology.* 22: 131-160.

Grande KD, PJL Williams, J Marra, DA Purdie, K Heinemann, RW Eppley and ML Bender. 1989. Primary production in the North Pacific gyre: a comparison of rates determined by the $^{14}C$, $O_2$ concentration and $^{18}O$ methods. *Deep-Sea Research.* 36(11): 1621-1634.

Greene RM, RJ Geider and PG Falkowski. 1991. Effect of iron limitation on photosynthesis in a marine diatom. *Limnology and Oceanography.* 36(8): 1772-1782.

Greene RM, RJ Geider, Z Kolber and PG Falkowski. 1992. Iron-induced changes in light harvesting and photochemical energy conversion processes in eukaryotic marine algae. *Plant Physiology.* 100(2): 565-575.

Greene RM, ZS Kolber, DG Swift, NW Tindale and PG Falkowski. 1994. Physiological limitation of phytoplankton photosynthesis in the eastern equatorial Pacific determined from variability in the quantum yield of fluorescence. *Limnology and Oceanography.* 39(5): 1061-1074.

Gregg WW and KL Carder. 1990. A simple spectral solar irradiance model for cloudless maritime atmospheres. *Limnology and Oceanography.* 35(8): 1657-1675.

Harris GP, FB Griffiths and DP Thomas. 1989. Light and dark uptake and loss of $^{14}C$: methodological problems with productivity measurements in oceanic waters. *Hydrobiologia.* 173(2): 95-105.

Hess WR, F Partensky, GWM van der Staay, JM García-Fernández, T Borner and D Vaulot. 1996. Coexistence of phycoerythrin and a chlorophyll $a/b$ antenna in a marine prokaryote. *Proceedings of the National Academy of Sciences of the United States of America.* 93:

11126-11130.

Holligan PM. 1992. Do marine phytoplankton influence global climate? In. *Primary productivity and biogeochemical cycles in the sea*, PG Falkowski and AD Woodhead, Eds. Plenum Press. New York, USA. pp. 487-501.

Holligan PM, E Fernandez, J Aiken, WM Balch, P Boyd, PH Burkill, M Finch, SB Groom, G Malin, K Muller, DA Purdie, C Robinson, CC Trees, SM Turner and P Vanderwal. 1993. A biogeochemical study of the coccolithophore, *Emiliania huxleyi*, in the North-Atlantic. *Global Biogeochemical Cycles.* 7(4): 879-900.

Holm-Hansen O, AF Amos and CD Hewes. 2000. Reliability of estimating chlorophyll a concentrations in Antarctic waters by measurement of in situ chlorophyll a fluorescence. *Marine Ecology Progress Series.* 196: 103-110.

Hooker SB, NW Rees and J Aiken. 2000. An objective methodology for identifying oceanic provinces. *Progress in Oceanography.* 45(3-4): 313-338.

Jassby AD and T Platt. 1976. Mathematical formulation of the relationship between photosynthesis and light for phytoplankton. *Limnology and Oceanography.* 21(4): 540-547.

Jeffrey SW, RFC Mantoura and SW Wright. 1997. *Phytoplankton pigments in oceanography: guidelines to modern methods.* UNESCO Publishing. Paris (France).

Joint I, A Pomroy, G Savidge and P Boyd. 1993. Size-fractionated primary productivity in the northeast Atlantic in May-July 1989. *Deep-Sea Research II.* 40(1/2): 423-440.

Jursinic P and R Dennenberg. 1985. Reconciliation of the absorption change at 325 nm and other flash-yield determinations of concentrations of active photosystem II centers. *Archives of Biochemistry and Biophysics.* 241(2): 540-549.

Kana TM. 1992. Relationship between photosynthetic oxygen cycling and carbon assimilation in *Synechococcus* WH7803 (Cyanophyta). *Journal of Phycology.* 28(3): 304-308.

Kautsky H and A Hirsch. 1931. Neue versuche zur kohlensäureassimilation. *Naturwissenschaften.* 19: 964.

Kawamura M, M Mimuro and Y Fujita. 1979. Quantitative relationship between two reaction centers in the photosynthetic system of blue-green algae. *Plant and Cell Physiology.* 20(4): 697-705.

Kiefer DA and RA Reynolds. 1992. Advances in understanding phytoplankton fluorescence and photosynthesis. In. *Primary productivity and biogeochemical cycles in the sea*, PG Falkowski and AD Woodhead, Eds. Plenum Press. New York, USA. pp. 155-174.

Kirk JTO. 1994. *Light and photosynthesis in aquatic ecosystems.* Cambridge University Press. Cambridge, UK. 509pp.

Kok B. 1956. On the inhibition of photosynthesis by intense light. *Biochimica et Biophysica Acta.* 21: 234-244.

Kolber Z. 1997. Principle of fast repetition rate (FRR) fluorometry. Chelsea Instruments Ltd. Surrey, UK.

Kolber Z, J Zehr and P Falkowski. 1988. Effects of growth irradiance and nitrogen limitation on photosynthetic energy conversion in photosystem II. *Plant Physiology.* 88(3): 923-929.

Kolber ZS. 1998. Fast repetition Rate Fluorometry - A method for assessing ocean photosyn-

thesis. *Oceanology International 98*, New Malden, Spearhead Exhibitions Ltd. 329-340.

Kolber ZS, RT Barber, KH Coale, SE Fitzwater, RM Greene, KS Johnson, S Lindley and PG Falkowski. 1994. Iron limitation of phytoplankton photosynthesis in the equatorial Pacific Ocean. *Nature*. 371(6493): 145-148.

Kolber Z and PG Falkowski. 1993. Use of active fluorescence to estimate phytoplankton photosynthesis *in situ*. *Limnology and Oceanography*. 38(8): 1646-1665.

Kolber ZS and PG Falkowski. 1992. Fast Repetition Rate (FRR) fluorimeter for making in situ measurements for primary productivity. *IEEE*. 0-7803-0838-7/92: 637-641.

Kolber ZS, O Prasil and PG Falkowski. 1998. Measurements of variable chlorophyll fluorescence using fast repetition rate techniques: defining methodology and experimental protocols. *Biochimica et Biophysica Acta*. 1367: 88-106.

Kooten O van and JFH Snel. 1990. The use of chlorophyll fluorescence nomenclature in plant stress physiology. *Photosynthesis Research*. 25: 147-150.

Krause GH and E Weis. 1991. Chlorohyll fluorescence and photosynthesis: the basics. *Annual Review of Plant Physiology and Plant Molecular Biology*. 42: 313-349.

Laney S (2001). Documentation for v5 fluorescence yield analysis software. http://picasso.oce.orst.edu/ORSOO/FRRF/code.html

Latasa M and RR Bidigare. 1998. A comparison of phytoplankton populations of the Arabian Sea during the spring intermonsoon and southwest monsoon of 1995 as described by HPLC-analyzed pigments. *Deep-Sea Research II*. 45(10-11): 2133-2170.

Laws EA. 1991. Photosynthetic quotients, new production and net community production in the open ocean. *Deep-Sea Research*. 38A(1): 143-167.

Legrand M, C Feniet-Saigne, ES Saltzman, C Germain, NI Barkov and VN Petrov. 1991. Ice-core record of oceanic emissions of dimethylsulphide during the last climate cycle. *Nature*. 350: 144-146.

Lehninger AL. 1970. *Biochemistry, the molecular basis of cell structure and function*. Worth Publishers. New York, USA.

Lokstein H, C Steglich and WR Hess. 1999. Light-harvesting antenna function of phycoerythrin in *Prochlorococcus marinus*. *Biochimica et Biophysica Acta*. 1410(1): 97-98.

Long SP, S Humphries and PG Falkowski. 1994. Photoinhibition of photosynthesis in nature. *Annual Review of Plant Physiology and Plant Molecular Biology*. 45: 633-662.

Longhurst A, S Sathyendranath, T Platt and C Caverhill. 1995. An estimate of global primary production in the ocean from satellite radiometer data. *Journal of Plankton Research*. 17(6): 1245-1271.

Longhurst A. 1998. *Ecological geography of the sea*. Academic Press. San Diego, USA.

Lorenzen CJ. 1966. A method for the continuous measurement of in vivo chlorophyll concentration. *Deep Sea Research*. 13: 223-227.

MacIntyre HI, TM Kana and RJ Geider. 2000. The effect of water motion on short-term rates of photosynthesis by marine phytoplankton. *Trends in Plant Science*. 5(1): 12-17.

Mackey DJ, HW Higgins, MD Mackey and D Holdsworth. 1998. Algal class abundances in the western equatorial Pacific: Estimation from HPLC measurements of chloroplast pigments using CHEMTAX. *Deep-Sea Research I*. 45: 1441-1468.

Mackey MD, HW Higgins, DJ Mackey and SW Wright (1997). *CHEMTAX User's Manual: a program for estimating class abundances from chemical markers - application to HPLC measurements*. Hobart, Australia, CSIRO: 41.

Mackey MD, DJ Mackey, HW Higgins and SW Wright. 1996. CHEMTAX - a program for estimating class abundances from chemical markers: applications to HPLC measurements of phytoplankton. *Marine Ecology Progress Series*. 144: 165-283.

Mann KH and JRN Lazier. 1996. *Dynamics of marine ecosystems: biological-physical interactions in the oceans*. 2nd Ed. Blackwell Sciences. Malden, USA. 394pp.

Manodori A, M Alhadeff, An Glazer and A Melis. 1984. Photochemical apparatus organization in *Synechococcus* 6301 (*Anacystis nidulans*). Effect of phycobilisome mutation. *Archives of Microbiology*. 139(2-3): 117-123.

Mantoura RFC and CA Llewellyn. 1983. The rapid determination of algal chlorophyll and carotenoid pigments and their breakdown products in natural waters by reverse-phase high-performance liquid chromatography. *Analytica Chimica Acta*. 151(2): 297-314.

Marañón E and PM Holligan. 1999. Photosynthetic parameters of phytoplankton from 50°N to 50°S in the Atlantic Ocean. *Marine Ecology Progress Series*. 176: 191-203.

Marañón E, PM Holligan, M Varela, B Mourino and AJ Bale. 2000. Basin-scale variability of phytoplankton biomass, production and growth in the Atlantic Ocean. *Deep-Sea Research I*. 47(5): 825-857.

Margalef R. 1978. Life-forms of phytoplankton as survival alternatives in an unstable environment. *Oceanologica Acta*. 1(4): 493-509.

Marquis P. 1999. *Method validator*. Biologiste des Hôpitaux, Metz, France (http://www.marquis-soft.com/methval.htm)

Marra J. 1978. Phytoplankton photosynthetic response to vertical movement in a mixed layer. *Marine Biology*. 46: 203-208.

Marra J. 1995. Primary production in the North Atlantic: measurements, scaling, and optical determinants. *Philosophical Transactions of the Royal Society of London, Series B*. 348: 153-160.

McCarthy JJ. 2002. Biological responses to nutrients. In. *The Sea*, Volume 12, AR Robinson, JJ McCarthy and BJ Rothschild, eds. John Wiley & Sons, Inc., New York, USA. pp. 219-244.

Mobley CD. 1994. The optical properties of water. In. *Handbook of optics*. Vol. I. 2nd Ed. M Bass, Ed., MacGraw-Hill. New York, USA. pp. 43.3-43.56.

Moore LR, R Goericke and SW Chisholm. 1995. Comparative physiology of *Synechococcus* and *Prochlorococcus*: influence of light and temperature on growth, pigments, fluorescence and absorptive properties. *Marine Ecology Progress Series*. 116: 259-275.

Morel A. 1988. Optical modeling of the upper ocean in relation to its biogenous matter content (Case I waters). *Journal of Geophysical Research*. 93(C9): 10749-10768.

Morel A, D Antoine, M Babin and Y Dandonneau. 1996. Measured and modeled primary production in the northeast Atlantic (EUMELI JGOFS program): the impact of natural variations in photosynthetic parameters on model predictive skill. *Deep-Sea Research I*. 43(8): 1273-1304.

Mueller JL and RE Lange. 1989. Bio-optical provinces of the Northeast Pacific Ocean: a

provisional analysis. *Limnology and Oceanography*. 34(8): 1572-1586.

Müller P, X-P Li and KK Niyogi. 2001. Non-photochemical quenching. A response to excess light energy. *Plant Physiology*. 125: 1558-1566.

Myers J. 1980. On the algae: thoughts about physiology and measurements of efficiency. In *Primary productivity in the sea*. Falkowski PG. Ed., Plenum Press. New York, USA. pp. 1-16.

Neale PJ. 1987. Algal photoinhibition and photosynthesis in the aquatic environment. In *Photoinhibition*, DJ Kyle, CB Osmond and CJ Arntzen, Ed., Elsevier Science Publishers. pp. 39-65.

Neale PJ and A Melis. 1986. Algal photosynthetic membrane complexes and the photosynthesis-irradiance curve: a comparison of light-adaptation responses in *Clamydomonas reinhardtii* (Chlorophyta). *Journal of Phycology*. 22(4): 531-538.

Nelson DL and MM Cox. 2000. *Lehninger principles of biochemistry*. 3rd Edition. Worth Publishers. New York (USA). pp. 487-501.

Niyogi KK, O Bjorkman and AR Grossman. 1997. The roles of specific xanthophylls in photoprotection. *Plant Biology*. 94: 14162-14167.

O'Reilly JE, S Maritorena, BG Mitchell, DA Siegel, KL Carder, SA Garver, M Kahru and C McClain. 1998. Ocean color chlorophyll algorithm for SeaWiFS. *Journal of Geophysical Research*. 103(C11): 24937-24953.

Parkhill J-P, G Maillet and JJ Cullen. 2001. Fluorescence-based maximal quantum yield for PSII as a diagnostic of nutrient stress. *Journal of Phycology*. 37: 517-529.

Partensky F, J Blanchot and D Vaulot. 1999. Differential distribution and ecology of Prochlorococcus and Synechococcus in oceanic waters: a review. *Bulletin de l'Institut ocanographique*. 19(spécial): 457-475.

Peterson BJ. 1980. Aquatic primary productivity and the $^{14}C$-$CO_2$ method: A history of the productivity problem. *Annual Review of Ecology and Systematics*. 11: 359-385.

Peterson RG and L Stramma. 1991. Upper-level circulation in the South-Atlantic Ocean. *Progress in Oceanography*. 26(1): 1-73.

Pickard GL and WJ Emery. 1990. *Descriptive physical oceanography: an introduction*. 5th Ed. Exeter, UK.

Pitcher GC, AJ Boyd, DA Horstman and BA Mitchell-Innes. 1998. Subsurface dinoflagellate populations, frontal blooms and the formation of red tide in the southern Benguela upwelling system. *Marine Ecology-Progress Series*. 172: 253-264.

Platt T, CL Gallegos and WG Harrison. 1980. Photoinhibition of photosynthesis in natural assemblages of marine phytoplankton. *Journal of Marine Research*. 38(4): 687-701.

Poulton AJ. 2002. *Spatial and temporal variability of phytoplankton community composition in the tropical and subtropical Atlantic Ocean (40 degrees N to 40 degrees S)*. University of Southampton, UK. PhD thesis.

Poole R and M Tomczak. 1999. Optimum multiparameter analysis of the water mass structure in the Atlantic Ocean thermocline. *Deep-Sea Research I*. 46(11): 1895-1921.

Pope RM and ES Fry. 1997. Absorption spectrum (380-700 nm) of pure water. II. Integrating cavity measurements. *Applied Optics*. 36(33): 8710-8723.

Prieur L and S Sathyendranath. 1981. An optical classification of coastal and oceanic waters based on the specific spectral absorption curves of phytoplankton pigments, dissolved organic matter, and other particulate materials. *Limnology and Oceanography.* 26(4): 671-689.

Redfield AC, BH Ketchum and FA Richards. 1963. The influence of organisms on the chemical composition of sea-water. In. *The sea.* MN Hill, Ed. Interscience. New York, USA. pp. 26-77.

Riebesell U and DA Wolf-Gladrow. 2002. Supply and Uptake of inorganic nutrients. In. *Phytoplankton productivity: carbon assimilation in marine and freshwater ecosystems*, Williams PJ le B, DN Thomas and CS Reynolds, Eds. Blackwell Science Ltd. Oxford, UK. pp. 109-140.

Ríos AF, FF Prez and F Fraga. 1992. Water masses in the upper and middle North Atlantic Ocean east of the Azores. *Deep-Sea Research.* 39(3/4): 645-658.

Robins DB, Bale AJ, Moore GF, Rees NW, Hooker SB, Gallienne CP, Westbrook AG, Marañón E, Spooner WH, Laney SR. 1996. AMT-1 Cruise Report and Preliminary Results. *NASA Tech. Memo.* 104566, Vol. 35, Hooker SB and Firestone ER, Eds., NASA Goddard Space Flight Center, Greenbelt, Maryland, 87.

Roesler CS. 1998. Theoretical and experimental approaches to improve the accuracy of particulate absorption coefficients derived from the quantitative filter technique. *Limnology and Oceanography.* 43 (7): 1649-1660.

Rowan KS. 1989. *Photosynthetic pigments of algae.* Cambridge University Press. Cambridge, UK.

Santamaría-del-Angel E, S Alvarez-Borrego and FE Müller-Karger. 1994. Gulf of California biogeographic regions based on coastal zone color scanner imagery. *Journal of Geophysical Research.* 99(C4): 7411-7421.

Sathyendranath S, AD Gouveia, SR Shetye, P Ravindran and T Platt. 1991. Biological control of surface temperature in the Arabian Sea. *Nature.* 349(3): 54-56.

Savidge G, P Boyd, A Pomroy, D Harbour and I Joint. 1995. Phytoplankton production and biomass estimates in the northeast Atlantic Ocean, May-June 1990. *Deep-Sea Research I.* 42(5): 599-617.

Sathyendranath S, A Longhurst, CM Caverhill and T Platt. 1995. Regionally and seasonally differentiated primary production in the North Atlantic. *Deep-Sea Research I.* 42(10): 1773-1802.

Schreiber U, H Hormann, C Neubauer and C Klughammer. 1995. Assessment of photosystem II photochemical quantum yield by chlorophyll fluorescence quenching analysis. *Australian Journal of Plant Physiology.* 22(2): 209-220.

Schreiber U, U Schliwa and W Bilger. 1986. Continuous recording of photochemical and nonphotochemical chlorophyll fluorescence quenching with a new type of modulation fluorometer. *Photosynthesis Research.* 10(1-2): 51-62.

Siedler G, N Zangenberg and R Onken. 1992. Seasonal changes in the tropical Atlantic circulation: observation and simulation of the Guinea Dome. *Journal of Geophysical Research.* 97(C1): 703-715.

Søndergaard M. 2002. A biography of Einer Steemann Nielsen: the man and his science.

In. *Phytoplankton productivity: carbon assimilation in marine and freshwater ecosystems*, Williams PJ le B, DN Thomas and CS Reynolds, Eds. Blackwell Science Ltd. Oxford, UK. pp. 1-15.

Sosik HM and RJ Olson. 2002. Phytoplankton and iron limitation of photosynthetic efficiency in the Southern Ocean during late summer. *Deep-Sea Research I.* 49(7): 1195-1216.

Sprintall J and M Tomczak. 1992. Evidence of the barrier layer in the surface layer of the tropics. *Journal of Geophysical Research.* 97(C5): 7305-3716.

Sprintall J and M Tomczak. 1993. On the formation of Central Water and thermocline ventilation in the southern hemisphere. *Deep-Sea Research I.* 40(4): 827-848.

Steeman Nielsen E. 1952. The use of radio-active carbon ($^{14}$C) for measuring organic production in the sea. *Journal du Conseil International pour l'Exploration de la Mer.* 16: 117-140.

Stón J and A Kosakowska. 2000. Qualitative and quantitative analysis of Baltic phytoplankton pigments. *Oceanologia.* 42(4): 449-471.

Suggett D, G Kraay, P Holligan, M Davey, J Aiken and R Geider. 2001. Assessment of photosynthesis in a spring cyanobacterial bloom by use of a fast repetition rate fluorometer. *Limnology and Oceanography.* 46(4): 802-810.

Sukenik A, J Bennett, A Mortainbertrand and PG Falkowski. 1990. Adaptation of the photosynthetic apparatus to irradiance in *Dunaliella tertiolecta*: A kinetic study. *Plant Physiology.* 92(4): 891-898.

Tassan S and GM Ferrari. 1995. An alternative approach to absorption measurements of aquatic particles retained on filters. *Limnology and Oceanography.* 40(8): 1358-1368.

Tchernia P. 1980. *Descriptive Regional Oceanography.* Pergamon Marine Series, 3. Pergamon Press. Oxford, UK.

Tomczak M and JS Godfrey. 2001. Regional oceanography: an introduction. PDF version (http://www.es.flinders.edu.au/∼mattom/regoc/pdfversion.html).

Trees CC, DK Clark, RR Bidigare, ME Ondrusek and JL Mueller. 2000. Accessory pigments versus chlorophyll *a* concentrations within the euphotic zone: A ubiquitous relationship. *Limnology and Oceanography.* 45(5): 1130-1143.

Varela RA, F Figueiras, S Agustíand B Arbones (1998) Determining the contribution of pigments and the non-algal fraction to total absorption: toward a global algorithm. *Limnology and Oceanography.* 43(3): 449-457.

Waldron HN and TA Probyn. 1992. Nitrate supply and potential new production in the Benguela upwelling system. *South African Journal of Marine Science.* 12: 29-39.

Welschmeyer, N. A. 1994. Fluorometric analysis of chlorophyll *a* in the presence of chlorophyll *b* and phaeopigments. *Limnology and Oceanography.* 39: 1985-1992.

Widdicombe CE, SD Archer, PH Burkill and S Widdicombe. 2002. Diversity and structure of the microplankton community during a coccolithophore bloom in the stratified northern North Sea. *Deep-Sea Research II.* 49(15): 2887-2903.

Williams PJ leB. 1993. Chemical and tracer methods of measuring plankton production. *ICES Marine Science Symposia.* 197: 20-36.

Williams PJ leB and JE Robertson. 1991. Overall planktonic oxygen and carbon dioxide

metabolisms: the problem of reconciling observations and calculations of photosynthetic quotients. *Journal of Plankton Research*. 13 Supplement: 153-169.

Woods KL. 2003. *Development and assessment of novel techniques to measure primary production in the Celtic Sea and English Channel*. University of Southampton, UK. PhD thesis.

Woodward EMS. 1994. *Nutrient Analysis techniques*. Plymouth Marine Laboratory. Plymouth, UK. 26p.

Zapata M, F Rodríguez and JL Garrido. 2000. Separarion of chlorophylls and carotenoids from marine phytoplankton: a new HPLC method using a reversed phase $C_8$ column and pyridine-containing mobile phases. *Marine Ecology Progress Series*. 195: 29-45.

Zubkov MV, MA Sleigh, PH Burkill and RJG Leakey. 2000. Picoplankton community structure on the Atlantic Meridional Transect: a comparison between seasons. *Progress in Oceanography*. 45(3-4): 369-386.

Zubkov MV, MA Sleigh, GA Tarran, PH Burkill and RJG Leakey. 1998. Picoplankton community structure on an Atlantic transect from 50 degrees N to 50 degrees S. *Deep-Sea Research I*. 45(8): 1339-1355.

# Appendix A

# Available data

Contour plots of AMT11 CTD data (1 m binned layer) do not have an indication of the sample location, from where the interpolation grid has been generated, to avoid overcrowding the figure. However because it is important to know the depth and latitude of data samples, they are shown in Fig. A.1. Other contour plots, for which the grid has not been derived from CTD samples, have their sample location indicated by filled black circle.

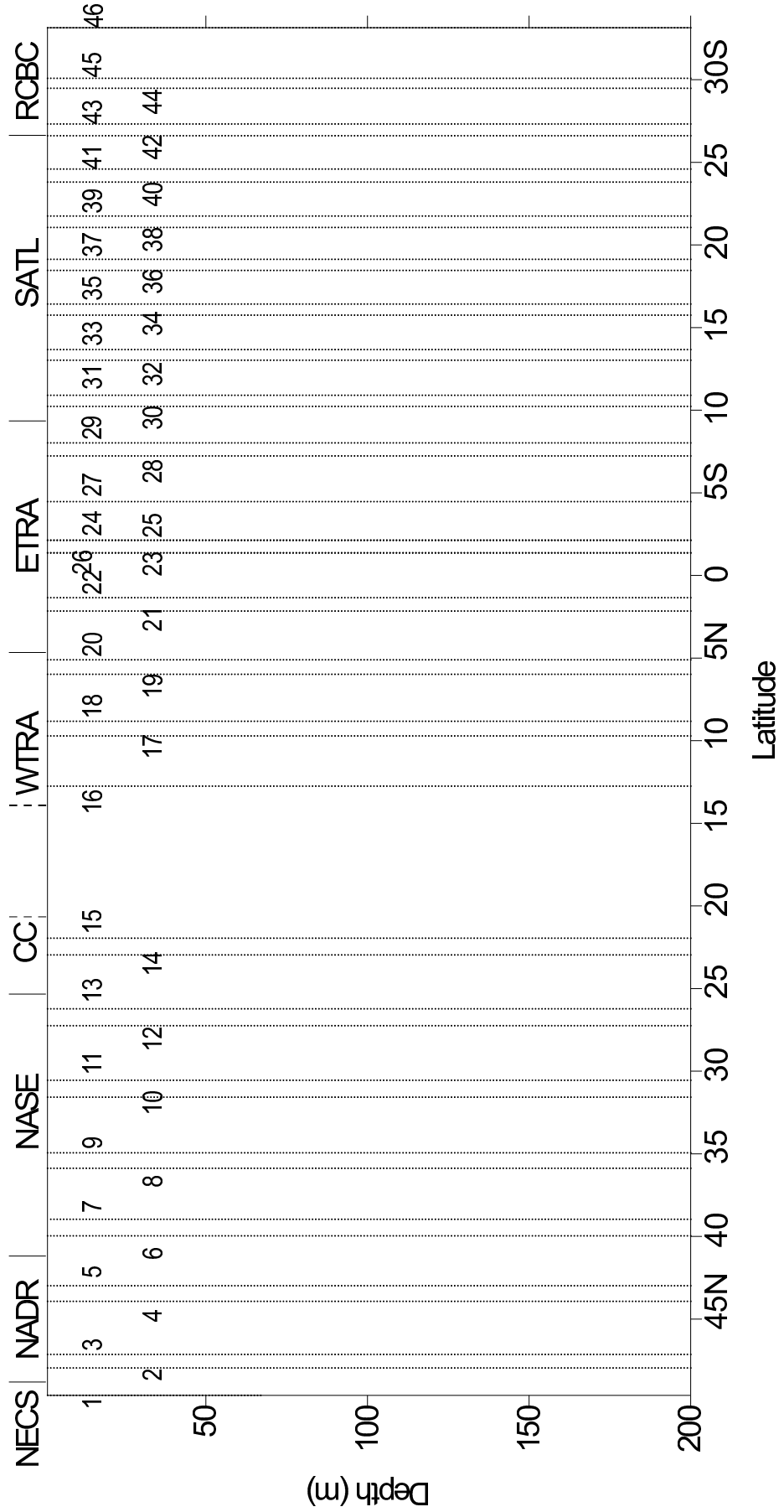


Figure A.1: Location of CTD samples for grid interpolation. There are CTD data at every 1 m depth. CTD mid-day and pre-dawn stations are indicated respectively in the upper and lower rows. The provinces are indicated in the top axis and the latitude in the bottom axis. Notice some stations have taken place at same latitude: 23/26 and 24/25.

# Appendix B

# Physical structure of the AMT11

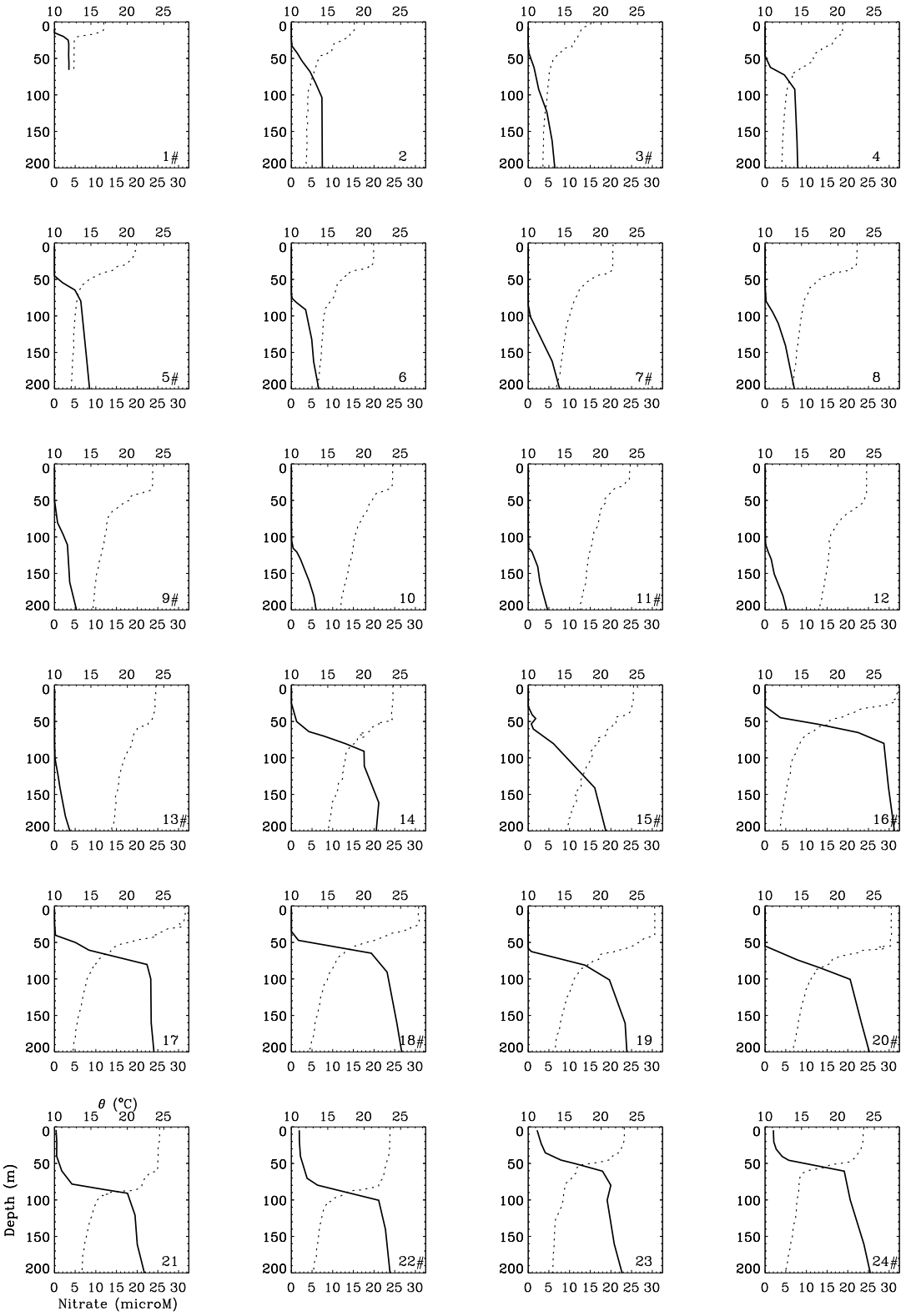


Figure B.1: Potential temperature ($\theta$ in °C, dotted line) and nitrate concentration ($\mu$M, solid line) along AMT11 transect, station 1 to 24. Day stations are indicated by #.

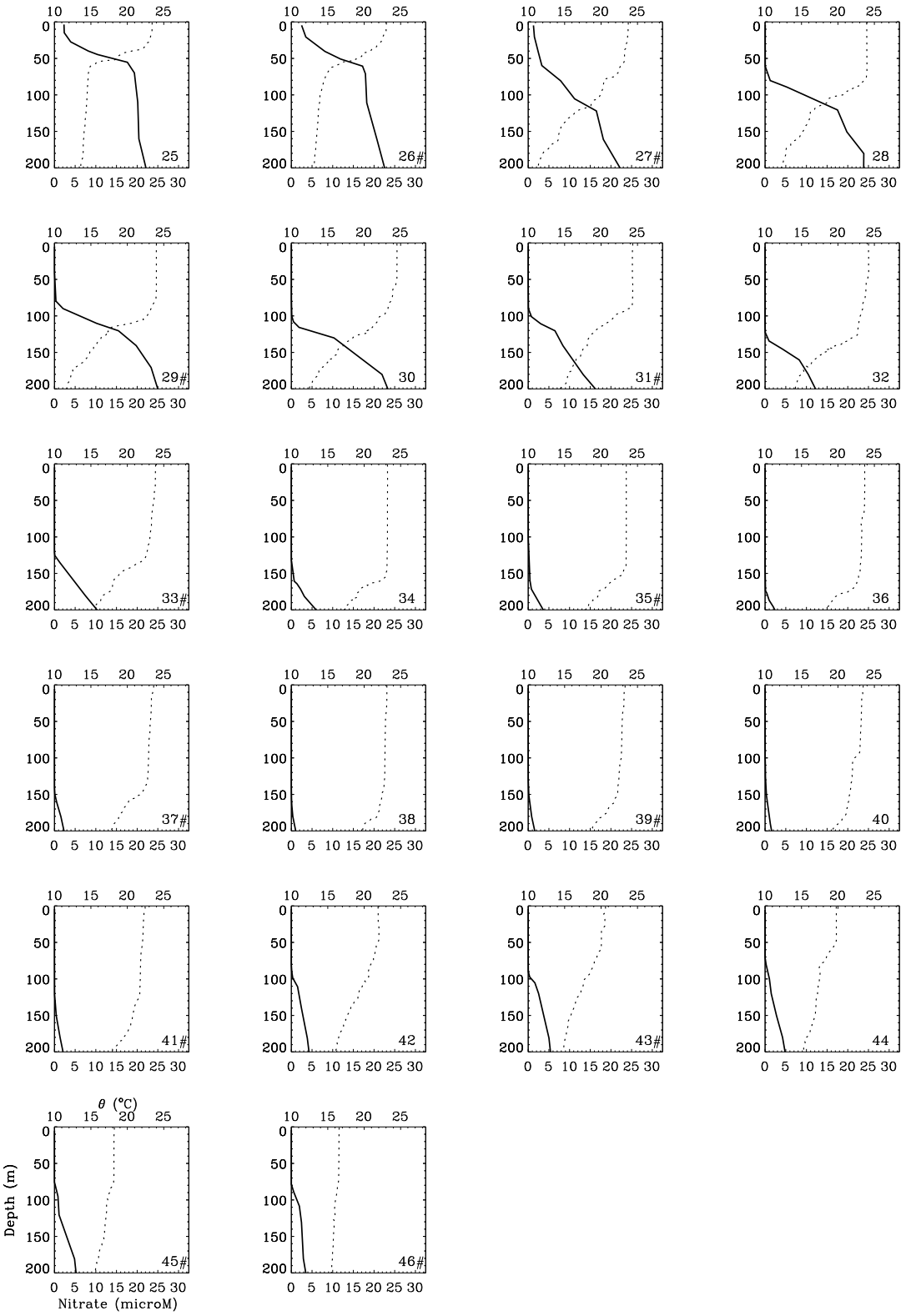


Figure B.2: Potential temperature ($\theta$ in °C, dotted line) and nitrate concentration ($\mu$M, solid line) along AMT11 transect, station 25 to 46. Day stations are indicated by #.

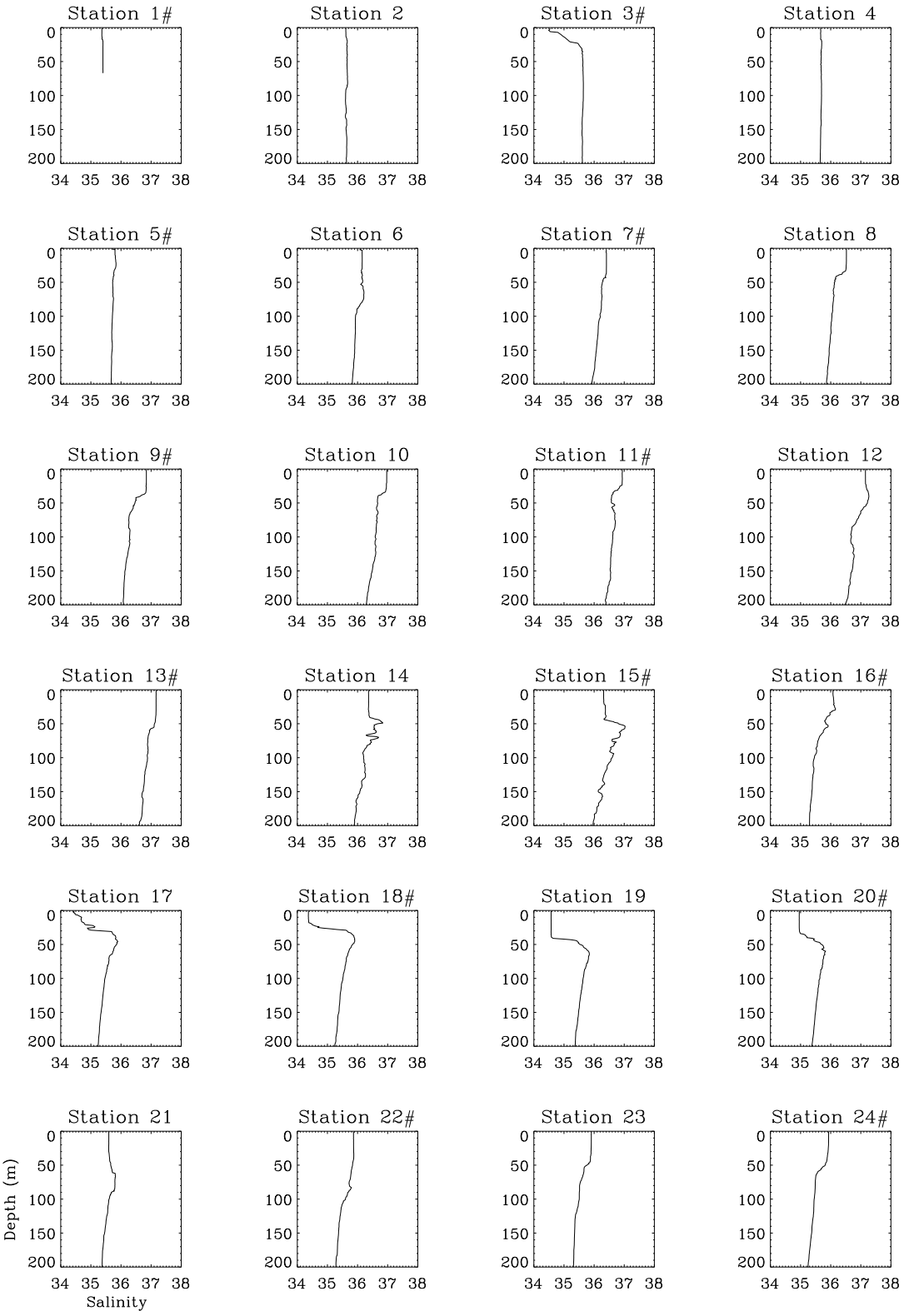


Figure B.3: Salinity profiles along AMT11 transect, stations 1 to 24. Day stations are indicated by #.

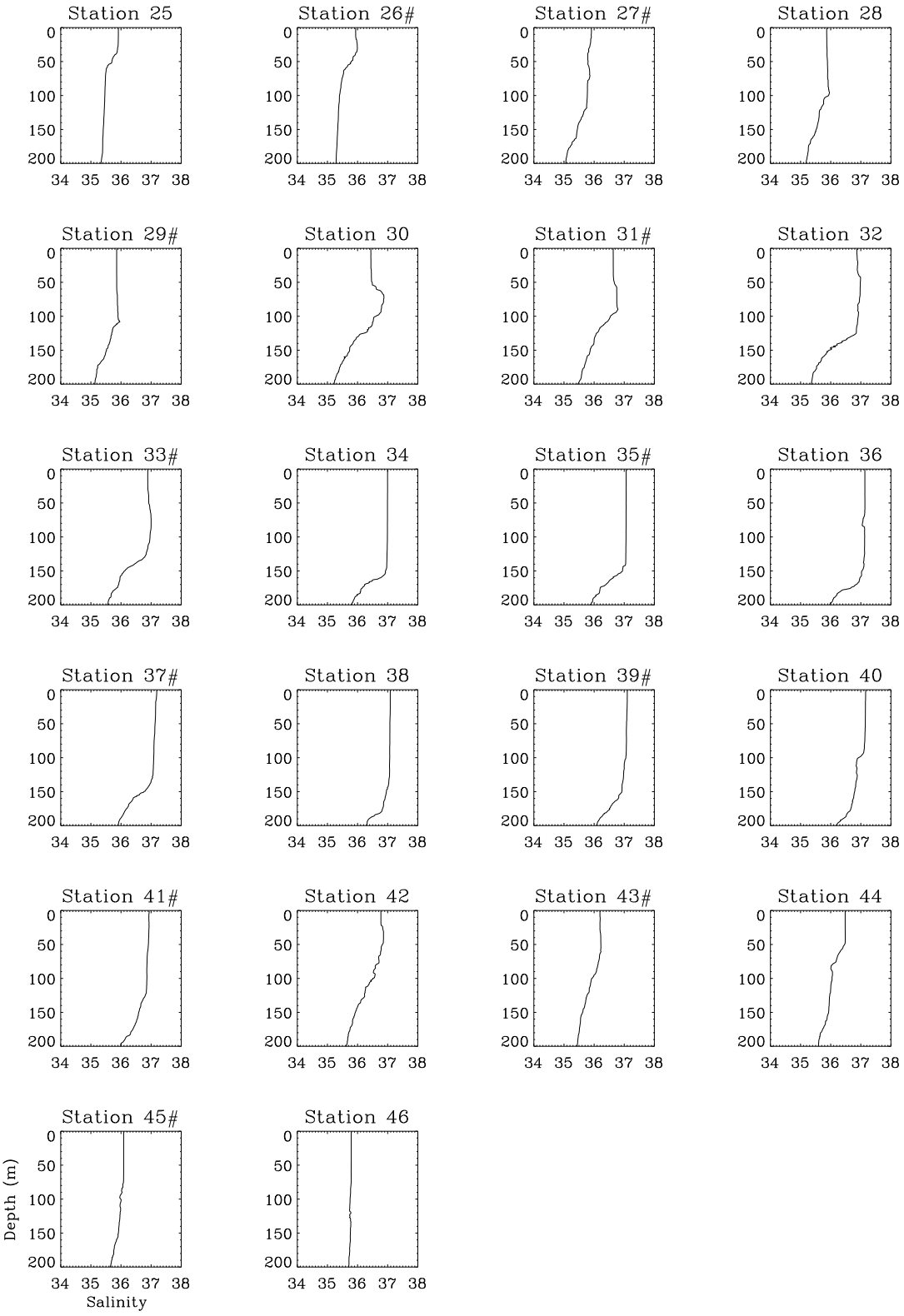


Figure B.4: Salinity profiles along AMT11 transect, stations 25 to 46. Day stations are indicated by #.

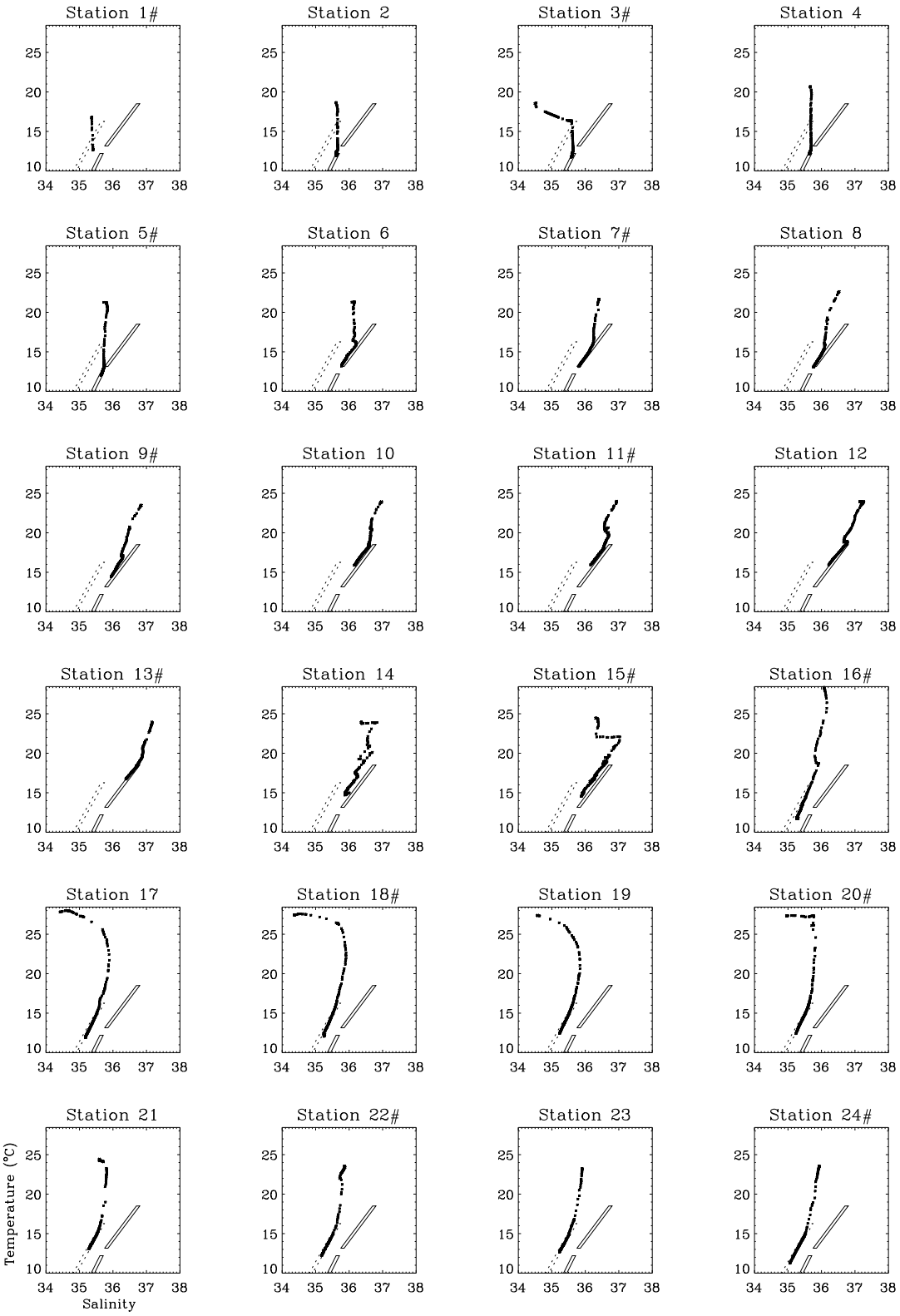


Figure B.5: T-S diagrams for the upper 200 m along AMT11 transect, stations 1 to 24. The parallelograms in solid lines represent the ENAWt (upper) and ENAWp (bottom) and the dotted parallelogram represents WSACW, as a guide for comparison between the provinces. Day stations are indicated by #.

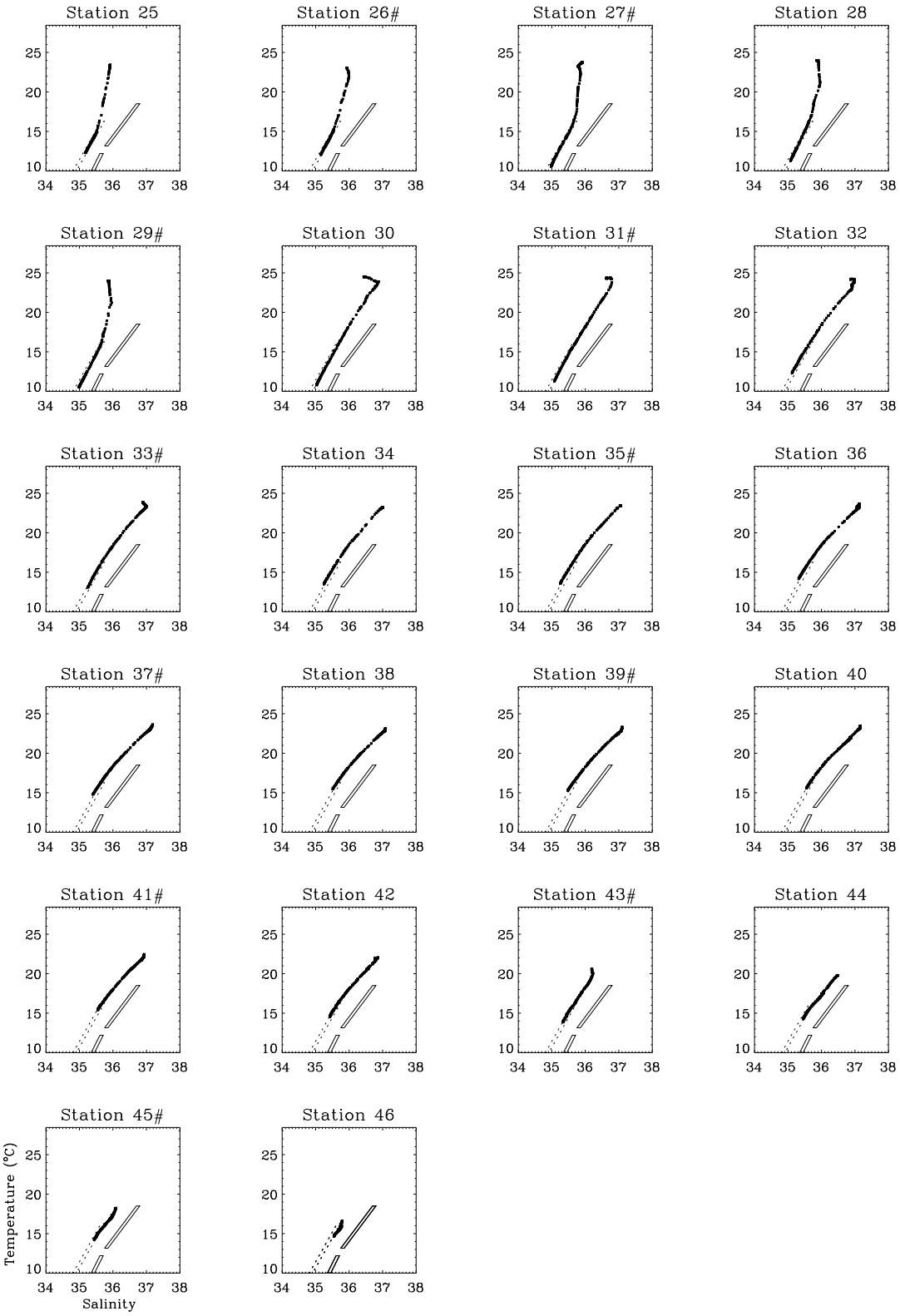


Figure B.6: T-S diagrams for the upper 200 m along AMT11 transect, stations 25 to 46. The parallelograms in solid lines represent the ENAWt (upper) and ENAWp (bottom) and the dotted parallelogram represents WSACW, as a guide for comparison between the provinces. Day stations are indicated by #.

# Appendix C

# Phytoplankton community structure

## C.1 Chl*b* as a marker pigment

When Chl*b* was detected (most of the samples), some assumptions were made to attempt to minimise underestimation or overestimation of nanoflagellates and dinoflagellates. The HPLC method applied in the AMT11 and BENEFIT-L1 cruises could not distinguish DVChl*b* from MVChl*b*, so the total Chl*b* measured (named Chl*b* from now on) accounted for DVChl*b* plus MVChl*b*. The former is found only in prochlorophytes and the latter can be found in green algae (Jeffrey *et al.* 1997) and also in prochlorophytes (Moore *et al.* 1995). Some dinoflagellates, lacking PER, also contain MVChl*b* from endosymbiont green algae (Jeffrey *et al.* 1997). The following analysis, summarised in Table C.1, was used to account for nanoflagellates and dinoflagellates. The presence/absence of green algae was assessed, by taking the pigments lutein (LUT), prasinoxanthin (PRA), violaxanthin (VIO) and neoxanthin (NEO) as marker pigments for the green algae (Jeffrey *et al.* 1997), named here as GREEN pigments. Although NEO may be due to Euglenophyceae, if the GREEN pigments are zero, green algae can be considered absent. If neither DVChl*a* nor GREEN pigments were detected but Chl*b* was found (Case 1 in Table C.1), then it was considered due to some endosymbiont green algae present in dinoflagellates, so Chl*b* together with PER accounted for the dinoflagellates. If Chl*b* and DVChl*a* were present with no GREEN pigments (Case 2 in Table C.1), then the Chl*b* was likely to be due to the prochlorophytes. In the absence of DVChl*a* but presence of GREEN pigments (Case 3 in Table C.1), the Chl*b* was attributed to the green algae. The most difficult case was when both the GREEN pigments and DVChl*a* co-occurred (Case 4 in Table C.1). In this

Table C.1: Marker pigments for nanoflagellates and dinoflagellates, depending on the presence (+)/absence (-) of DVChl*a* and GREEN pigments. GREEN is the sum of the marker pigments for green algae (LUT+PRA+VIO+NEO). Chl*b* column represents the phytoplankton group to which the Chl*b* content is attributed. P represents prochlorophytes, D is dinoflagellates and G the green algae. $Chlb_{green}$ is the Chl*b* due to the green algae.

| Case | DVChl*a* | GREEN | Chl*b* | nanoflagellates | dinoflagellates |
|---|---|---|---|---|---|
| 1 | - | - | D | HEX+BUT+ALL | PER+Chl*b* |
| 2 | + | - | P | HEX+BUT+ALL | PER |
| 3 | - | + | G | HEX+BUT+ALL+Chl*b* | PER |
| 4 | + | + | G + P | HEX+BUT+ALL+$Chlb_{green}$ | PER |

case the Chl*b* may be due to either the green algae or the prochlorophytes, or to both and the procedure to estimate the Chl*b* fraction due to the green algae would depend on the prochlorophyte type and its growth light level, as explained in Section C.1.1.

### C.1.1 Estimating Chl*b* due to the green algae

The method to estimate the amount of Chl*b* due to the green algae, was based on results of Moore *et al.* (1995). They analysed two types of prochlorophytes, one population from the surface of the Mediterranean Sea, the *Prochlorococcus marinus* MED4 (MED4-type) with high light adaptation and another from the deep water of the Sargassum Sea adapted to low ligh, the *Prochlorococcus marinus* SS120 (SS120-type). According to their results, the SS120 cannot grow at light levels higher than 100 $\mu$E m$^{-2}$ s$^{-1}$ and has higher DVChl*b* to DVChl*a* ratio (Chl$b/a > 1$) than the MED4-type (Chl$b/a < 0.2$). The classification of the prochlorophytes to one of these two types of population was based on the physical structure of the water column. The Chl$b/a$ ratio values were chosen following the method below and they are summarised in Table C.2. The difference between the measured Chl*b* and estimated $Chlb_{prochl}$ was the Chl*b* due to the green algae ($Chlb_{green}$).

Table C.2: Estimating Chl$b_{green}$ fraction from Chl$b$ and DVChl$a$. For the P.marinus MED4-type, Chl$b_{green}$ = Chl$b$ - DVChl$a$ × Chl$b/a$. PAR in $\mu$E m$^{-2}$ s$^{-1}$.

| samples | P-type | Chl$b/a$ ratio |
|---|---|---|
| AMT11 z>ILD | SS120 | 1 (e.g. Chl$b_{green} = 0$) |
| AMT11 z<ILD and | MED4 | PAR $> 100 \Rightarrow$ Chl$b/a = 0.055$ |
| all BENEFIT-L1 | | $60 <$ PAR $< 100 \Rightarrow$ Chl$b/a = 0.12$ |
| | | $20 <$ PAR $< 60 \Rightarrow$ Chl$b/a = 0.15$ |
| | | PAR $< 20 \Rightarrow$ Chl$b/a = 0.2$ |

**SS120-type**

All the AMT11 samples deeper than the ILD were considered to be the SS120-type. Because the Chl$b/a$ ratio for SS120-type was between 0.9 and 2.0 (Moore *et al.* 1995) and most of these field samples had the Chl$b$ concentrations double to that of DVChl$a$ concentrations, it was assumed that most of the Chl$b$ was due to the prochlorophytes and not to the green algae, hence only HEX, BUT and ALL (Chl$b_{green} = 0$) accounted to the nanoflagellates (Table C.2). This assumption may underestimate the nanoflagellates.

**MED4-type**

This type of Prochlorococcus tolerates fluctuating high light and can grow at high light exposure (Moore *et al.* 1995), so the prochlorophytes confined within the ILD of the AMT11 transect and all the BENEFIT-L1 samples were more likely to be this type of population. For these samples, Chl$b$ was split into DVChl$b$ and MVChl$b$, depending on the light level, which determined the ratio of Chl$b/a$ (Moore *et al.* 1995). During the AMT11, water sampling for HPLC pigments was carried out at local noon, so the PAR measured at the depth and time of sampling was assumed to be the growth light level. For the BENEFIT-L1 oligotrophic stations that took place at the dusk or dawn, with very low or no light and where both GREEN and DVChl$a$ pigments were present (bio-optical stations 15, 17 and 19), the growth light level was assumed to be equal to that from the station B16 (Figure 5.1), an oligotrophic station in the vicinity area, sampled at local

midday under clear sky conditions. The Chl$b$ due to the prochlorophytes (Chl$b_{\mathrm{prochl}}$) was estimated by applying the Chl$b/a$ ratio to the measured DVChl$a$ (Table C.2).

# Appendix D

# Phytoplankton physiology

## D.1 Instrument and methodology assessment

Fast repetition rate (FRR) fluorometry was applied to collect physiological parameters of the phytoplankton across the Atlantic Ocean during the AMT11 in two different ways. The FRR fluorometer was used in the bench-top mode for on board measurements of the water sampled at discrete depths with the rosette bottles (Chapter 6). Each measurement was carried out in the dark chamber only. This method was applied on the pre-dawn stations. At mid-day stations, the instrument was attached to the bio-optical rig and deployed vertically for *in situ* profiling measurement. Both chambers were used for measurements, the light chamber to assess the phytoplankton physiology under ambient light and the dark chamber to asses without ambient light effect. Because during the pre-dawn station the measurement was taken in the dark chamber only and because one of the parameters needed for primary production estimate should be taken in the light chamber, the intercalibration between the chambers was very important. To assess the performance of the instrument and the methodologies applied during the thesis, data collected at five pre-dawn stations of BENEFIT-L1 (see Chapters 5) and three samplings at the E1 station were analysed. At pre-dawn, the absence of natural light assured the same light conditions for the light and dark chambers. Also, the phytoplankton population had time enough to recover from the light exposure, so that the time delay between the discrete bench top-mode and *in situ* profiling methods did not affect the physiological state of the phytoplankton since the water sample was kept in the darkness.

### D.1.1 E1 sampling

The E1 is a sampling station located at latitude 50°02' N and longitude 04°22'W, 22 nautical miles southwest of Plymouth where the local depth is around 75 m. This sampling was planned to investigate the agreement between two sampling methods for fast repetition rate fluorometry (FRRf). Three measurements were carried out: at 11:00 pm (16 May 2002), 02:00 am and 05:00 am (17 May 2002) on board Research Vessel Squilla.

The FRR fluorometer was set to autoranging mode and deployed attached to the bio-optical rig, down to about 5.0 m deeper than the DCM and held there for 2 min (gain setting time), then brought to the surface, stopping for water collection with bottles and extended fluorescence acquisitions at 4 depths. For every bottle fired, the rig was brought 0.7 m shallower and held for about 20 s (about 30 acquisitions) for FRR fluorescence sampling. This 0.7 m correction was due to the distance between the bottles and the FRR fluorometer. The water was analysed by bench-top mode just after the sampling, as described above but with the same gain automatically set by the instrument during the *in situ* profiling.

### D.1.2 Dark chamber versus light chamber

The measurements from light and dark chambers were compared to check whether the chambers was retrieving the same values. The FRR fluorometer was profiled vertically with auto-ranging mode and the data from the upper part of the water column only, e.g. from the surface to the depth of maximum fluorescence, were analysed. The data were binned into 1 m layer and those resulting from one measurement only were discarded. Data processing and quality control was explained in the Chapter 6.

### D.1.3 Discrete bench-top mode method versus *in situ* profiling method

Water samples from the CTD bottles were analysed as soon as the data from *in situ* profiling methods were analysed and the gain set for the *in situ* profiling (auto-ranging mode) was available. The whole procedure to finish the bench-top mode measurement took less than 2 hours from the time of the water collection. Depth correction was applied

for matching up of the water column structure (Chapter 6). Data processing and quality control was explained in Chapter 6.

### D.1.4 Statistics for data analysis

The comparison between the two chambers or between the two methods was examined using the Bland-Altman method, which consists of a graphical analysis, plotting the difference between the two measurements against the average of the two measurements (Bland and Altman 1986). The mean difference and the limits of agreement[1] are plot as a guide for the analysis. Correlation and linear regression techniques were usually applied to assess the agreement between the two measurements (Boyd and Abraham 2001). Deming regression was used to estimate the slope and intercept of the relationship between the measurements. This regression method provided unbiased estimates of the slope and intercept by applying the orthogonal least-squares technique where deviations were drawn perpendicular to the regression line. This accounted for the errors not only in the y-axis but also in the x-axis. Deming regression was applied using the Method Validator version 1.1.10.0 (1999, Philippe Marquis, Metz-France).

## D.2 Results

### D.2.1 Comparison between light and dark chambers

The comparison between the chambers is shown in Figure D.1 and Table D.1.

**Fo, Fm, Fv:** Graphical analysis through Bland-Altman plots (Figure D.1) showed differences in the fluorescence measurements but most of the data were within the limits of agreement (Figure D.1 Fo, Fm and Fv). The mean differences were very small for all the three parameters relative to the measurement values. Statistically, there was no significant differences in fluorescence (Fo, Fm, Fv) measurements from the two chambers, with $R^2$ bigger than 0.975, a slope close to 1.0 ($b > 0.95$) and a small intercept ($|a| < 0.1$).

[1] limits of agreement is the mean difference $\pm$ 1.96 $\times$ sd, where sd is the standard deviation of the differences between the two measurements.

**Fv/Fm:** Measurement was also within the limits of agreement and the average difference was null (-0.001), but there was an evident proportional bias between the two chambers (Figure D.1 Fv/Fm). The dark chamber overestimated Fv/Fm at values lower than 0.35 and underestimated at values bigger than 0.4 (Figure D.1). The bias was proportional to the value of Fv/Fm yielding a consistent relationship between the chambers ($R^2 > 0.95$) with a slope of 0.79 and an intercept of 0.075 (Table D.1). This high $R^2$ was also an indication of high precision. The proportional bias between measurements of light and dark chambers proved necessary to introduce a correction for the dark chamber even for the *in situ* profiling measurements of Fv/Fm. Perhaps a more frequent calibration followed by a test to check agreement between the chambers is required for better performance of the instrument.

$\sigma_{\mathrm{PSII}}$: The dark chamber overestimates the light chamber measurement of $\sigma_{\mathrm{PSII}}$ across the range investigated (constant bias) with a small mean difference ($= 21 \times 10^{-20}$ m$^2$ photon$^{-1}$). There was also an increasing imprecision with increasing $\sigma_{\mathrm{PSII}}$. The $R^2$ was smaller than 0.9 (Table D.1), showing a weak relationship between the two chambers, e.g. imprecision. The intercept value for $\sigma_{\mathrm{PSII}}$ was small (a = -19.8) relative to the measurement ($\sigma_{\mathrm{PSII}} > 450 \times 10^{-20}$ m$^2$ photon$^{-1}$) and the intercept was close to 1. At $\sigma_{\mathrm{PSII}} < 650 \times 10^{-20}$ m$^2$ photon$^{-1}$, it can be considered that the two chambers yielded the same measurement of $\sigma_{\mathrm{PSII}}$, with high precision. The $R^2$ had poorer value due to bigger imprecision at $\sigma_{\mathrm{PSII}} > 650 \times 10^{-20}$ m$^2$ photon$^{-1}$, so increasing the number of acquisitions may reduce the effect of the imprecision and improve the measurement, since the mean difference was small.

$\tau_{\mathrm{QA}}$: Differences of this parameter between the two chambers were bigger (higher imprecision). Although the biases were related to the value of the measurements, there was no linearity as that found for Fv/Fm. The bias was considered for three sub-ranges of $\tau_{\mathrm{QA}}$ as indicated in Figure D.1. The bias decreased with increasing $\tau_{\mathrm{QA}}$ but the imprecision (sd) increased with increasing $\tau_{\mathrm{QA}}$.

The FRR fluorometer had one photomultiplier only for the measurement of the fluorescence emitted by both chambers, so the difference between the measurements with the light and dark chambers was not due to the sensor (Figure 2.7). There may be a difference in the excitation energy since each chamber has its own array of LEDs. However that was corrected by taking a little sample of emission light as a reference signal which was

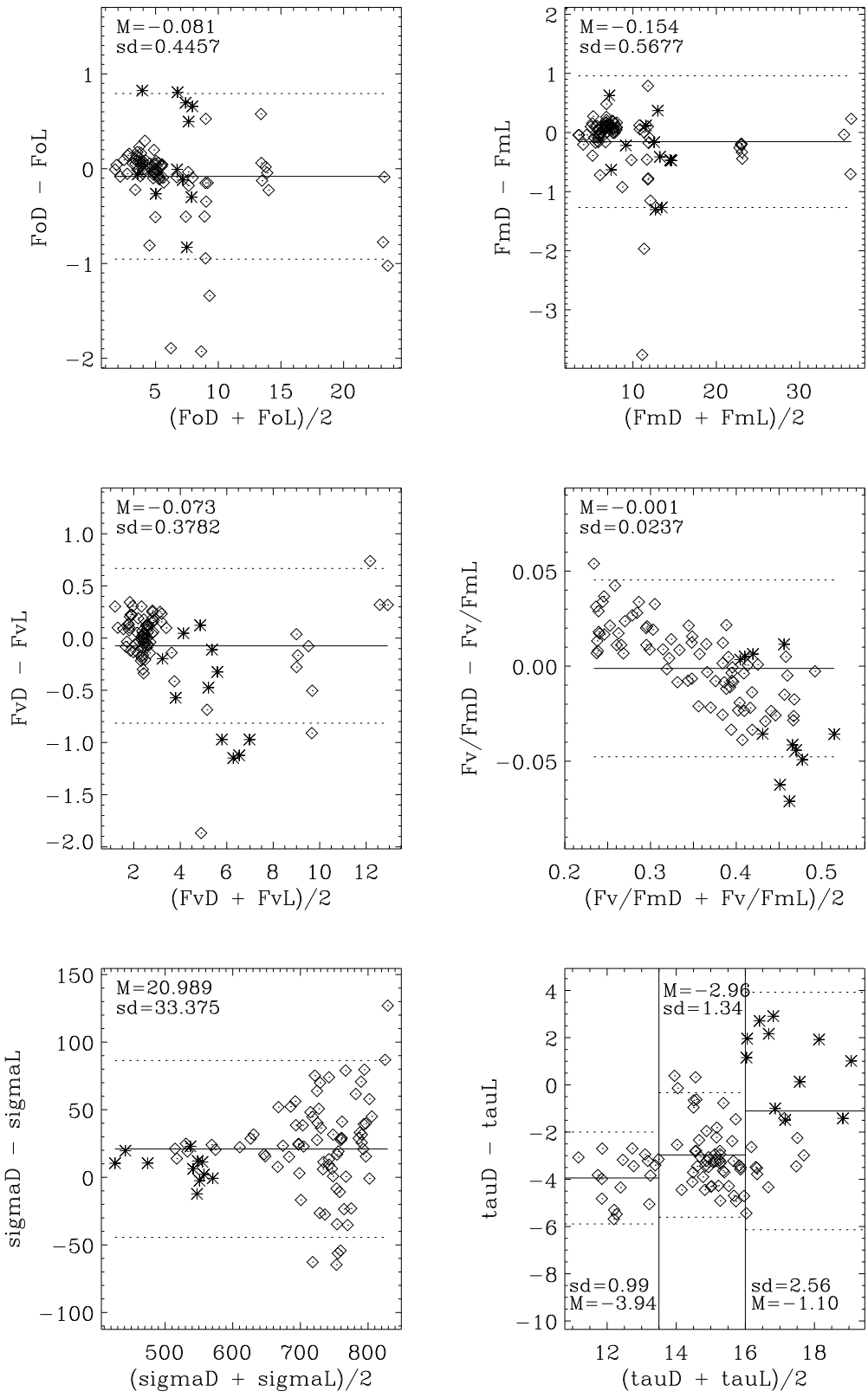


Figure D.1: Bland-Altman plots for comparison of measurements of FRRF-derived phytoplankton physiological data with light chamber (suffix L) and dark chamber (suffix D) at pre-dawn stations of BENEFIT-L1 (diamond) and E1-sampling (*). The solid line is the mean difference between light and dark chambers (bias) and the dotted lines are the limits of agreement (±1.96 sd). For $\tau_{QA}$ three limits were considered as indicated. Fo, Fm and Fv in arbitrary units, $\sigma_{PSII}$ in $\times 10^{-20}$ m$^2$ photon$^{-1}$ and $\tau_{QA}$ in ms.

Table D.1: Comparison of measurements of FRRF-derived phytoplankton physiological data with light chamber and dark chamber. $R^2$ is the adjusted coefficient of determination. The slope (b) and intercept (a) and the 95% confidence interval (in brackets) were estimated with Deming regression. The number of data analysed was 88. Fo, Fm and Fv in arbitrary units, $\sigma_{PSII}$ in $\times 10^{-20}$ $m^2$ $photon^{-1}$.

| | Fo | Fm | Fv | Fv/Fm | $\sigma_{PSII}$ |
|---|---|---|---|---|---|
| $R^2$ | 0.990 | 0.993 | 0.980 | 0.960 | 0.867 |
| b | 0.971 | 0.985 | 0.968 | 0.788 | 1.059 |
| $[b]$ | 0.950 to 0.993 | 0.969 to 1.001 | 0.914 to 1.022 | 0.749 to 0.827 | 0.995 to 1.123 |
| a | 0.105 | -0.002 | 0.043 | 0.075 | -19.8 |
| $[a]$ | -0.023 to 0.233 | -0.167 to 0.163 | -0.113 to 0.198 | 0.062 to 0.089 | -58.9 to 19.4 |

recorded with the corresponding set of fluorescences (Chapter 2). Another difference between the light and dark chambers was structural: the PVC housing built-in for the dark chamber and the pipes attached on it to prevent the sample from ambient light. However, this housing also restricted the volume of water to be sampled. The dark chamber has a smaller volume of water contained in the PVC housing (Figure 2.7). Because of the restriction of the water volume by the PVC housing of the dark chamber and that it may have higher scattering properties, the fluorescence may be more scattered, increasing the pathway to the optical window, increasing water absorption of red light (fluorescence), decreasing the actual fluorescence that reaches the detector. In the other hand, dark chamber may also increase scattering of blue light not absorbed initially by the phytoplankton, increasing the probability of absorption by the phytoplankton, increasing the effect of excitation energy, so increasing the fluorescence measured by the dark chamber. Although the open volume of water in the light chamber, the sun-block installed in parallel to light chamber optical window (see Figure 2.7 in Chapter 2) for fluorescence collection restricted the pathway as short as in the dark chamber. Emitted fluorescence was collected perpendicular to the excitation beam, so the increase in sample volume would not increase the fluorescence within the range of the collector. Further research is still needed to assess the measurements from light and dark chamber.

### D.2.2 Comparison between discrete bench-top mode measurement and *in situ* profiling measurement

Results of comparison between measurements from discrete bench-top mode and *in situ* profiling methods with FRR fluorometry are presented in Table D.2 and Figure D.2.

**Fo, Fm, Fv**: Scattering in the discrete mode was expected to be higher since bubbles could be trapped either in the pipes or in the dark chamber, or in both. Trapped bubbles increase scattering which increases fluorescence yields. Therefore both Fo and Fm from discrete bench-top mode were expected to be bigger than the measurements from the *in situ* profiling method. However the opposite was observed in the experiment: the discrete bench-top mode method underestimated the *in situ* profiling method (Figure D.1) with a small mean difference between the two methods for Fo, Fm and Fv. Deming regression confirmed that with a slope smaller than 0.95 for all the three fluorescences (Table D.2). All the three fluorescences produced $R^2$ higher than 0.90 but less than 0.95, so the relationship between the two methods to estimate Fo, Fm and Fv was weaker than the relationship between the chambers. Because the agreement between chambers[2] was more consistent and precise than the agreement between the methods, it can be concluded that the *in situ* profiling method was more precise than the discrete bench-top mode method. In terms of fluorescences, it can be considered that they are measuring the same value although the discrete bench-top mode seems more imprecise. The increase in acquisition numbers can improve and overcome the imprecision of the discrete bench-top mode method.

**Fv/Fm:** Although giving good performances in fluorescence measurements, the discrete bench-top mode method underestimated the *in situ* profiling method for Fv/Fm with mean difference of -0.023, e.g. constant bias across the range analysed (0.2 to 0.5). This was less than 10 % at Fv/Fm of 0.25 and less than 5 % at Fv/Fm of 0.5. The slope was closer to the equality line (b = 1.039) than the three previous measurements (Fo, Fm and Fv) but $R^2$ was smaller ($R^2 = 0.79$), probably due to the noise relatively big to the Fv/Fm range investigated (sd of differences was 0.034). The discrete bench-top mode showed small constant bias but was imprecise. Increasing the number of acquisitions can improve the estimate of Fv/Fm with the discrete bench-top mode method.

[2]Agreement between chambers was carried out through *in situ* profiling method.

Table D.2: Comparison of FRRF-derived phytoplankton physiological measurements with the discrete bench-top mode and the *in situ* profiling FRRF, both with dark chambers. $R^2$ is adjusted squared multiple R. The slope (b) and intercept (a) and their 95% confidence interval (in brackets) were estimated with Deming regression. Number of data analysed was 30. Fo, Fm and Fv in arbitrary units, $\sigma_{\mathrm{PSII}}$ in $\times 10^{-20}$ m$^2$ photon$^{-1}$.

| | Fo | Fm | Fv | Fv/Fm | $\sigma_{\mathrm{PSII}}$ |
|---|---|---|---|---|---|
| $R^2$ | 0.940 | 0.951 | 0.938 | 0.787 | 0.871 |
| b | 0.925 | 0.927 | 0.932 | 1.039 | 1.022 |
| [*b*] | 0.837 to 1.012 | 0.858 to 0.996 | 0.857 to 1.008 | 0.859 to 1.220 | 0.87 to 1.175 |
| a | 0.314 | 0.183 | -0.139 | -0.038 | 6.9 |
| [*a*] | -0.272 to 0.900 | -0.631 to 0.997 | -0.462 to 0.184 | -0.108 to 0.032 | -84.5 to 98.4 |

**$\sigma_{\mathrm{PSII}}$:** The mean difference was $21.3 \times 10^{-20}$ m$^2$ photon$^{-1}$, a constant bias with the discrete bench-top mode method overestimating the *in situ* profiling method (Figure D.2). The mean difference was small relative to the $\sigma_{\mathrm{PSII}}$ range (450 to 800 $\times 10^{-20}$ m$^2$ photon$^{-1}$), with a slope close to 1 (b = 1.022) and a small intercept (a = 6.9 $\times 10^{-20}$ m$^2$ photon$^{-1}$). The noise was big enough to decrease the relationship between the two measurements ($R^2$ = 0.87), revealing imprecision in the discrete bench-top mode method.

**$\tau_{\mathrm{QA}}$:** There was an increasing bias with increasing $\tau_{\mathrm{QA}}$ although no linear relationship was observed for such increase. The three sub-ranges showed increasing bias and the imprecision was nearly constant across the whole range.

The main conclusion was that the *in situ* profiling method is more precise than the discrete bench-top mode. The imprecision in the latter method can be minimised by increasing the number of acquisitions because the mean difference is small for either Fv/Fm or $\sigma_{\mathrm{PSII}}$.

## D.3 Conclusions

Data collected at night and pre-dawn stations were analysed to compare the physiological parameters retrieved from the two chambers when *in situ* measurements were taken

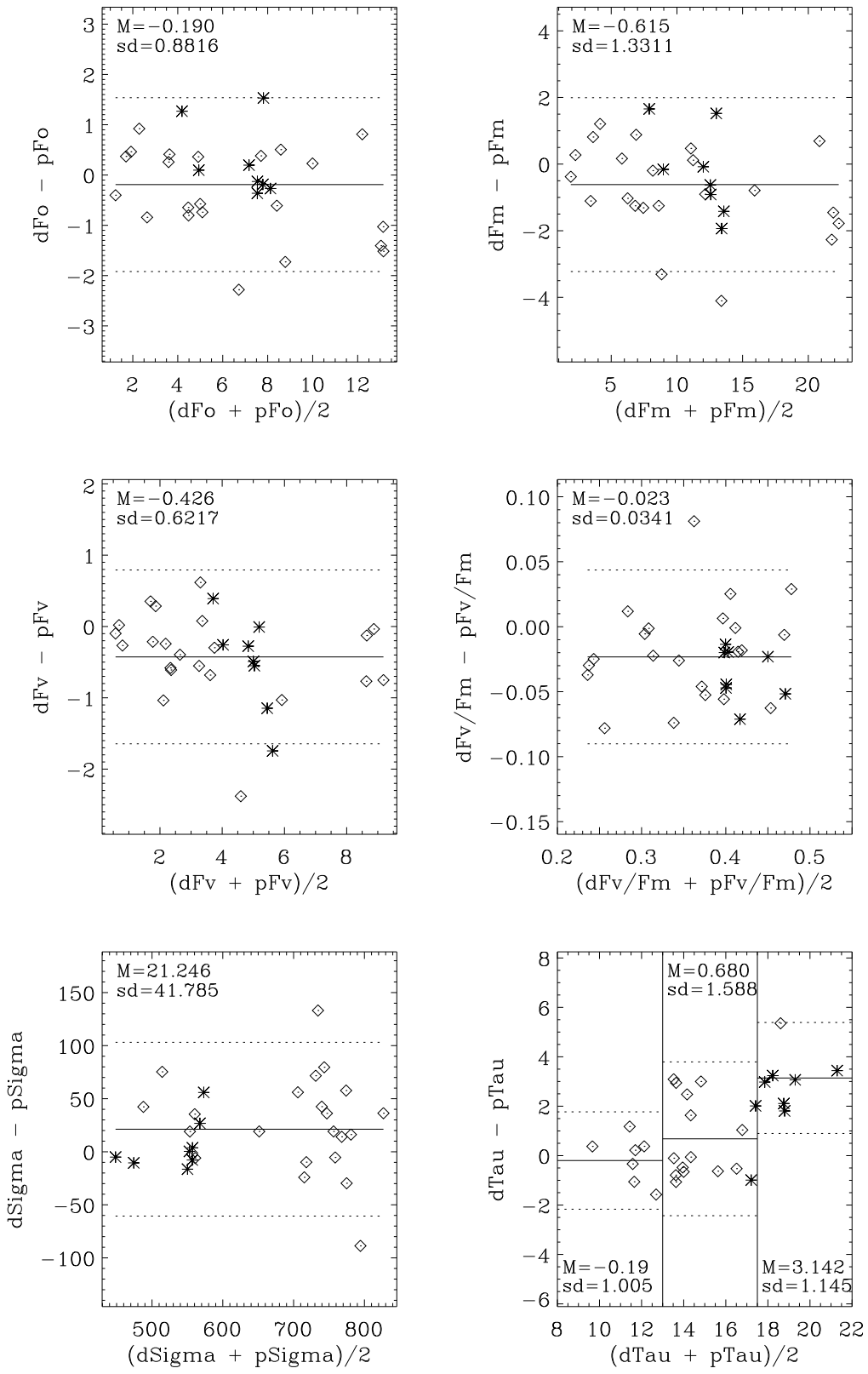


Figure D.2: Bland-Altman plot for FRRF-derived phytoplankton physiological data measured with discrete bench-top mode (prefix d) and profiling (prefix p) methods, both with dark chambers, for BENEFIT-L1 (diamond) and E1-sampling (*). The solid line represents the mean difference between light and dark chambers (bias) and the dotted lines represent limits of agreement (±1.96 sd). For $\tau_{QA}$ 3 limits were considered as indicated. Fo, Fm and Fv in arbitrary units, $\sigma_{PSII}$ in $\times 10^{-20}$ m$^2$ photon$^{-1}$ and $\tau_{QA}$ in ms.

profiling the FRR fluorometer vertically in the water column. Also at the same time of the profiling, discrete water samples were collected for analysis on board with the FRR fluorometer set for bench-top mode method. Then the measurements of the two methods (profiling and bench-top mode) were compared.

The two chambers and the two methods retrieved biased values, so it is suggested that the results from these comparisons be applied for correction of the physiological parameters.

From the two chambers comparison Fv/Fm measurement presented a proportional bias and constant precision, so a linear correction is suggested. $\sigma_{\mathrm{PSII}}$ between 400 and 650 $\times 10^{-20}$ m$^2$ photon$^{-1}$ had a bias of less then 5 % of the measurement value and the measurements were quite precise in this range. For $\tau_{\mathrm{QA}}$ it is suggested that a correction depending on the range of the measurement be applied.

The discrete bench-top mode was less precise than the *in situ* profiling method, so the more measurements obtained with the bench-top mode, the better. A constant bias correction is suggested for Fv/Fm and $\sigma_{\mathrm{PSII}}$ whilst a bias correction depending on the range of measurements seems more adequate for $\tau_{\mathrm{QA}}$.

It is suggested a correction for the methods be applied first and then the correction for the chambers difference.

# Appendix E

# Primary productivity

## E.1 Calibration of CTD fluorescence for Chl*a* estimate

Higher irradiance in the upper layer of the water column causes quenching of fluorescence. The depth of such a light effect depends on how much light can penetrate in the water column which is not an easy task to determine. This light effect over fluorescence decreases the power to estimate Chl*a* concentration from fluorescence measurements. To overcome this problem, results from the phytoplankton community analysis presented in Chapter 5 were recalled. That pigment analysis presented three distinct phytoplankton assemblages along the AMT11 transect. In the surface waters of oligotrophic gyres, Cluster A, an assemblage of prochlorophytes and nanoflagellates with high photoprotection was detected. Cluster B was found where the depth of the nitracline was deep, so low light, and a community with high Chl*b* content with nanoflagellates was dominating over prochlorophytes. At depths where nitrate was more abundant at shallower water, so high light, a mixed community of phytoplankton with nanoflagellates domination (Cluster C) was detected. Considering this difference along the AMT11 transect, a linear regression analysis was applied to obtain an equation specificly to describe the relationship between the fluorescence from the CTD (CTDf) and the Chl*a* concentration for each Cluster (Table E.1). Apart from station 1, the AMT11 data had very similar relationship (Table E.1), independent on the differences presented by the Cluster analysis. The derivation of specific relationship for each of the Clusters resulted in lower values in the errors and in

Table E.1: Linear regression analysis between CTD fluorescence and totChl*a* from HPLC for all the data excluding station 1 (W1), station 1 only and for Clusters A, B and C are presented with respective number of samples (N) and adjusted coefficient of determination (adj_$R^2$). Standard error of estimate for constant and slope is presented in brackets. The model is Chl*a* = slope × CTDf - constant for all the data sets but for Station 1 is in the log space Chl*a* = 10^(slope × CTDf - constant).

| Data | N | adj_$R^2$ | constant | slope |
|---|---|---|---|---|
| Station 1 | 6 | 0.997 | -3.190 (0.061) | 1.625 (0.036) |
| W1 | 110 | 0.705 | -0.489 (0.041) | 0.482 (0.030) |
| Cluster A | 28 | 0.621 | -0.465 (0.080) | 0.464 (0.069) |
| Cluster B | 38 | 0.519 | -0.468 (0.101) | 0.453 (0.071) |
| Cluster C | 38 | 0.702 | -0.392 (0.069) | 0.430 (0.458) |

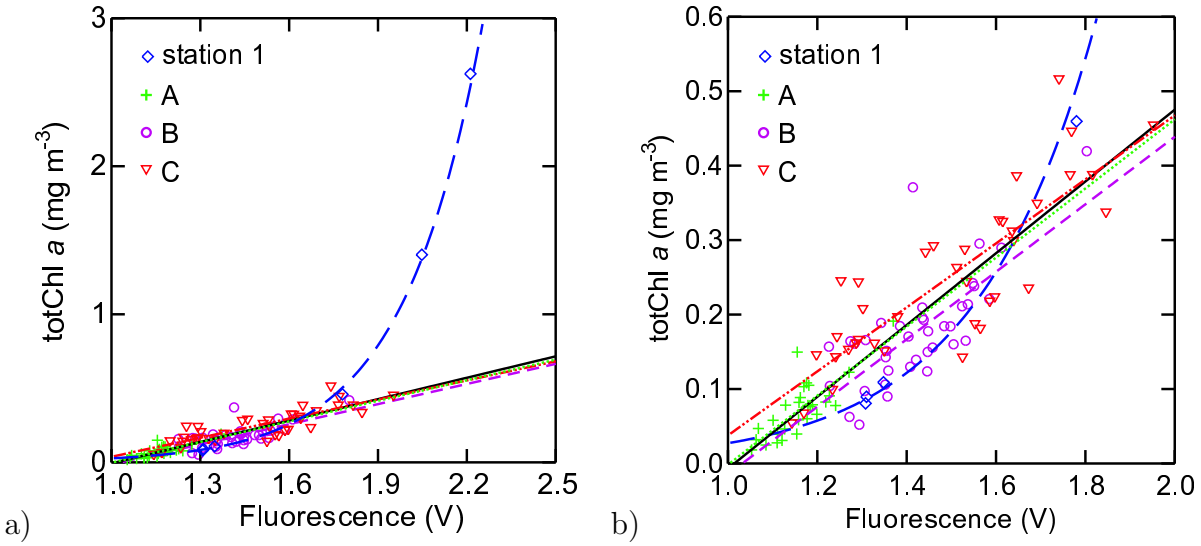


Figure E.1: Differences in the relationship between CTD fluorescence and Chl*a* concentration for a) all the AMT11 data and b) with detailed view at concentrations lower than 0.6 mg $m^{-3}$. Equations presented in Table E.1 are overplotted for Station 1 (long dashed line), W1 (solid line), Cluster A (dotted line), Cluster B (dashed line) and Cluster C (dash dot dotted line). The Clusters are indicated.

the coefficient of determination (Table E.1). However, because Cluster B and C had a more distinct relationship between CTDf and Chl*a*, it was decided to use Cluster specific relationships to derive the Chl*a* concentrations.

## E.2 Chl*a* estimates from CTD fluorescence

At each station the water column was split according to the Clusters of phytoplankton assemblage. Figure E.2 shows how Chl*a* was estimated. Because the pigment analysis was done for discrete samples, it was assumed that a depth interval was dominated by one of the Clusters when two consecutive discrete samples were classified as the same Cluster. When two discrete consecutive samples were identified as different Clusters, that depth interval was analysed as in transition from one Cluster to another with 100 % domination of the Cluster in its respective extreme. The domination of those Clusters were considered gradual and estimated linearly (Figure E.2).

## E.3 Other measurements

**Size-fractionated Chl*a* concentration**

At pre-dawn stations of AMT11, about 0.3 L of water were drawn and filtered sequentially through 0.2, 2 and 20 $\mu$m polycarbonate filters. Immediately after the filtration, the filter was placed in a glass vial with 8 mL of 90 % acetone for at least 20 h for extraction at -20 °C. Chl*a* was measured in a 10-AU Turner Design digital fluorometer calibrated against a standard Chl*a* stock solution prior to the cruise.

### E.3.1 Size-fractionated $^{14}$C uptake

At every pre-dawn stations of AMT11, five depths were sampled for size-fractionated primary production rate determination. For each sampled depth four 70 mL acid-cleaned polypropylene bottles (3 transparent + 1 dark) were filled with the water sample. Each bottle was inoculated with 333 to 814 kBq (9-22 $\mu$Ci) $NaH^{14}CO_3$, depending on the phytoplankton biomass, to yield activities exceeding 3000 dpm. The incubation was set before sunrise for 24 h, in an on-deck incubator with filters to reduce the irradiance to

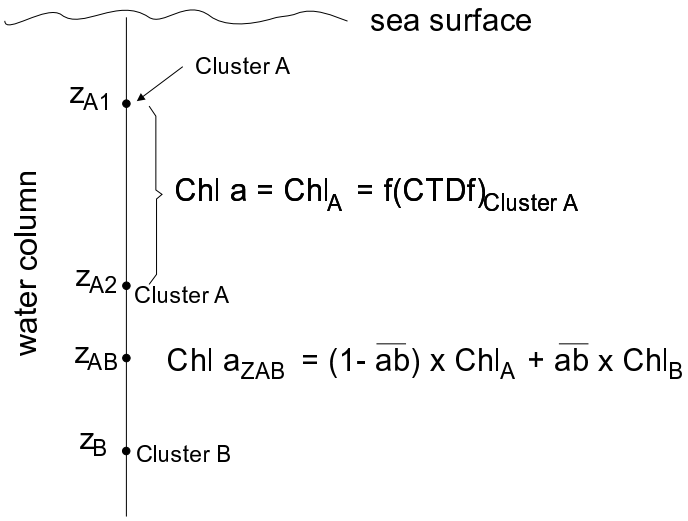


Figure E.2: Chl*a* concentration estimated from the CTD fluorescence (CTDf) accounting for the phytoplankton community structure differences. Discrete samples are represented by dots with indication of depth and the Cluster as they were classified. A layer of water column where both extremes had discrete water sample classified as the same Cluster, for example the layer between $Z_{A1}$ and $Z_{A2}$, the Chl*a* was estimated with the regression line obtained for that Cluster, e.g. Cluster A. A layer with different Clusters in the extremes like the layer between $Z_{A2}$ and $Z_B$, Chl*a* at depth $Z_{AB}$ was estimated accounting proportionally the distance from each of the end-Clusters to estimate the transition from one Cluster to the other, where $\overline{ab} = (Z_{AB} - Z_{A2})/(Z_B - Z_{AB})$. $Chl_A$, $Chl_B$ and $Chl_C$ are totChl*a* estimated as function of CTDf specific for respectively Clusters A, B and C.

approximately those experienced by the cells at the sampling depths. The samples were then filtered at vacuum pressure $< 50$ mmHg through a cascade of 20, 2 and 0.2 $\mu$m polycarbonate filters. After filtration, the filters were fumed with concentrated HCl for decontamination for 20 to 22 h and then placed in plastic scintillation vials. Each vial was filled with 3 mL of Ultima GOLD XR LSC scintillation cocktail and the radioactivity determined on board with a Beckman LS600SC liquid scintillation counter. Internal quenching correction was performed.

### E.3.2 $^{14}$C photosynthesis-irradiance (P-E) curve experiment

The relationship between irradiance and the rate of carbon incorporation by phytoplankton was evaluated at 3 depths down to the DCM in every mid-day station. Thirteen 70 mL Corning bottles of were filled from each depth, inoculated with 333 to 814 kBq (9 to 22 mCi) $NaH^{14}CO_3$ and incubated for approximately 2 hours with a halogen lamp with near-solar spectrum. The incubators were cooled with near sea-surface water (18.5-23C). The PAR irradiance of each incubator cell (corresponding to the light each Corning bottle should receive) was measured before every incubation with a LI-COR 1000 quantometer equipped with a LI-COR plate sensor. The last Corning bottle from each depth was protected against light with aluminium foil and used as a dark reference. After the incubation, the samples were filtered through Millipore GF/F filters, which were processed as described above for the determination of size-fractionated primary production.

## E.4 Auxiliary results

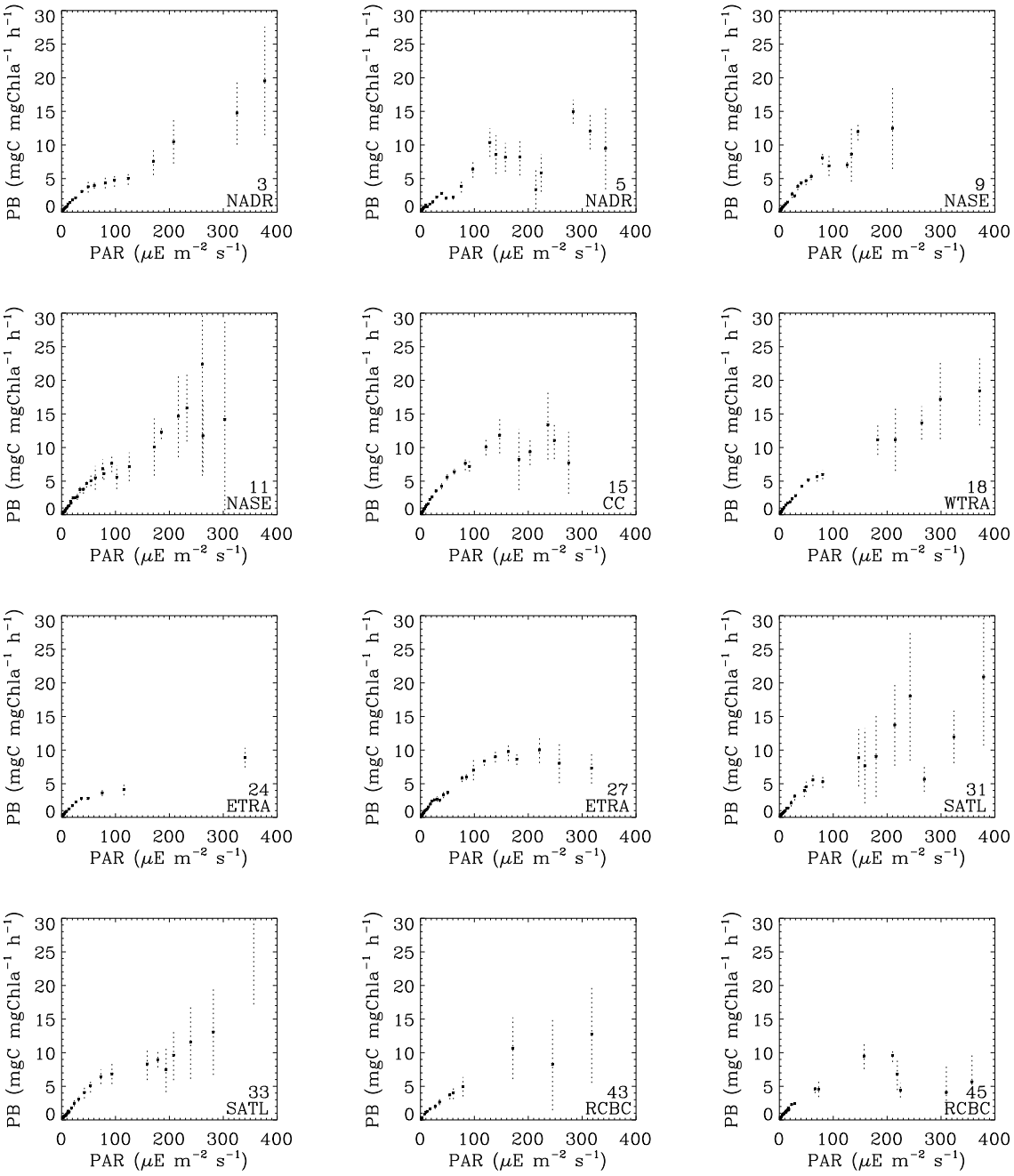


Figure E.3: Biomass specific primary production estimated from FRRF against PAR. Stations with bigger errors (in dotted line) are shown. The scales are the same for all the stations. Same data plotted in log-log scale are presented in Chapter 7, Figure 7.2.